Factors Affecting Mercury Capillary Pressure Measurements

by

Maung Than Htay Akbar Ali

A Thesis Presented to the

FACULTY OF THE COLLEGE OF GRADUATE STUDIES

KING FAHD UNIVERSITY OF PETROLEUM & MINERALS

DHAHRAN, SAUDI ARABIA

In Partial Fulfillment of the
Requirements for the Degree of

MASTER OF SCIENCE

In

PETROLEUM ENGINEERING

December, 1991

Order Number 1354101

Factors affecting mercury capillary pressure measurements

Ali, Maung Than Htay Akbar, M.S.

King Fahd University of Petroleum and Minerals (Saudi Arabia), 1991

U·M·I

300 N. Zeeb Rd.
Ann Arbor, MI 48106

FACTORS AFFECTING MERCURY CAPILLARY PRESSURE MEASUREMENTS

BY

MAUNG THAN HTAY AKBAR ALI

A Thesis Presented to the

FACULTY OF THE COLLEGE OF GRADUATE STUDIES

KING FAHD UNIVERSITY OF PETROLEUM & MINERALS

DHAHRAN, SAUDI ARABIA

In Partial Fulfillment of the
Requirements for the Degree of

MASTER OF SCIENCE

In

PETROLEUM ENGINEERING

DECEMBER 1991

KING FAHD UNIVERSITY OF PETROLEUM AND MINERALS
DHAHRAN, SAUDI ARABIA

COLLEGE OF GRADUATE STUDIES

This thesis, written by Mr. Maung Than Htay Akbar Ali under the direction of his Thesis Advisor and approved by his Thesis Committee, has been presented to and accepted by the Dean of the College of Graduate Studies, in partial fulfillment of the requirements for the degree of MASTER OF SCIENCE in Petroleum Engineering.

Thesis Committee:

Dr. Khalid Al-Fossail
Thesis Advisor

Dr. Abdulaziz U. Al-Kaabi
Member

Dr. Abdulaziz A. Al-Majed
Member

Dr. Salih Saner
Member

Dr. Khalid Al-Fossail
Department Chairman

Dr. Ala H. Al-Rabeh
Dean, College of Graduate Studies

Date: 8.2.92

DEDICATED TO MY MOTHER

ACKNOWLEDGEMENTS

Acknowledgement is due to King Fahd University of Petroleum and Minerals for providing financial support during the entire period of study .

My sincere gratitude and appreciation is due to my thesis committee chairman, Dr. Khalid Al-Fossail for his beneficial help and invaluable guidance throughout the course of thesis work. He offered me lot of his time for useful discussions and remarkable ideas . I wish to express my deep appreciation to my thesis committee, Dr. Abdulaziz U. Al-Kaabi, Dr. Salih Saner and Dr. Abdulaziz A. Majed whose effort, support, and guidance throughout this study made this research possible.

I wish to express my special thanks to Mr. Hayri Alpustun and all RI staff from Petroleum Engineering section of Division 1, KFUPM Research Institute, for providing every possible facility for this research work and for their guidance.

Finally , I am thankful to my colleagues and friends for the friendly treatment offered to me during my study.

TABLE OF CONTENTS

LIST OF TABLES

LIST OF FIGURES

THESIS ABSTRACT

Full Name of Student : MAUNG THAN HTAY AKBAR ALI

Title of Study : FACTORS AFFECTING MERCURY CAPILLARY PRESSURE MEASUREMENTS

Major Field : PETROLEUM ENGINEERING

Date of Degree : DECEMBER 1991

The factors that influence the mercury capillary pressure data of Berea sandstone and carbonate rocks were investigated. These factors include sample size, epoxy coating and equilibrium time as studied by Wardlaw et al. [8]. Katz and Thompson's [18] method was applied to estimate the liquid permeability from capillary pressure data and a comparison was carried out with Swanson's [14] correlation method. Finally, the experimental data was presented using the J-function put forth by Leverett [1].

The Experimental results show that capillary pressure curves are insensitive to the sample size of sandstone samples regardless of equilibrium time and epoxy coating. Studies on the coated carbonate rock samples show that forming of the injection capillary pressure curves depend on the sample size. As the sample size increased, the injection curves moved to a lower saturation and the displacement pressure decreased. Estimation of permeability using the two methods showed that while Swanson's correlation approach gave a standard deviation error of 72%, the Katz and Thompson's percolation theory gave a standard deviation error of 45%. In an attempt to obtain a better correlation, pore throat sorting (PTS) was used as a parameter in the extended J-function for sandstone rocks, and critical length (l_c) was considered in the correlation function for carbonate samples that have a permeability range from 20 md to 800 md.

MASTER OF SCIENCE

KING FAHD UNIVERSITY OF PETROLEUM & MINERALS

DHAHRAN, SAUDI ARABIA

ملخص بحث

اسم الطا لب : مون تان تيه أكبر علي
مسمى البحث : العوامل التي تؤثر علي قياس الضغط الشعري بالزئبق
القسم : هند سة البترول
تاريخ منح الدرجه : جمادي الثانيه١٤١٢هـ

تم في هـذه الدراسه بحث العوامل التي تؤثر عاى قياسات الضغط الشعري لعينات صخور رمليه وأخرى جيريه. والعوامل التي تم دراستها هي طول العينه الصخريه والغلاف الايبوكسي وزمن التوازن. في هذه الدراسه تم تقدير النفاذيه باستخدام طريقه كاتز و ثومبسون وتم مقارنتها بتلك المستخلصه من طريقه سوانسن للعلائق وأخيرا تم عرض البيانات التي وجدت في التجارب باستخدام دالة جيه كماإقترحه ليفرت.

ولقد أظهرت النتائج أن منحنيات الضغط الشعري لاتتأثر بطول العينه للصخور الرمليه. في حاله وجود الغطاء الايبو كسي لعينات الصخور الجيريه أن منحنيات الضغط الشعري للضخ تعتمد عاى طول العينه فكلما زاد طول العينه كلما زاحت منحنيات الضخ إلى قيم صغيره. وقد أظهرت الدراسه أيضا أن تقدير قيم النفاذيه بإستخدام طريقة سوانسن يعطي إنحراف معياري قدره ٧٢٪ بينما استخدام طريقة كاتز وثومبسن مع نظريه الرشح يعطي إنحراف معياري قدره ٤٥٪ وفي محاوله لتحسين هذه النتائج تم إدراج معامل تصنيف عنق المسام في دالة جيه بالنسبه لعينات الصخور الرمليه وإدراج الطول الحرج للعينه في داله العلائق بالنسبه لعينات الصخور الجيريه التي تتراوح نفاذيتها بين ٢٠ و ٨٠٠ مليدارسي.

الما جستير في العلوم
جامعة الملك فهد للبترول والمعادن
الظهران-المملكة العربية السعوديه

CHAPTER 1

CHAPTER 1

INTRODUCTION

Capillary pressure, which is a unique function of fluid saturation, is defined as the pressure difference at the interface between two immiscible fluids, such as oil and water or gas and water, existing in the reservoir rocks or the porous system. The relation between fluid saturation and capillary pressure gives the physical properties of the rock samples such as pore geometry, porosity and permeability. Therefore, capillary pressure measurement is not only important for obtaining the reservoir rock properties but it also plays a major role in waterflooding or in secondary oil recovery.

The techniques which have been used to measure capillary pressure of the reservoir rocks are porous diaphragm method, centrifuge method and mercury injection method. there are serious limitations in porous diaphragm and centrifuge methods. While in the porous diaphragm method, the time that is needed to obtain a capillary pressure curve may be months rather than hours, in the centrifuge method, the calculation of capillary pressure will be a tedious work although equilibrium time is short. On the other hand, the centrifuge method allows the determination of capillary pressure curves of small consolidated core sample quickly and conveniently [2].

Although mercury is a nonwetting liquid and it must be forced under pressure into the evacuated core sample, the capillary pressure curves

determined by the mercury injection method can be converted to equivalent oil-water system or gas-water system. [3,5]

The measurement of capillary pressure by mercury injection, as mentioned above, is the commonly used and reliable method. Therefore, some of the literatures on the subject have concentrated their studies on the pore geometry and fluid distribution in the petroleum reservoir rock from capillary pressure data [6,7,8,9,10]. The advantages of the method lie in the fact that the experimental data, capillary pressure curves, can be obtained quickly in a matter of hours rather than days, and even small irregular shaped samples can also be handled in the same manner as that of large regular shaped samples.

Considering from theoretical as well as practical aspects, the capillary pressure curve provides the characterization of the capillary properties of the porous system and also the degrees of properties which are related to fluid behavior in porous media. [4]

The study of this thesis is devoted to the capillary pressure measurements and capillary function. It is planned to study the factors which affect the capillary pressure curve by using mercury injection method. The sample size influences the surface area to volume ratios, and therefore it can be expected to affect the shape of capillary pressure curve. The effect of surface area size which has epoxy coating was investigated for Berea, Bentheimer and

carbonate samples. The results obtained from capillary pressure data can be used to determine the equivalent oil-water system which can be related to the rock properties of actual reservoir.

In this study, Leverett capillary pressure function [1], J-function, was utilized to correlate the capillary pressure-saturation relation and a modification to it will be carried out to obtain a better correlation. Since fluid flow in the porous media is controlled by the pore throat size ratio, the pore size distribution plays a crucial role in fluid flow. Therefore, permeability was calculated from mercury capillary pressure data using Katz and Thompson's percolation theory approach [18] and a comparison of it with Swanson's correlative approach was carried out.[17].

CHAPTER 2

CHAPTER 2

LITERATURE REVIEW

There is a limited number of publications in the literature that studied the factors affecting capillary pressure on limestone core samples using mercury injection method. This is true due to the fact that sufficiently accurate results can never be obtained directly and mercury does not always act as a strongly nonwetting liquid. However, the method described for determination of capillary pressure involves a porous solid and a single nonwetting fluid, i.e., mercury, which forms a contact angle of 140° against the solid.

Leverett, M.C. [1] proposed a correlation function called J-function in order to normalize the capillary pressure curves in which physical properties of the rock and fluid properties were used. He found that J-function-saturation relation correlated well in all clean unconsolidated sands.

Hassler, G.L. [2], who studied and developed capillary pressure measurements in small core samples using centrifuge method, showed that difficulties were encountered in calculating capillary pressure if the experimental data were not smooth enough. His method can be used with liquid or gas, and the capillary pressure can be measured directly.

Purcell, W.R. [3] pointed out that the capillary pressure curve derived by mercury injection method has been found to be in close agreement with that obtained by the conventional method called porous diaphragm for the various formations if the constant conversion factor was used to account for the differences between surface tensions and contact angles. Most probably, in the air-mercury system, mercury is the nonwetting liquid and in the oil-water system, water is the wetting liquid. In his paper, he further showed that capillary pressure curve could be obtained very quickly in less than an hour and core samples of any shape, whether regular or irregular, could be handled regardless of the size of the cores. He also calculated the permeability of the core from mercury capillary pressure data.

Rose Walter and Bruce, W.A. [4] proposed a new technique in which single or multiple displacing cell can be used to determine the capillary pressure curve. The data obtained by their method can be applied to express the characteristics of the reservoir rock. They also stated that extended J-function can be employed to correct the capillary pressure data. The characteristics such as fluid distribution, orientation of shape and tortuosity, the interfacial surface area and relative permeability of the wetting phase can be investigated by interpreting capillary pressure data.

Brown, Harry W., [5] showed that the results obtained from mercury injection method vary widely from sample to sample when converting to

water/gas system which is most commonly used method in restored-state. Considering both the methods, the same trend for capillary pressure curve was found if the same conditions were kept unchanged. In converting air-mercury to oil-water system, a proper conversion factor has to be chosen. The factors 6.4 and 7.2 are for limestone and sandstone samples respectively. He further stated that the drainage capillary pressure curve derived from restored state method can be utilized in the solution of dynamic problem of fluid flow of oil and gas system. He also pointed out that the use of J-function invented by Leverett for the correlation of capillary pressure saturation had given a good correlation for a specific geologic formation. The results can be improved by grouping formations according to their lithologies or rock textures.

Pickell, J.J.[6] found from a laboratory investigation that air-mercury capillary pressure data studies of hysteresis can sufficiently indicate the fluid distribution in a water-oil system when the rock is strongly water-wet. Mercury can be recovered more efficiently from a well-sorted rock in which higher saturation exists in uniform pores. Somehow, the recovery of mercury is less from poorly sorted rock, because of existence of lower saturation in discrete small pores. However, residual oil saturation can be forecasted from the air-mercury capillary data similar to that of oil-water system.

The Scientific Software Corporation [7] presented a geologic survey on

the studies of air-mercury capillary pressure for different types of core samples. According them, only very low initial displacement pressure is required to fill the mercury into the porous media if the sample is highly permeable at about 430 md. It is due to the fact that most of the large porosities lie in fairly large and uniform pores.

Wardlaw, N.C. and Taylor, R.P., [8] studied several factors that affect the capillary pressure curve using mercury injection method. These factors included sample size, epoxy coating and equilibrium time. They found that the sample size was not significantly affected in Indiana limestone, as shown in Fig. (2.1). The temperature effect, which might change the volume of mercury, can be neglected if the laboratory was controlled thermostatically before the experiment started. The same trends of capillary pressure curves were found in both epoxy coated samples and uncoated samples, regardless of the size except for the injection curve in region A-B, Fig. (2.2). It is due to the influence of surface area which allows intrusion of more fluids into the uncoated sample. Therefore, the displacement pressure is less for uncoated sample than that for coated sample. Equilibrium time was studied for both rapid rates and slow rates on a sample of Indiana limestone. There were no significant effects on the withdrawal capillary pressure curve for both cases, Fig. (2.3). It was found that less equilibrium time was required for epoxy coated sample because only a small surface area existed compared to the sample volume. The studies of hysteresis effect on capillary pressure curve of

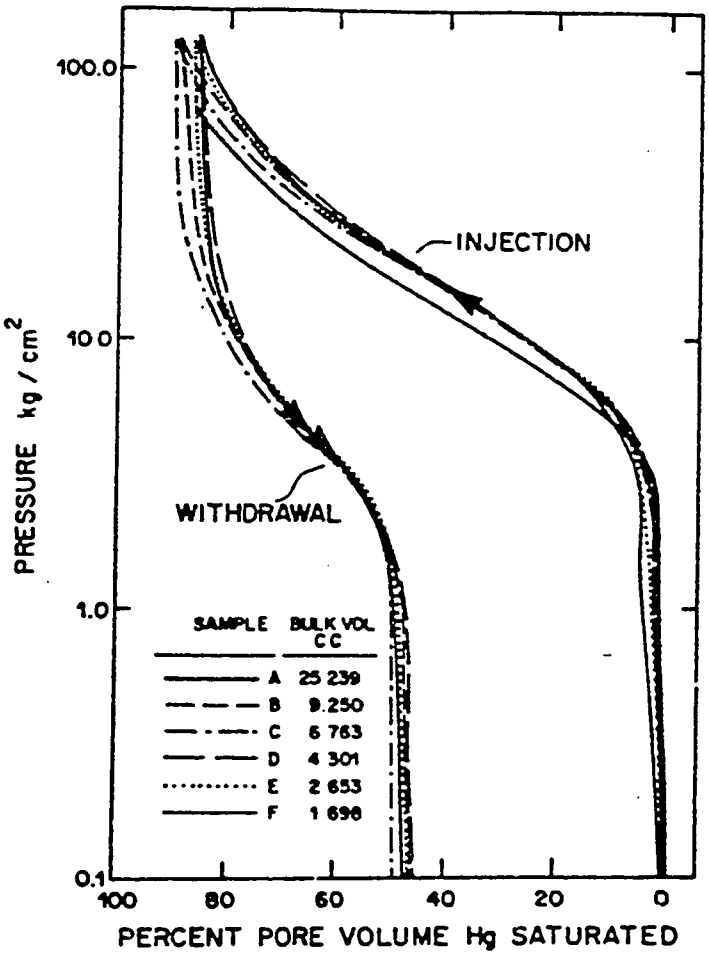

Fig.(2.1) : Capillary Pressure Curves for Different Samples Showing The Effect of Sample Sizes (Ref. 8)

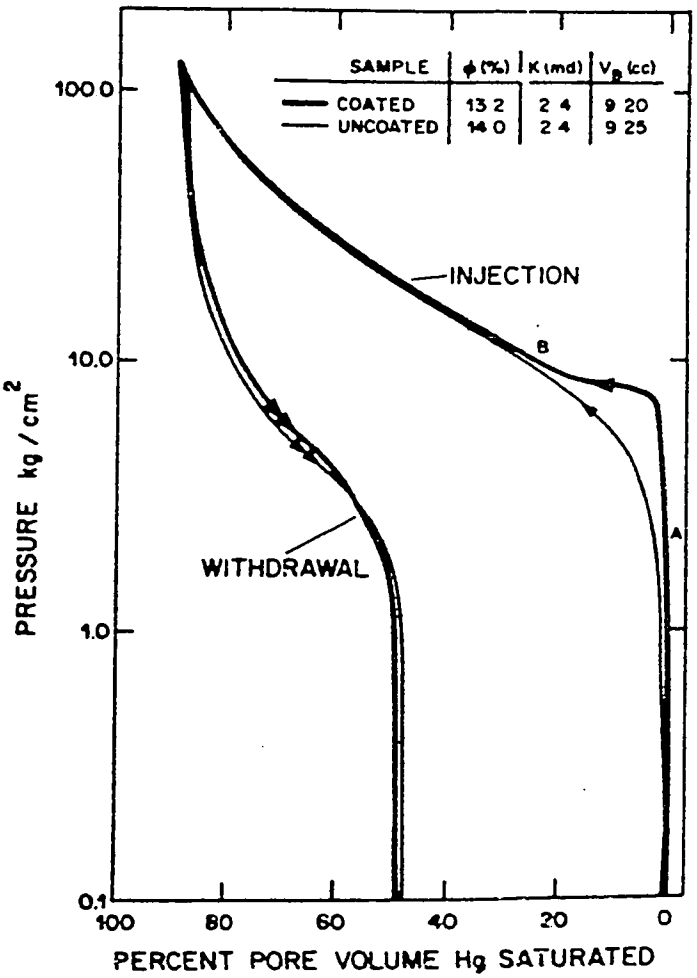

Fig.(2.2) : Capillary Pressure Curves for Duplicate Samples Showing The Effect of Epoxy Coating (Ref. 8)

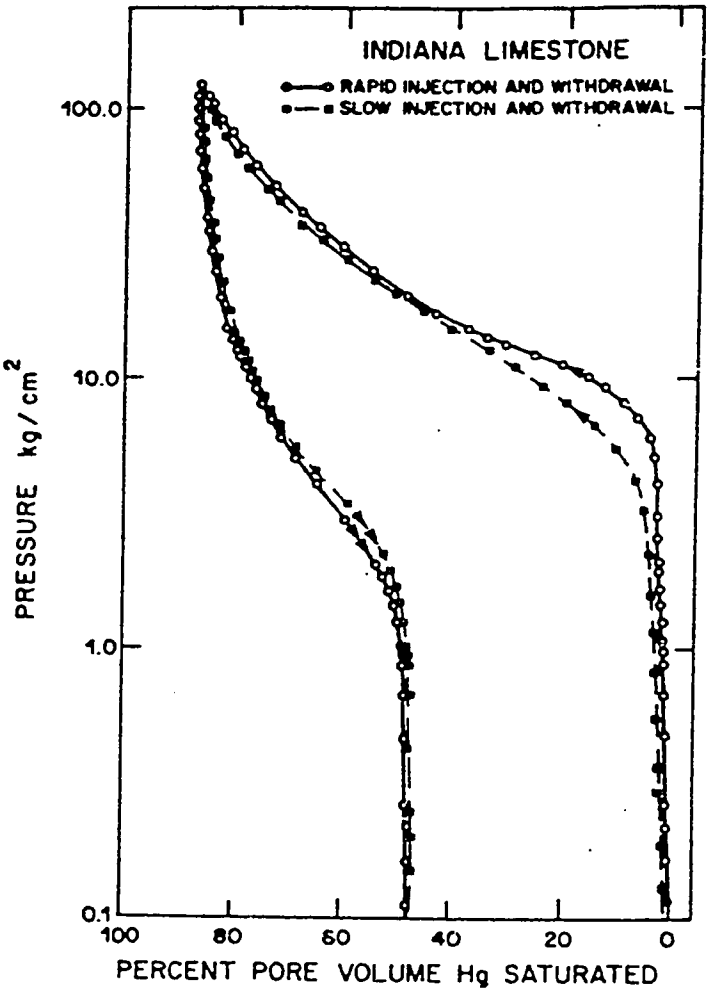

Fig.(2.3) : Capillary Pressure Curves for Duplicate Samples Showing The Effect of Equilibrium (Ref. 8)

Indiana limestone suggested that, in spite of doing hysteresis loops for intermediate saturation, the residual saturation can be computed from any initial saturation provided the initial injection curve and the final re-injection curves are known.

Wardlaw, N.C. [9] stated that the decrease of ejection or withdrawal efficiency (defined as ejected mercury volume at minimum pressure divided by injected mercury volume at maximum pressure) had depended on the increase of pore to throat sizes ratio or the decrease in porosity of dolomite core samples. On the other hand, the withdrawal efficiency increases with the increase in porosity. Therefore, withdrawal efficiency bound to vary widely from one sample to another in the same geological formation according to their homogeneity.

Wardlaw, N.C. and Cassan, J.P. [10] determined the recovery efficiency using mercury capillary pressure data and their results were compared to the oil recovery efficiency obtained from the relative permeability tests. They found that no significant correlations had existed between permeability, threshold pressure and mercury recovery efficiency, although porosity of the samples significantly correlated with mercury recovery efficiency. They also noted that the recovery of oil at breakthrough had a better relation with the relative permeability to water at residual oil saturation and also to porosity and pore-to-throat size ratio.

Wardlaw, N.C. and McKellar M. [11] pointed out that trapping of mercury in the pore had depended on pore to throat sizes ratio, throat to pore coordination number, random and non-random heterogeneity, and surface condition or roughness of the pore and throat. They also added that the injection curve gradient was significant upon which pore to throat sizes ratio was considered as a large number, as also the pore system arrangement should be non-randomly distributed. Thus the withdrawal and re-injection curve can be drawn for any initial saturation if the residual saturation is known.

Larson, R.G. and Morrow, N.R. [12] studied the effect of sample thickness on capillary curves using the theoretical approach based on the percolation concept. A comparison was made with mercury injection method. They used the glass capillary cell which has a purex fritted dics of 4.0-5.5 μm pore size as a porous material. They found that the sample thickness effects were significant when the pore size of about 10 times the particle diameter or the pore throat size of about 30 times the particle diameter was used. The effect becomes insignificant when the pore throat diameter is greater than 70 μm. The effect of sample thickness increased the accessibility of pore space which reduced the sharpness of the injection curves knee.

Sampath Krishnaswamy and Raible, Clarence J. [13] determined the absolute permeability, porosity, and pore size distribution from mercury

capillary pressure data. The permeability estimation from experimental data was found lower than the measured value at high saturation levels. It is due to the initial water saturation value which is higher than zero. The porosity values which was obtained from the pore size data and the saturation experiment were found to have a maximum deviation of ± 3 . In the study of pore size distribution, the results showed that medium pore throats did not have any contribution to pore volume as compared with large pore throats.

Swanson, B.F. [14] developed a new correlation to determine brine and air permeability from mercury capillary pressure data. He pointed out that sidewall chips or ditch cuttings could be used to calculate permeability.

Thomeer, J.H. [15] proposed a new equation to determine air permeability from mercury capillary pressure data. Three parameters such as pore geometrical factor, mercury saturation at infinite pressure and displacement pressure were used in his equation. The goal of his study was to compare measured and calculated permeability. He found a new correlation between measured and calculated permeability within an estimated error factor of 1.85.

Swanson, B.F. [16] used the mercury porosimetry to define the normalized capillary pressure P_c/σ from mercury/vacuum system. The results of water-oil system and mercury-air system were compared. The surface

tension, σ , and contact angle, θ , were measured during the experiment. The mercury contact angle on smooth quartz surface on behalf of sandstone was found to be 130° to 140° , measured through the mercury phase and the surface tension was found to be 484 dynes/cm. Figure (2.4) shows the agreement between mercury-air and water-oil for several samples of chloritic sandstone.

Omoregie, Z.S. [17] studied the factors affecting capillary pressure measurement using different methods on North Sea sandstone samples. The results showed that most of the samples had good agreement between centrifuge and mercury data, through most of the saturation range, on normalized capillary pressure curves as shown in Fig. (2.5). The effect of wettability on both the methods was studied. He assumed a contact angle of 40° for mercury system and that of 30° for oil-water system. The Plot of J-function versus wetting phase saturation is shown in Fig. (2.6). Significant differences were found between the oil-water centrifuge data and the mercury injection data. The reason was that the contact angle of 30° for J-function calculation was insufficient. He suggested that a mixed wettability system actually holds more than one contact angle.

Katz, A.J., Thompson, A.H., and Raschke, R.A.[18,19,22] studied the determination of absolute permeability by percolation concept from the mercury capillary pressure data. They suggested that rock sample of any type

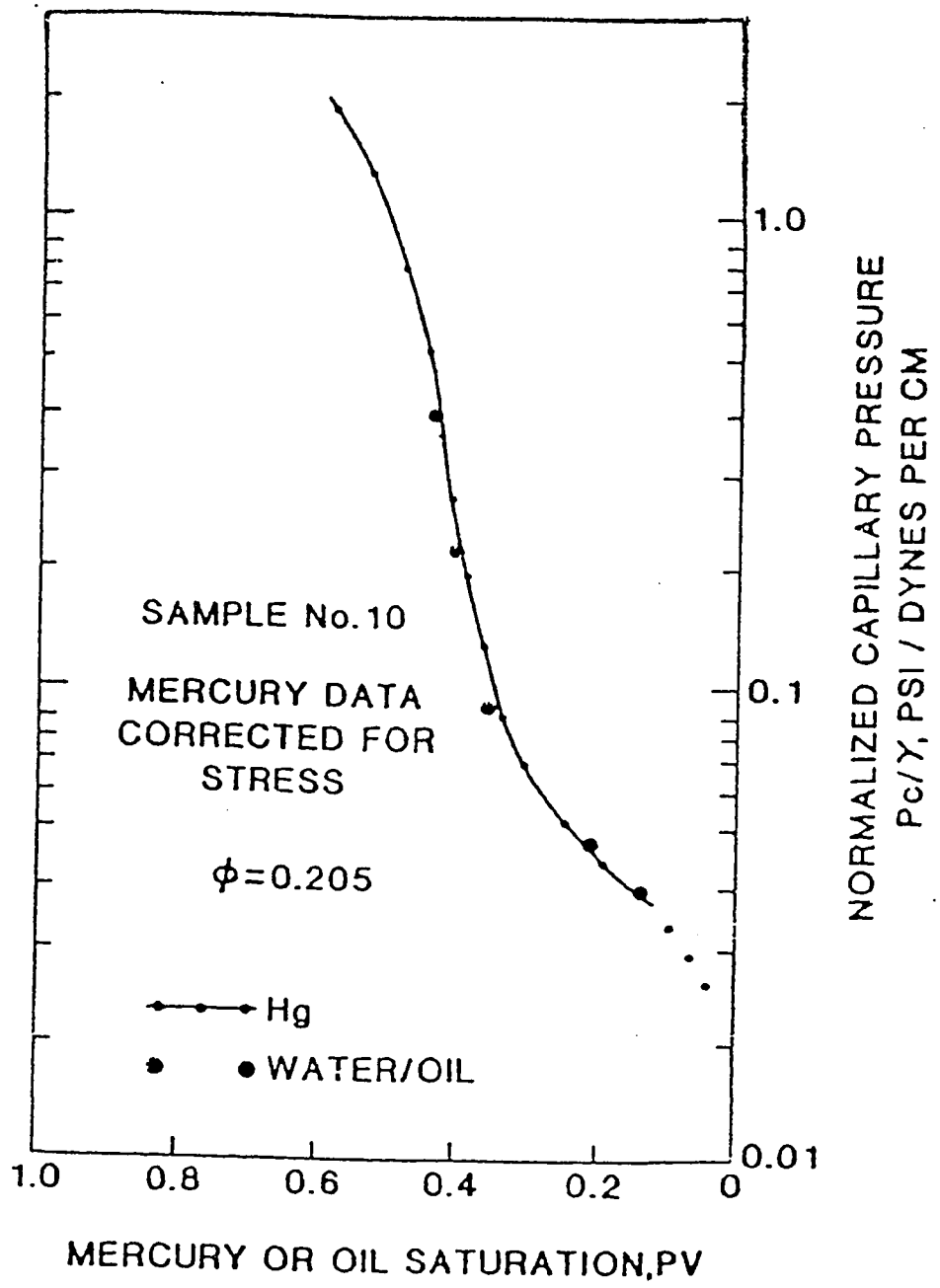

Fig.(2.4) : Comparison of Normalized, Stress-corrected Mercury Data with Water/Oil Data (Ref. 16)

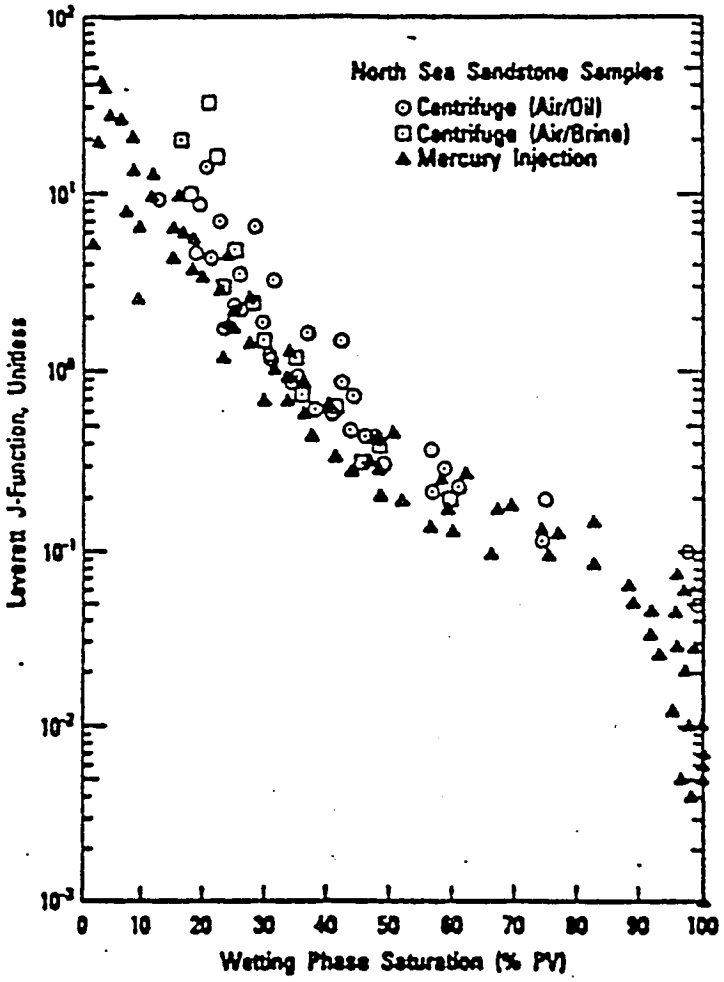

Fig.(2.5) : Comparison of Normalized Capillary Pressure Curves Obtained by Different Methods (Ref. 17)

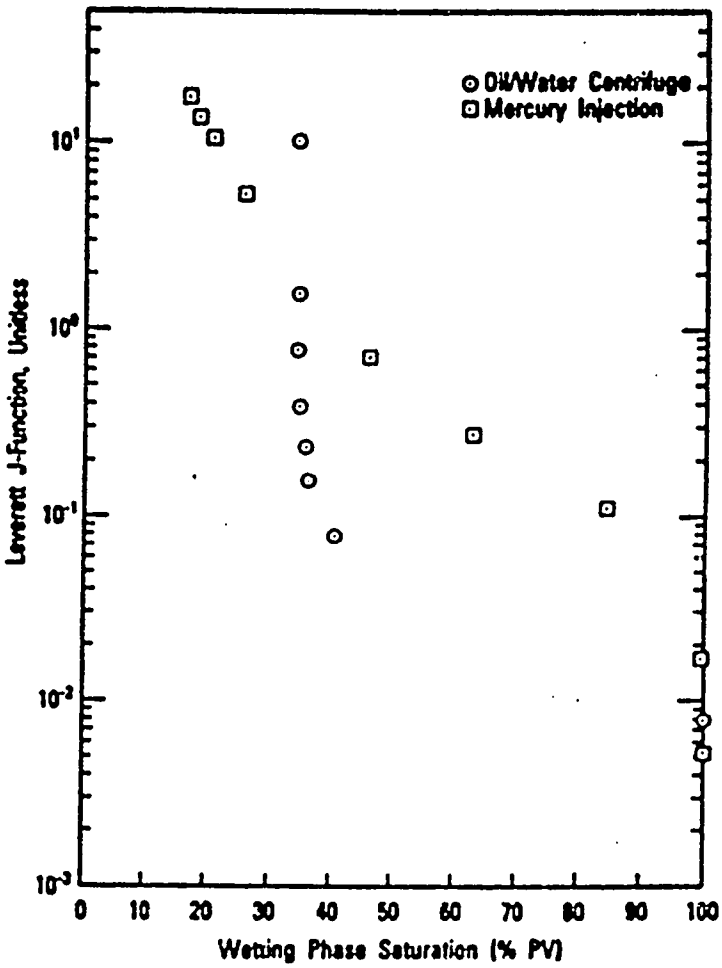

Fig.(2.6) : Comparison of Normalized Capillary Pressure Curves for an Intermediate Wettability Samples (Ref. 17)

whether sandstone or limestone, cylinder core sample or drill chips samples can be used to determine permeability using the equation shown below without adjusting any parameter involved in that equation. They further showed that agreement between calculated and measured permeability is within the acceptable errors which are estimated to be a factor of ± 2.

$$k = c \times l_c \times \frac{\sigma}{\sigma_o}$$

Those errors must be attributed to l_c calculation method and inhomogeneity of sample.

Thompson et al. [20] suggested that mercury injection capillary pressure data could be used to determine the permeability which can be presented in terms of a single effective pore diameter for essentially all porous media. They used the same equation as that used by Katz and Thompson (1986). They found that the errors resulted from the comparison of measured and calculated values were within the range. This is due to the sample inhomogeneity and the constant $c = 1/226$ which is estimated to be a factor of 2. The sample size and shape effect were studied for four cylindrical samples and chip samples of the Berea sandstone. The results are shown in Fig. (2.7). The spread in entry pressure is almost 10 to 15 % which means the threshold pressure is relatively insensitive to the shape factors. It was also pointed out

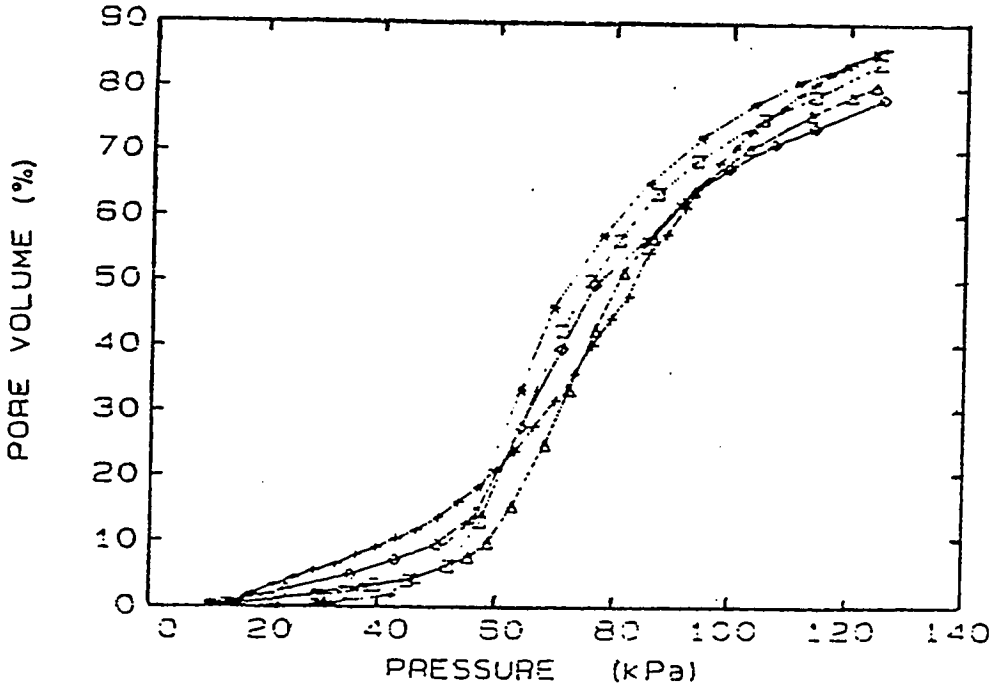

Fig.(2.7) : Comparison Between Different Shaped samples of Berea Sandstone and The Chips sample (Ref. 20)

that mercury injection curves were available for interpretation and estimation of transport properties such as permeability and conductivity.

Kent, D.M. [21] obtained information on the interaction between nonwetting fluids and reservoir porosity for carbonate rock samples using mercury injection capillary pressure data. The curves can be established in terms of intercrystal, cavity and mixed (combined intercrystal and cavity) porosity samples. The shallow slope of the plateau, as shown in Fig. (2.8), suggested a relatively uniform distribution of pore throat sizes on a dolomite which has intercrystal porosity. Mixed pore system which sloping plateaus are the norm, indicated that a poor uniform of pore throat size distribution had existed in a combination of vugs and intercrystal porosity as shown in Fig. (2.9). For cavity porosity, no plateau is discernible on the curve indicating a wide distribution of pore throat sizes. He discussed the clay content which might decrease the effective size of the pore throat, resulting in a decrease in withdrawal efficiency and an increase in irreducible water saturation.

Jenning, Jeffrey B. [23] showed that capillary pressure curves play a crucial role in exploration and developing geology. After converting from a mercury air capillary system to an oil-water capillary system, oil column can be estimated from capillary pressure data. The parameters such as pore throat sorting (PTS), reservoir grade (RG), and oil column for 50 % and 70 % oil saturations can be obtained from the capillary pressure data. He

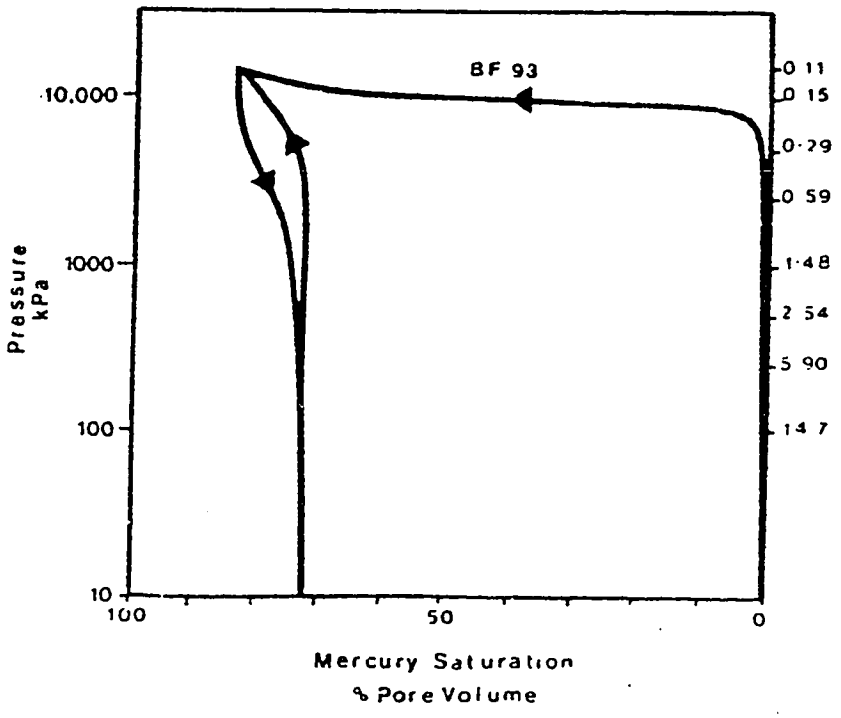

Fig.(2.8) : Mercury Injection Capillary Pressure Curve for Intercrystal Porosity in Dolomitized Micrite (Ref. 21).

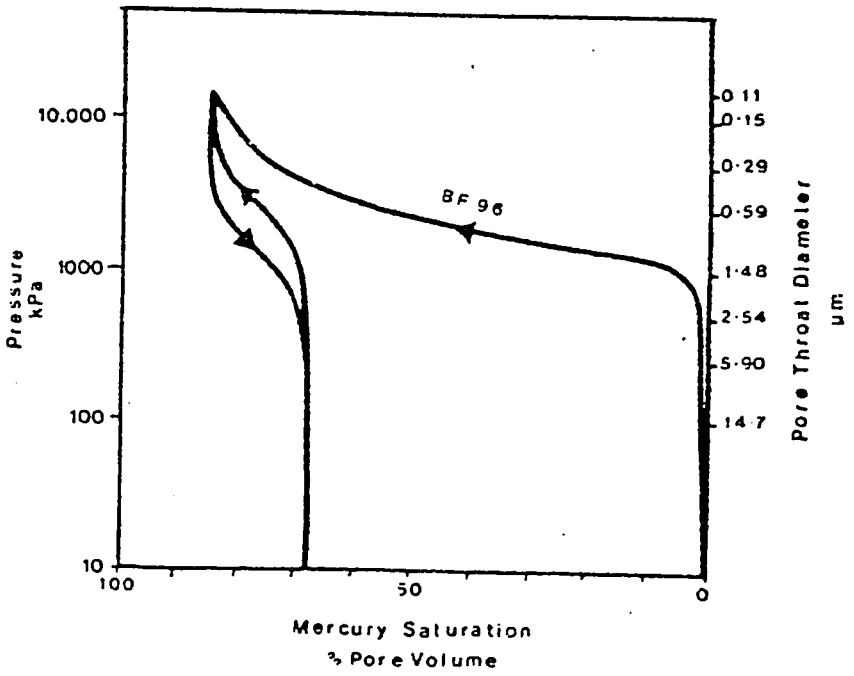

Fig.(2.9) : Mercury Injection Capillary Pressure Curve for Mix Porosity in Cemented skeletal Grainstone (Ref. 21).

pointed out that in well-sorted rocks, where a PTS value of 1.0 represents a perfectly horizontal plateau, oil will rapidly saturate after the threshold pressure is obtained. If the RG number is large, the pore throats will be smaller and much larger buoyancy pressure is needed to obtain economic oil saturation. The nonwetting phase (oil) relative permeability can be determined by construction of J-function vs. saturation on log-log plot. The pore geometry factor is obtained from the slope.

Mishra, B.K., and Sharma, M.M. [24] developed a method using capillary tube model to determine the pore size distribution in which mercury capillary pressure data were applied. They pointed out that this method will lead to a much better estimate of the true pore size distribution for small samples. They found that the use of Bethe Tree as a model for pore space had given good approximation.

Tsang, Y.W., and Hale, F.V. [25] used the mercury porosimetry to study and simulate the fracture reservoir. They assumed a constant contact angle of 180° throughout the calculation. They found that 65 % of the total volume of mercury was trapped in the fracture when the external pressure was reduced to zero.

Kamath, J. [26] developed a new correlation to estimate air permeability from mercury injection data. He also studied the effect of sample dimensions

on the estimation of air permeability and found that the sample dimensions have small effect on the permeability estimation method.

Chowdiah, P. [27] showed that gas-water capillary pressure data obtained by displacement test on tight sands was compared with capillary pressure data determined by mercury injection porosimetry. The value of conversion factor of 5 was used based on interfacial tension in the range of 470 to 480 dynes/cm and contact angle in the range of 130° to 140° for the mercury-vacuum system, and corresponding values of 70 dynes/cm and 0° for the gas-water system. For the sample with permeability of 9.2 μm and a porosity of 11.4 % at 1440 psi net stress, a significant difference between gas-water and mercury-vacuum was found, but for the sample with 31.9 μm permeability and a porosity of 13.7 % at 4735 psi net stress, the difference was found to be insignificant. He suggested that this might be due to difference in pore morphology of these rocks and pointed out that confining stress could have a significant effect on capillary pressure.

Yuan, H.H., and Swanson, B.F. [28] found that the pore space of the rock samples could be obtained by monitoring the mercury capillary pressure fluctuations during the injection period when the mercury was intruded into the sample as a constant slow rate. In this study, capillary pressure curves were divided into two parts, subison and risons. The subison-pore system distributions were focused on Berea sandstone and San Andres dolomite.

They found that the median subison-pore system volume (25 to 50 nl) for Berea sandstone was roughly double the median subison-pore system volume (12 to 25 nl) for San Andres dolomite.

Morrow, N.R. [29] used two methods; the first is a standard technique (centrifuge) in which pressure was increased steadily at preprogrammed time intervals and the second involved equilibration of mercury volume at each pressure step before proceeding to next level of pressure (mercury injection). The biggest differences between the standard and equilibrium analyses are at the lowest (less than 1000 psi) pressures and at highest pressures (40,000 psi and above). The measurements were found to be in reasonable agreement at intermediate capillary pressure. This suggested that at a high capillary pressure, the true equilibrium in the mercury-vacuum system would require substantially longer times at this pressure.

Tsakiroglou, Christos D., and Payatakes, Alkiviades C. [30] developed a reliable mercury intrusion-withdrawal simulation for three dimensional chamber and throat networks. They found that the withdrawal curve and the residual mercury saturation value had depended strongly on the ratio of the mean diameters. The residual mercury saturation increased sharply as the ratio of mean chamber diameter to mean throat diameter increased, as shown in Fig. (2.10). The intrusion curve became wider or narrower according to the width of the throat size distribution (see fig. 2.11). The two contact angles (

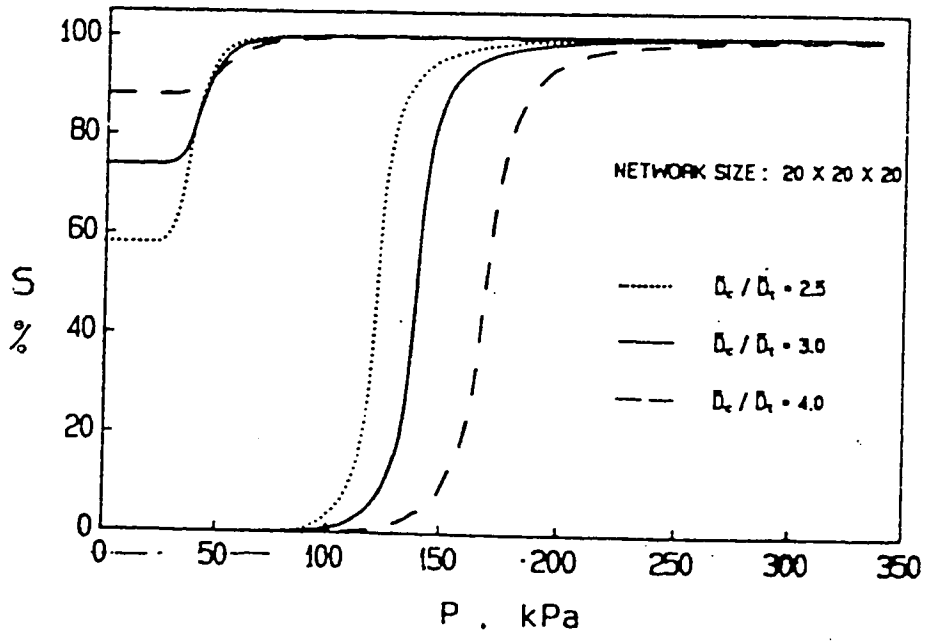

Fig.(2.10) : Simulated Mercury Capillary Pressure Curves Showing The Effect of Pore to Throat Diameter Ratio (Ref. 30).

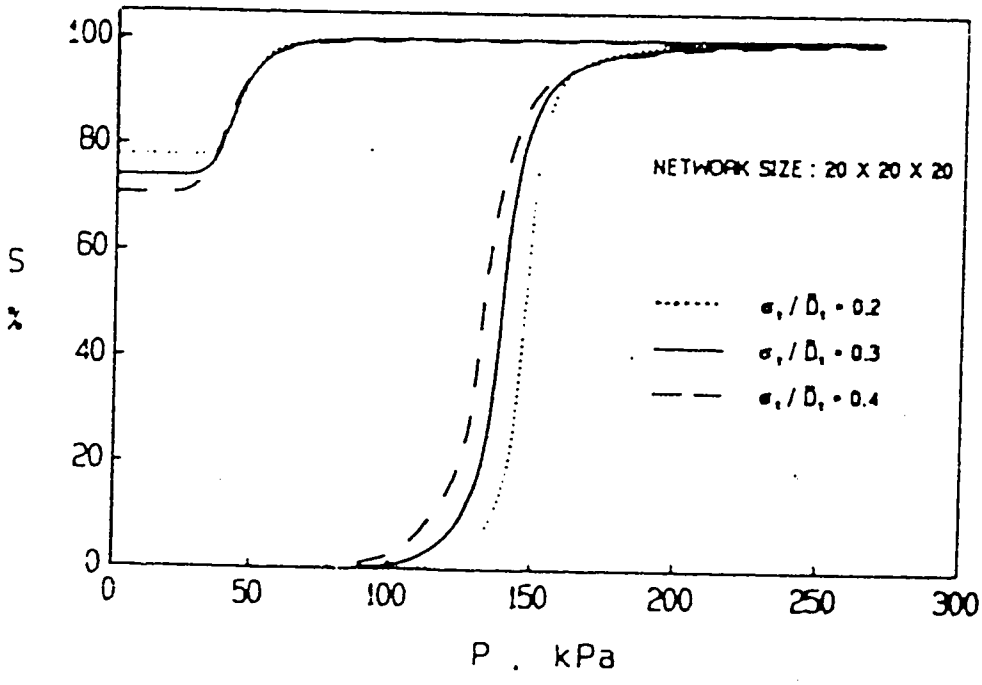

Fig.(2.11) : Simulated Mercury Capillary Pressure Curves Showing The Effect of Throat to Pore Diameter Ratio (Ref. 30).

θ_i and θ_r) are important parameters affecting the shapes and positions of the capillary pressure curves and the degree of hysteresis between the intrusion and retraction curves as shown in Fig. (2.12).

Maloney et al. [31] used two types of sandstone samples to describe the saturation and pore-throat size distribution using mercury injection method. The results indicated that approximately 80 % of the pore throats within both Berea and Bentheimer samples were in the range of 1 to 60 μm as shown in Figs. (2.13) and (2.14), respectively. They found that the Berea samples had slightly larger pore throat diameter as well as microporosity than the Bentheimer samples.

It can be readily inferred from the foregoing literature review that there is only a limited literature available about the study of capillary pressure by mercury injection method. Although considerable methods for studying the capillary pressure on Berea sandstone and limestone for a specific formation has been presented in some literature, necessary investigation is still needed to study the measurement of capillary pressure for carbonate rocks which have least permeability and varying lithology.

The objective of this study is to evaluate various factors that may influence the mercury injection, withdrawal, and re-injection curves.

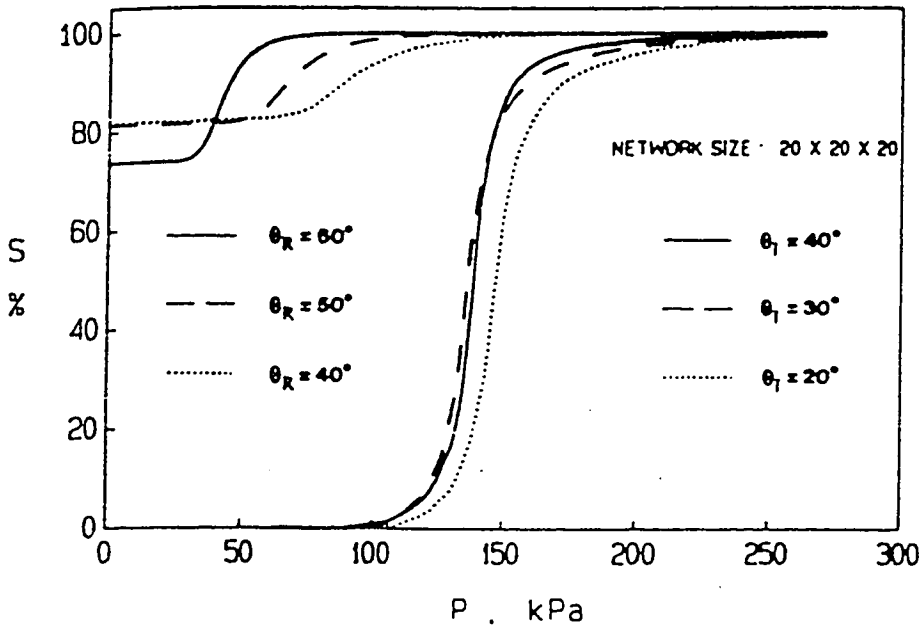

Fig.(2.12) : Simulated Mercury Capillary Pressure Curves Showing The Effect of Contact Angle (Ref. 30).

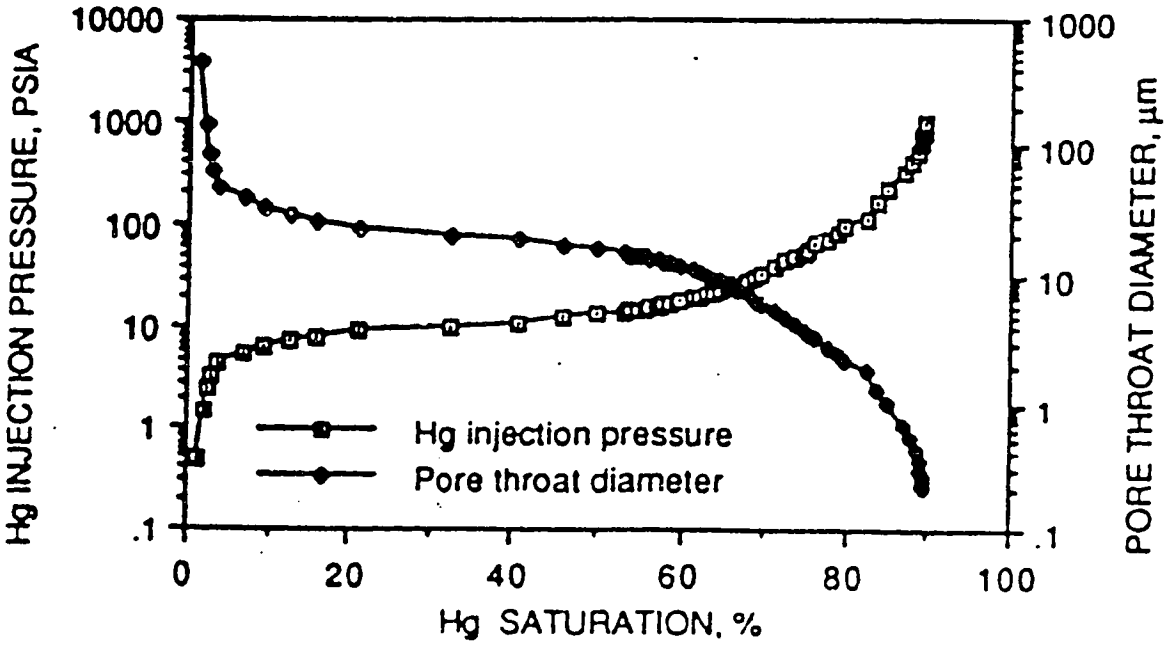

Fig.(2.13) : Mercury Injection Capillary Pressure and Pore Throat Diameter as a Function of Saturation for Berea Sandstone (Ref. 31)

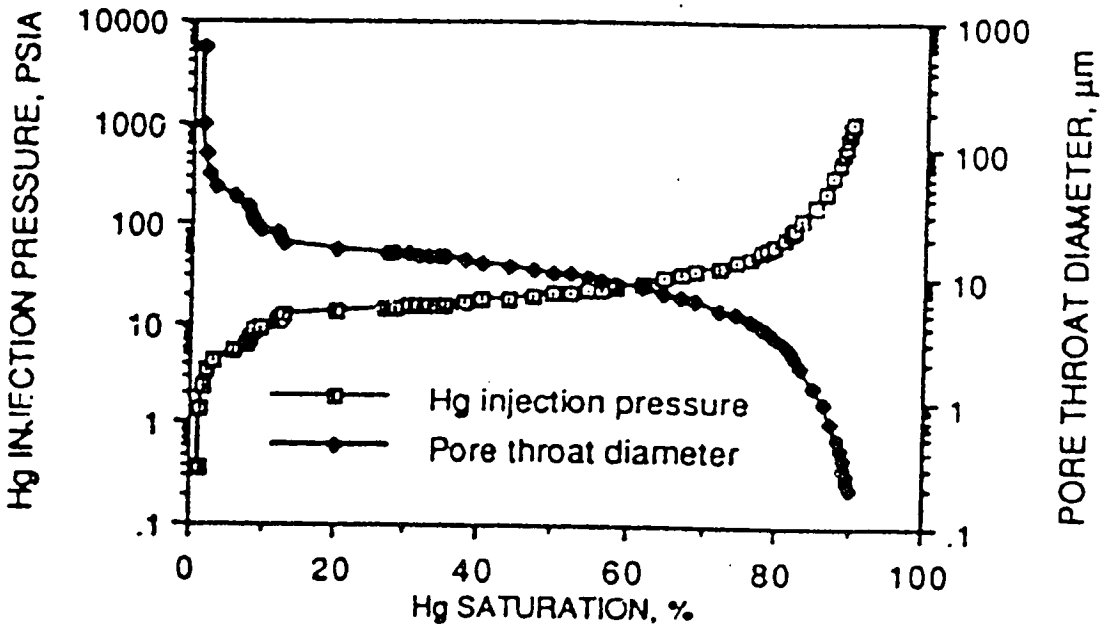

Fig.(2.14) : Mercury Injection Capillary Pressure and Pore Throat Diameter as a Function of Saturation for Bentheimer Sandstone (Ref. 31)

The specific objectives are :

1 .The influence of sample size on the capillary pressure saturation relation.

2 .The influence of equilibrium time.

3 .The effect of epoxy coating.

4 .Determination of the parameters which influence the forms of the capillary pressure curves, other than those three studied earlier.

5 .Capillary pressure data will be used to calculate permeability and comparison will be made with the previous studies.

6 .Correlating the experimental data using J-function or an extended J-function.

J-function or correlating function was proposed by Leverett as an expression,

$$J(S_w) = \frac{P_c}{\sigma} \times [\frac{k}{\Phi}]^{1/2}$$

Modification of J-function will be determined in order to represent a single reservoir.

CHAPTER 3

CHAPTER 3

EXPERIMENTAL APPARATUS AND PROCEDURES

Mercury injection experiments were conducted with high pressure of about 2000 psi on cylindrical shape core samples of different sizes. In this chapter, the description of the apparatus, materials and experimental procedures are presented as follows :

3.1 EXPERIMENTAL APPARATUS

The experimental apparatus used in the present study is shown in Fig. (3.1). It consists of a volumetric pump, a high pressure pycnometer, pressure control panel and vacuum pump. A brief description of each component are given in the next sections.

3.1.1 Mercury Injection Pump

The Mercury injection pump developed by core laboratories, Inc. is a high pressure volumetric displacement pump. The displacement is performed by a screw-actuated plunger which operates through a packing gland into a cylinder. The stainless steel plunger and an alloy steel measuring screw are precisely attached with micrometer scale which permits direct volume readings up to 0.01 cc. The pump scale indicates the volume of mercury charged to/or withdrawn from sample by movement of the pump metering

1. Yoke and Screw
2. To Panel
3. Micrometer Scale
4. Handle
5. Linear Scale
6. Auxiliary Linear Scale
7. Needle Valve
8. Sample Chamber
9. Packing Gland
10. Cylinder
11. High Pressure Gauge
12. High Pressure Valve
13. Displacement Plunger
14. Locking cap
15. Observation Port

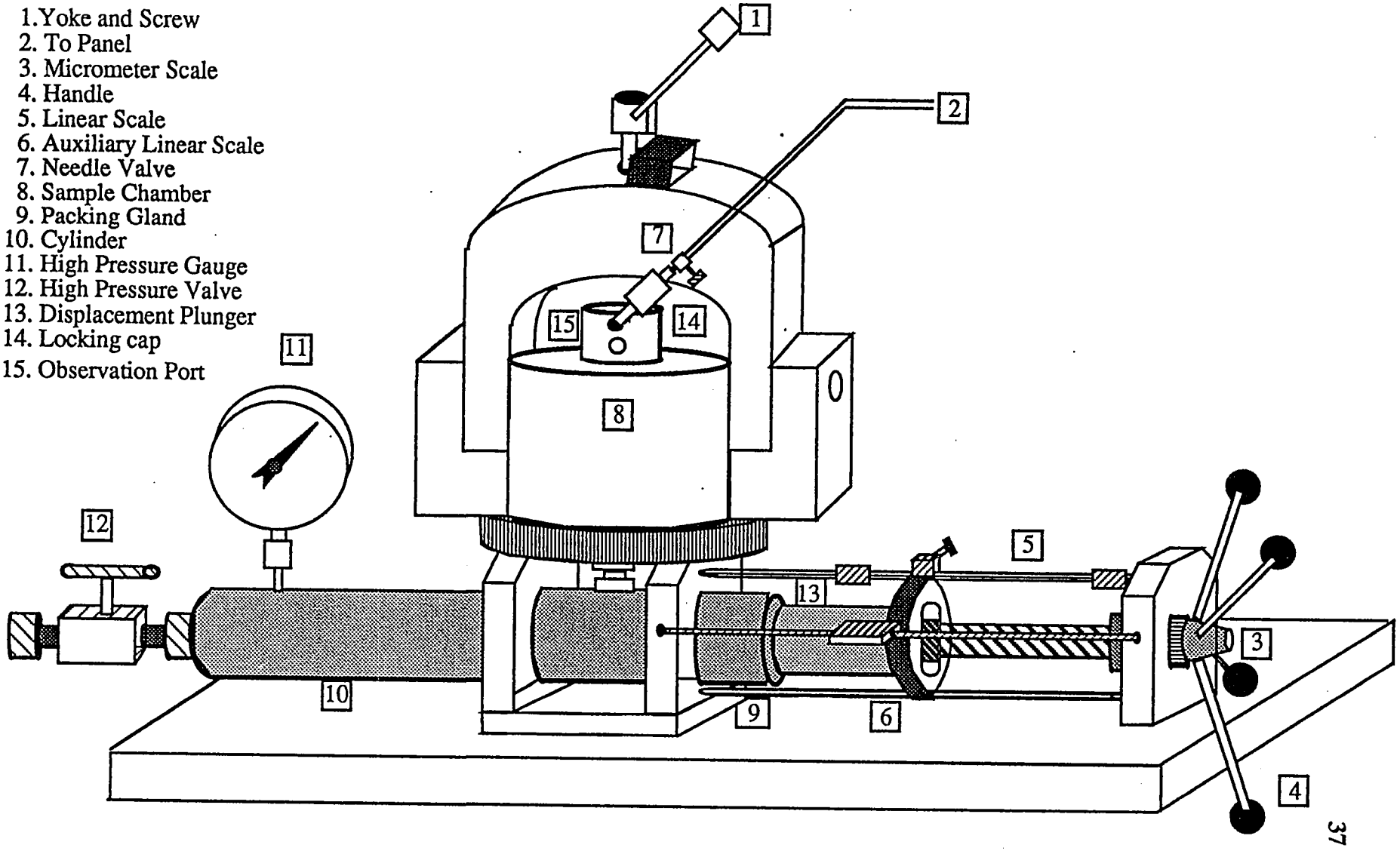

Fig. (3.1) Mercury Injection Apparatus

plunger.

3.1.2 Pycnometer

The pycnometer serves as a sample chamber and can hold a pressure of about 2000 psi. It is made of stainless steel. The sample chamber can handle samples size up to 2.5 *inch* (6.25 cm) in diameter and 3.5 *inch* (8.75 cm) length. The sample chamber is closed by a cap forming a pressure and vacuum tight seal. The pycnometer is provided with lucite window (observation port) at the top of the chamber which would indicate the mercury level in the sample chamber.

3.1.3 Pressure Control Panel

The pycnometer cap is connected to the pressure control assembly by a 1/8 *inch* stainless steel high pressure tubing. The regulation of gas pressure using nitrogen in the pycnometer and accurate measurements are done by the control equipment which is shown in Fig. (3.2). The assembly consists of two precise pressure gauges, regulator, relief valve and five pressure control valves. The small gauge can precisely measure pressure ranges from -30 to 30 psi. The large gauge can precisely handle pressure ranges of 0-2000 psi. All the gauges and control valves including the regulator are interconnected behind the panel as shown in Fig. (3.3). To prevent damage from accidental overpressure, the small gauge is equipped with pressure relief valve. The four

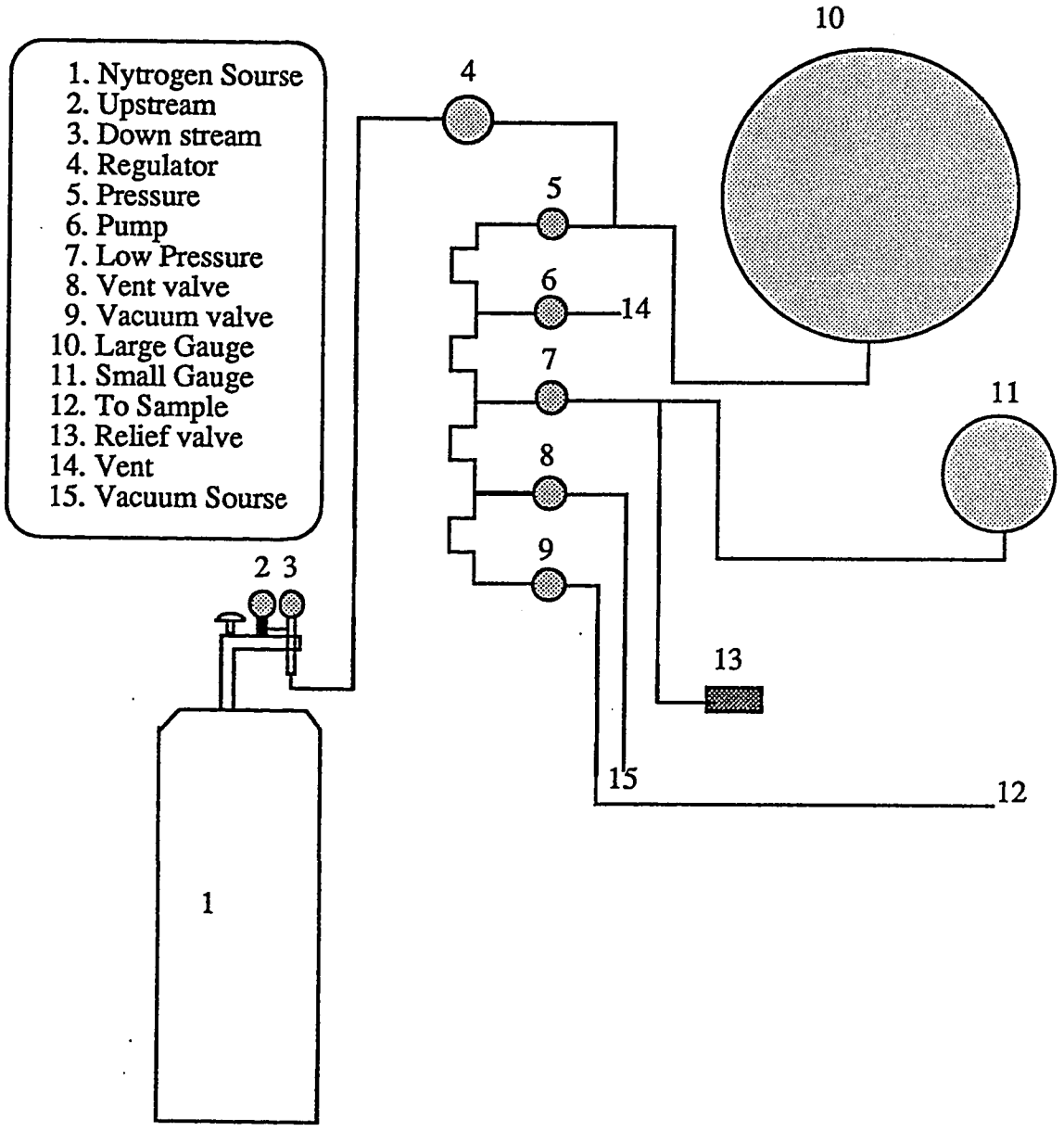

Fig (3.3). Piping diagram for panel rear view

valves, whose functions are indicated on the control panel, are used to connect the pycnometer system with the vacuum source, high pressure nitrogen, low pressure gauge for small pressure and an atmospheric vent.

3.1.4 Auxiliary Equipment

An auxiliary equipment which include the vacuum pump, nitrogen cylinder and lamb is used in this system. The vacuum pump is established for releasing pressure from atmospheric pressure to zero atmospheric, the nitrogen cylinder is commonly used for the high pressure gas source, and the lamb is used to see the mercury level through the observation port in the pycnometer clearly.

3.2 MATERIALS

The reservoir rocks such as Berea cores, Bentheimer cores and carbonate cores, from Saudi Arabian reservoirs have been used to measure capillary pressure. Berea sandstone has been used extensively because its general characteristics are well known. Bentheimer sandstone, a rock from german quarry, was selected as the second sandstone type because of its high permeability and homogeneity.

3.2.1 Preparation of Cores

A Berea core of 5 feet in length and 2 inch in diameter has been cut into

core pieces of 6 inch length and 1 inch diameter. The cores were then cut into different lengths so as to have the maximum length that has to fit inside the sample chamber. Therefore, the 6 inch length and 1 inch diameter core were cut into three different pieces of about 2 cm, 4 cm, and 6 cm in length. The same procedures were also followed in Bentheimer cores. The cores were dried in the oven for 6 hours with a temperature of $110°F$.

The carbonate core samples were 2.5 cm in diameter and 5 cm in length. The carbonate samples were cleaned with toluene and dried in a vacuum oven whose temperature was set at $110°F$ for 6 hours.

A helium porosimeter and a gas permeameter were used to determine the porosity and permeability values respectively. Basic core properties, such as dimension of the plug samples, porosity and permeability are shown in Tables 4.1 through 4.2.

3.3 EXPERIMENTAL PROCEDURES

A pressure-volume correction curve called blank or reference run is established for the apparatus before each sample run. To determine the mercury capillary pressure curve by Core lab equipment or Ruska pump, the blank test is needed to account the compression and expansion effects of mercury and the air present in the system.

3.3.1 The Pressure-Volume Correction

Once the required parts of the apparatus are cleaned, the equipment is ready for blank run. The blank run was carried out for each sample. The total system is evacuated by turning vacuum pump on until an absolute pressure of zero psi is read in the pressure gauge. Approximately 30 minutes are required for the evacuation process.

When the mercury level reaches the reference mark, which is located in an observation port, the auxiliary linear scale and the micrometer scale were set to zero. Linear scale is fixed at some number which will be used later to calculate the bulk volume of the sample. Pressure is released from nitrogen cylinder into the mercury pump. Gas is admitted to the system until the desired predetermined pressure of 1, 2, 3, 5, ----------etc. has reached. At each pressure, the displacement readings on the pump scale were recorded. At predetermined pressure 1 to 1800 psi, the above procedure was followed and the cumulative pump readings were recorded for each pressure increase. The results were arranged in tabular form in Appendix A.

3.3.2 Operation of Sample Test

(a) Injection Capillary Pressure Curve

The core sample is placed in the sample chamber after its porosity, permeability and dry weight are measured. The equipment is shown in Fig.

(3.1). The system pressure is reduced to zero psi absolute. While the system is vacuuming, the pump piston is advanced to raise the mercury level in the sample chamber up to the reference mark. Then the linear scale reading is recorded at the preadjusted mark.

By subtracting the known volume, whose index mark has been recorded in blank run, from linear scale reading would yield the bulk volume of the sample. The micrometer hand wheel and auxiliary linear scale are readjusted to zero; pressure is then applied to the system step by step. The pump is operated so as to displace mercury into the sample chamber and again raise the level to the reference mark. Mercury is injected as required until its level remains constant at the reference mark. One has to wait until mercury level no longer recedes or mercury no longer penetrates the pore spaces at each pressure increase. Therefore, pump readings need to be taken and recorded at predetermined pressure. The pressure and volume data from the above measurements are shown in tabular form in Appendix A. The apparent volumes of mercury entering the samples are obtained by subtracting the volumes indicated by the blank run.

(b) Ejection or Withdrawal Capillary Pressure Curve

After the injection process is completed at maximum pressure, mercury is ejected from the sample by reducing the pressure from the sample chamber. Once the pressure is released, the mercury level somewhat over-comes the

reference line of the observation port. The pump piston is withdrawn so as to maintain the mercury level at the reference mark. If mercury level overrides the reference line, unnecessary problems arise and it can delay the process, because mercury enters into the valve assembly and blocks the valve seat and port. Hence, it is necessary to be aware of the mercury level should not exceed the lucite window, which will involve cleaning problem and extra work.

The mercury level is accurately positioned at the reference mark for each pressure decrease, then scale reading is recorded which indicates the amount of mercury that comes out from the pore spaces. Repeat the same procedures until the pressure is equal to zero psi absolute. On reaching atmospheric pressure, reduction at each pressure decrease is effected by cracking vacuum valve using vacuum pump. For each pressure decrease in the system, the resultant volume reading and corresponding pressure are noted. The measurement data are shown in Appendix A.

After the withdrawal stages are accomplished, re-injection process is continued. The mercury injection is continued until the maximum pressure is reached. The re-injection experiment was conducted without taking the sample out from the sample chamber. The pressure and volume are recorded at each pressure increase. The intrusion pressure value and the unsaturated pore volume obtained at maximum observed pressure from injection process should be the same as the value from re-injection process.

CHAPTER 4

CHAPTER 4

RESULTS AND DISCUSSIONS

Mercury injection experiments using Berea sandstone, Bentheimer sandstone, and carbonate core samples were conducted to study the influence of sample sizes, epoxy coating, and equilibrium on the capillary pressure-saturation relationship. Three samples of different lengths were tested with a slow injection rate while the other three samples were tested with a rapid injection rate to determine the equilibrium effect on sample sizes. The three samples with different lengths were tested without coating on the sample surface while the other three sample surfaces were coated with thin layer of epoxy to investigate the surface effect on sample sizes. Before the actual test was carried out for all the samples, mercury injection experiment was performed with Berea sandstone of three different sizes to check the accuracy of the apparatus. Based on the results of the above experiments (J-function), Leverett's correlation function was used to correlate the experimental data.

Besides studying those factors which affect the mercury capillary pressure curve in the actual injection runs, the permeability calculation for all the types of samples was investigated. A summary of the core properties which were used in this study are given in Tables 4.1 and 4.2. The raw experimental data of the two sample runs are given in Appendix A.

Table (4.1) physical properties of the Barea & Bentheimer samples

Sample #	Dia (cm)	Length (cm)	Buck Vol. (cc)	Pore Vol (cc)	Porosity (%)	Permeability (md)	Dry Wt. (gm)	Grain Dens. (gm/cc)
S1	2.43	2.24	10.34	2.26	21.856	680	21.031	2.6028
S6	2.41	2.02	9.14	1.93	21.115	671	18.783	2.6051
S7	2.41	4.15	18.687	4.097	21.924	773	38.036	2.6069
S10C	2.42	4.12	18.95	4.09	21.58	610	38.658	2.6000
S12	2.43	4.13	19.05	4.07	21.364	834	39.063	2.6076
S13C	2.43	6.38	29.59	6.9885	23.62	864	59.867	2.6500
S14C	2.43	6.33	29.36	6.3866	21.76	817	60.509	2.6300
S16	2.41	6.35	28.965	6.365	21.974	925	58.837	2.6034
S18	2.4	6.28	28.396	5.996	21.115	856	58.232	2.5996
S20C	2.4	1.85	8.37	1.6542	19.77	529	17.582	2.6200
S21C	2.4	1.885	8.53	1.8175	21.31	507.3	17.418	2.6000
S22C	2.43	4.19	19.43	3.9619	20.39	605.2	39.500	2.5500
B1	2.5	1.875	8.86	1.85	20.88	905.5	18.111	2.58
B2	2.5	1.89	9.10	2.06	22.64	908	18.291	2.60
B3	2.5	4.18	20.17	4.49	22.26	1352	40.392	2.58
B4	2.5	3.89	19.00	4.35	22.89	1232	38.051	2.6
B5C	2.5	3.855	18.92	3.993	21.10	1403	38.385	2.56
B6C	2.5	4.0	19.63	4.4349	22.59	1077	39.033	2.57
B7C	2.5	5.87	28.81	7.2142	25.04	1632	56.985	2.64
B8	2.5	5.875	28.71	6.73	23.44	1591	57.048	2.60
B10C	2.5	2.01	9.87	2.3565	23.88	917	19.294	2.57
B12C	2.5	2.01	9.87	2.1865	22.16	871	19.784	2.58
B13C	2.5	5.81	28.52	6.6197	23.21	1646	57.042	2.6
B14	2.5	5.86	28.67	6.67	23.26	1623	57.392	2.61

Table (4.2) physical properties of the carbonate samples

Sample #	Lithology	Dia (cm)	Length (cm)	Buck Vol. (cc)	Pore Vol (cc)	Porosity (%)	Permeability (md)	Dry Wt. (gm)	Grain Dens. (gm/cc)
32	Bicl Incl Grst	2.5	3.78	18.21	4.64	25.48	839.41	36.45	2.69
34	Bicl Incl Grst	2.48	3.81	17.8	4.56	25.61	874.54	36.02	2.72
36	Bicl Incl Grst	2.48	3.82	17.87	4.62	25.85	699.25	35.88	2.71
38	Bicl Incl Grst	2.52	3.27	15.82	3.77	23.83	1267.2	32.8	2.72
54	Bicl Incl Grst	2.49	3.82	18.55	4.11	22.16	81.46	39.13	2.71
56	Bicl Incl Grst	2.49	3.83	18.38	3.98	21.65	118.7	38.79	2.69
58	Biocl wkst	2.5	4.39	21.4	4.05	18.93	20.43	47.59	2.74
74	Dol Mdst	2.52	5.11	25.38	1.88	7.41	0.325	64.43	2.74
82A	Sil Dol	2.53	1.93	9.64	0.49	5.08	0.425	25.02	2.73
82	Sil Dol	2.53	3.01	15.07	0.25	1.67	0.425	40.416	2.73
90A	Biocl Wkst	2.53	1.93	9.64	0.42	4.35	0.69	24.87	2.70
90	Biocl Wkst	2.525	2.99	14.97	1.97	13.17	0.69	35.51	2.73
96	Incl Bcl pk	2.515	5.105	25.3	3.3	13.04	5.3	60.058	2.73
101A	Calc Dol	2.52	3.01	15.01	1.06	7.08	2.71	37.61	2.70
101	Calc Dol	2.52	1.93	9.63	1.3	13.46	2.71	22.57	2.71
105	Vuggy	2.5	5.11	23.59	3.68	15.6	181.45	53.63	2.69

Essential features of the experimental results are presented and discussed in the following sections.

4.1 SAMPLE SIZE EFFECT

4.1.1 Effect of Sample Size on Sandstone Rocks

Mercury injection curves for sample sizes of about 2 cm, 4 cm, and 6 cm in diameter, as shown in Figs. (4.1) through (4.8) were generated for equilibrium studies as well as epoxy coating studies on the sample sizes. For equilibrium, the tests were performed in two ways such as a rapid injection rate which means the volume reading is taken immediately after adjusting the mercury level at reference mark, and a slow injection rate which means the volume reading is recorded after the mercury level is maintained at the reference mark for about 10 minutes.

The relationships between capillary pressure and mercury saturation studied from the slow and rapid injection rates of varying lengths for Berea sandstone are presented in Figs. (4.1) and (4.2) respectively. Similar results, obtained from the slow and rapid injection rates for coated samples with similar varying lengths are shown in Figs. (4.3) and (4.4) respectively. For Berea samples which have permeability ranging from 500 to 900 md, shown in Figs.(4.1) through (4.3), the injection curve shape is essentially independent of

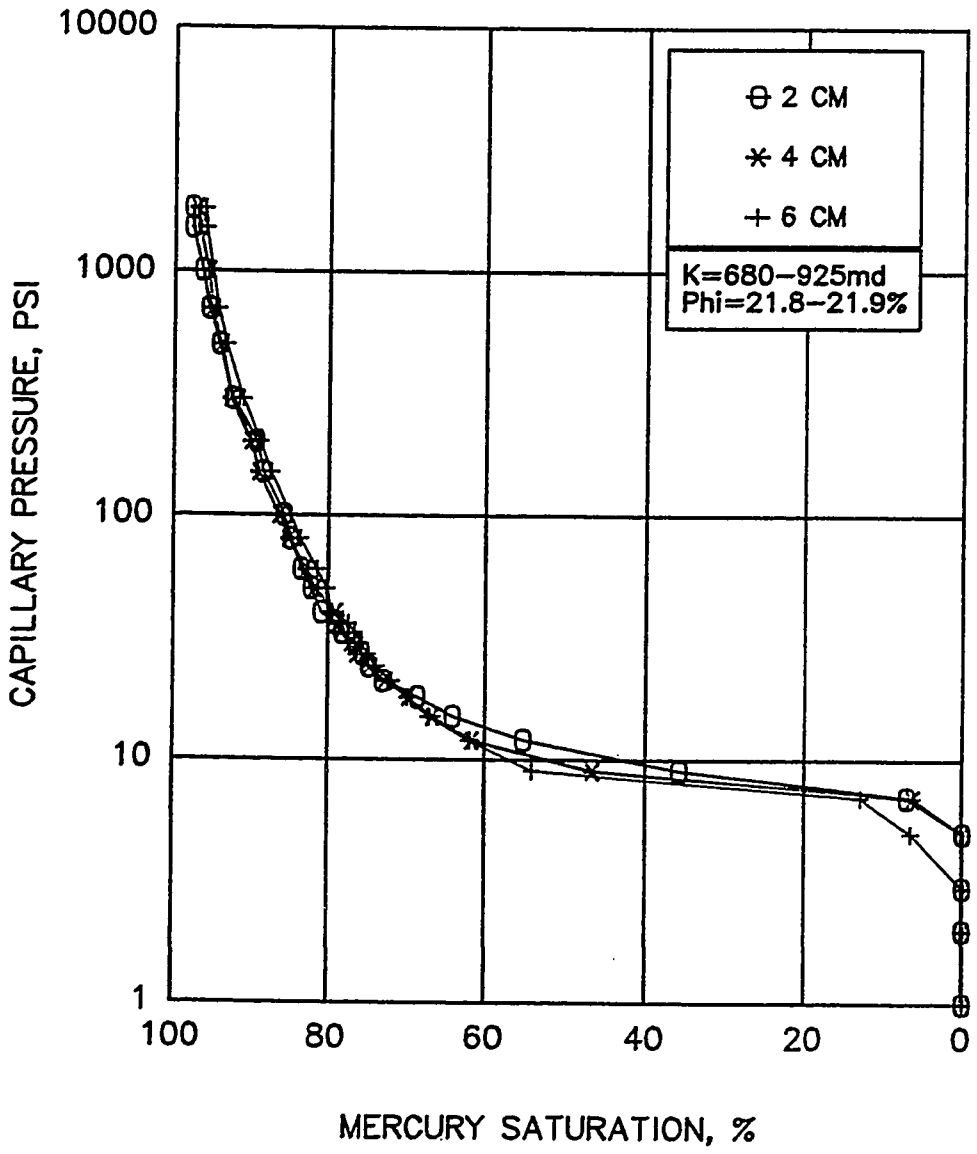

Fig(4.1). Comparison of Injection Capillary Pressure Curves for Different Size of Berea Uncoated Samples with Slow Rate of Injection.

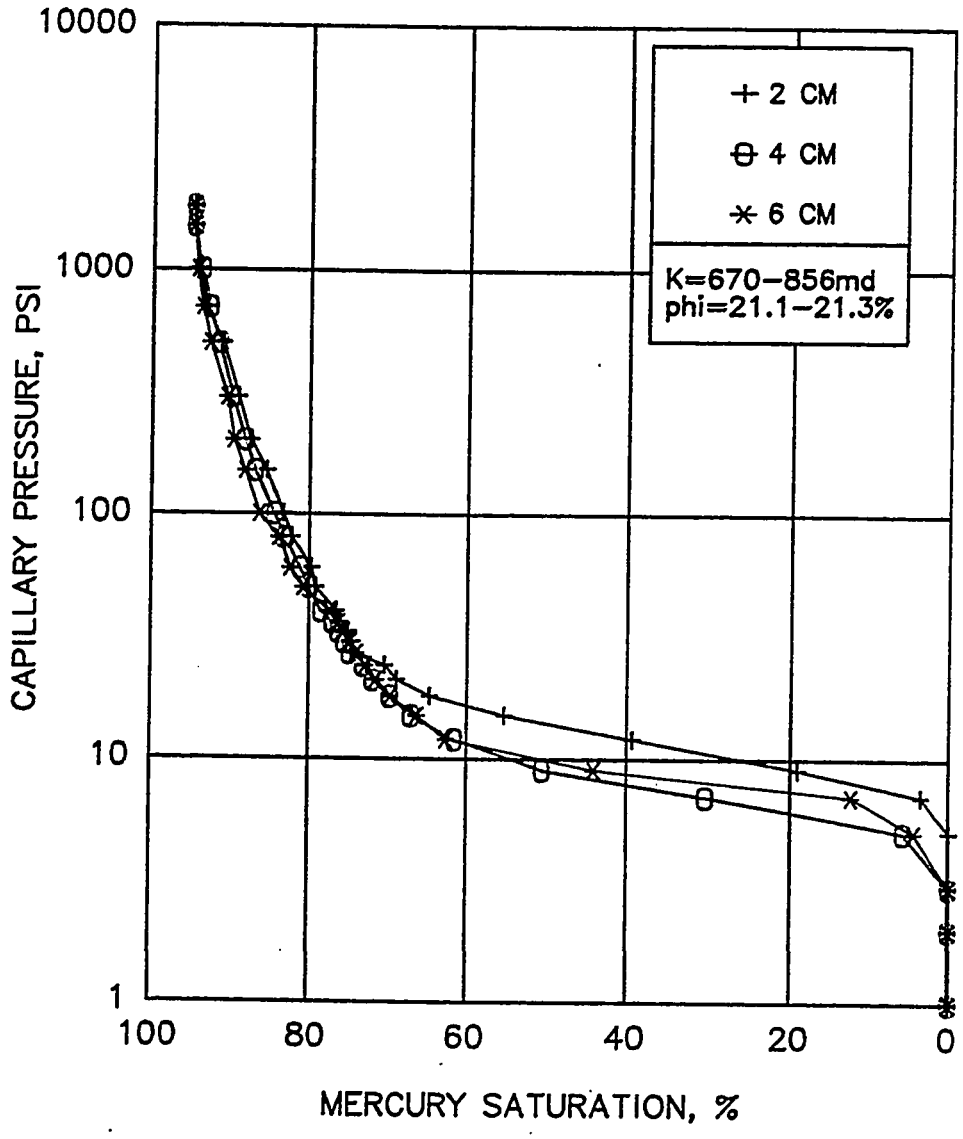

Fig(4.2). Comparison of Injection Capillary Pressure Curves for Different Size of Berea Uncoated Samples with Rapid Rate of Injection.

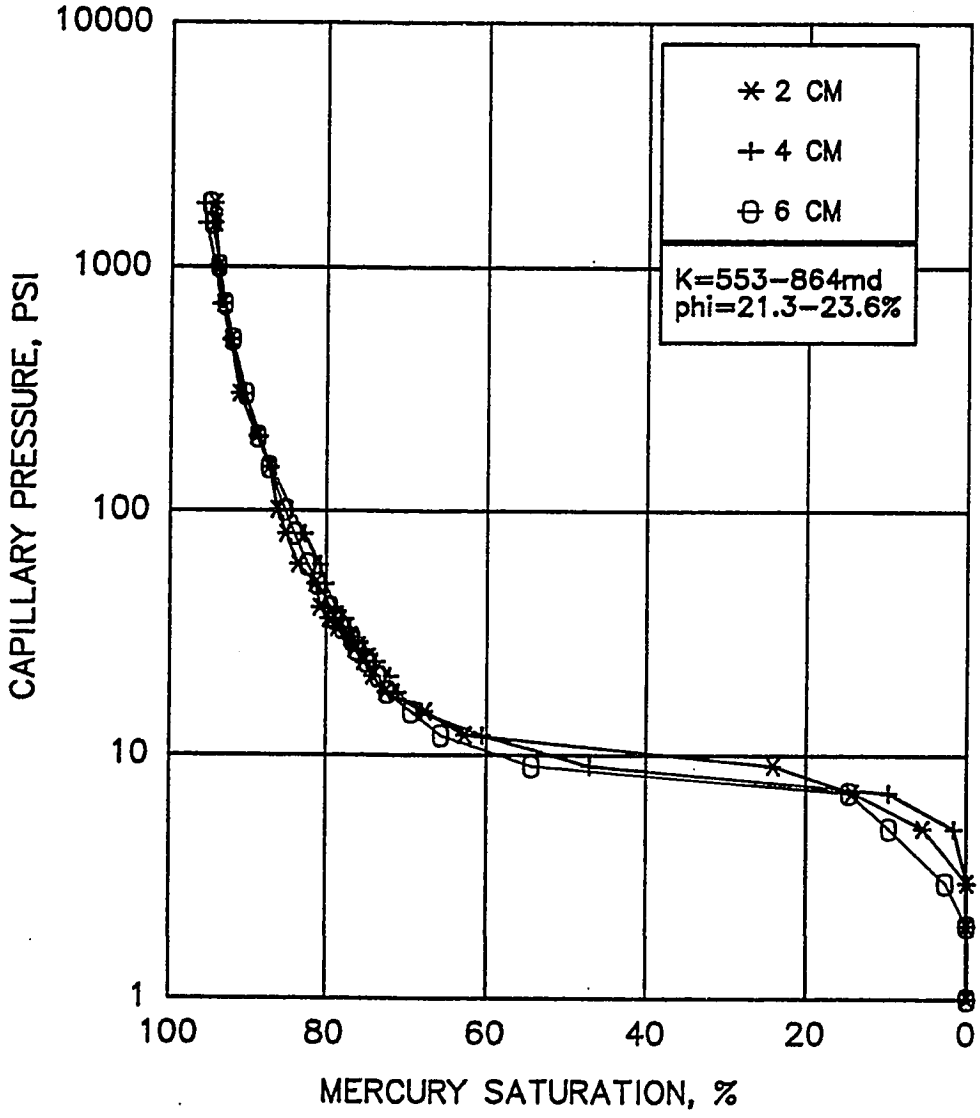

Fig(4.3). Comparison of Injection Capillary Pressure Curves for Different Size of Berea Coated Samples with Slow Rate of Injection.

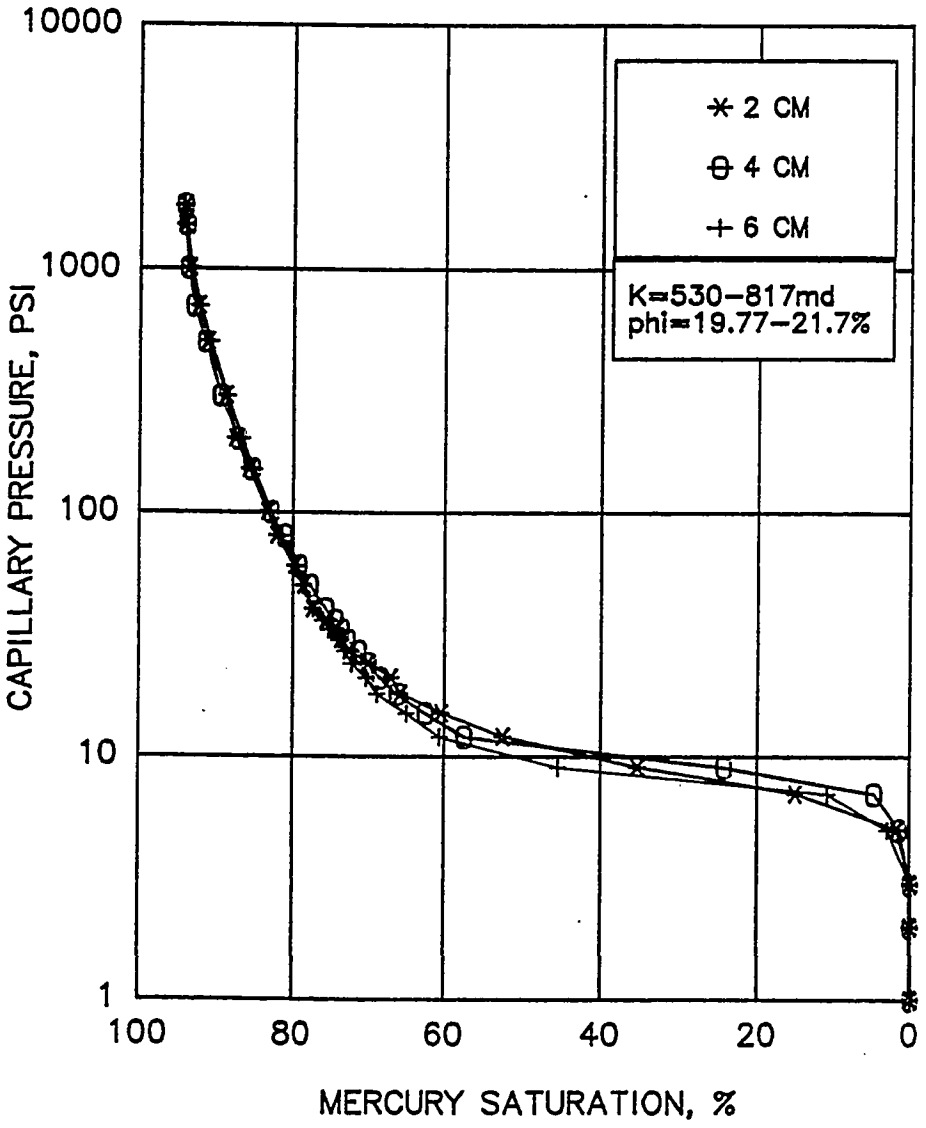

Fig(4.4). Comparison of Injection Capillary Pressure Curves for Different Size of Berea Coated Samples with Rapid Rate of Injection.

sample size. All the data for the coated and uncoated samples fell within the same region. Above 50 % mercury saturation, there was no significant effect of sample size; all the data fell within the same region. Except for the uncoated samples which are run rapidly, the injection curve shape which changed with sample size, is believed to be due to an experimental error.

The Bentheimer sandstone which is a type of Berea, was tested to investigate the effect of the sample size. The Volume of mercury occupied in the pores is converted to mercury saturation (i.e., percentage of pore volume occupied) and it is plotted against capillary pressure as shown in Figs. (4.5) through (4.8).

Bentheimer samples of 2 cm, 4 cm, and 6 cm in length, the permeability ranged from 900 to 1650 md and the porosity remained almost the same which is about 23 %, were tested with a slow rate to study the equilibrium effect as shown in Fig. (4.5). It was found that the displacement pressures were relatively insensitive to the sample size. However, the surface effects were indicated in the low pressure regions of the saturation where the positive curvature encountered at which the mercury started to enter the sample.

The samples with higher surface area of 6 cm, exhibit low entry pressure. Similar results obtained for coated samples are shown in Fig. (4.7). The samples were prepared in such a way that the whole surface of the sample was coated with thin layer of epoxy resin except one side of the sample. The three

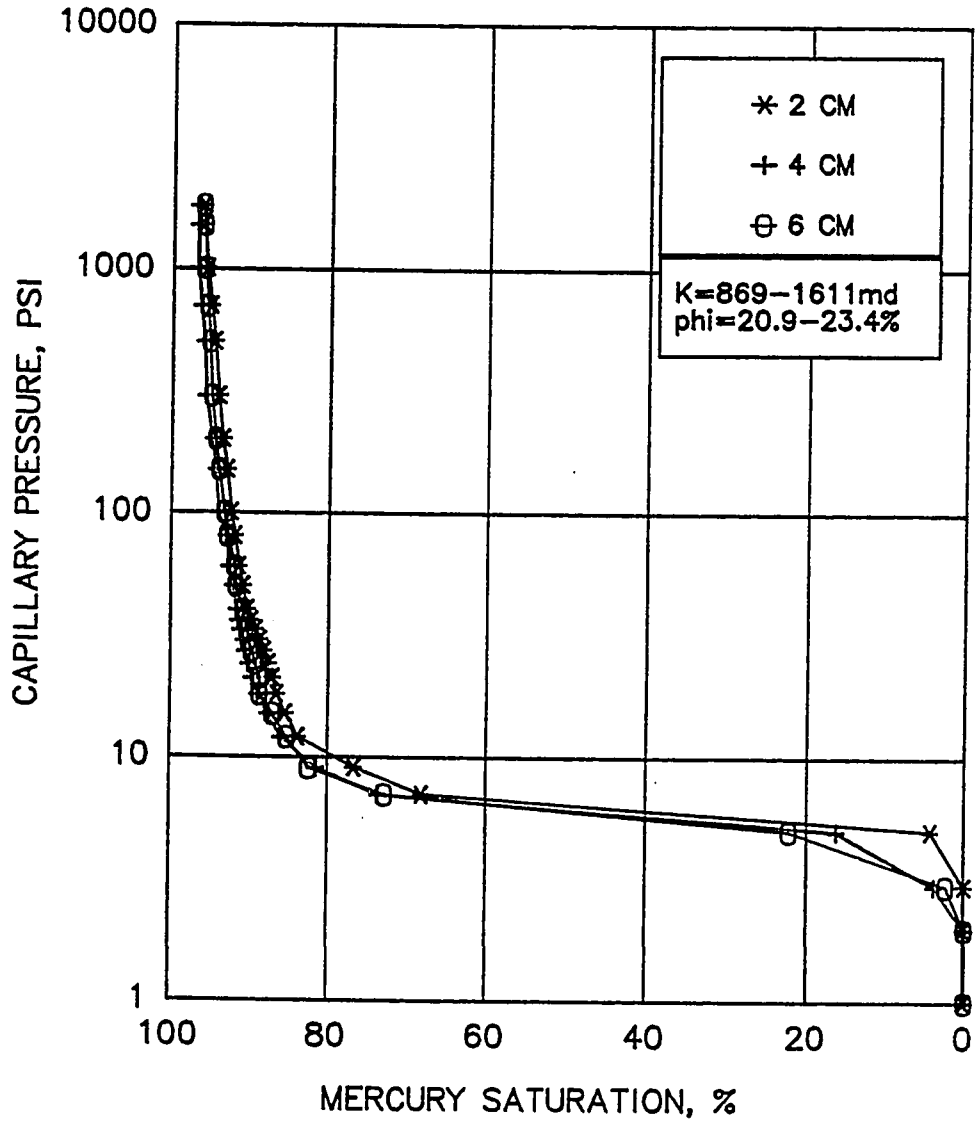

Fig(4.5). Comparison of Injection Capillary Pressure Curves for Different Size of Bentheimer Uncoated Samples With Slow Rate of Injection.

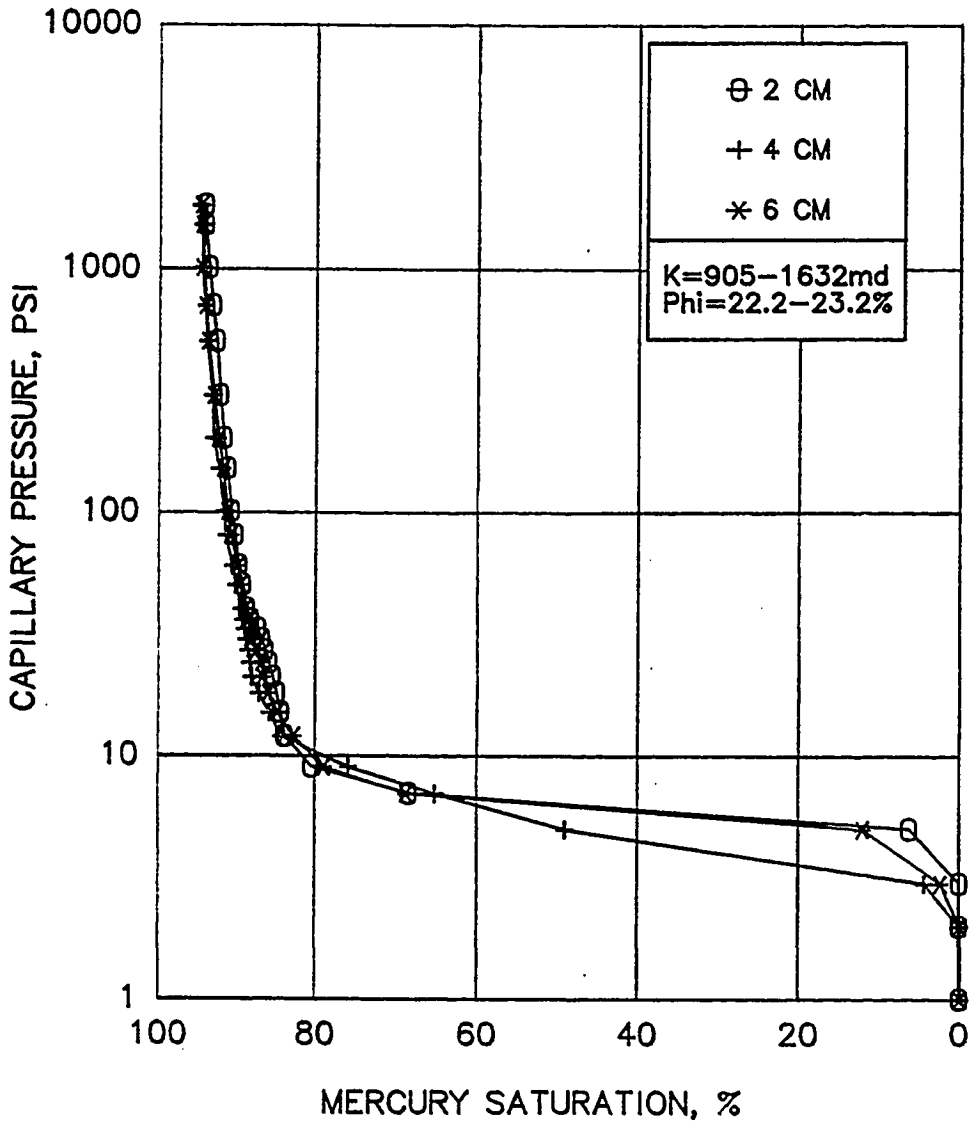

Fig(4.6). Comparison of Injection Capillary Pressure Curves for Different Size of Bentheimer Uncoated Samples with Rapid Rate of Injection.

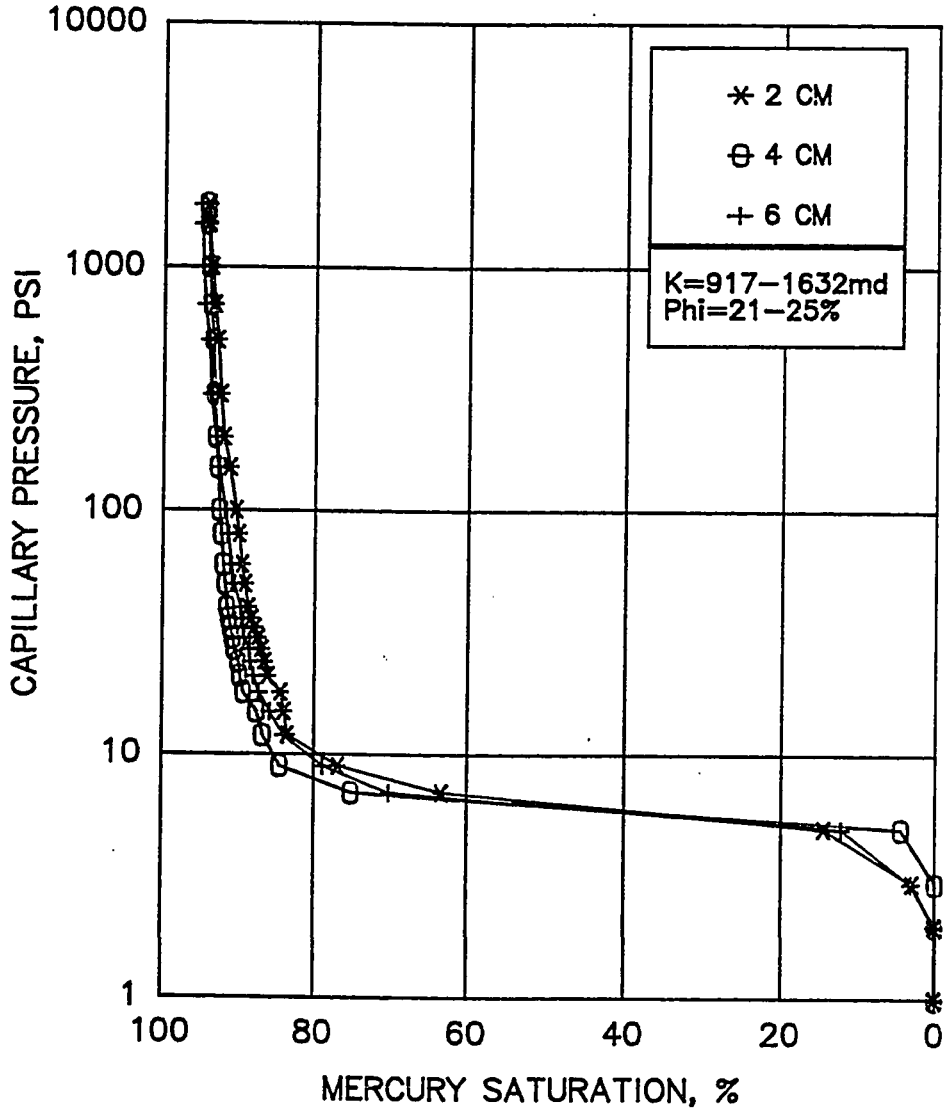

Fig(4.7). Comparison of Injection Capillary Pressure Curves for Different Size of Bentheimer Coated Samples with Slow Rate of Injection.

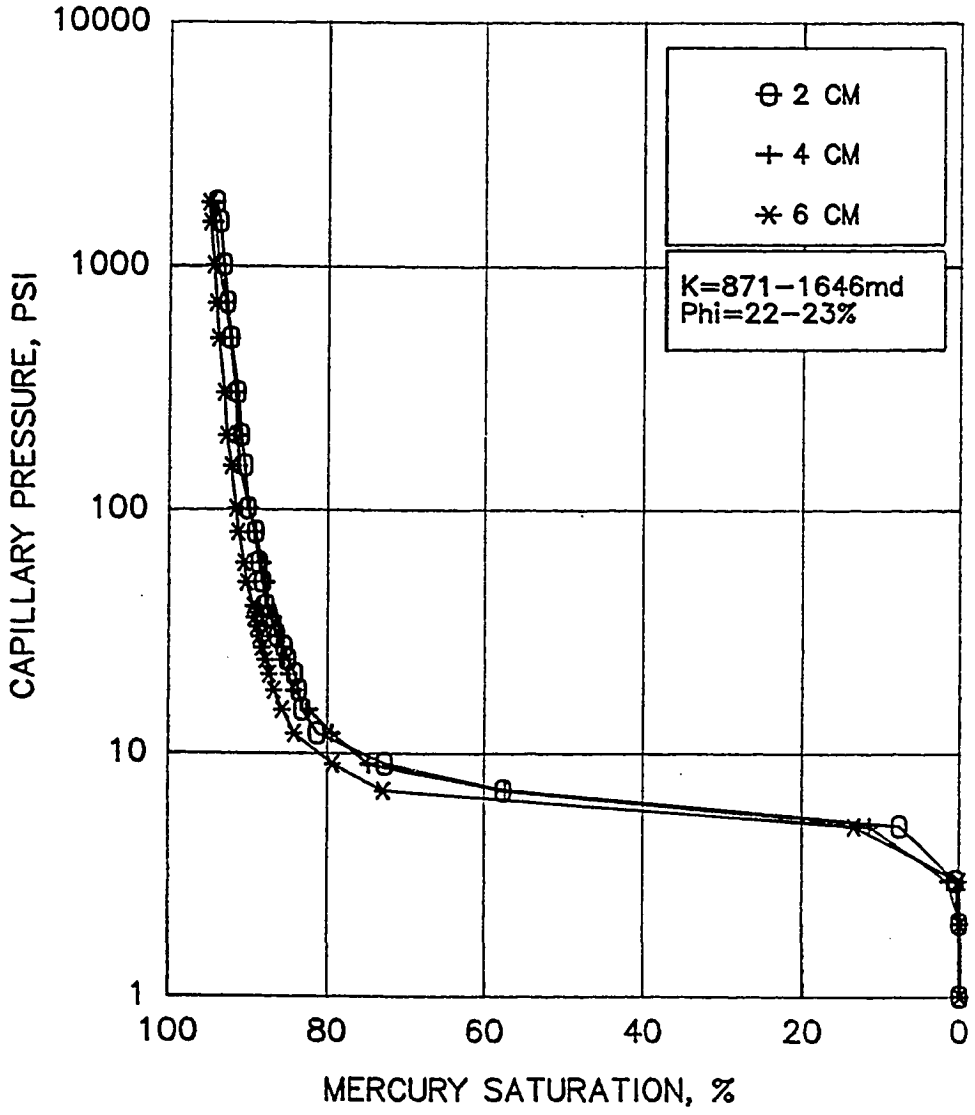

Fig(4.8). Comparison of Injection Capillary Pressure Curves for Different Size of Bentheimer Coated Samples with Rapid Rate of Injection.

different sizes of the samples studied are those which correspond to the ones studied in Fig. (4.5). The mercury injection tests were performed with the slow rate.

Figures. (4.6) and (4.8) show the results of the coated and uncoated Bentheimer samples in which injection tests were performed rapidly. No differences were observed between the coated and uncoated samples of different sizes except for the one which is shown in Fig. (4.6) wherein the displacement pressure was observed to be low as compared with that of the other two samples which may be due to an experimental error. As given in the literature, the displacement pressure, for the rapid injection case should be higher because of insufficient time which was allowed to reach the equilibrium.

Figures. (4.1) through (4.8) illustrate that the irreducible saturation (unsaturated pore volume) observed is likely to be the same for different sizes of samples and the displacement pressure measured from the injection curve is also seen to be the same for different sample sizes. It can be concluded from this study that the injection capillary pressure curves are insensitive to the sample sizes regardless of the coating or equilibrium time.

The effect of sample size on withdrawal capillary pressure curves is shown in Figs. (4.9) through (4.12) in which the same samples as those tested in the previous discussions, are used for the ejection process. The mercury was withdrawn rapidly allowing a few seconds between the pressure decreases. In

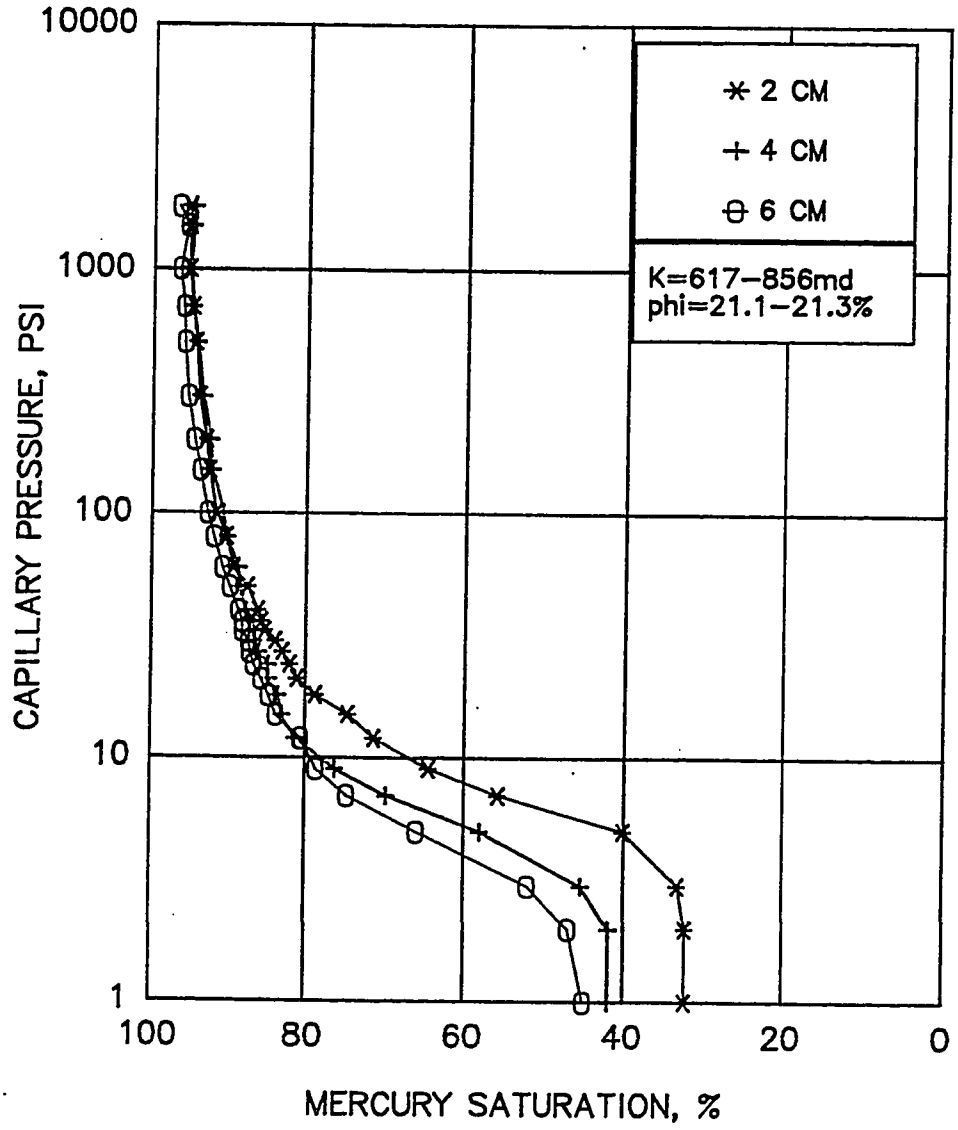

Fig(4.9). Comparison of Withdrawal Capillary Pressure Curves For Different Size of Berea Uncoated Samples with Rapid Rate of Ejection.

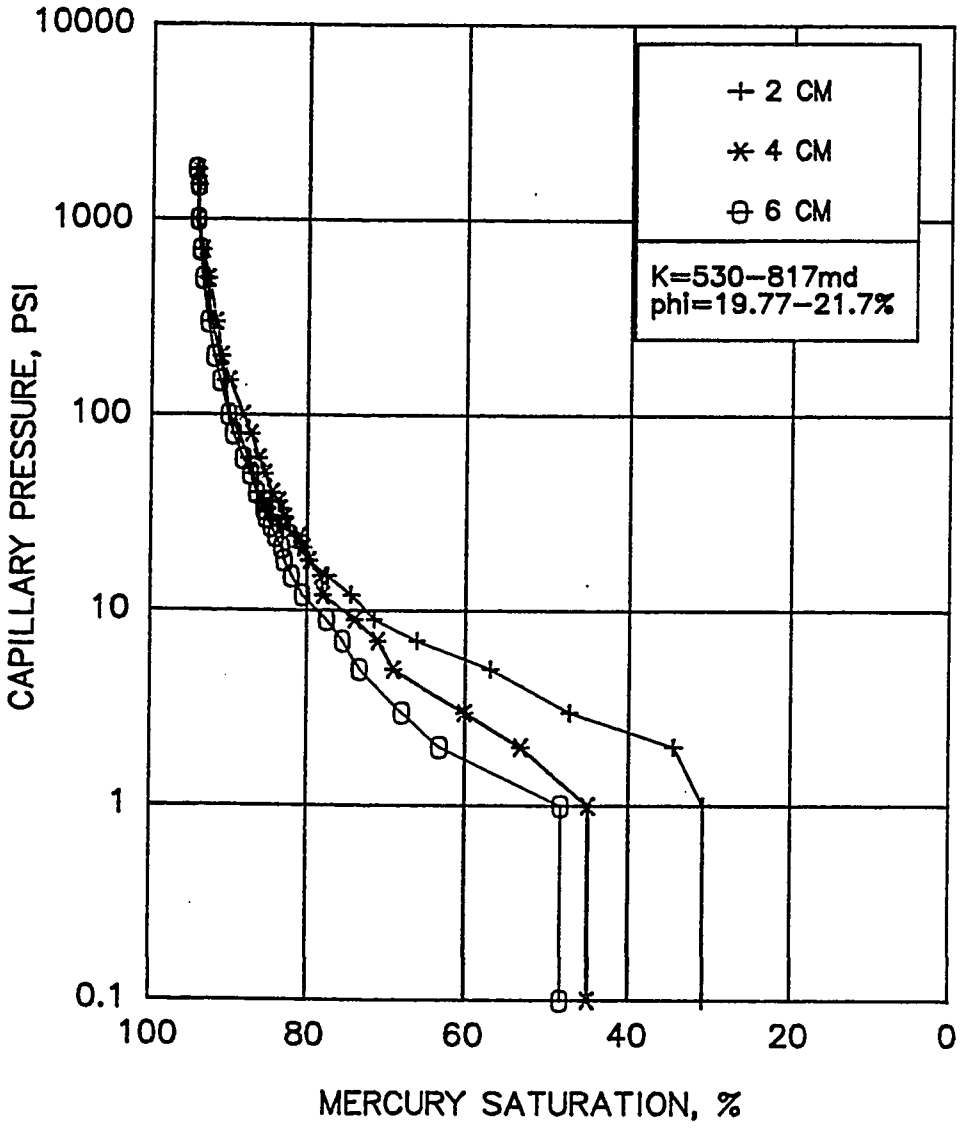

Fig(4.10). Comparison of Withdrawal Capillary Pressure Curves For Differet Size of Berea Coated Samples with Rapid Rate of Ejection.

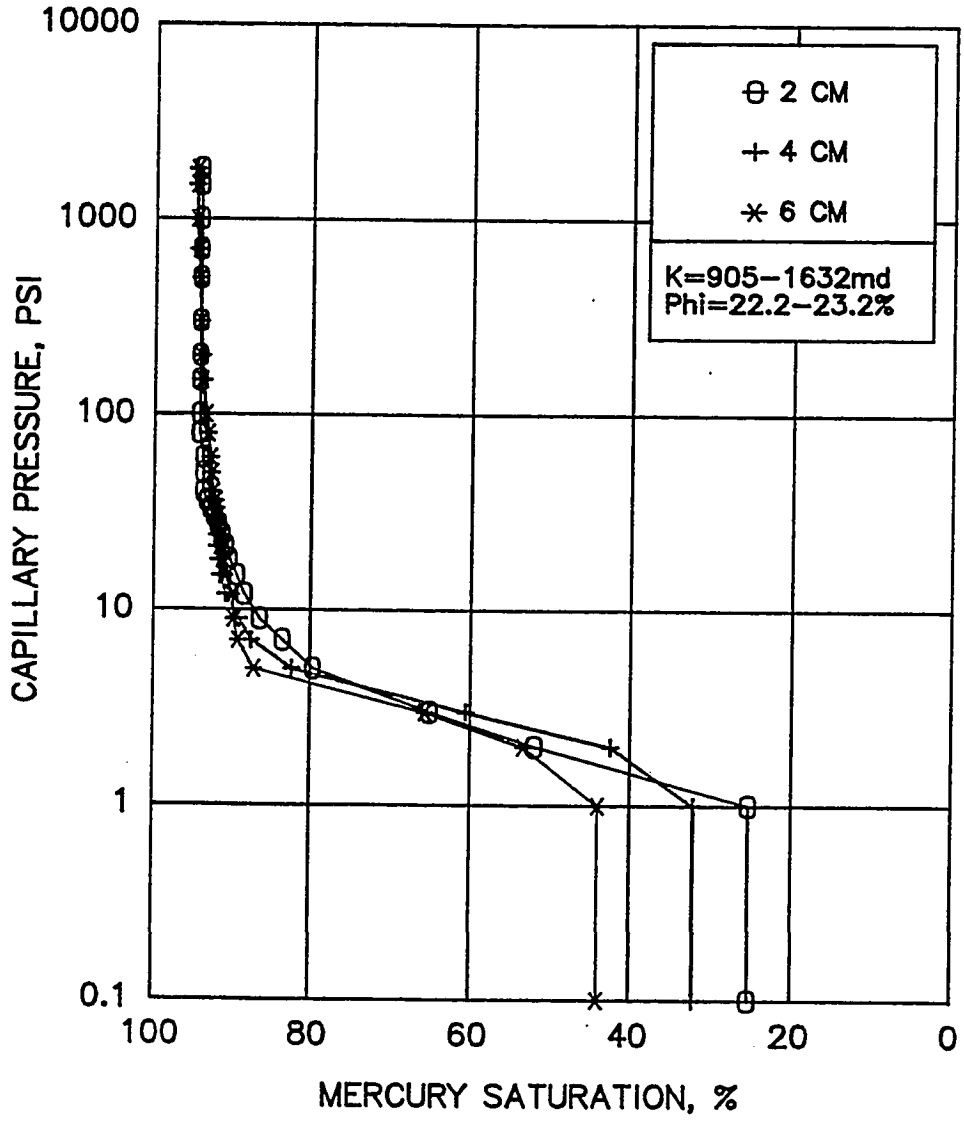

Fig(4.11). Comparison of Withdrawal Capillary Pressure Curves For Different Size of Bentheimer Uncoated Samples with Rapid Rate of Ejection.

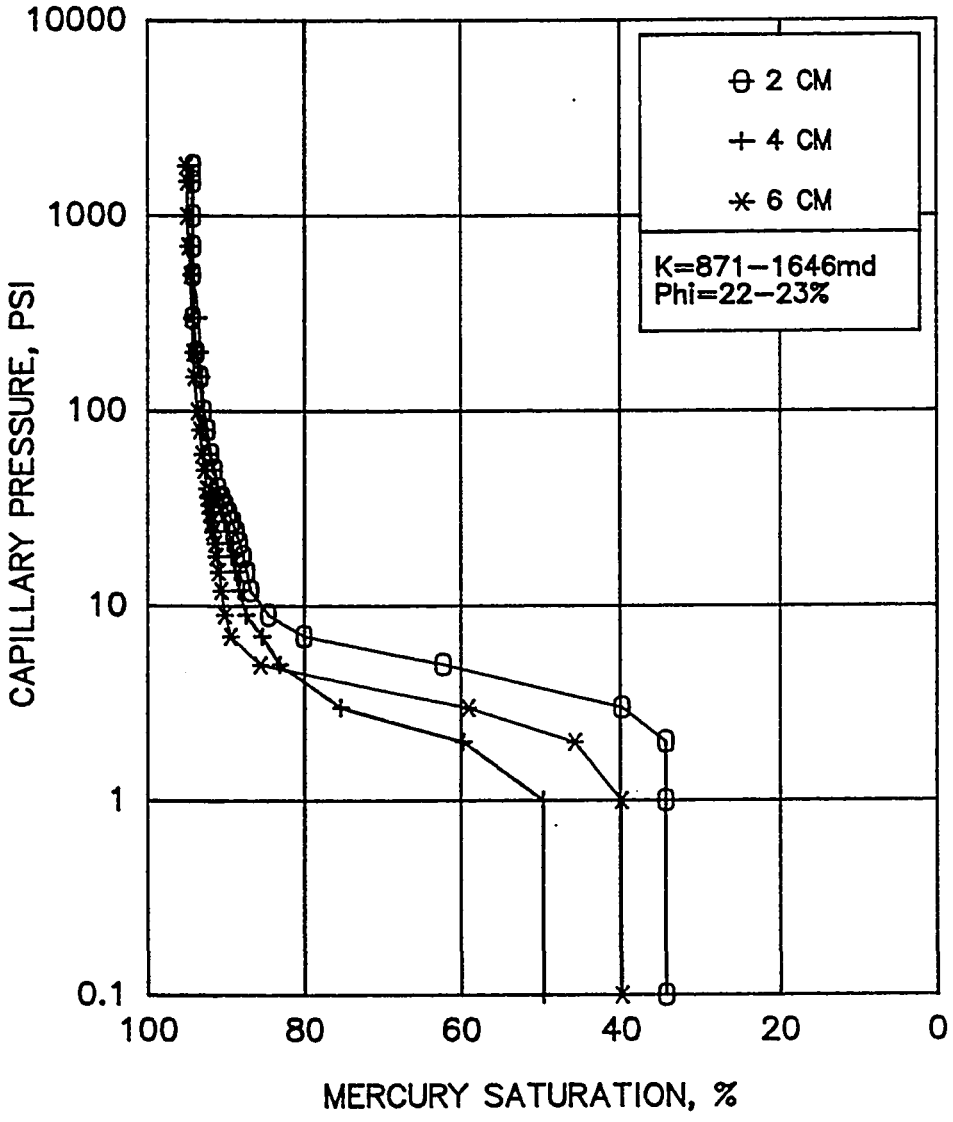

Fig(4.12). Comparison of Withdrawal Capillary Pressure Curves For Different Size of Bentheimer Coated Samples with Rapid Rate of Ejection.

such cases, the effect of the sample size was observed to be sensitive to the capillary pressure curve. The data in Figs. (4.9) and (4.10) show that the residual mercury saturation increases as sample size increases. Similar results were obtained for coated and uncoated samples in the case of rapid withdrawal rate as shown in Figs. (4.11) and (4.12). It is apparent from these figures that the amount of trapped mercury increases as the sample size increases. In fact, enough time is required to extract the mercury from the pore space specially for larger core samples.

4.1.2 Effect of Sample Size on Carbonate Rocks

The mercury injection is controlled solely by the size of the throats. When the injection capillary pressure experiment starts, the nonwetting fluid completely surrounds the exterior of the rock sample. Normally, the nonwetting fluid does not enter the pore system except through the largest pore openings available on the surface of the rock. Therefore, it is noticed that the sample size influences the surface area to volume ratios which in turn affects the form of the capillary pressure curves.

Figure (4.13) displays the injection and withdrawal curves for the carbonate rock samples. Six carbonate rock samples with bulk volumes ranged from 15 to 19 cc were tested to analyze the effects of the sample size. The lithology of the sample is bioclast intraclast grainstone. The same lithological group of carbonate samples was chosen to minimize the effect of heterogeneity.

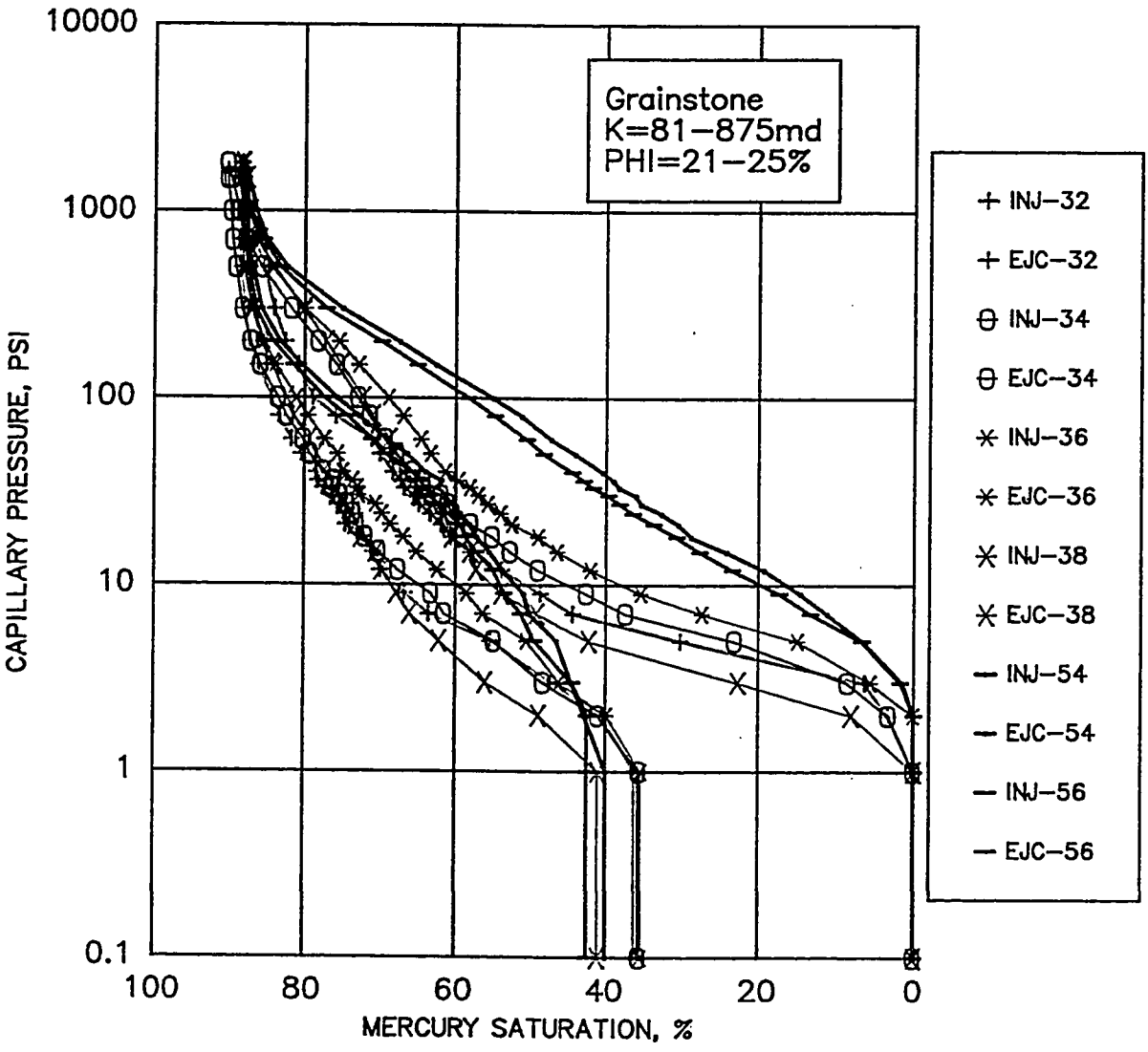

Fig(4.13). Comparison of Injection and Ejection Capillary Pressure Curves Obtained from Uncoated Carbonate Samples.

Wardlaw [8] studied the sample size effect of the Indiana limestone. He concluded that the sample size did not significantly affect the shape of the curves. It can be seen from Fig. (4.13) that the sample size affects the shape of the capillary pressure curves. But one thing I share with Wardlaw's suggestion is that slight variations were observed in the minimum unsaturated pore volume, which is believed to be inaccuracies of pore volume measurements. It is apparent that the displacement pressure varied from one sample to another according to their pore throat diameters. It can thus be concluded that for larger pore throat samples, the injection curve has moved to lower pressure ranges.

The study of the sample size effect on the withdrawal curves in the same figure revealed that the residual saturation decreases as the pore throat of the sample diameter increases. It can be explained as follows. If P_c is reduced, the nonwetting fluid will withdraw from the pore system until P_c becomes smaller than the pressure necessary to support a continuous nonwetting fluid phase at the smallest pore bottle neck (constriction). At this point, the continuous nonwetting fluid finger is broken, and some nonwetting fluid is trapped in the pore system behind this constriction.

Comparison between injection curves for different size of samples with epoxy coating are shown in Fig. (4.14). In this experiment, 5 cm length carbonate samples were cut into two pieces of 2 cm and 3 cm in length. Both

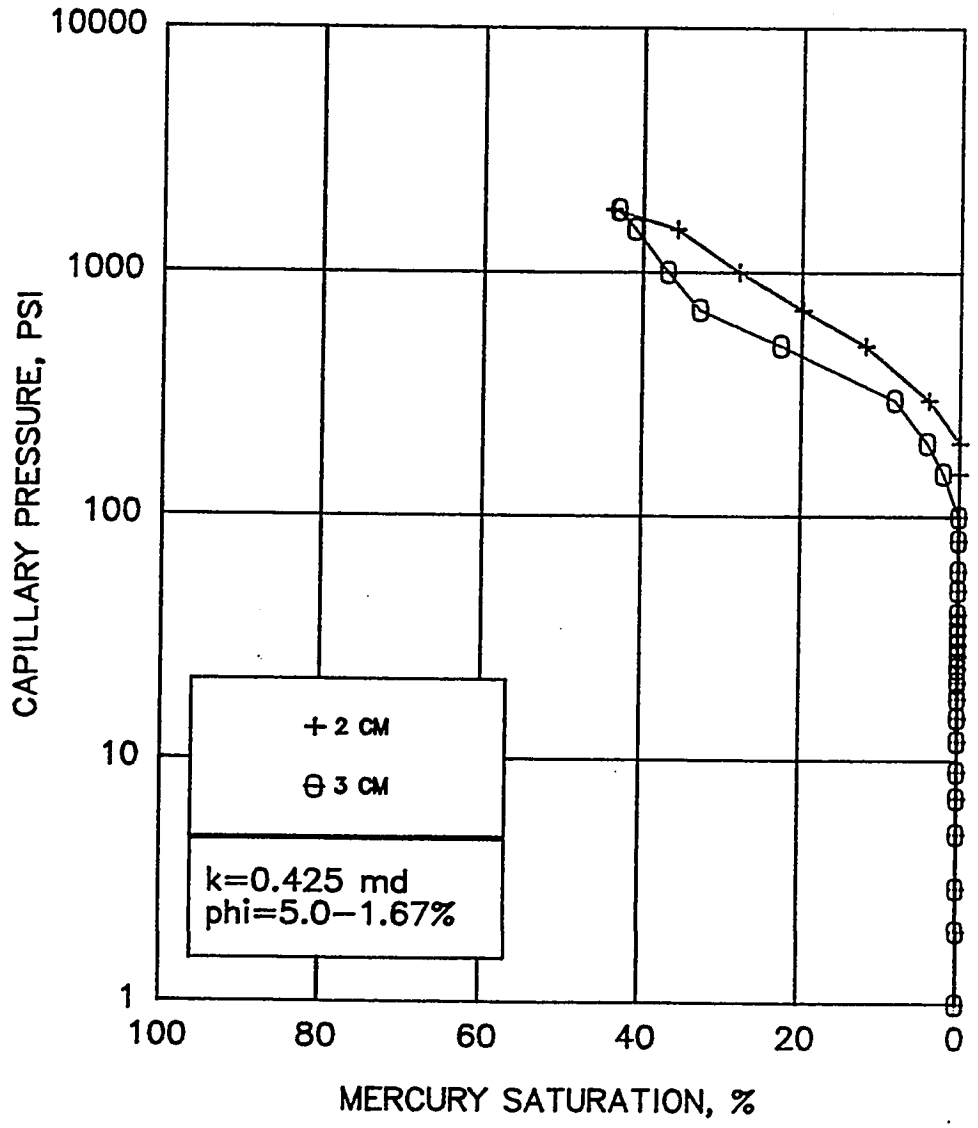

Fig(4.14). Comparison of Injection capillary pressure curves Obtained from The Slow Rate for Diffrent Size Coated Carbonate Samples. The Lithology Is Sil Dol.

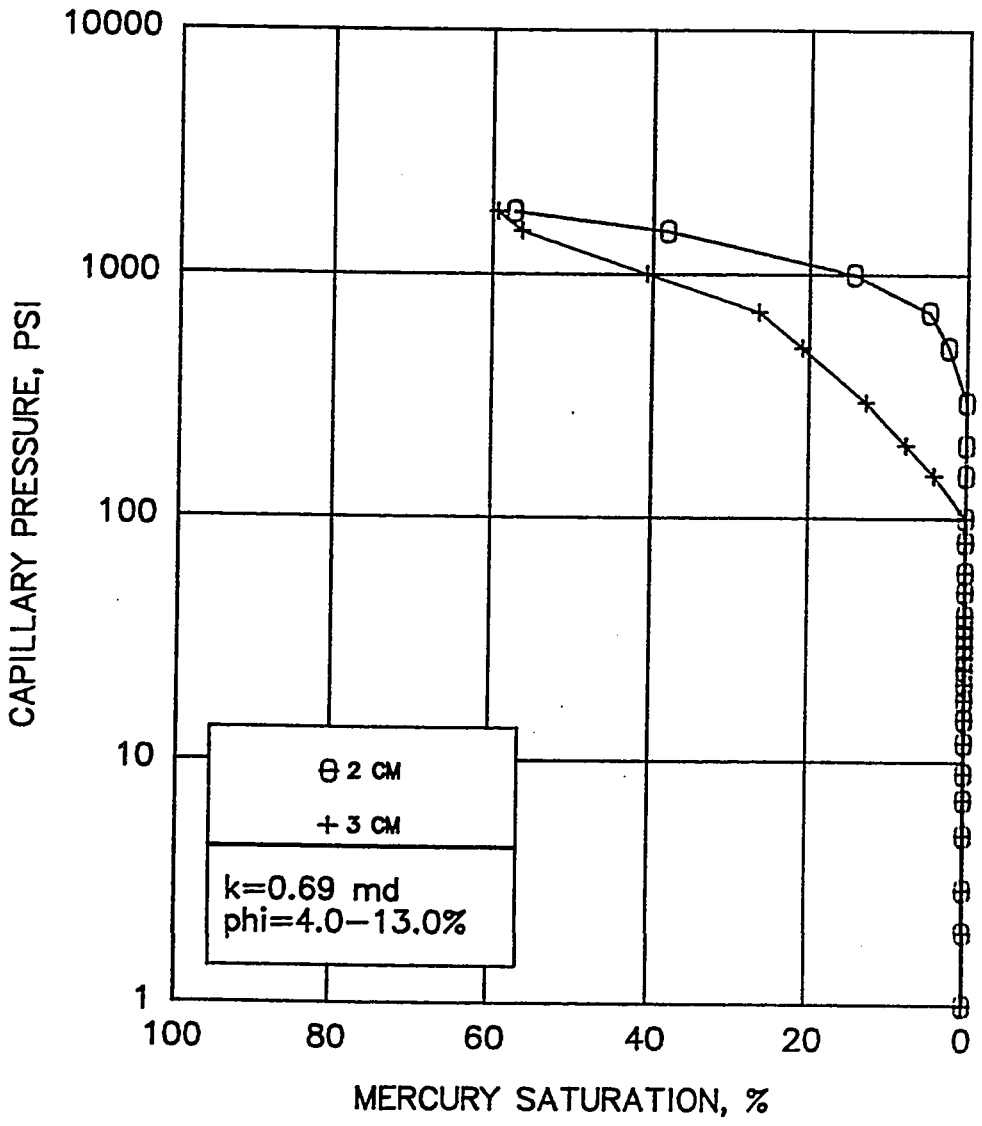

Fig(4.15). Comparison of Injection Capillary Pressure Curves Obtained from The Slow Rate for Different Size Coated Carbonate Samples. The Lithology is Boicl Wkst.

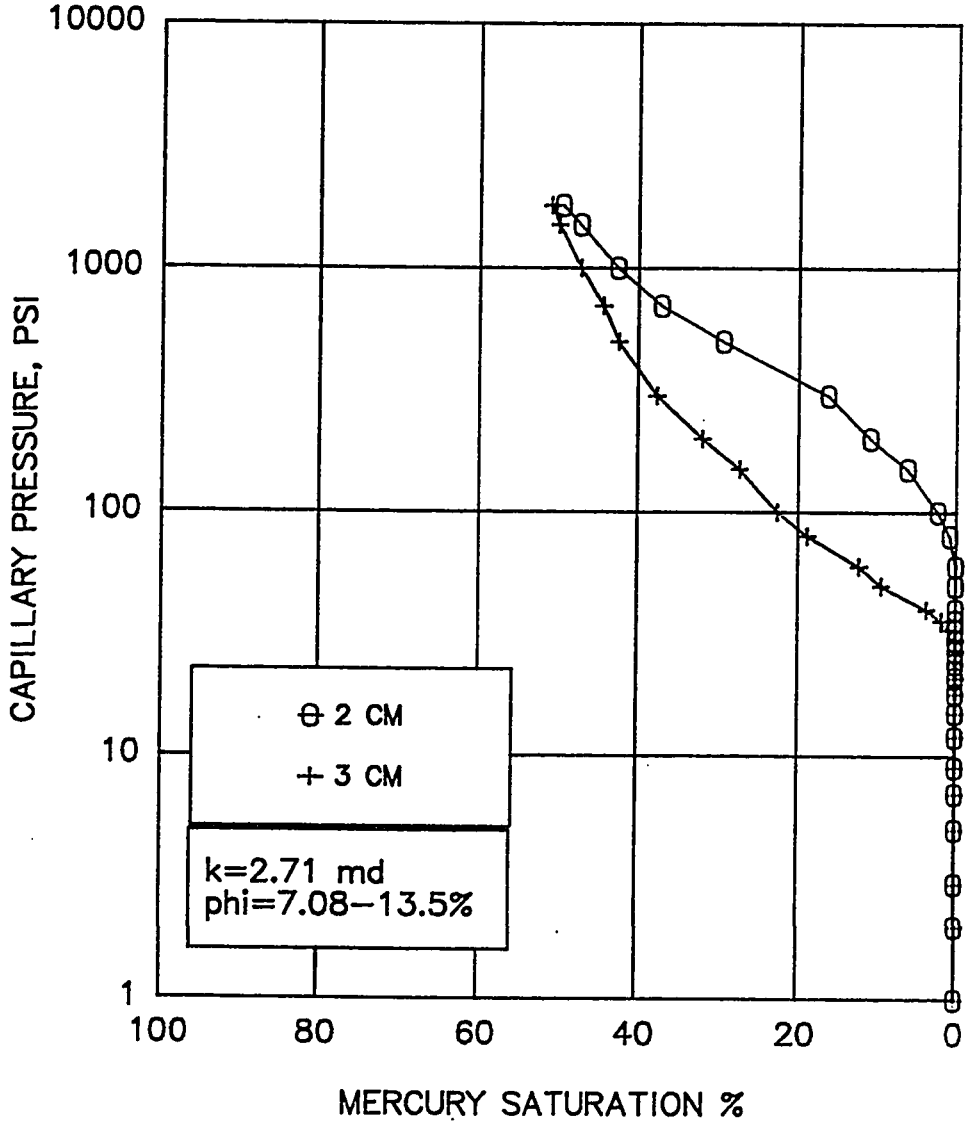

Fig(4.16). Comparison of Injection Capillary Pressure Curves Obtained from The Slow Rate for Different Size Coated Carbonate Samples. The Lithology is Calc Dol.

the samples were coated with thin layer of epoxy resin to minimize the surface effect. Results in this figure show that the injection capillary pressure curve moves to a lower pressure range as the sample size increases. The lower the mercury saturation at a given pressure, the smaller will be the observed displacement pressure in the curves of large size samples. Similar results were obtained when the sample size effect for epoxy coated sample of the other two types of carbonate rocks was studied. The injection capillary pressure curves for these samples are shown in Figs. (4.15) and (4.16).

4.2 EQUILIBRIUM EFFECT

4.2.1 Injection Capillary Pressure

Two methods were employed to study the effect of equilibrium on the samples of Bentheimer and Berea sandstone. The first method is a normal technique, i.e., rapid injection, where pressure is increased steadily without allowing enough time for mercury to enter in the pore space at predetermined pressure intervals. The second method involves equilibration of mercury volume at each pressure step, i.e., slow injection, before proceeding to the next level of pressure. The Bentheimer sandstone sample was cut into 2 pieces in each of 2 cm, 4cm, and 6 cm in length. Figs. (4.17), (4.18), and (4.19) compare the mercury injection results by the two methods for duplicate samples. From these plots, it is inferred that the samples examined by the

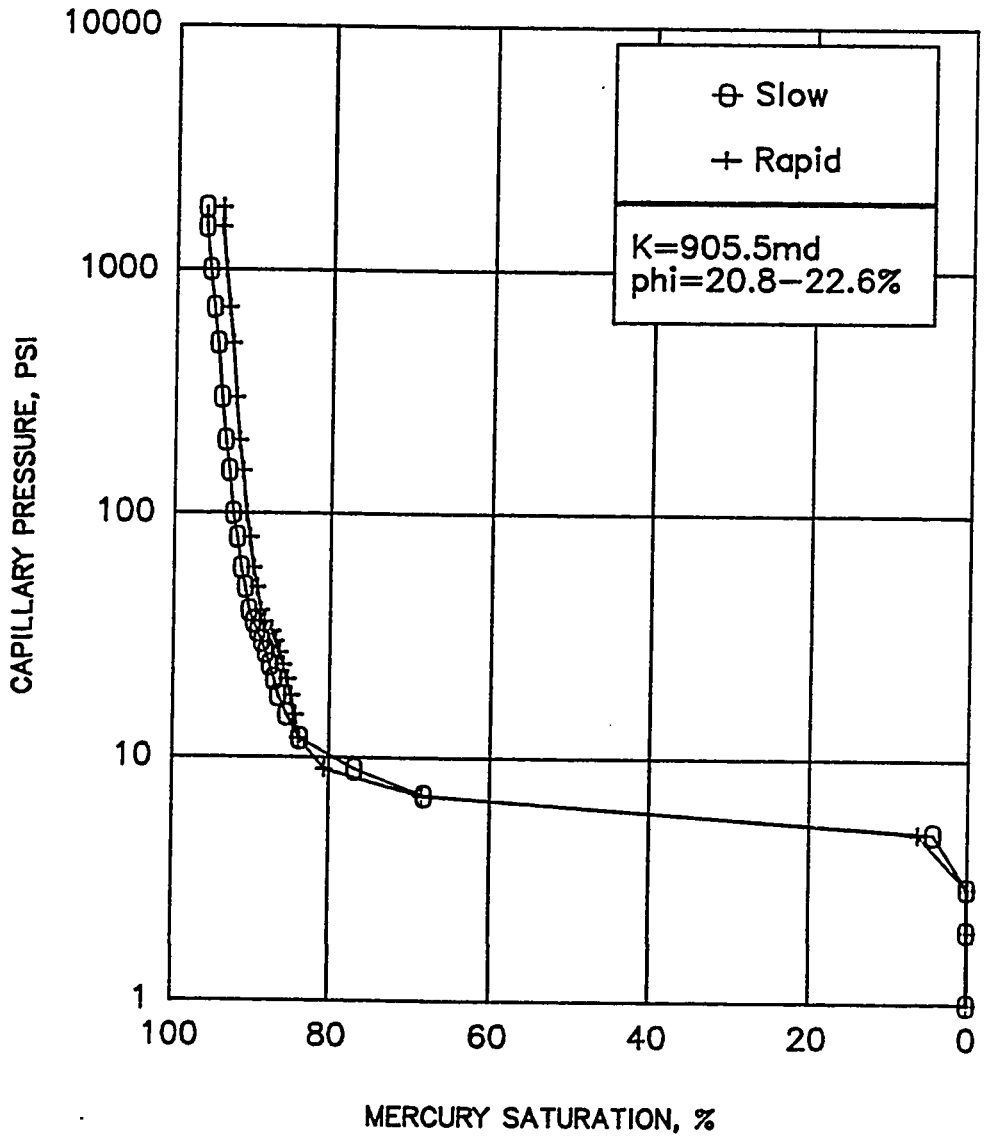

Fig(4.17). Comparison of Injection Capillary Pressure Curves for 2 cm Uncoated Bentheimer Samples.

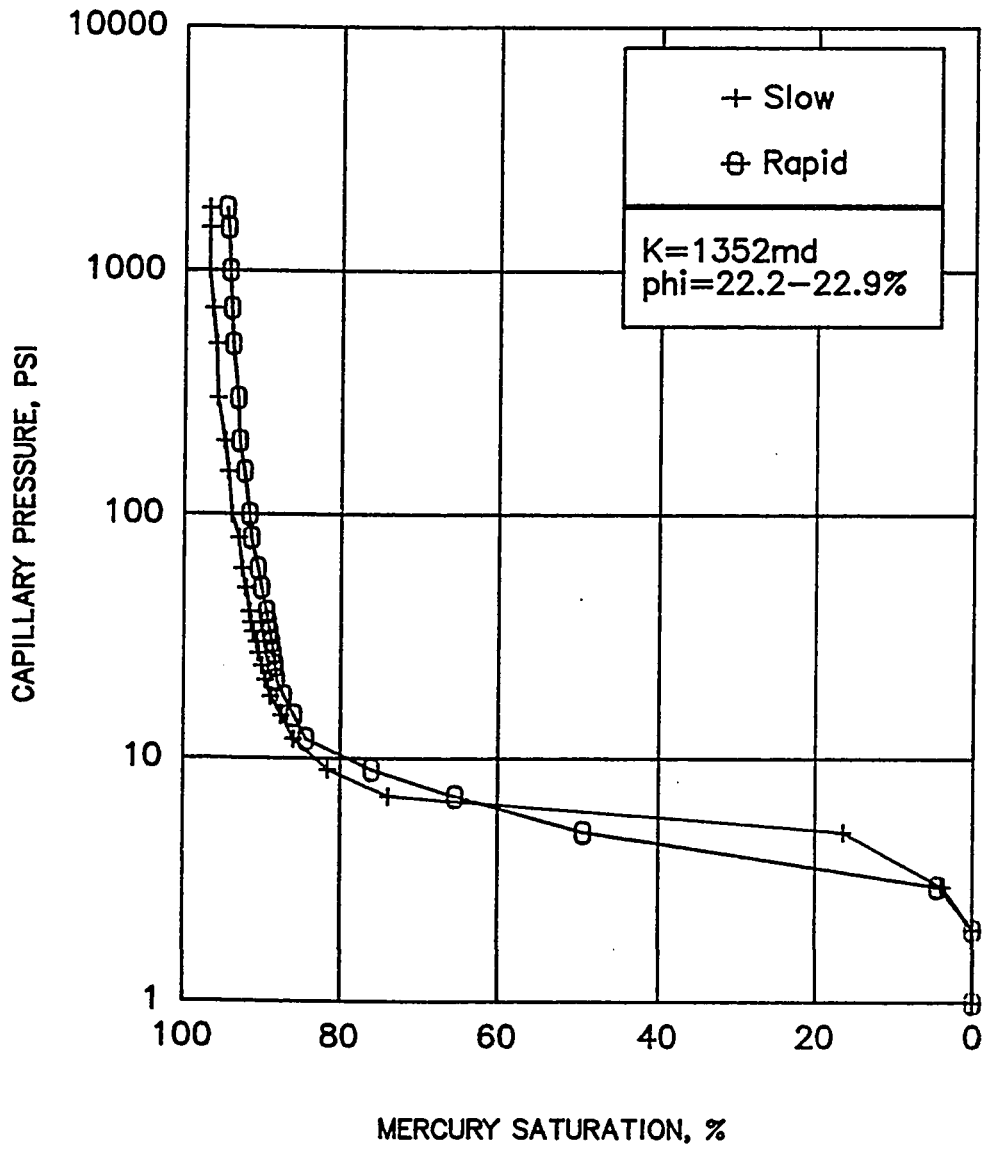

Fig(4.18). Comparison of Injection Capillary Pressure Curves for 4 cm Uncoated Bentheimer Samples

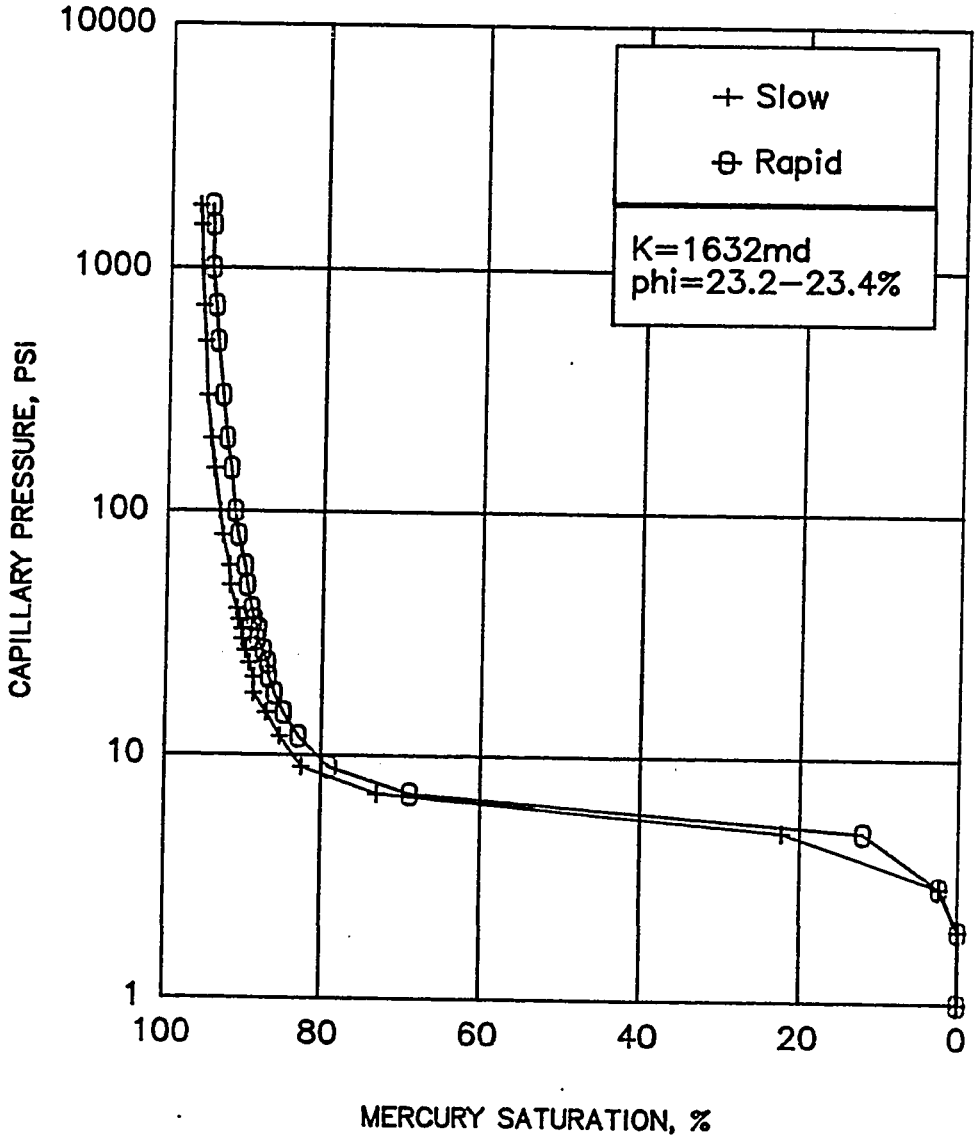

Fig(4.19). Comparison of Injection Capillary Pressure curves for 6 cm Uncoated Bentheimer Samples

rapid injection rate reached a lower nonwetting phase saturation, i.e., above 70% mercury saturation, at a given pressure than that obtained by the slow injection rate. The differences between the slow rate and the rapid rate analyzes are not significant. Below the saturation of about 70%, the two capillary curves coincide with each other. The displacement pressures are the same whether the tests were performed rapidly or slowly regardless of the difference in size of the Bentheimer samples. Except in Fig. (4.18), the displacement pressure is quite different between the two methods on the Bentheimer sample of 4 cm length. This may be due to an experimental error.

The results of the study of equilibrium effect on Berea samples are shown in Figs. (4.20) through (4. 22). Berea samples were treated in the same way as the Bentheimer samples. A comparison of slow injection with rapid injection for Indiana limestone samples, as indicated by Wardlaw [8] . showed that rapid injection curve shows higher displacement pressure. He explained that allowing insufficient time had increased the displacement pressure. In the instant study, the displacement pressure was kept the same for both the methods applied on Berea and Bentheimer sandstone samples. It is due to the reasons that first, the Berea and Bentheimer sandstones are permeable and secondly, the pore sizes are distributed homogeneously. However, there is a general agreement in the shape of the capillary pressure curves for the various studies. Unsaturated pore volumes were higher for slow injection cases. But in

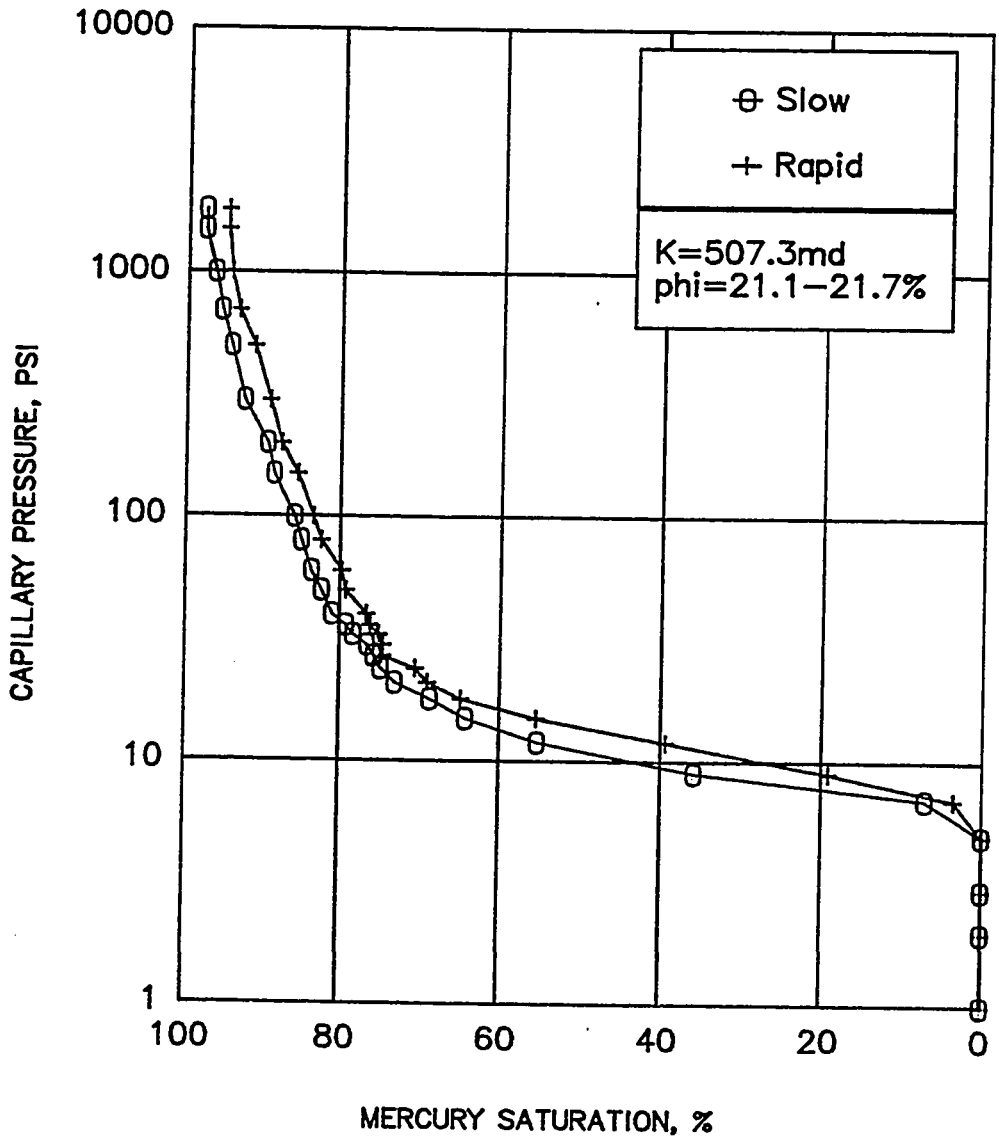

Fig(4.20). Comparison of Injection Capillary Pressure Curves for 2 cm Uncoated Berea Samples.

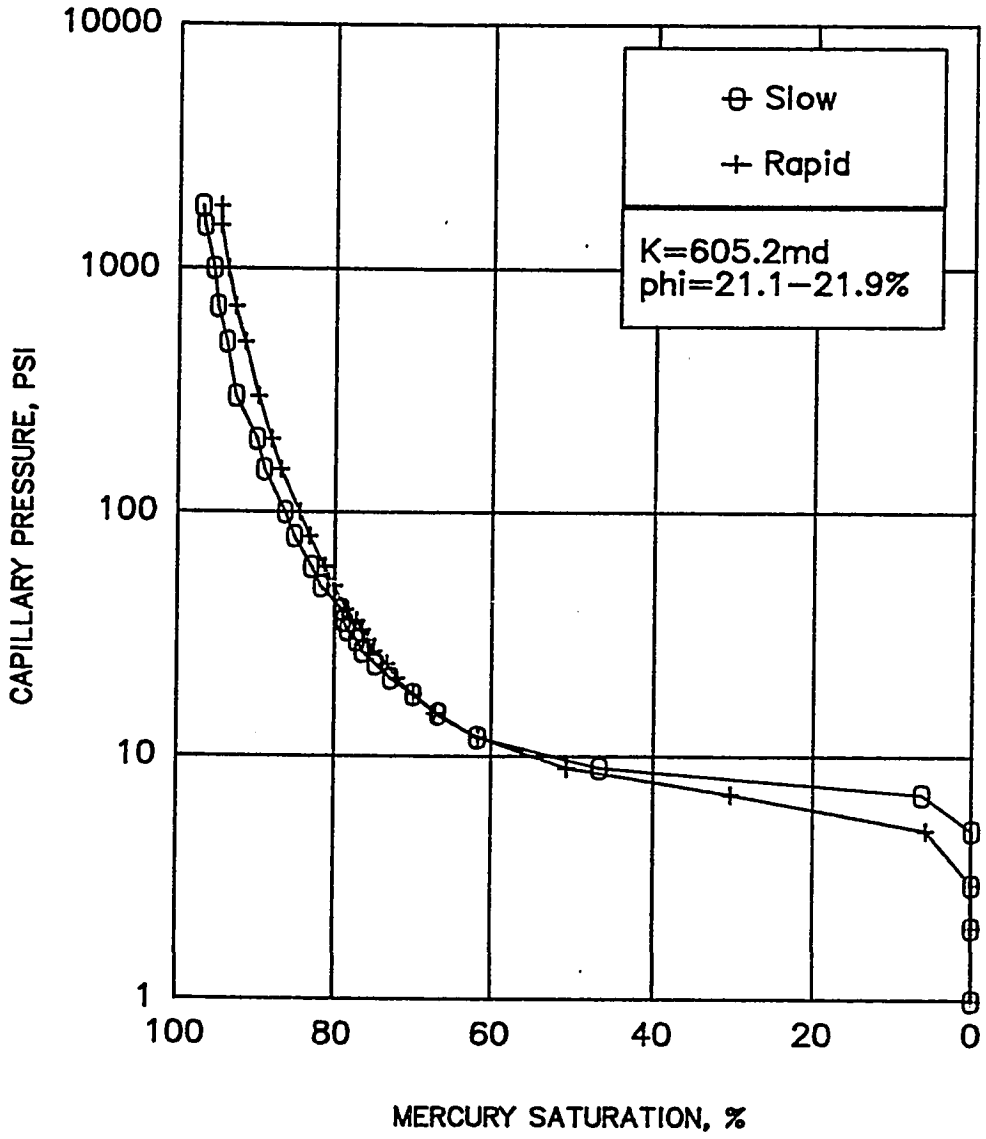

Fig(4.21). Comparison of Injection Capillary Pressure Curves for 4 cm Uncoated Berea Samples.

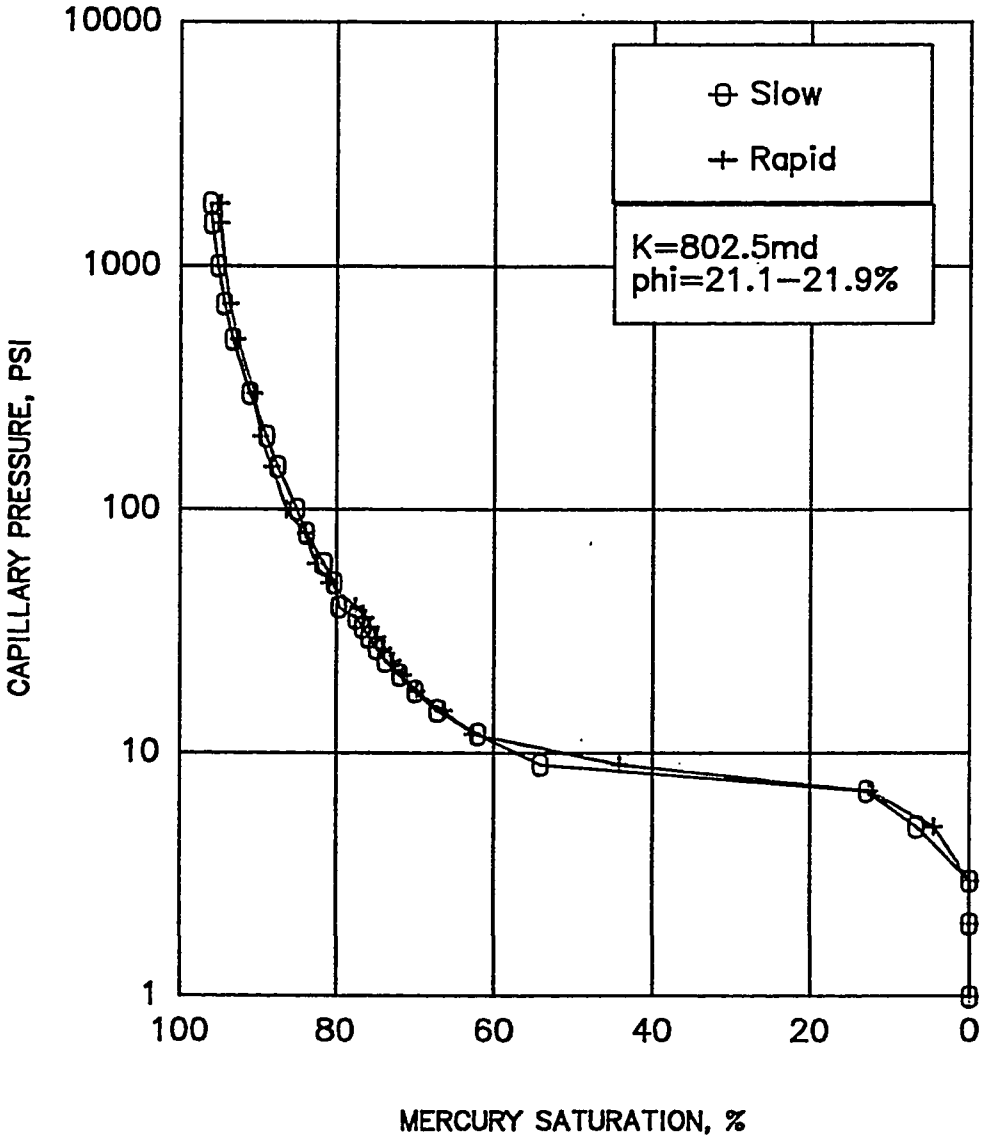

Fig(4.22). Comparison of Injection Capillary Pressure Curves for 6 cm Uncoated Berea Samples.

Fig. (4.22) irreducible mercury saturations are the same for both the methods applied.

It can be inferred that mercury injection at high pressure especially for those samples of larger size may indicate that true equilibrium in the mercury-air system would require substantially longer time at these pressures. In Fig. (4.21), the displacement pressure was observed to be higher in slow rate tests than that in rapid rate tests. It is due to the experimental error.

4.2.2 Withdrawal Capillary Pressure

The relationship of volume of mercury leaving from the pore system to pressure during pressure reduction defines the ejection capillary curves. The retraction begins at the point at which the intrusion ends and the pore system is filled with mercury partially or completely. The study of equilibrium effect on Bentheimer sandstone samples is shown in Figs. (4.23) through (4.25). For the experiments described here, duplicate samples of 2 cm, 4 cm, and 6 cm in length Bentheimer sandstone samples were used. The ejection capillary pressure results indicate that the residual nonwetting phase saturation increases when rapid rates were applied. On the other hand, as the samples length increases, the residual saturation increases. As can be seen from Fig. (4.25), the equilibrium effect is an important parameter affecting the shape and positions of the capillary pressure curves.

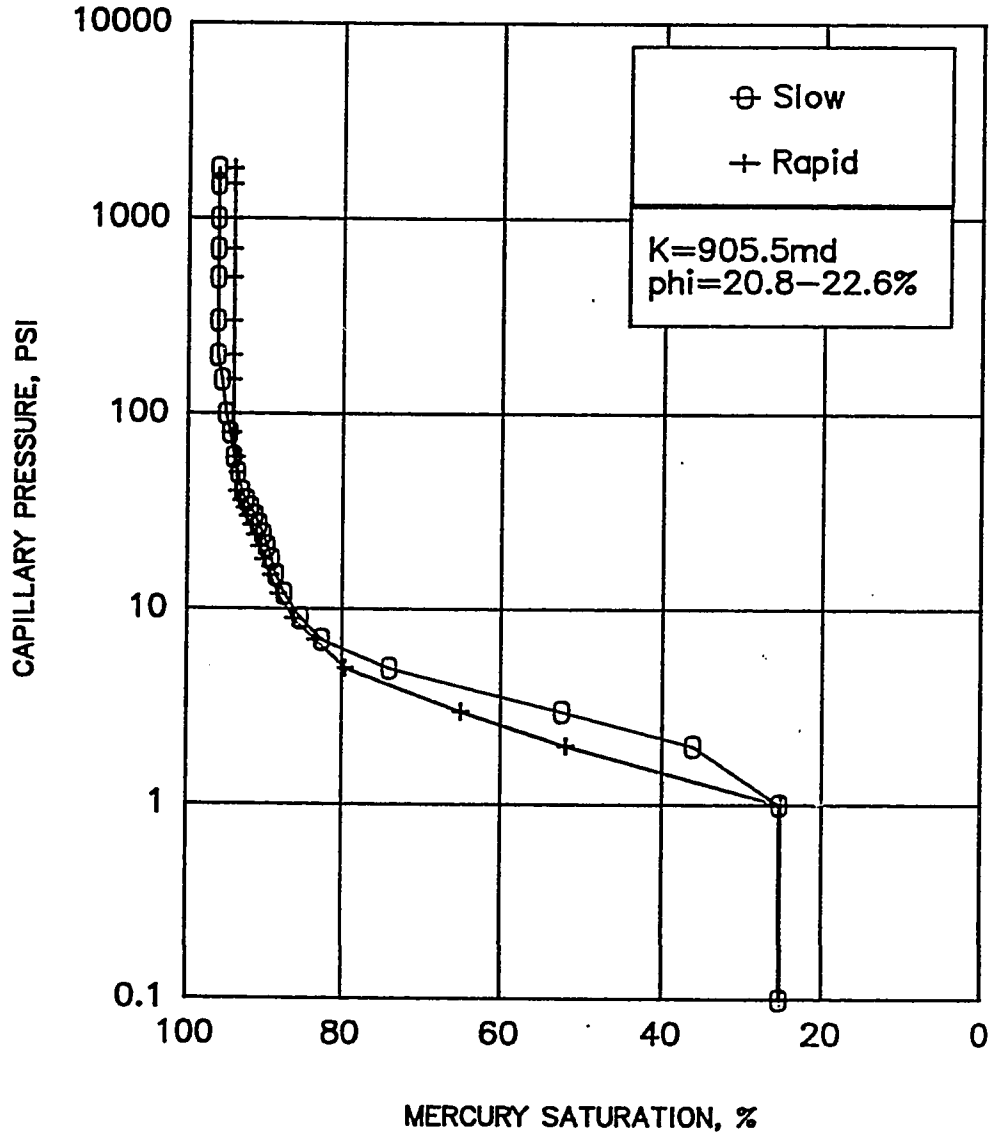

Fig(4.23). Comparison of Withdrawal Capillary Pressure Curves for 2 cm Uncoated Bentheimer Samples.

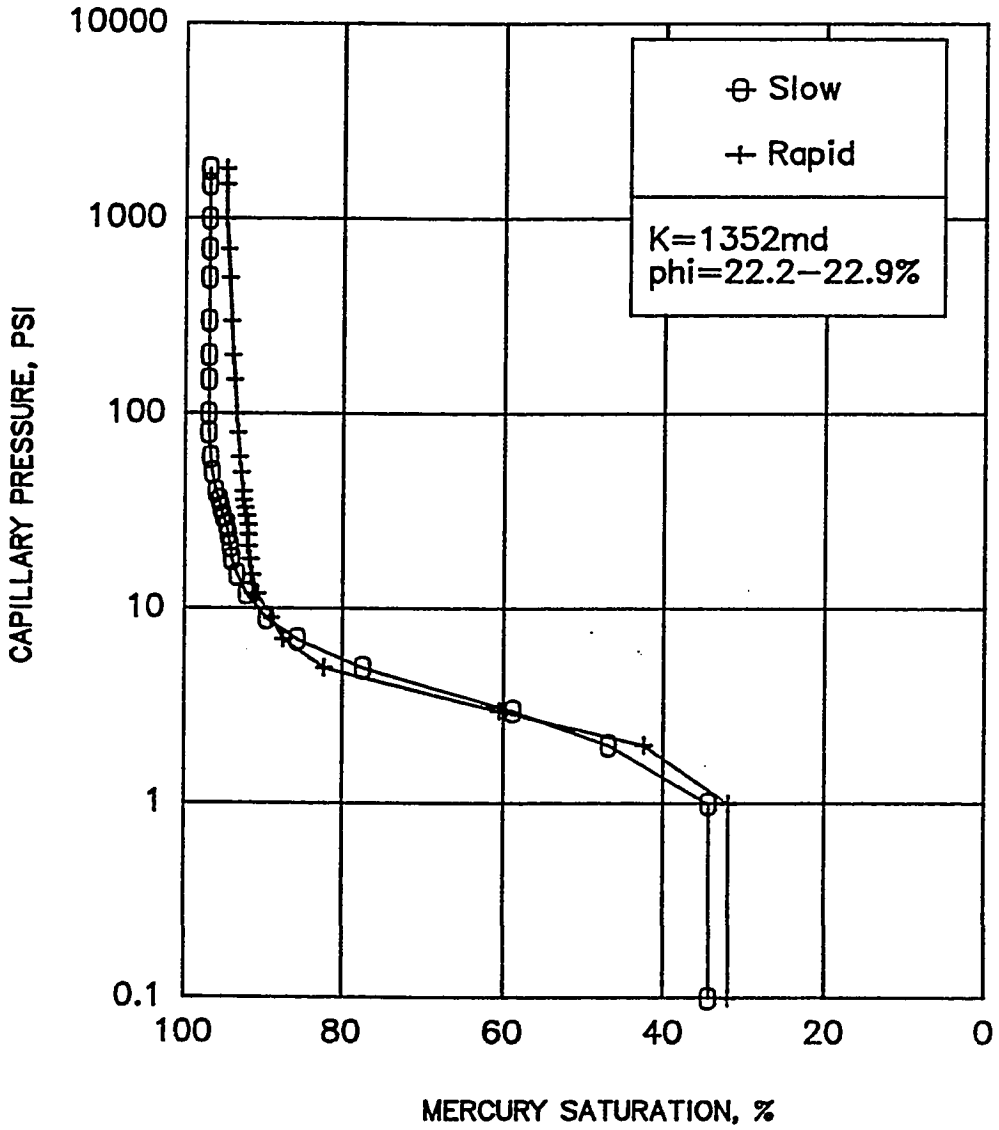

Fig(4.24). Comparison of Withdrawal Capillary Pressure Curves for 4 cm Uncoated Bentheimer Samples.

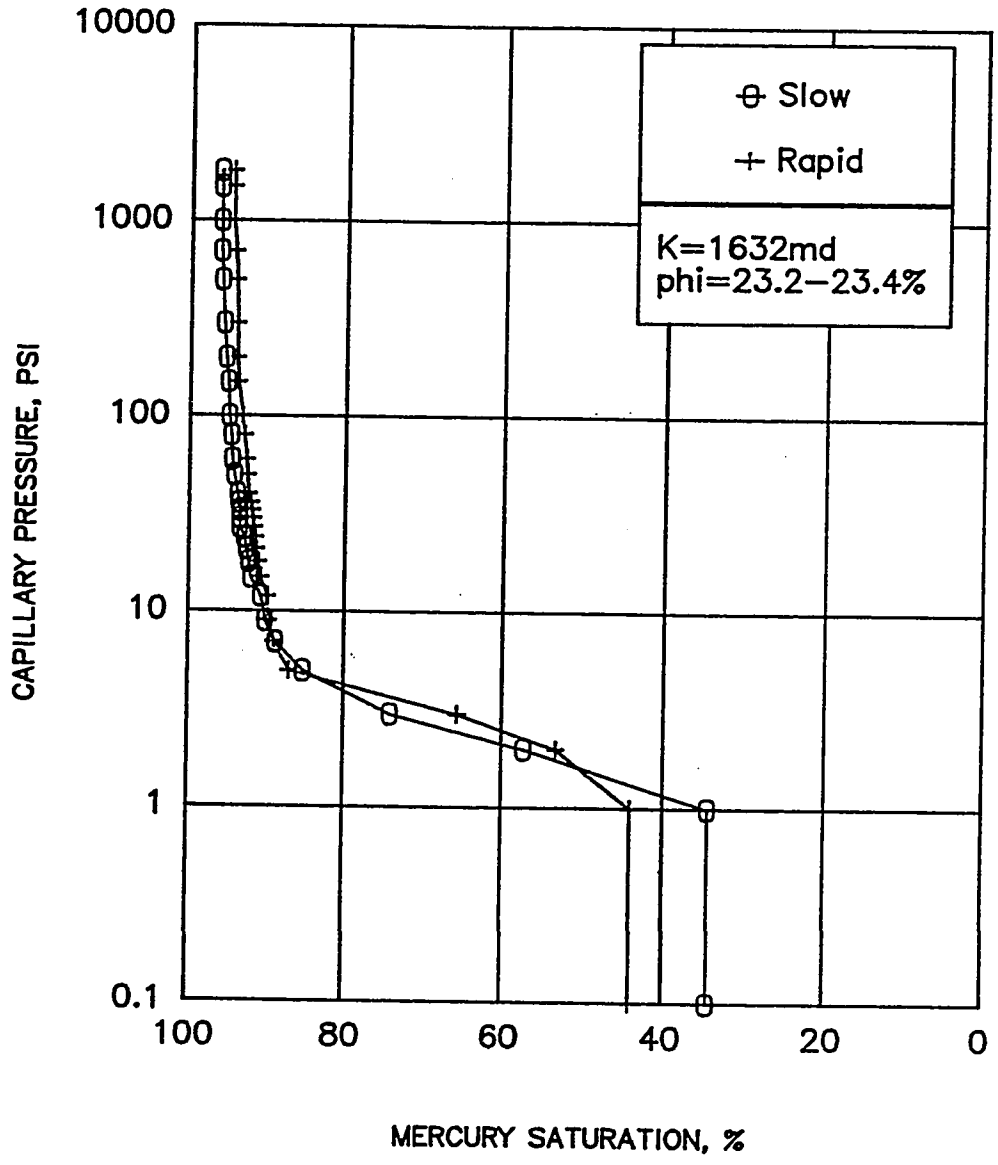

Fig(4.25). Comparison of Withdrawal Capillary Pressure Curves for 6 cm Uncoated Bentheimer Samples.

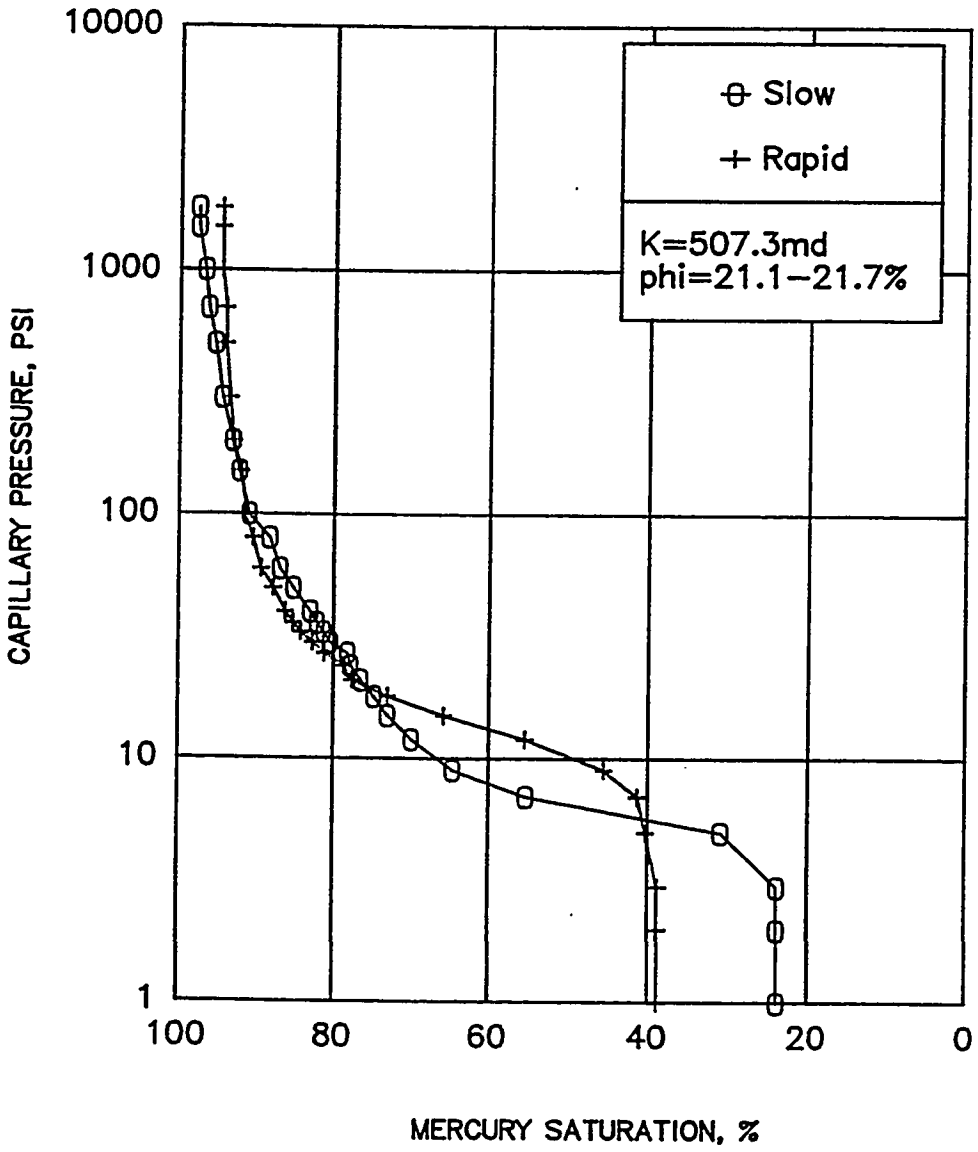

Fig(4.26). Comparison of Withdrawal Capillary Pressure Curves for 2 cm Uncoated Berea Samples.

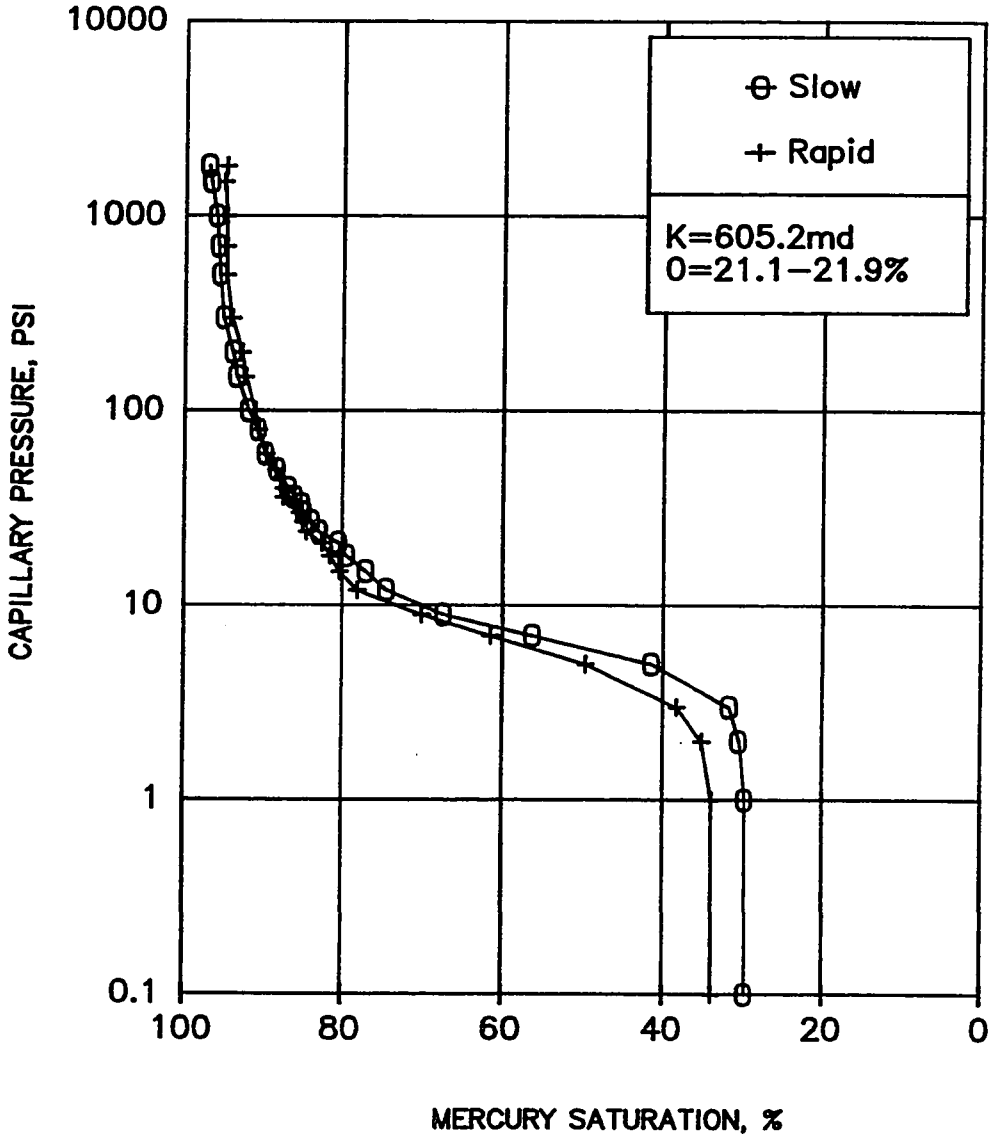

Fig(4.27). Comparison of Withdrawal Capillary Pressure Curves Obtained from The Slow and The Rapid Rate for 4 cm Uncoated Berea Samples.

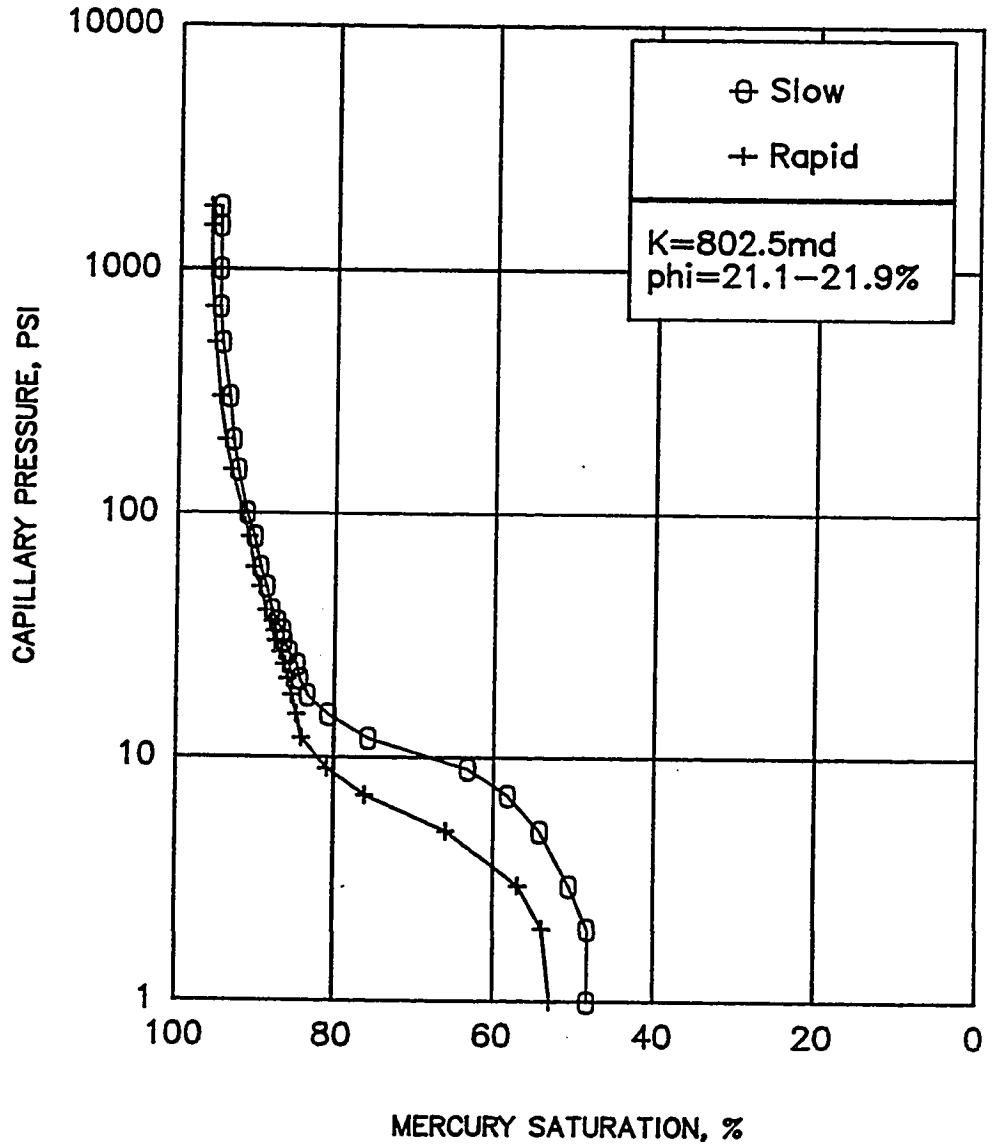

Fig(4.28). Comparison of Withdrawal Capillary Pressure Curves for 6 cm Uncoated Berea Samples.

The ejection capillary pressure curves for Berea samples of the same sizes for the two techniques of slow and rapid ejections, are given in Fig. (4.26, 4.27, and 4.28). It is apparent from these figures that the residual mercury saturation increases sharply as the length of samples increases and the rapid rate forms widened ejection capillary curves. A very important result is that both forms of the retraction curve and the residual mercury saturation value depend mainly on the method applied. Rapid ejection increases the volume of mercury trapped in the pore system because the time requirement is insufficient to withdraw the mercury from the system.

4.3 EPOXY COATING EFFECT

4.3.1 Injection Capillary Pressure Curves

Twin samples of the length of 2 cm, 4 cm, and 6 cm were tested to investigate the coating effect on sample sizes. The three samples were coated with a thin layer of epoxy resin on the surface of the sample except for one side while the other samples were uncoated. The epoxy coating effect using rapid injection techniques for the Bentheimer samples is given in Figs. (4.29) through (4.31). It can be seen from these figures that epoxy coating effect is insensitive to the shape of the capillary pressure curve. Displacement pressure and irreducible saturation are almost the same for each sample size. Except in the Fig. (4.30), lower nonwetting phase saturation occurred at pressures above

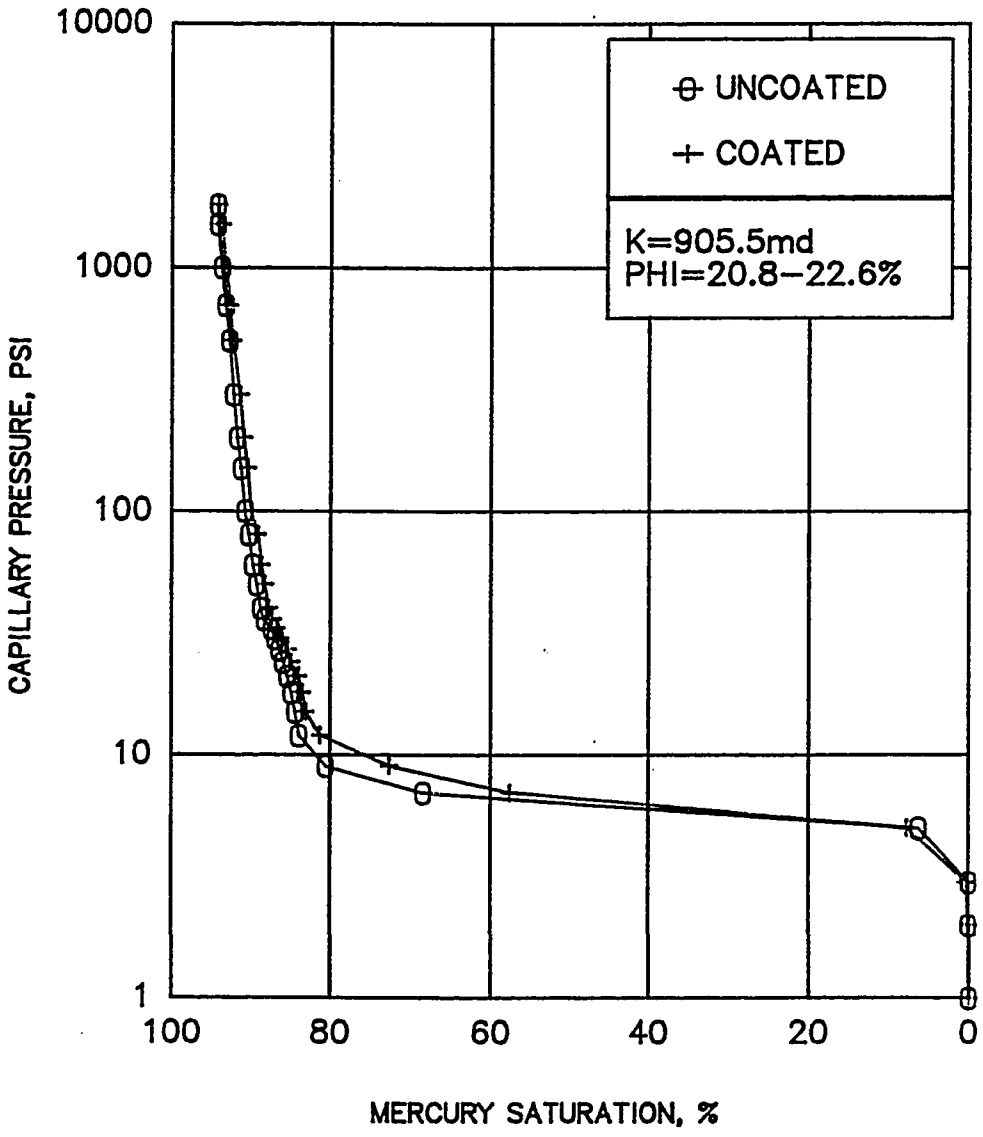

Fig(4.29). Comparison of Injection Capillary Pressure Curves Obtained from The Rapid Rate for 2 cm Bentheimer Samples.

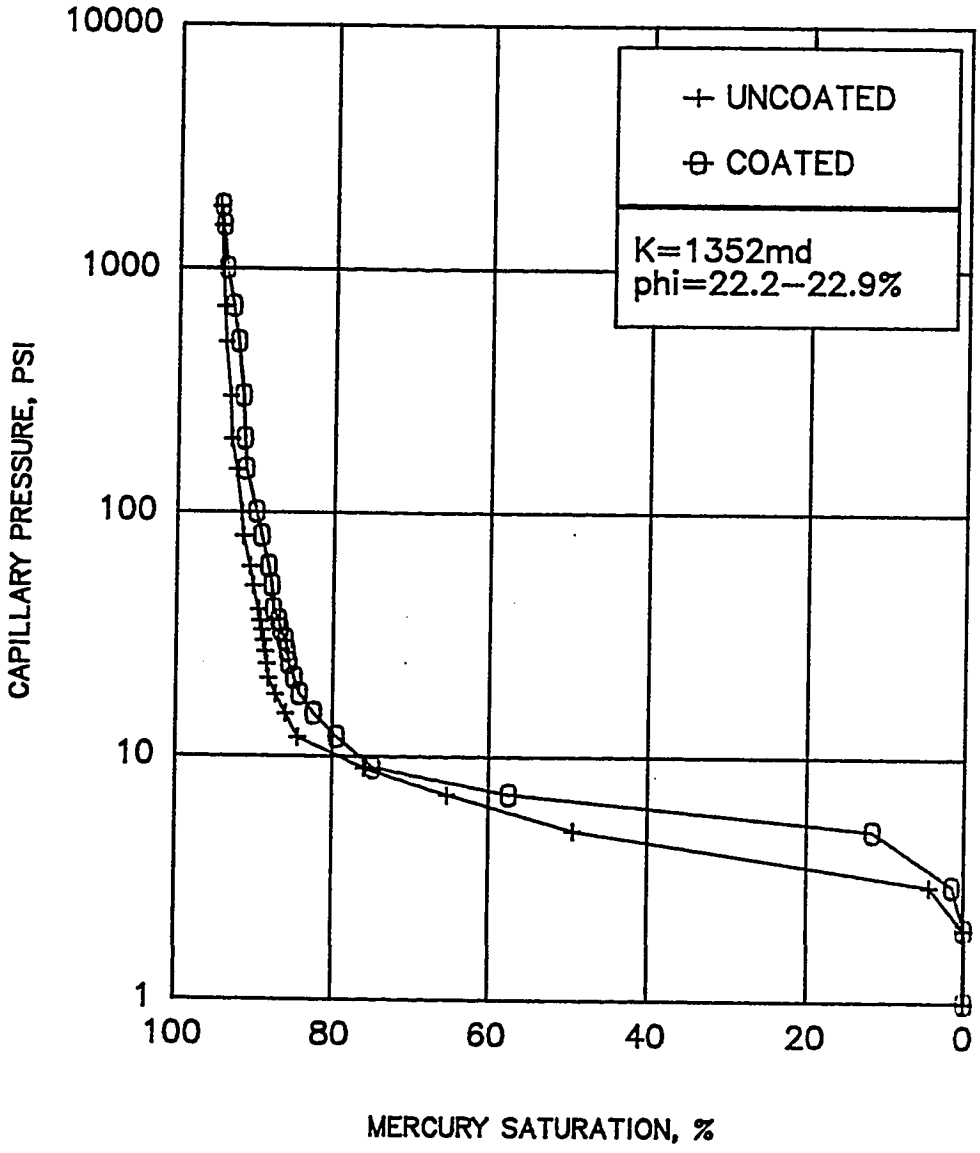

Fig(4.30). Comparison of Injection Capillary Pressure Curves Obtained from The Rapid Rate for 4 cm Bentheimer Samples

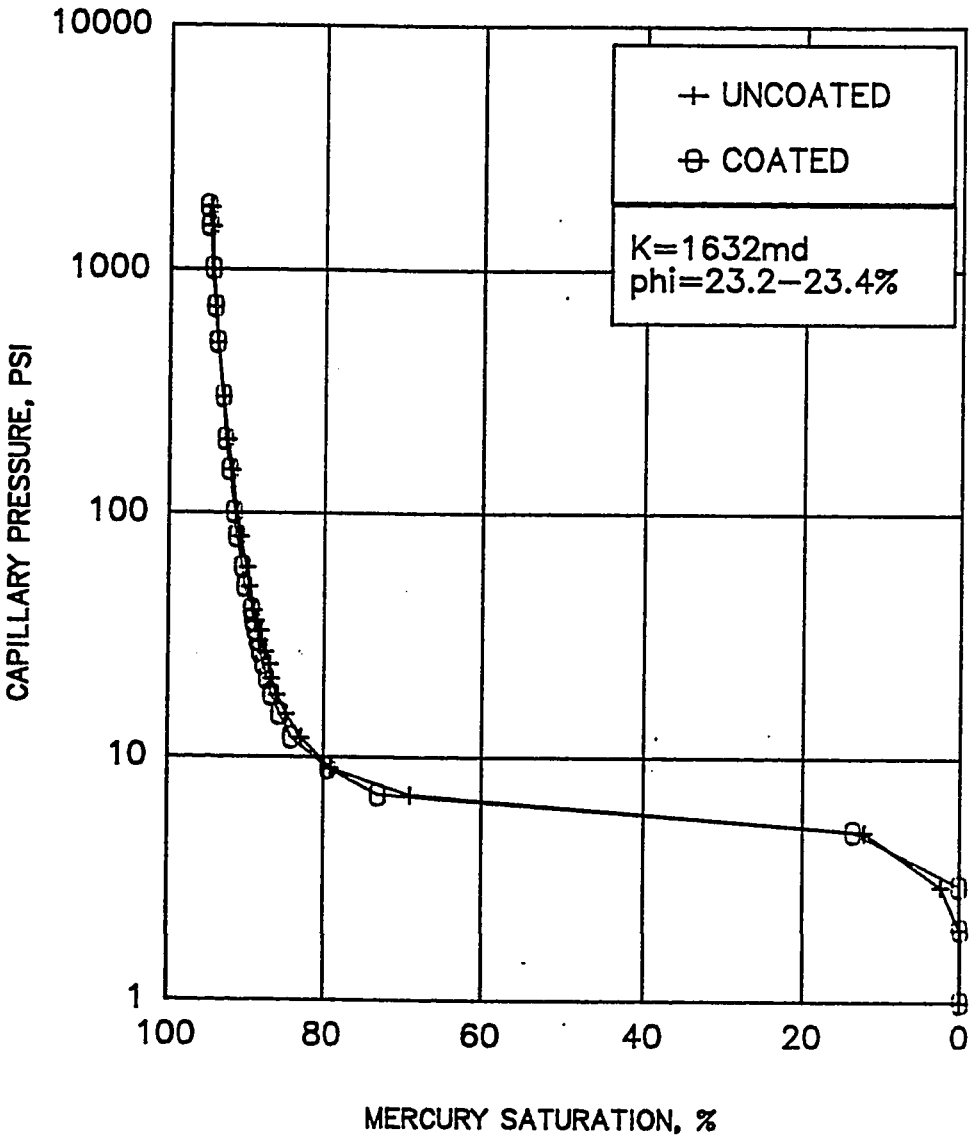

Fig(4.31). Comparison of Injection Capillary Pressure curves Obtained from The Rapid Rate for 6 cm Bentheimer Samples.

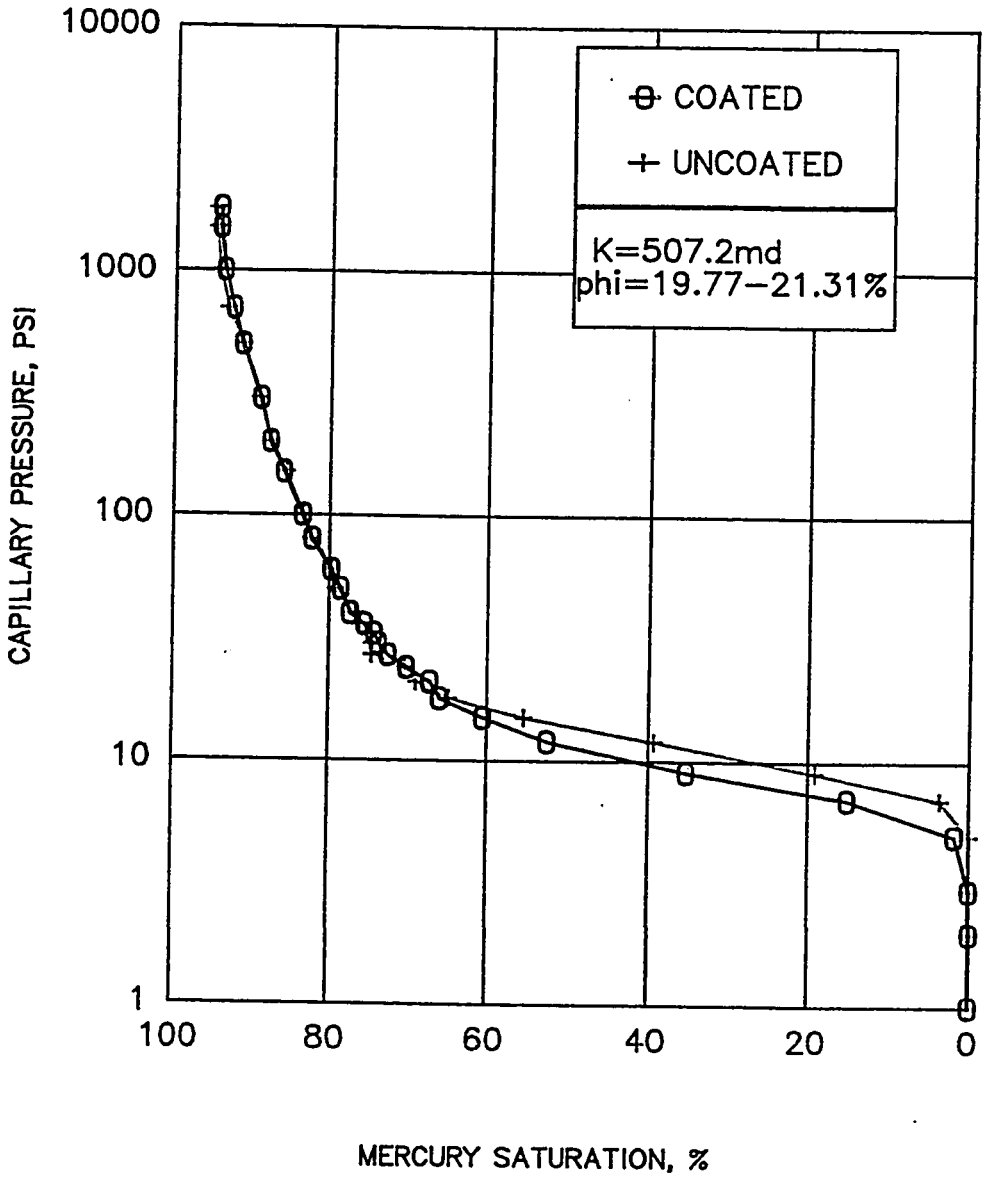

Fig(4.32). Comparison of Injection Capillary Pressure Curves Obtained from The Rapid Rate for 2 cm Berea Samples.

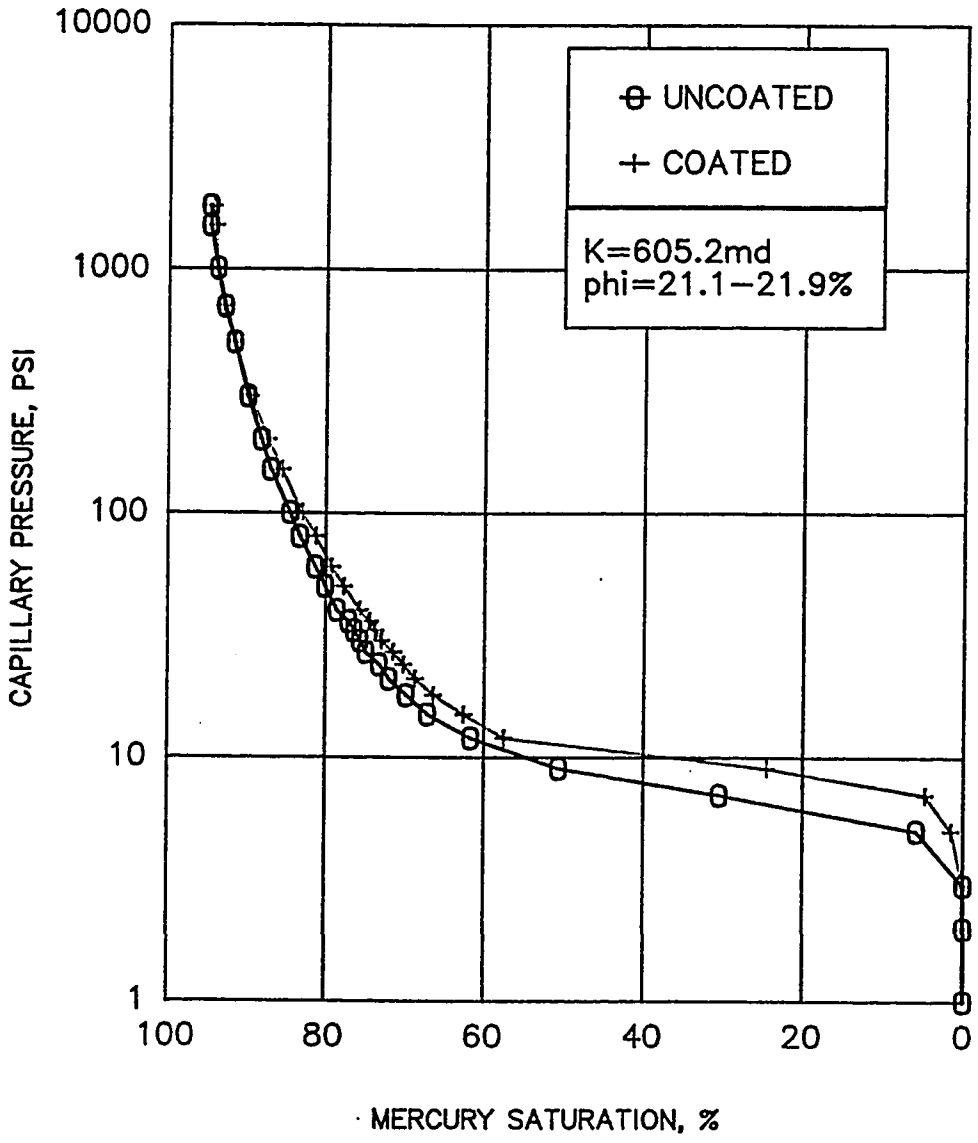

Fig(4.33). Comparison of Injection Capillary Pressure Curves Obtained from The Rapid Rate for 4 cm Berea Samples.

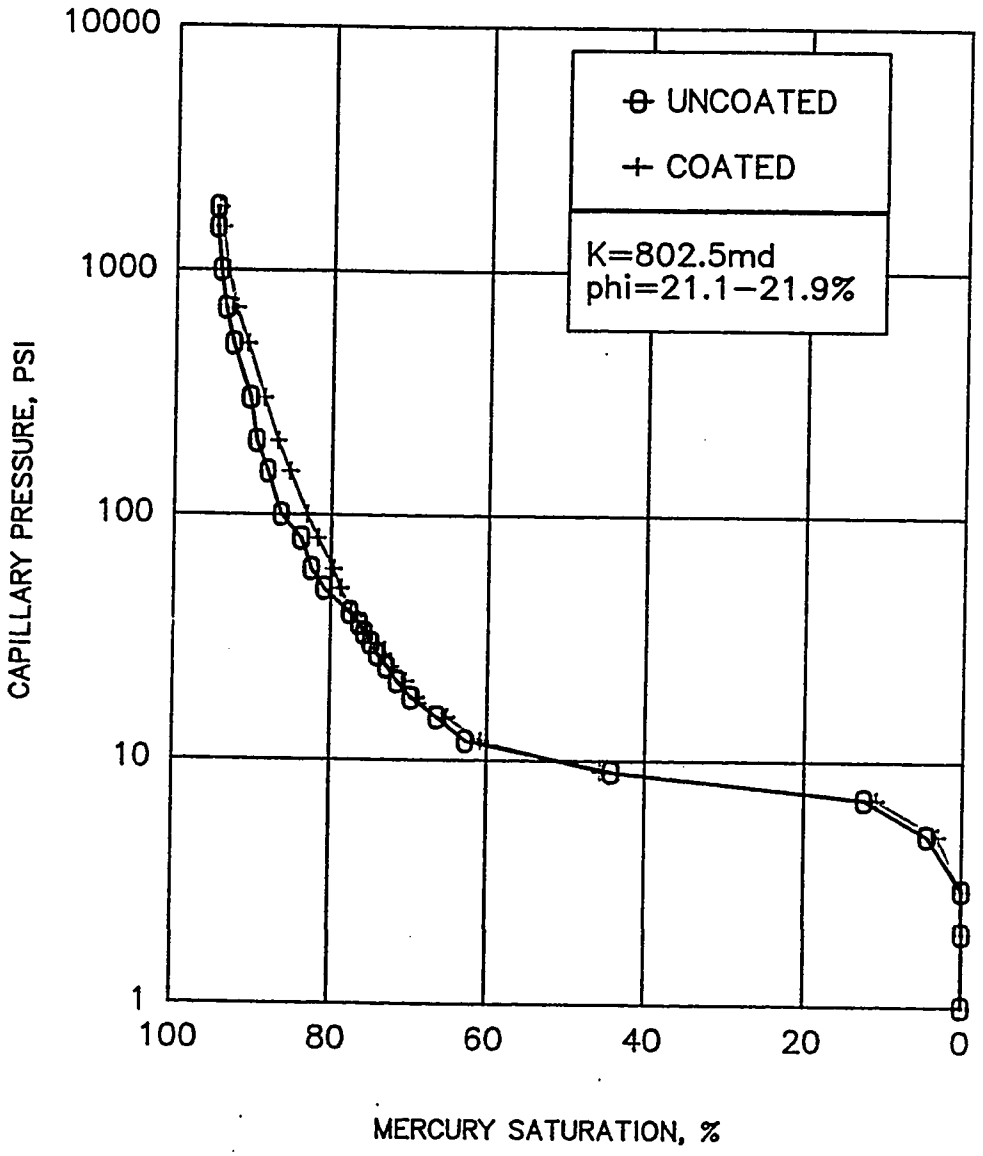

Fig(4.34). Comparison of Injection Capillary Pressure Curves Obtained from The Rapid Rate for 6 cm Berea Samples.

10 psi for coated sample. The results from injection capillary pressure test performed on the Berea samples were very similar to those obtained in Bentheimer sample tests. No differences between coated and uncoated samples were found on the study of coating effect. Figures (4.32, 4.33, and 4.34) show the capillary pressure curves for coated and uncoated Berea sandstone samples. The results shown in these figures indicate that lower pressure contribution at a given saturation below 60 % was observed for the coated samples. The irreducible saturation is the same for all cases.

4.3.2 Ejection Capillary Pressure Curves

Withdrawal capillary pressure experiments were conducted to determine the effect of equilibrium on the coated samples at the end of the injection experiment. Figures (4.35) through (4.40) show not only the rapid ejection on the coated and uncoated samples of Bentheimer and Berea sandstone, but they also illustrate a comparison of the residual saturation. The results of these studies confirm that the residual saturation increases for the coated sample as compared with that of the uncoated sample for the samples of 2 cm, 4 cm, and 6 cm in length. In the case of the Bentheimer samples, the residual saturation increases with the increase the sample size, whereas the residual saturation increases with the increase in the sample size for Berea samples. The Berea samples had slightly larger pore throat diameters than the Bentheimer samples.

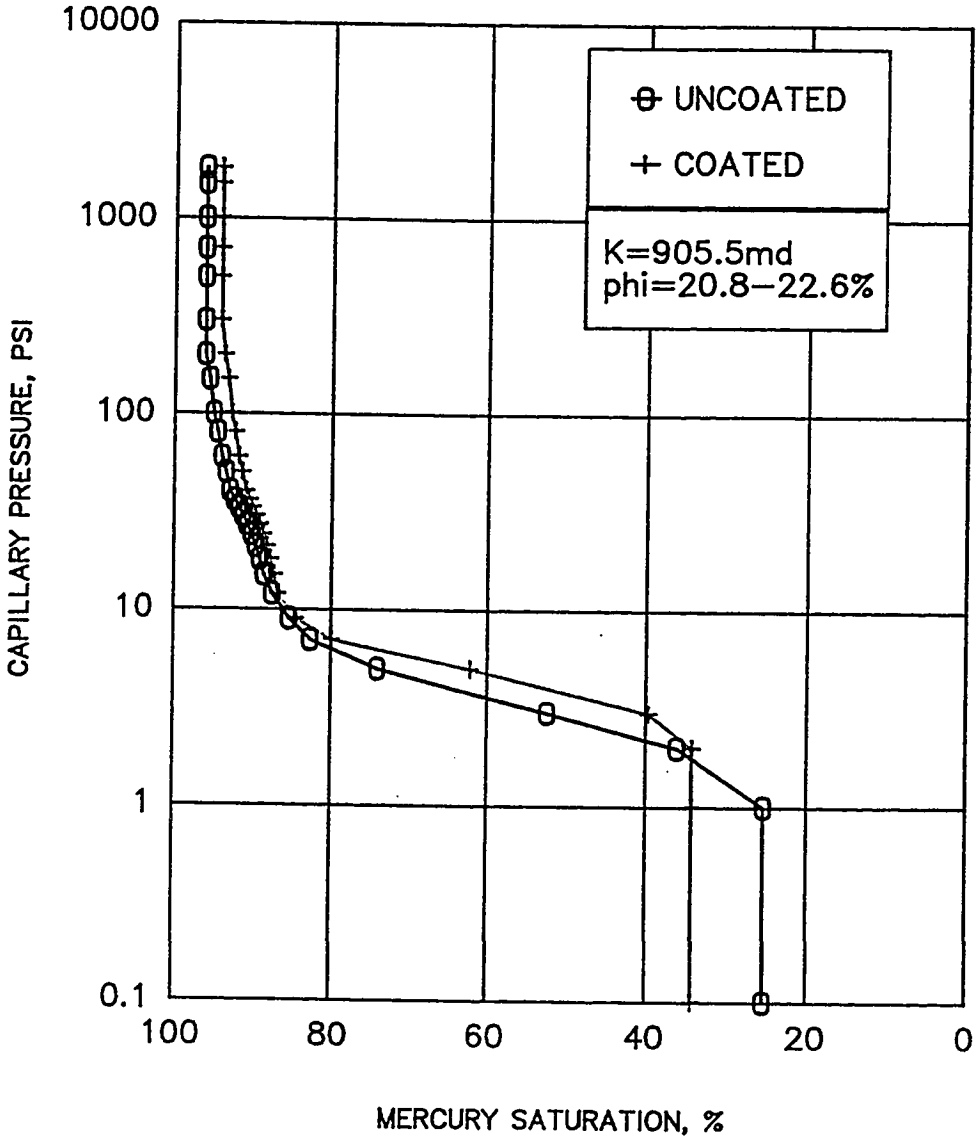

Fig(4.35). Comparison of Withdrawal Capillary Pressure Curves Obtained from The Rapid Rate for 2 cm Bentheimer Samples.

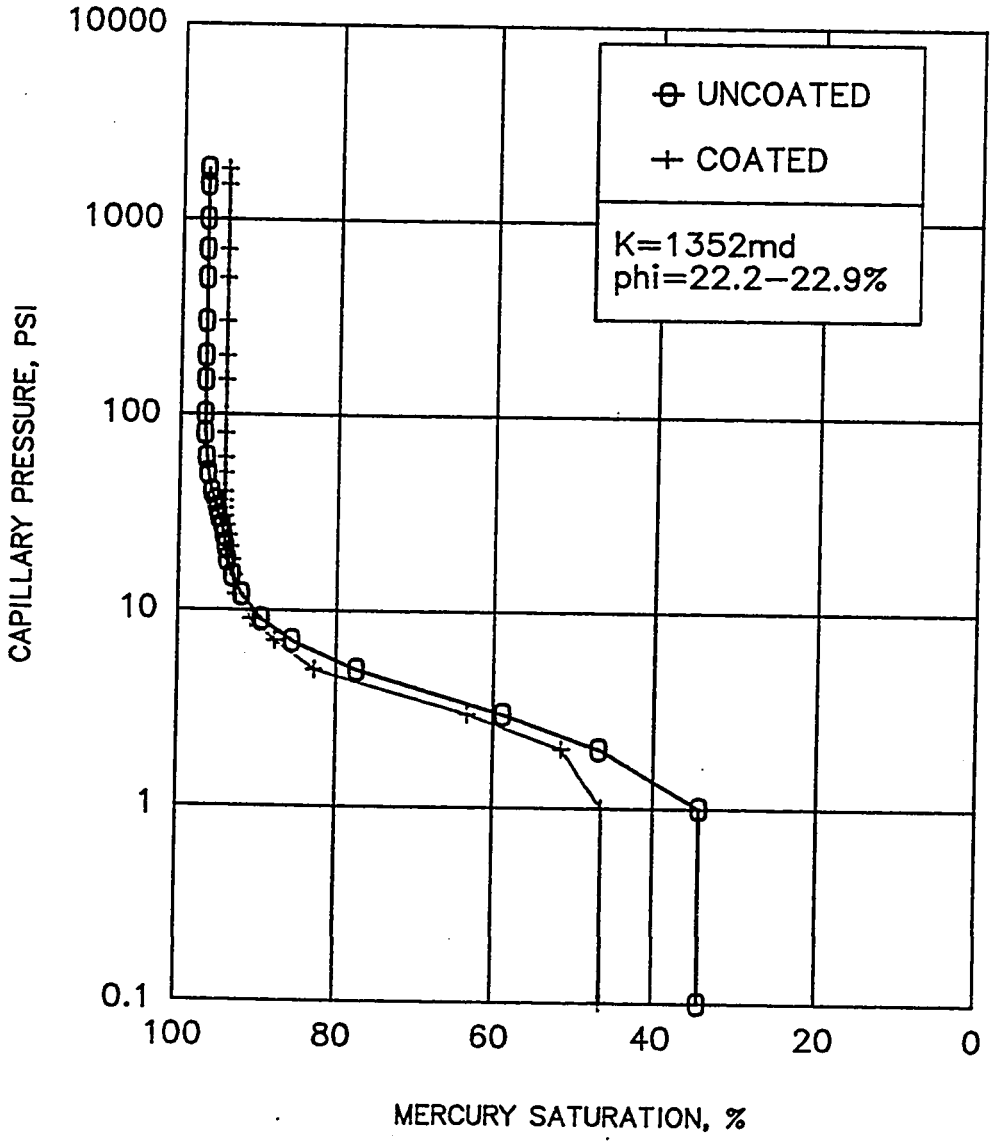

Fig(4.36). Comparison of Withdrawal Capillary Pressure Curves Obtained from The Rapid Rate for 4 cm Bentheimer Samples.

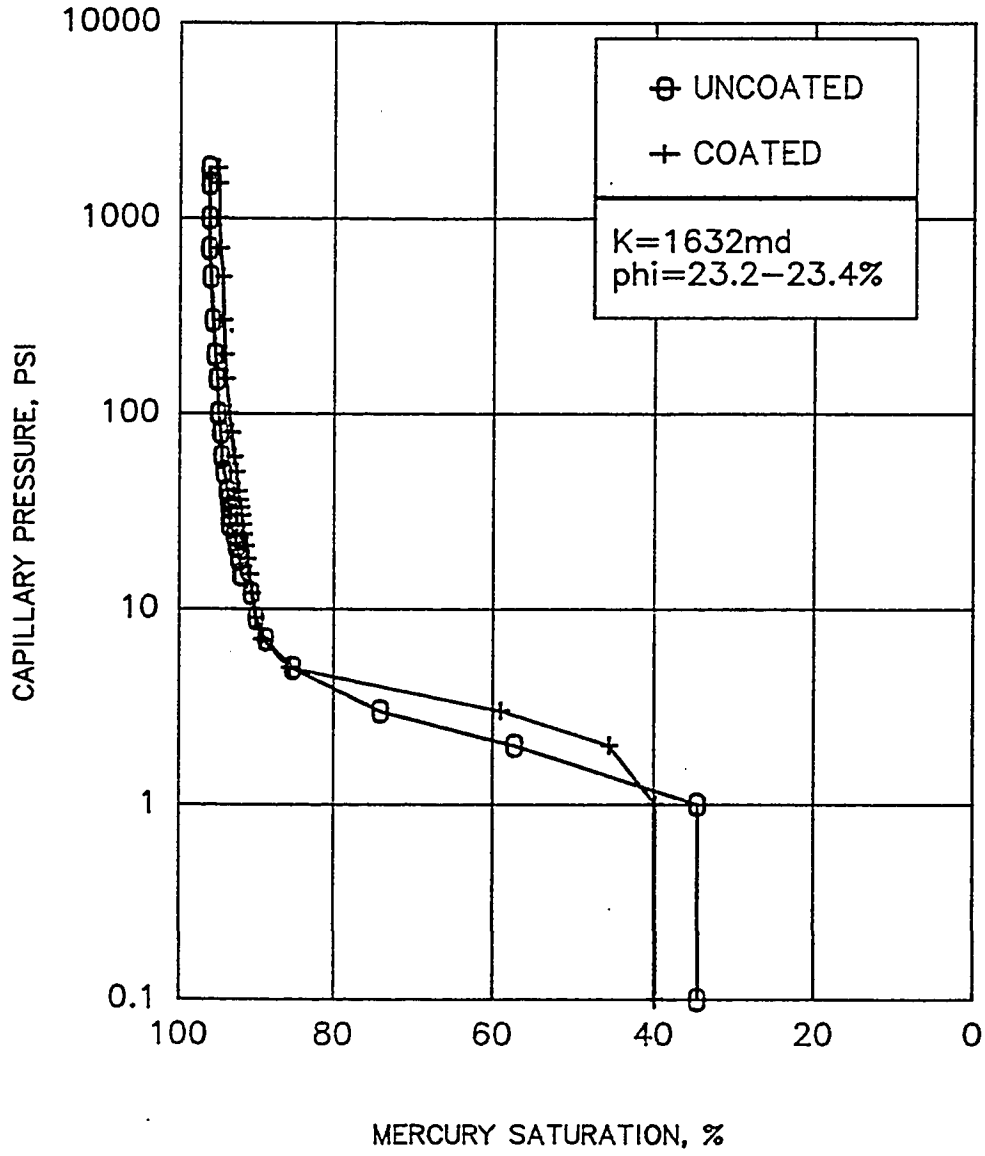

Fig(4.37). Comparison of Withdrawal Capillary Pressure Curves Obtained from The Rapid Rate for 6 cm Bentheimer Samples.

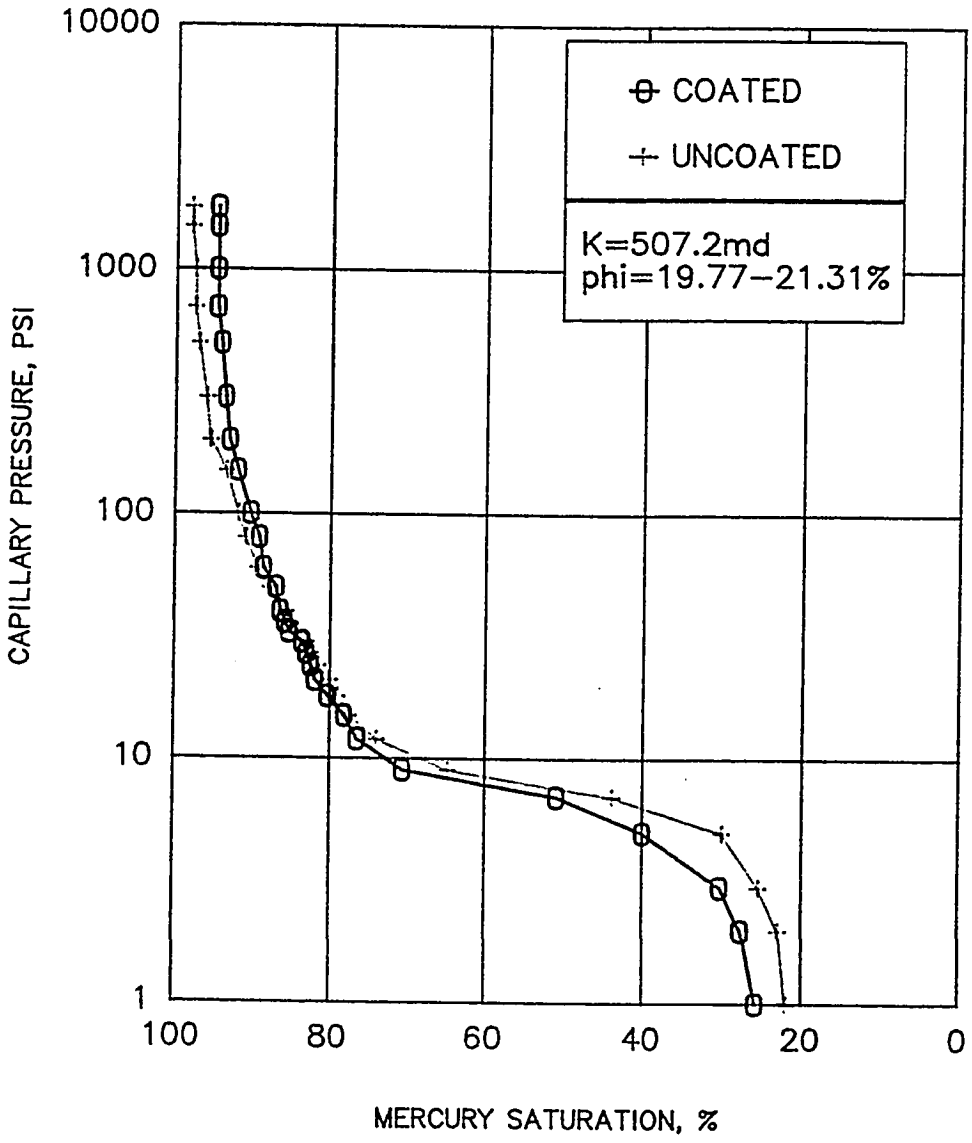

Fig(4.38). Comparison of Withdrawal Capillary Pressure Curves Obtained from The Rapid Rate for 2 cm Berea Samples.

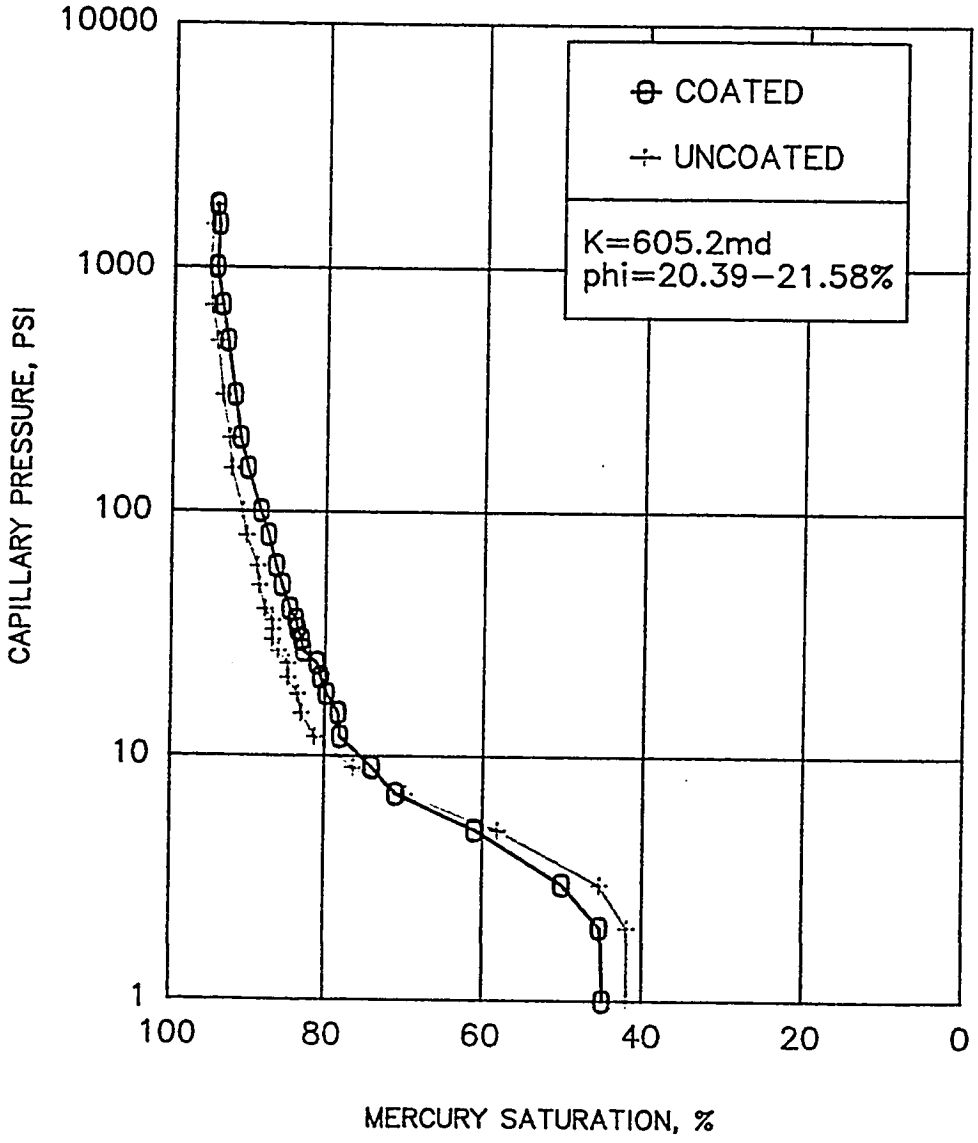

Fig(4.39). Comparison of Withdrawal Capillary Pressure Curves Obtained from The Rapid Rate for 4 cm Berea Samples.

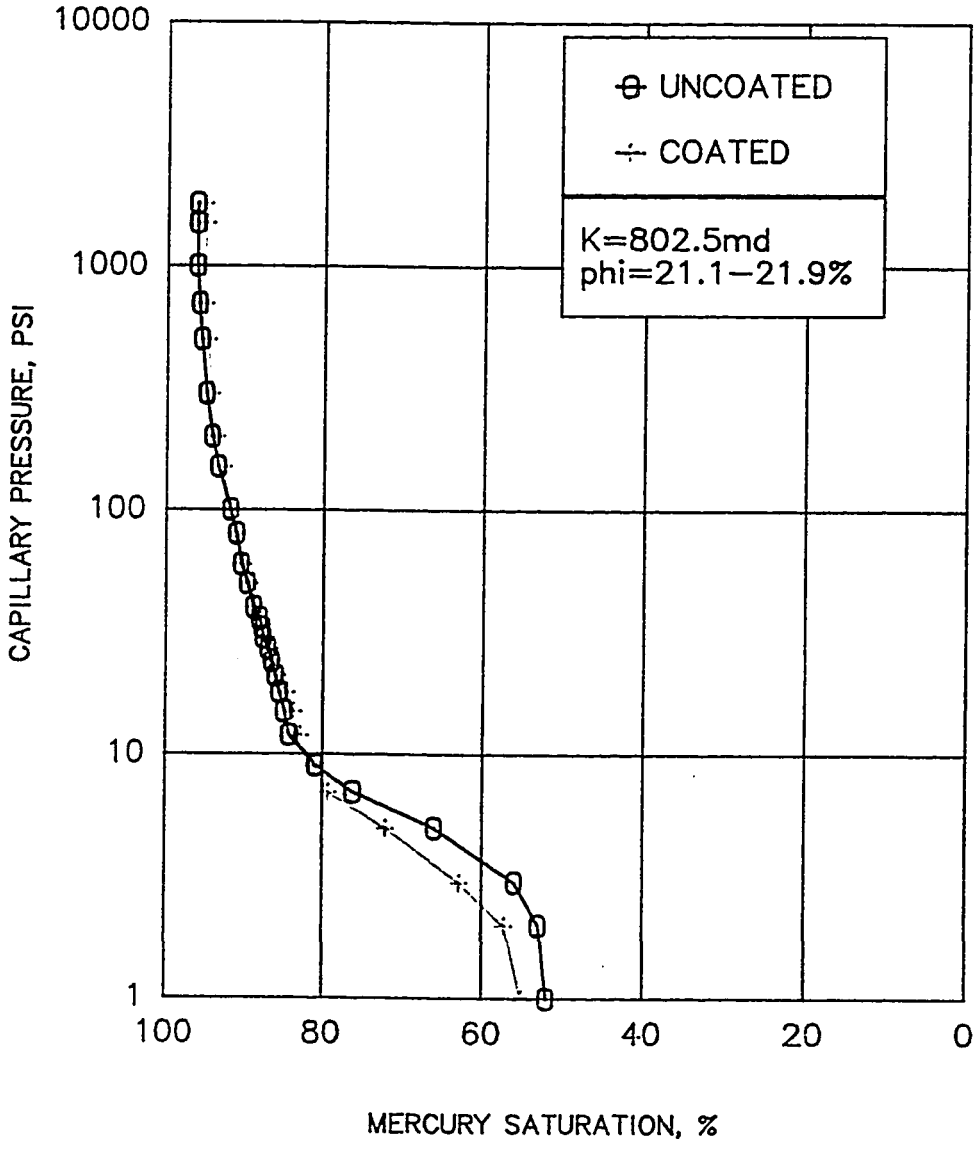

Fig(4.40). Comparison of Withdrawal Capillary Pressure Curves Obtained from The Rapid Rate for 6 cm Berea Samples.

In summary, for both coated and uncoated samples, the time required to obtain equilibrium is mainly dependent on the filling of throats, despite the relatively large volume of the pore. During ejection, the mercury gradually loses its continuity, and thus the paths through which mercury can flow out of the pore space become narrow. From the above studies, it is found that the withdrawal capillary pressure curve is sensitive to the rapid rate for the coated sample. Therefore, during ejection it is necessary to wait at each pressure stage for a time span longer than that required during injection, if equilibrium is to be attained at that pressure increase.

4.4 EFFECT OF PORE THROAT SIZE DISTRIBUTION

Varying of pore throat size affects the injection capillary pressure curves in which pressure ranges become wider. the injection mercury capillary pressure curves for all types of carbonate rocks studied are shown in Fig. (4.41). The sandstone samples and carbonate samples studied are shown in Fig. (4.42). If the rate of occurrence of large throats in the space is increased, the injection starts at lower pressures, and the injection curves are moved to lower pressure ranges. For instance, in the cases of Berea, Bentheimer and grainstone carbonate samples the curves of which are shown in Fig. (4.42), the intrusion started at lower pressure. It can be concluded, in general, that the injection curve becomes wider according to the pore size distribution.

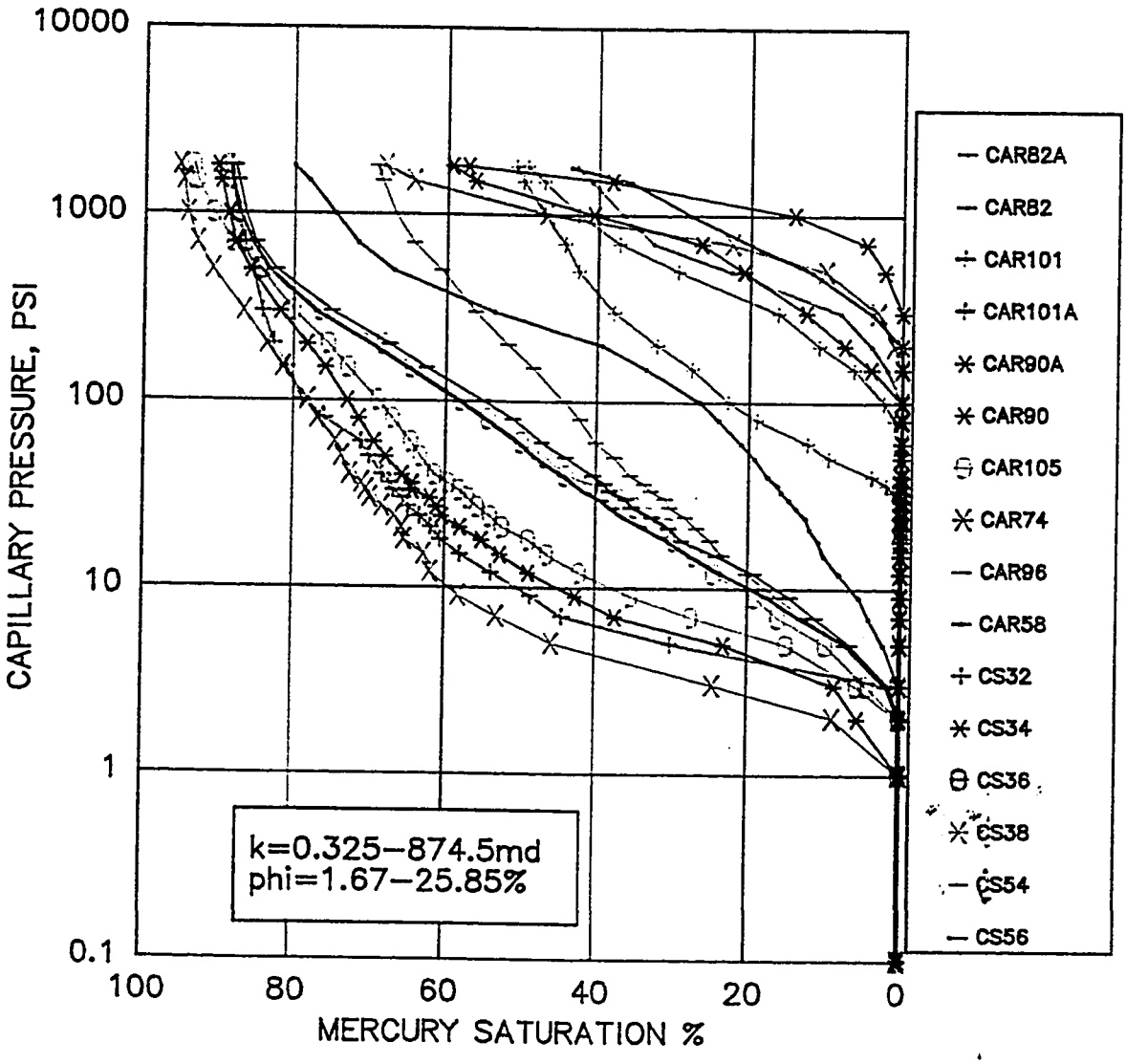

Fig(4.41). Injection capillary pressure curves for Carbonate Rocks.

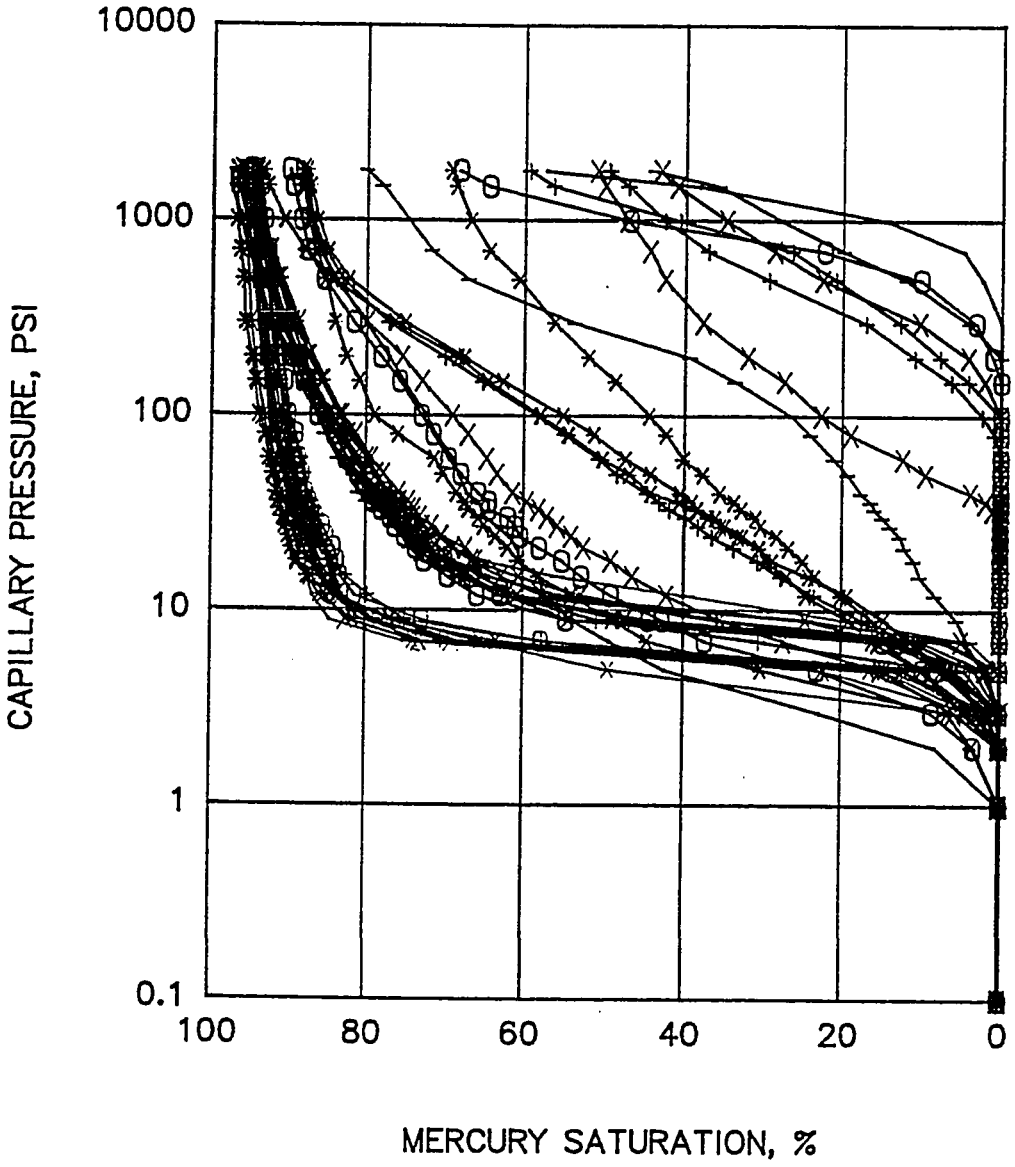

Fig(4.42). Injection Capillary Pressure Curves for All Samples Including Sandstone and Carbonate.

The pore size distributions for some samples are given in Figs. (4.43) through (4.61). In fact, pore size distribution is related to the pore throat sorting. It can be seen from these figures and Tables (4.3) and (4.4), that the calculated pore throat sorting for each sample is given in the last column of the Tables. Pore throat sorting (PTS) is a measurement of the sorting of the pore throats within a rock sample. The numbers range from 1.0 (perfect sorting) to 8.0 (essentially no sorting), with most of the rock samples falling between 1.2 and 5.0. The pore throat sorting can be determined by using the following equation :

$$PTS = \left[\frac{P_c@75\ H_g saturation}{P_c@25\ saturation}\right]^{1/2}$$

However, the 25 % and 75 % mercury saturation need to be adjusted for irreducible saturation. On the other hand, the pore throat sorting can be predicted from the injection curves. If the injection curve plateau is close to the horizontal, the pore throats are sorted perfectly. If the injection curve plateau is far from the horizontal or the plateau becomes steep, the pore throats are sorted poorly. Injection, ejection and re-injection curves for each sample are shown in Figs. (4.62) through (4.80). In well sorted rocks, pore throats were distributed uniformly and the pore throat sorting values are in the range of 1.2 to 1.6. In this study, Berea, Bentheimer and 2 types of carbonate samples were found well sorted and the rest of the carbonate samples were found poorly

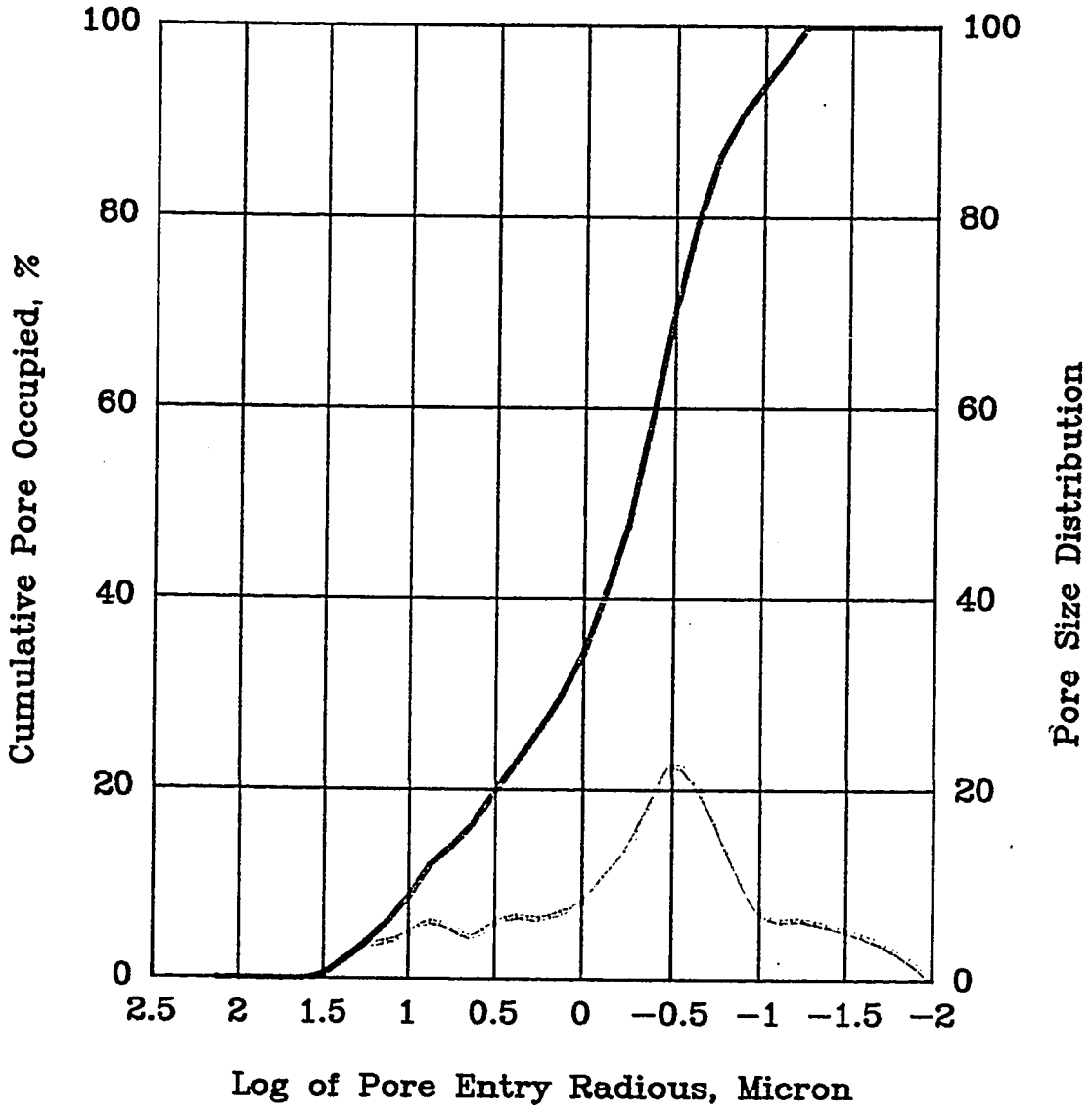

Fig (4.43). Pore Throat Size Distribution for Sample No. Carbonate−58

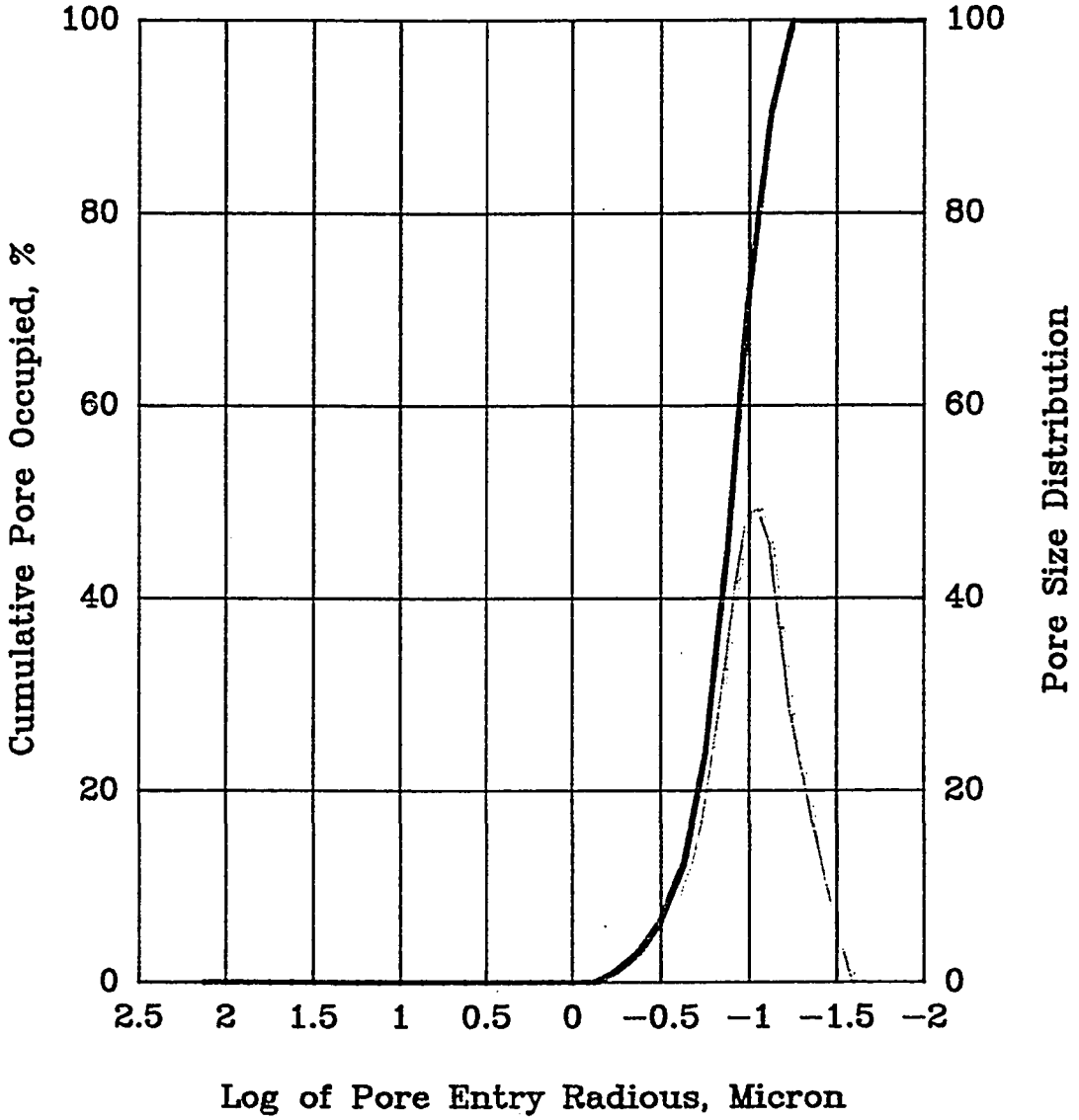

Fig (4.44). Pore Throat Size Distribution for Sample No. Carbonate−74

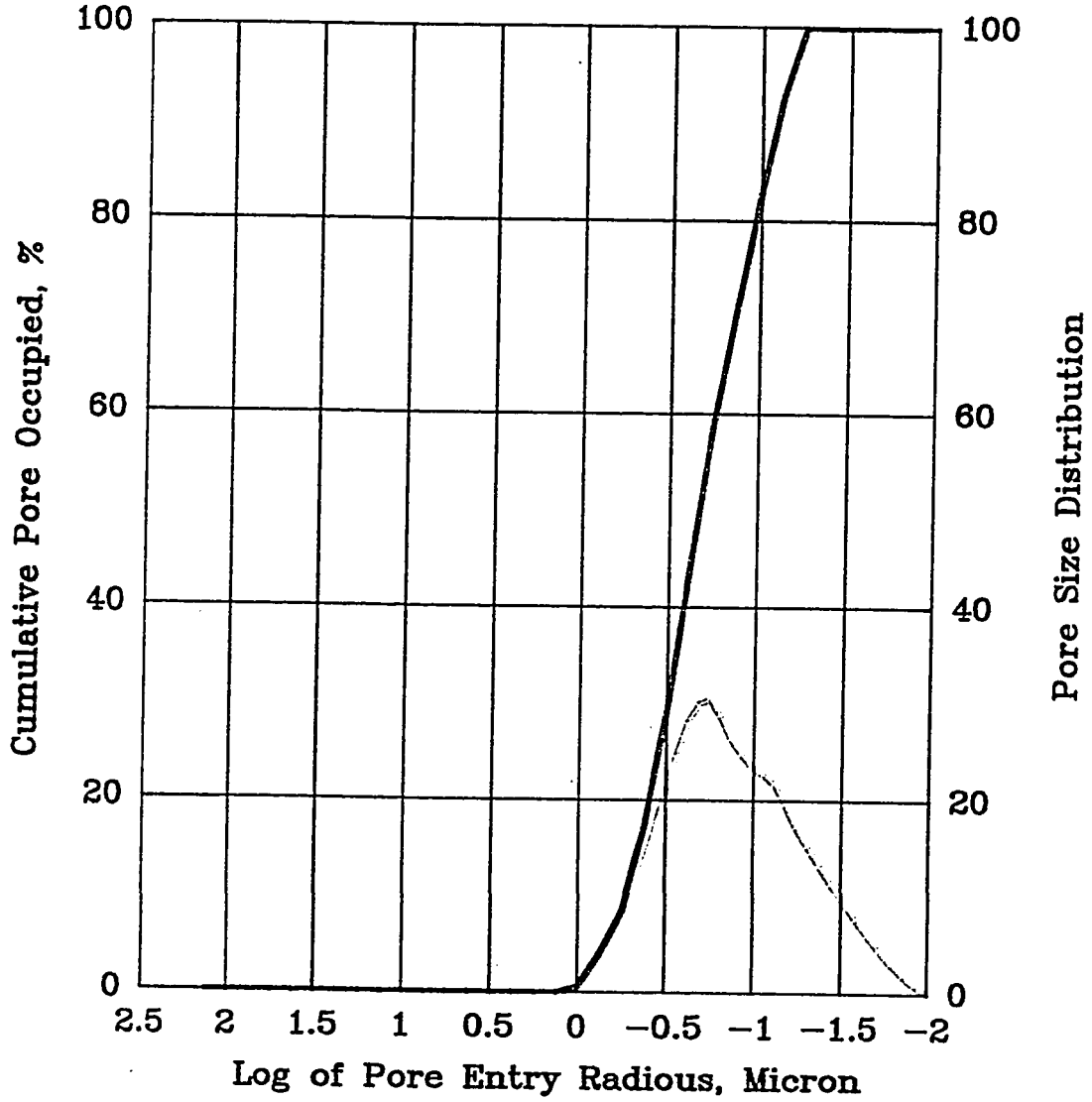

Fig (4.45). Pore Throat Size Distribution for Sample No. Carbonate–82

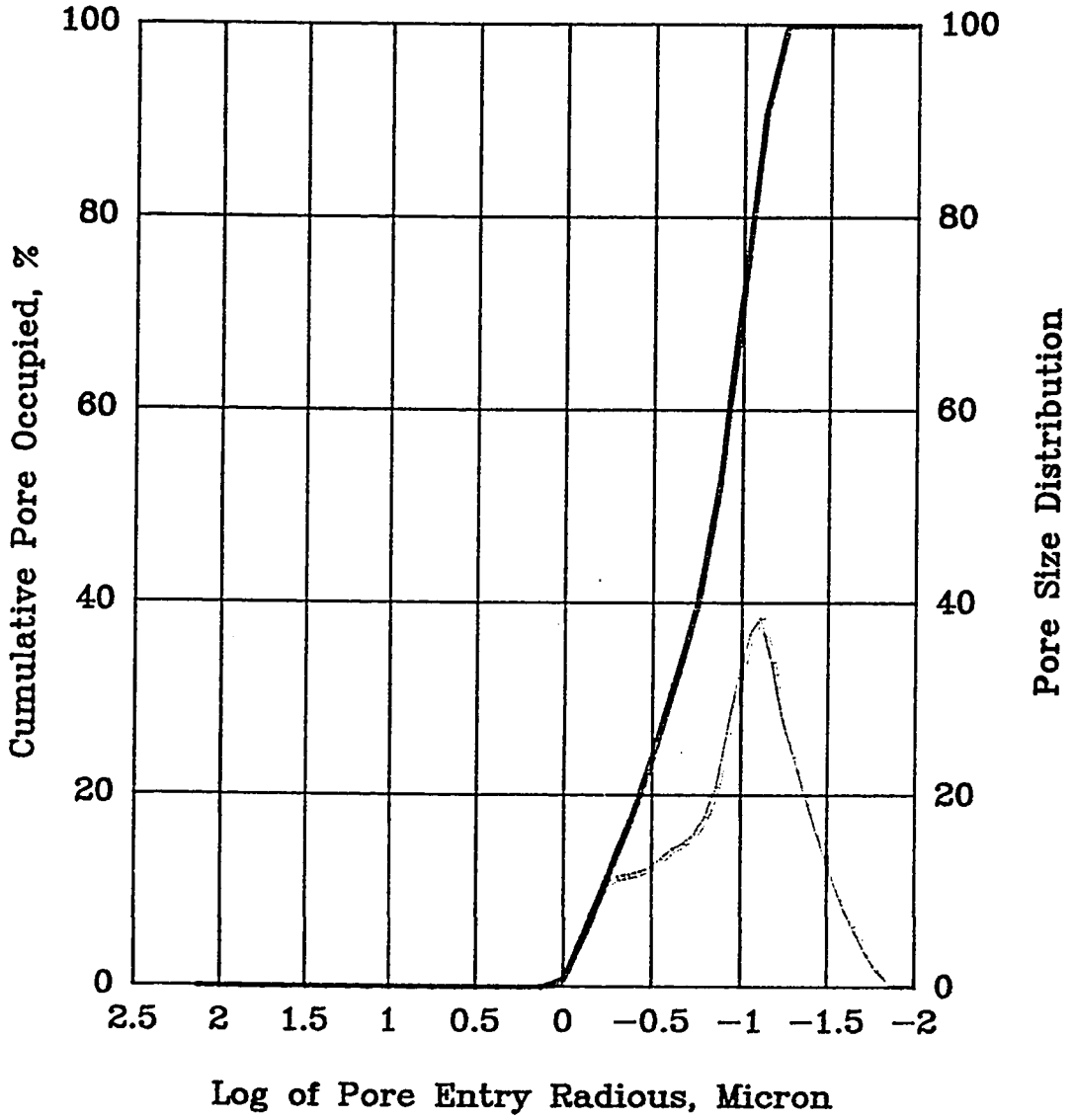

Fig (4.46). Pore Throat Size Distribution for Sample No. Carbonate−90

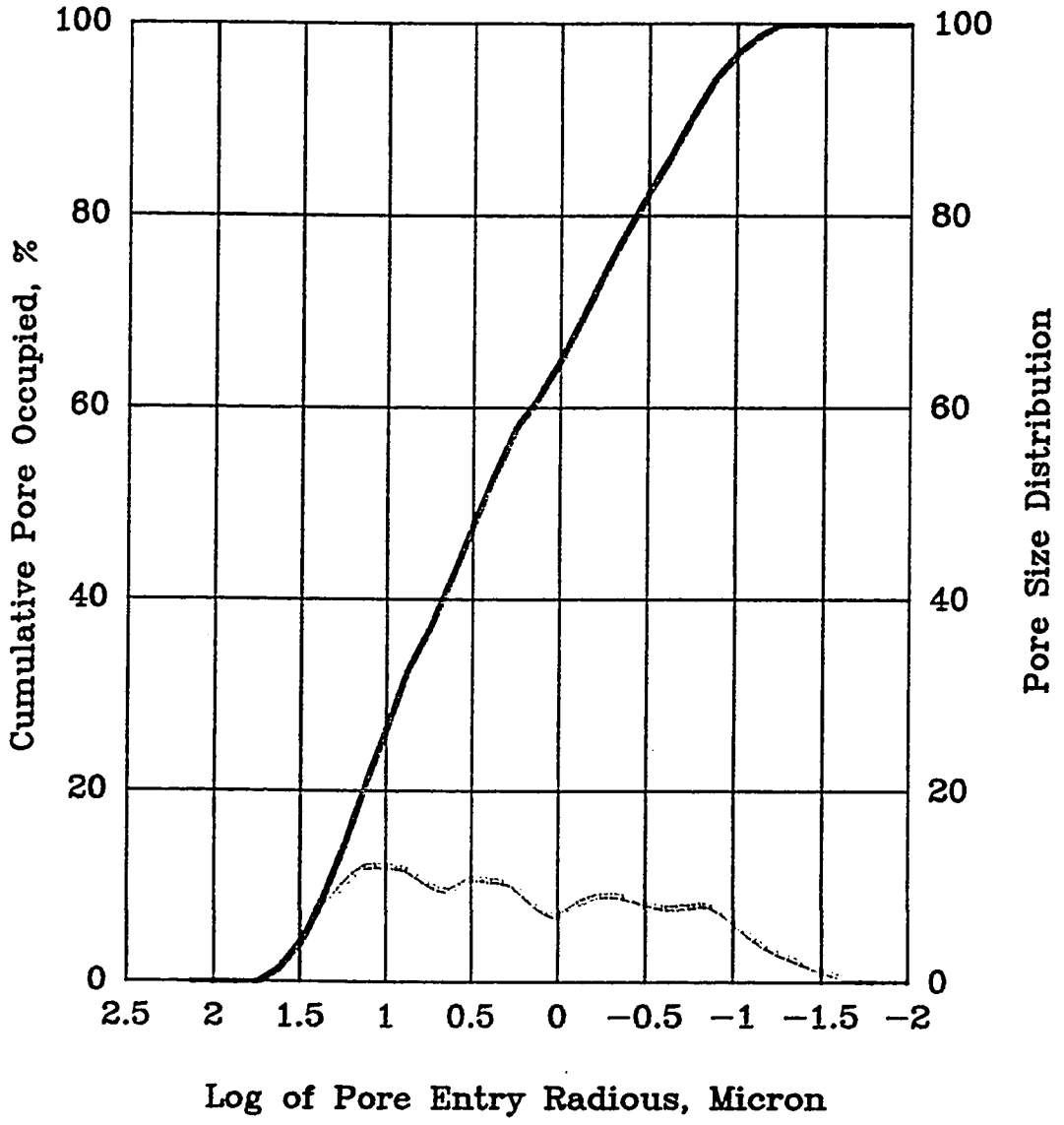

Fig (4.47). Pore Throat Size Distribution for Sample No. Carbonate−96

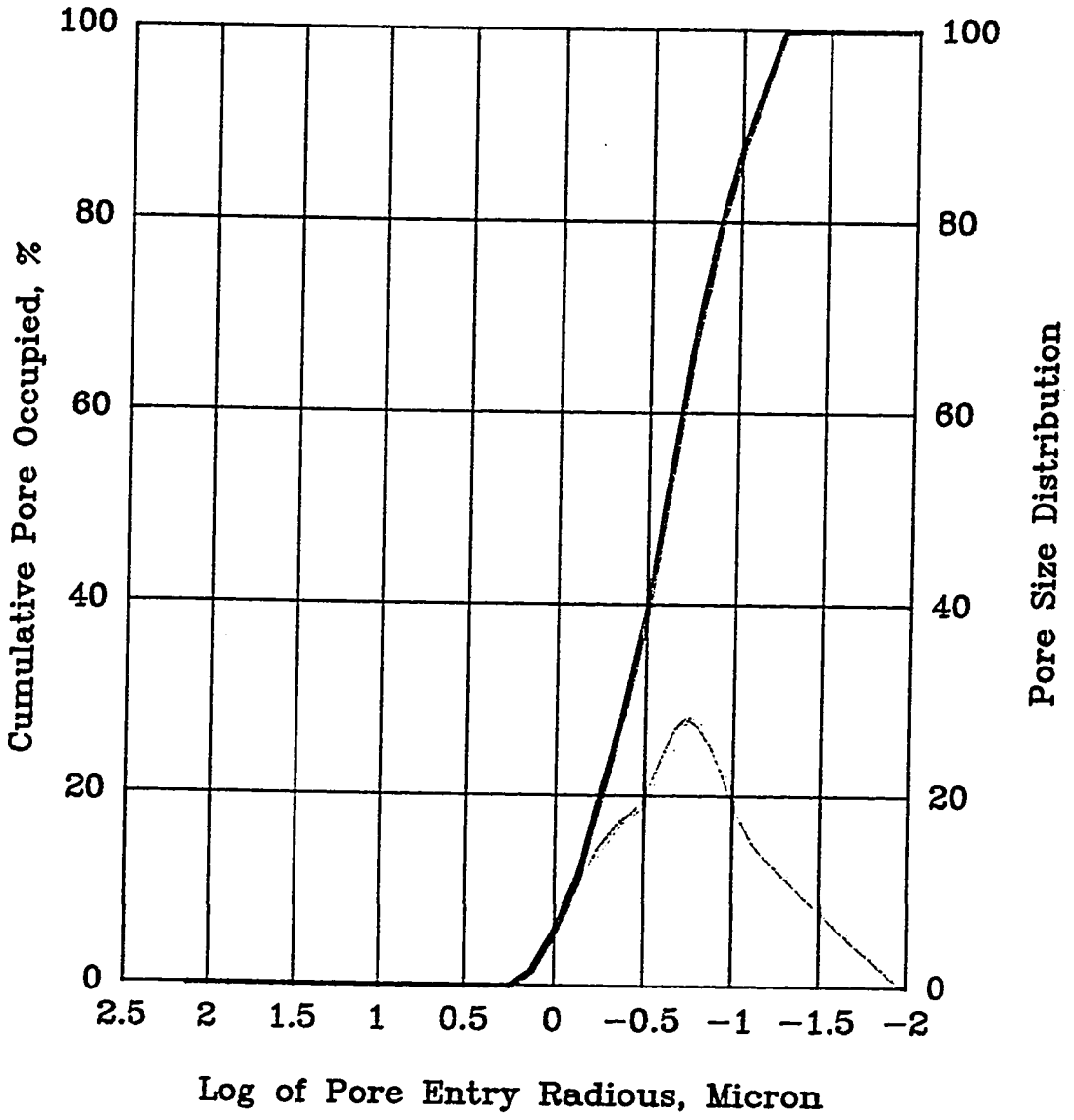

Fig (4.48). Pore Throat Size Distribution for Sample No. Carbonate−101

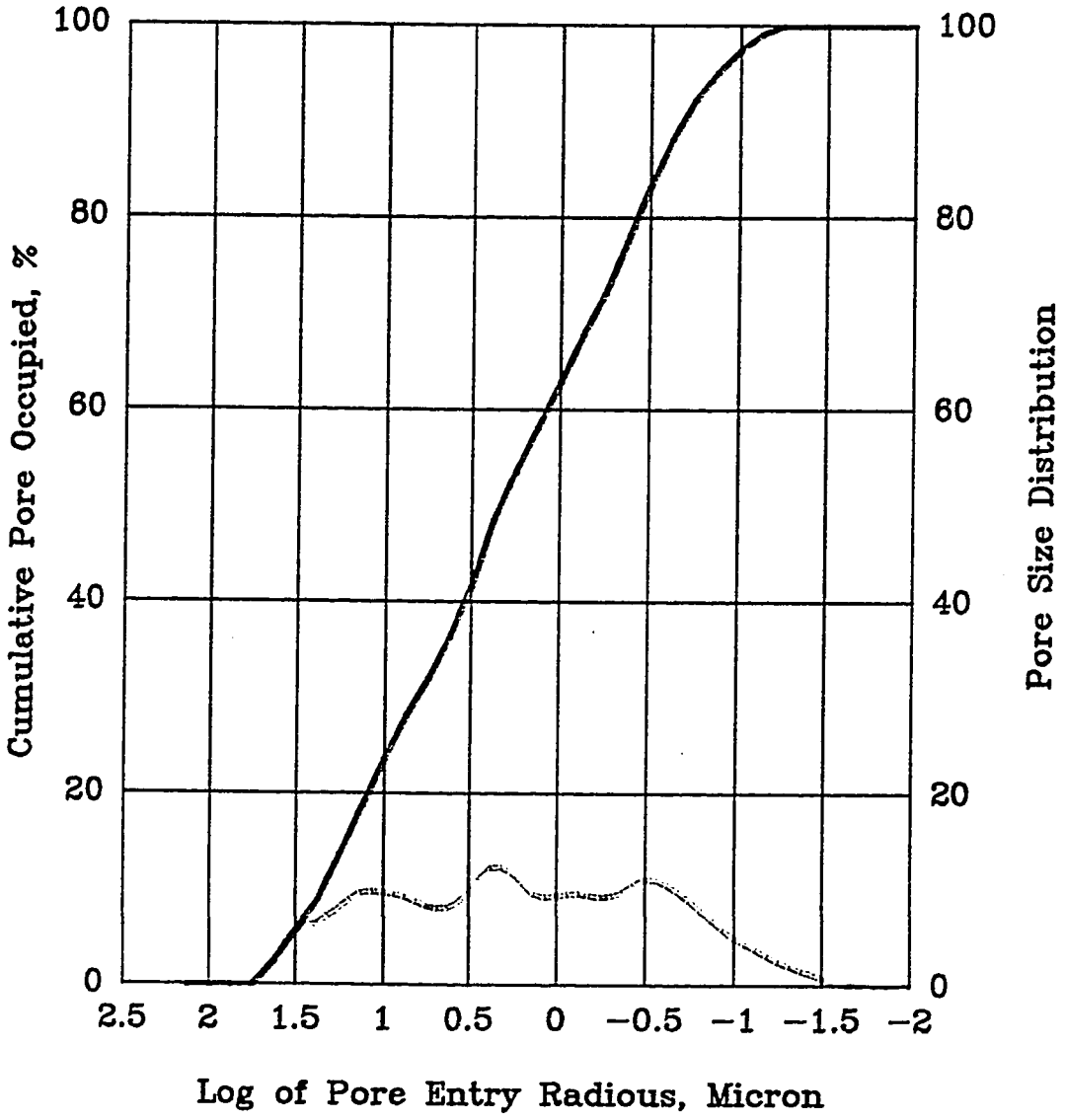

Fig (4.49). Pore Throat Size Distribution for Sample No. Carbonate−105

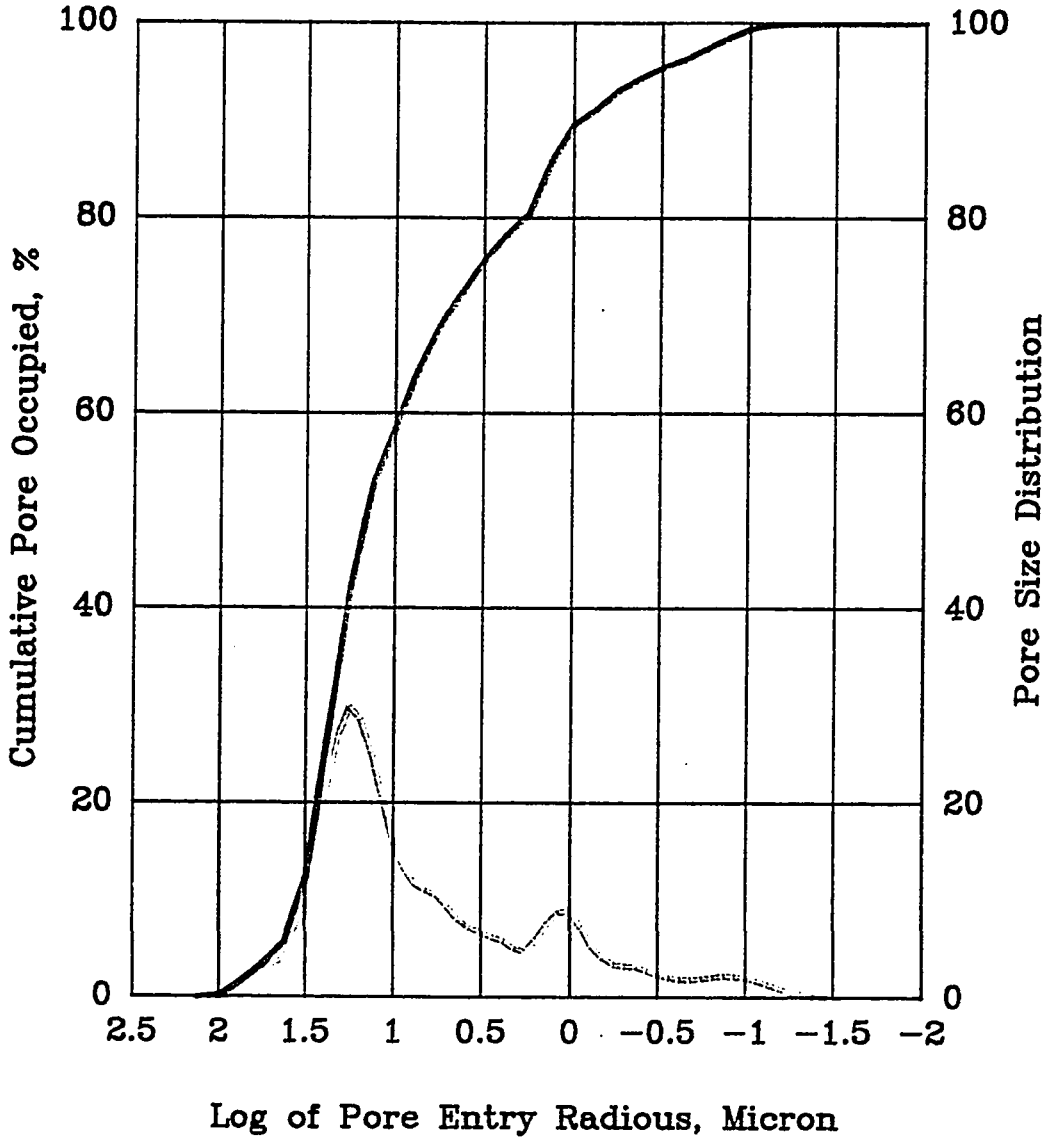

Fig (4.50). Pore Throat Size Distribution for Sample No. Carbonate−32

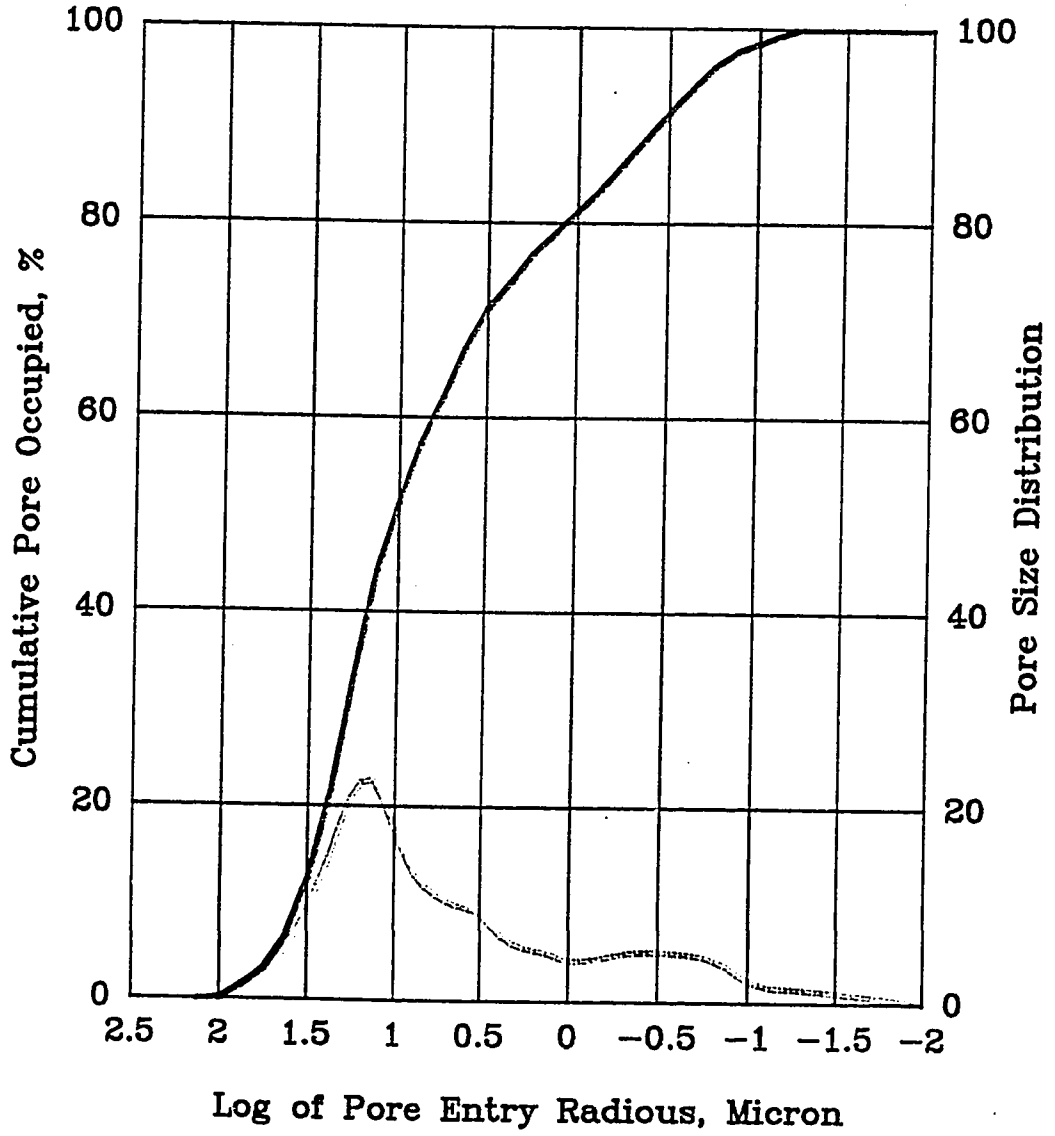

Fig (4.51). Pore Throat Size Distribution for Sample No.Carbonate−34

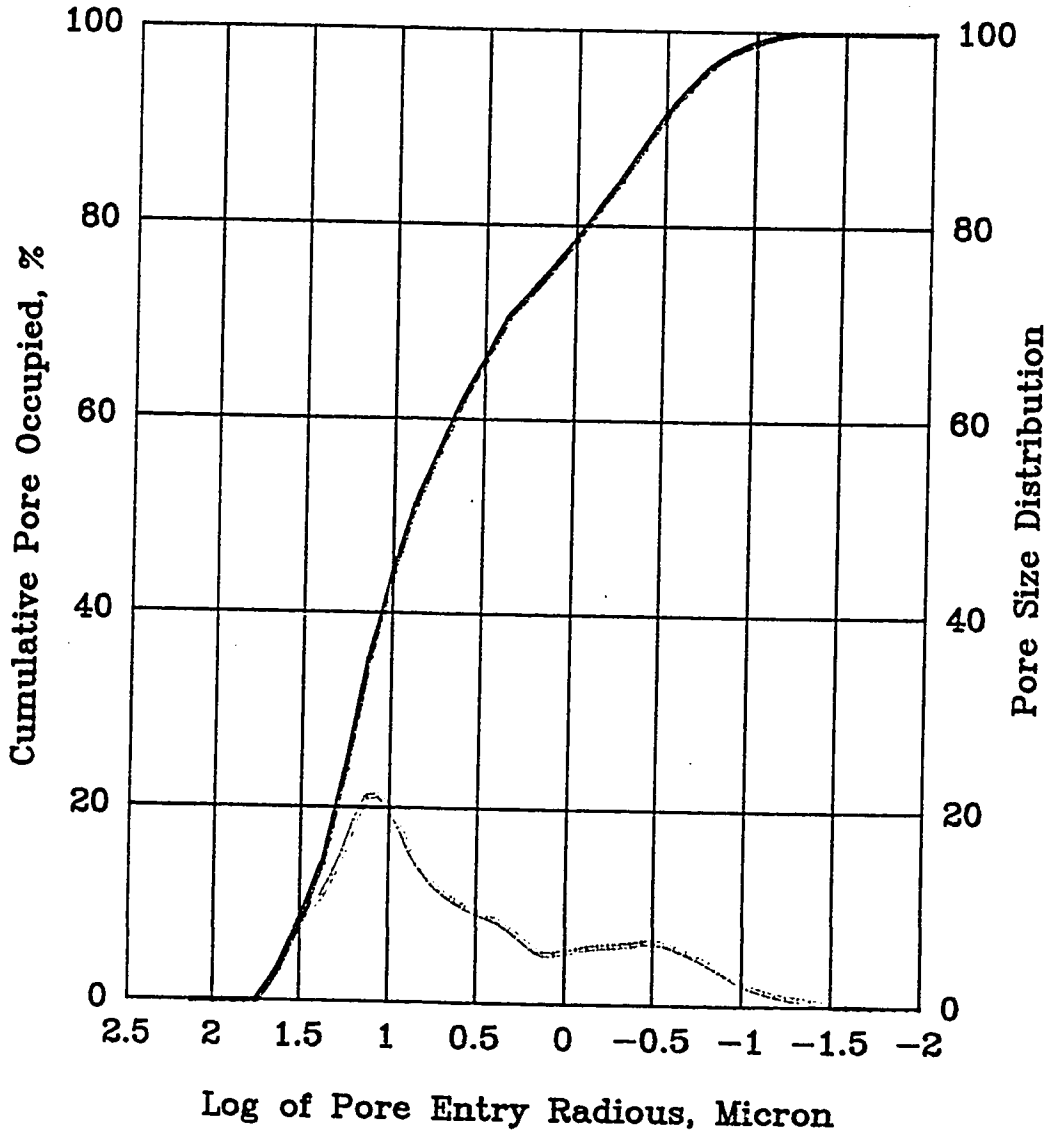

Fig (4.52). Pore Throat Size Distribution for Sample No. Carbonate–36

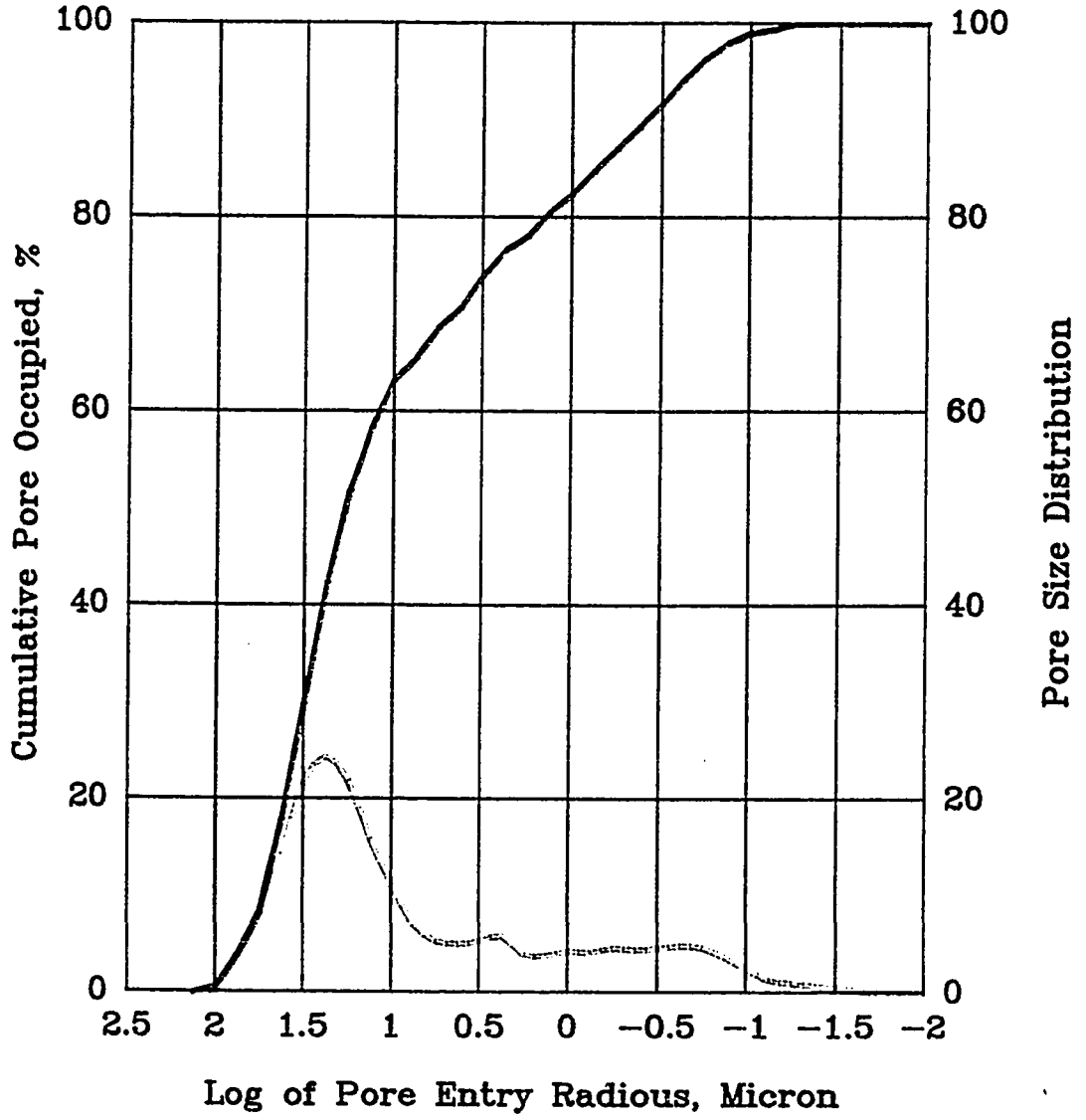

Fig (4.53). Pore Throat Size Distribution for Sample No. Carbonate−38

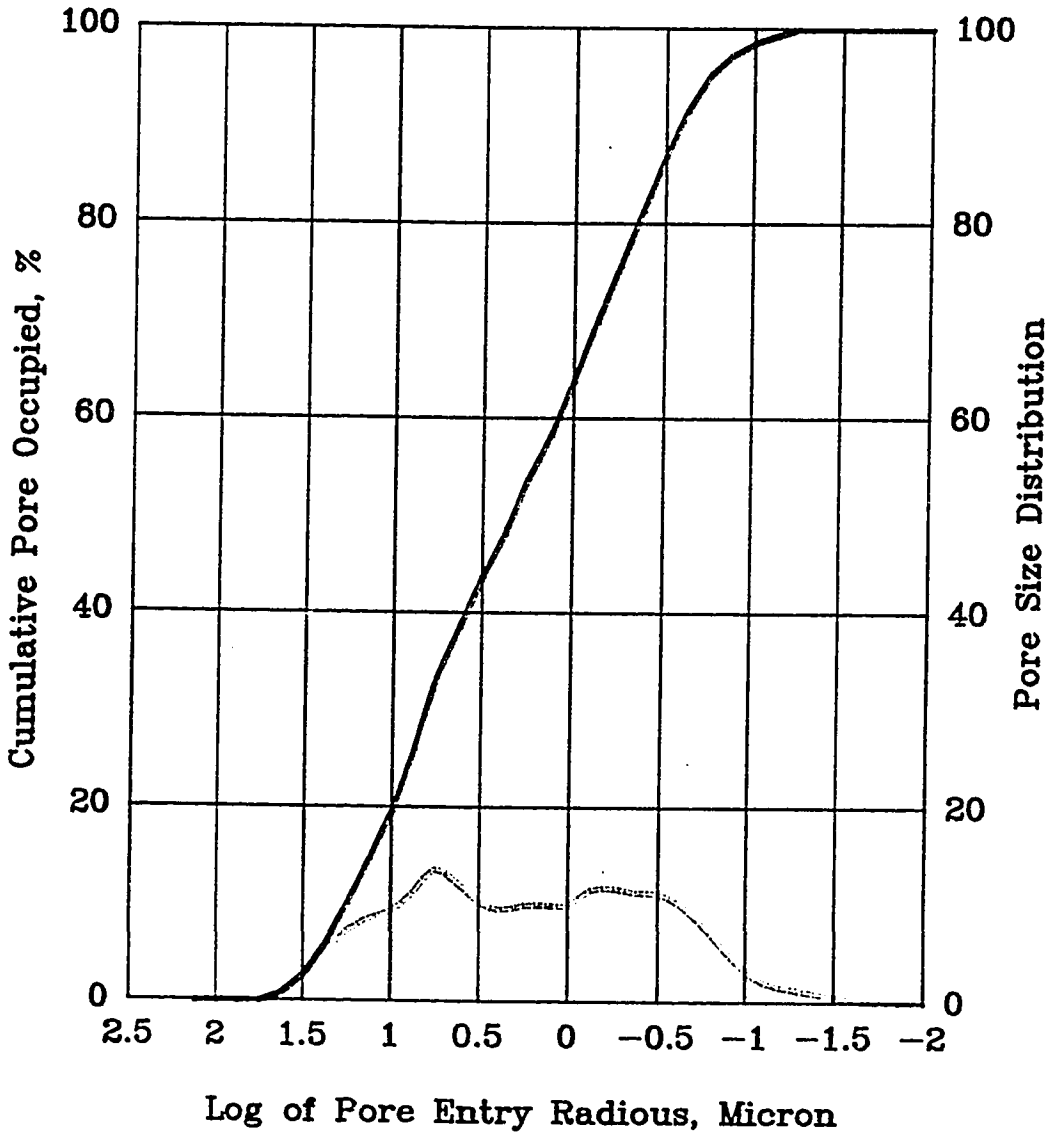

Fig (4.54). Pore Throat Size Distribution for Sample No. Carbonate−54

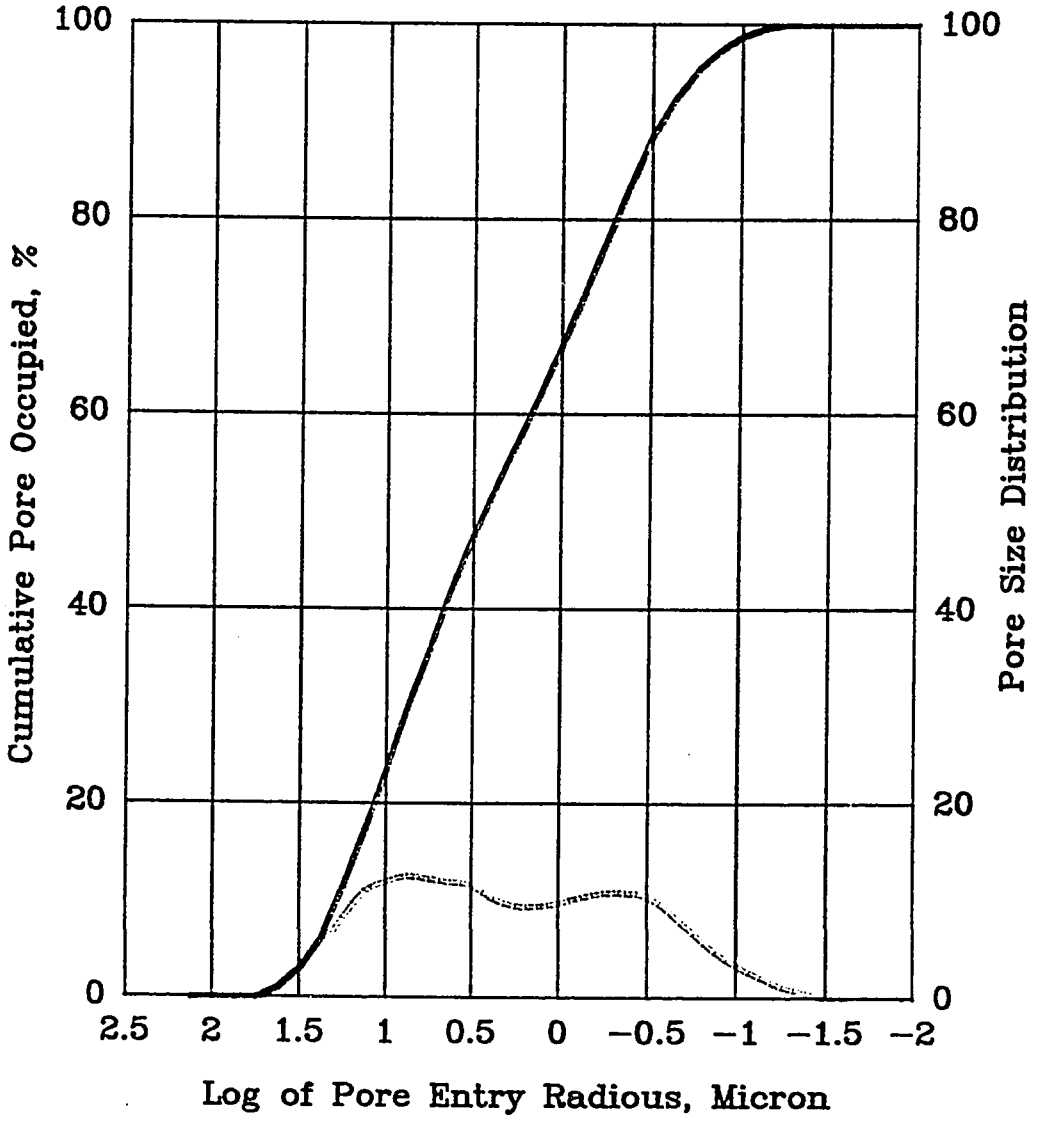

Fig (4.55). Pore Throat Size Distribution for Sample No. Carbonate−56

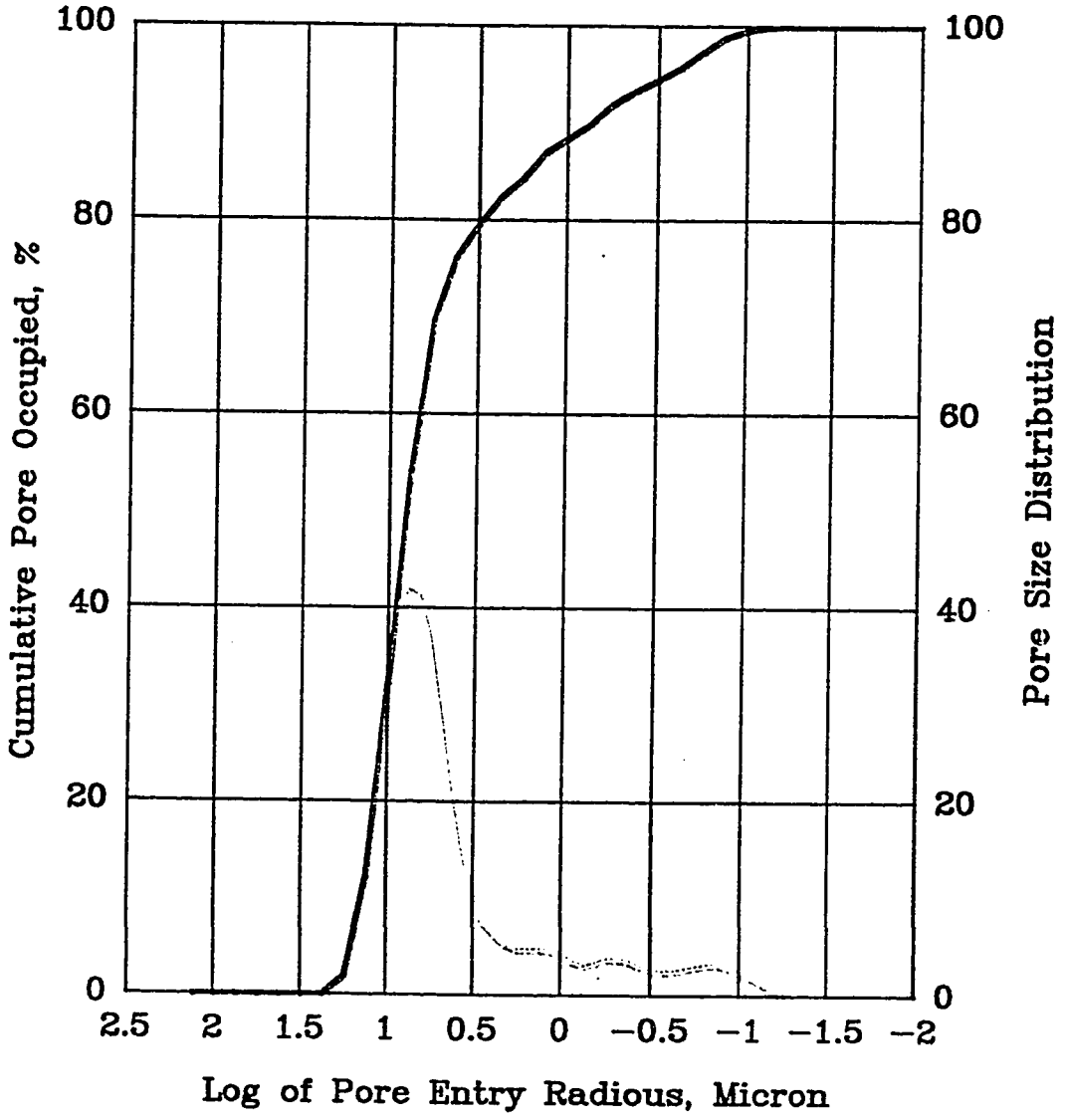

Fig (4.56). Pore Throat Size Distribution for Sample No. Berea−2 cm

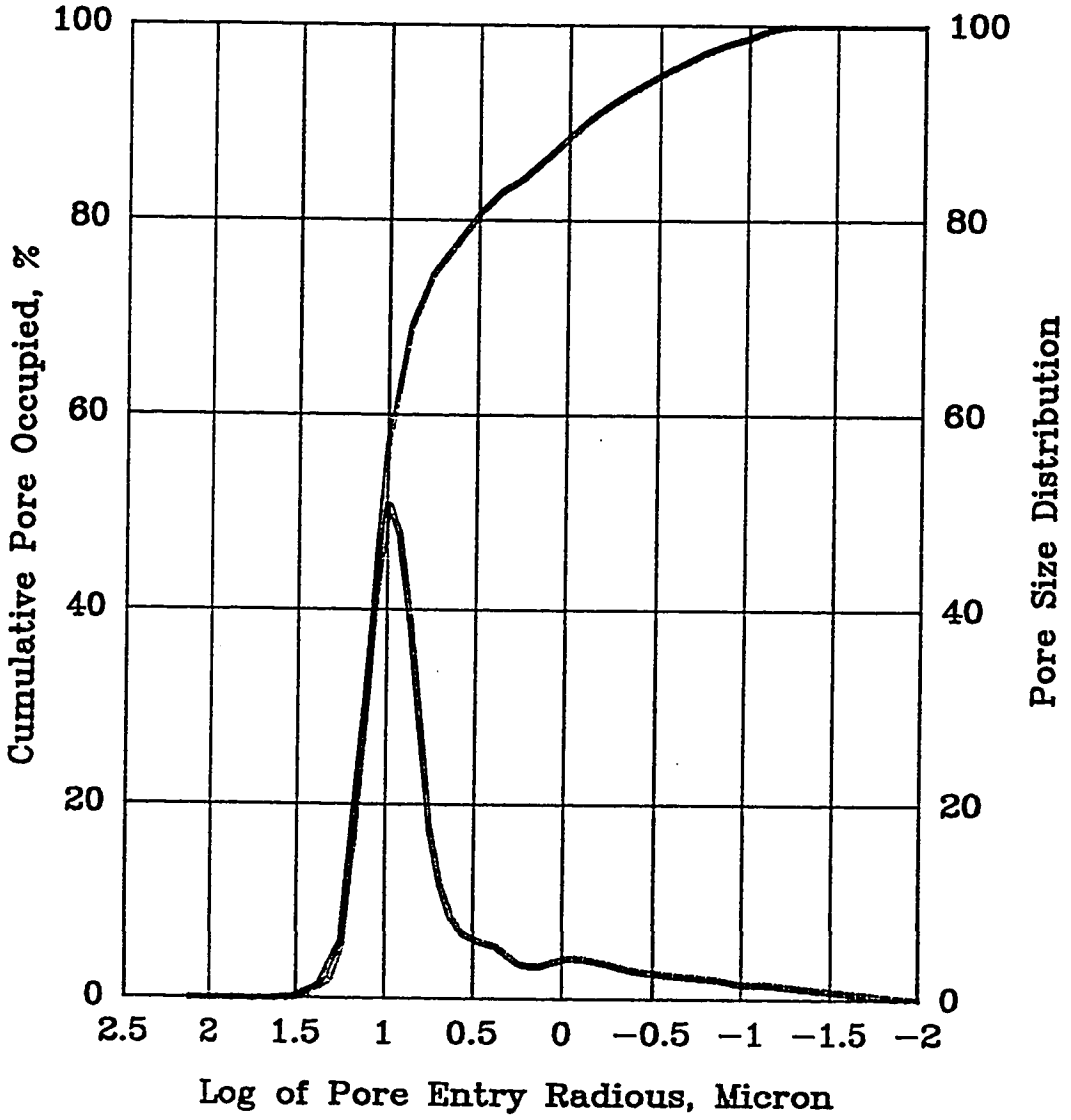

Fig (4.57). Pore Throat Size Distribution for Sample No. Berea−4 cm

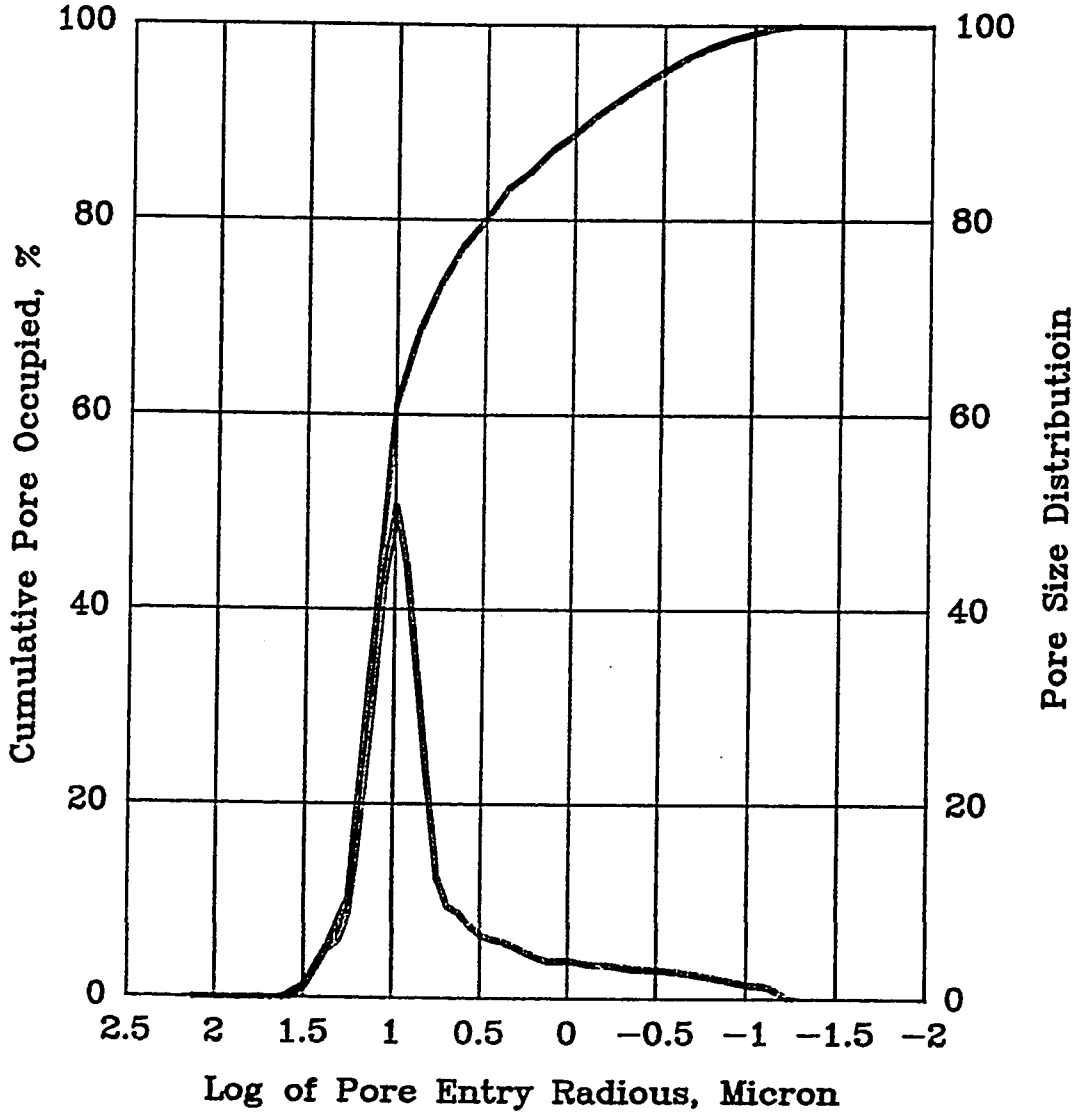

Fig (4.58). Pore Throat Size Distribution for Sample No. Berea–6 cm

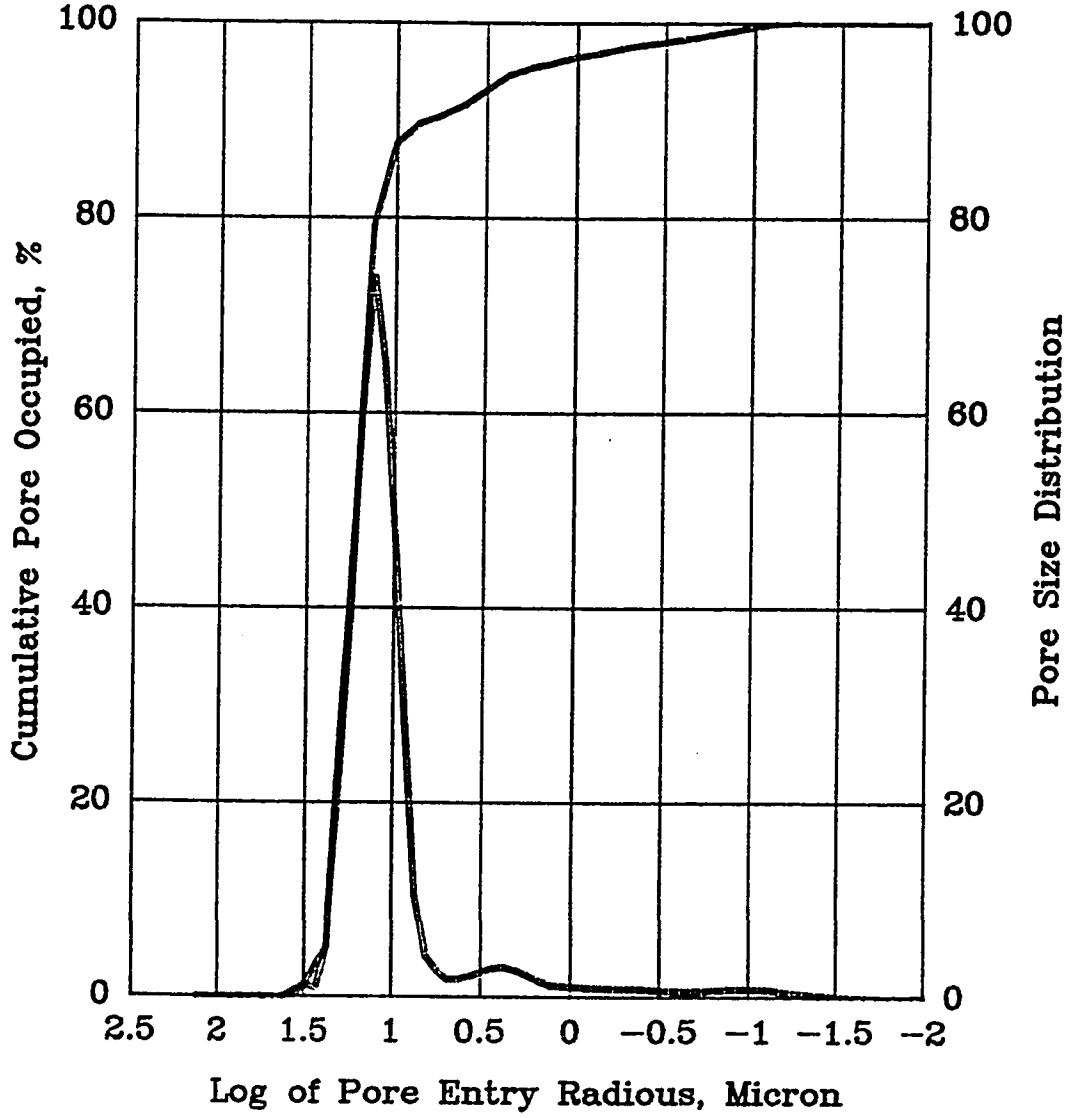

Fig (4.59). Pore Throat Size Distribution for Sample No. Bentheimer–2 cm

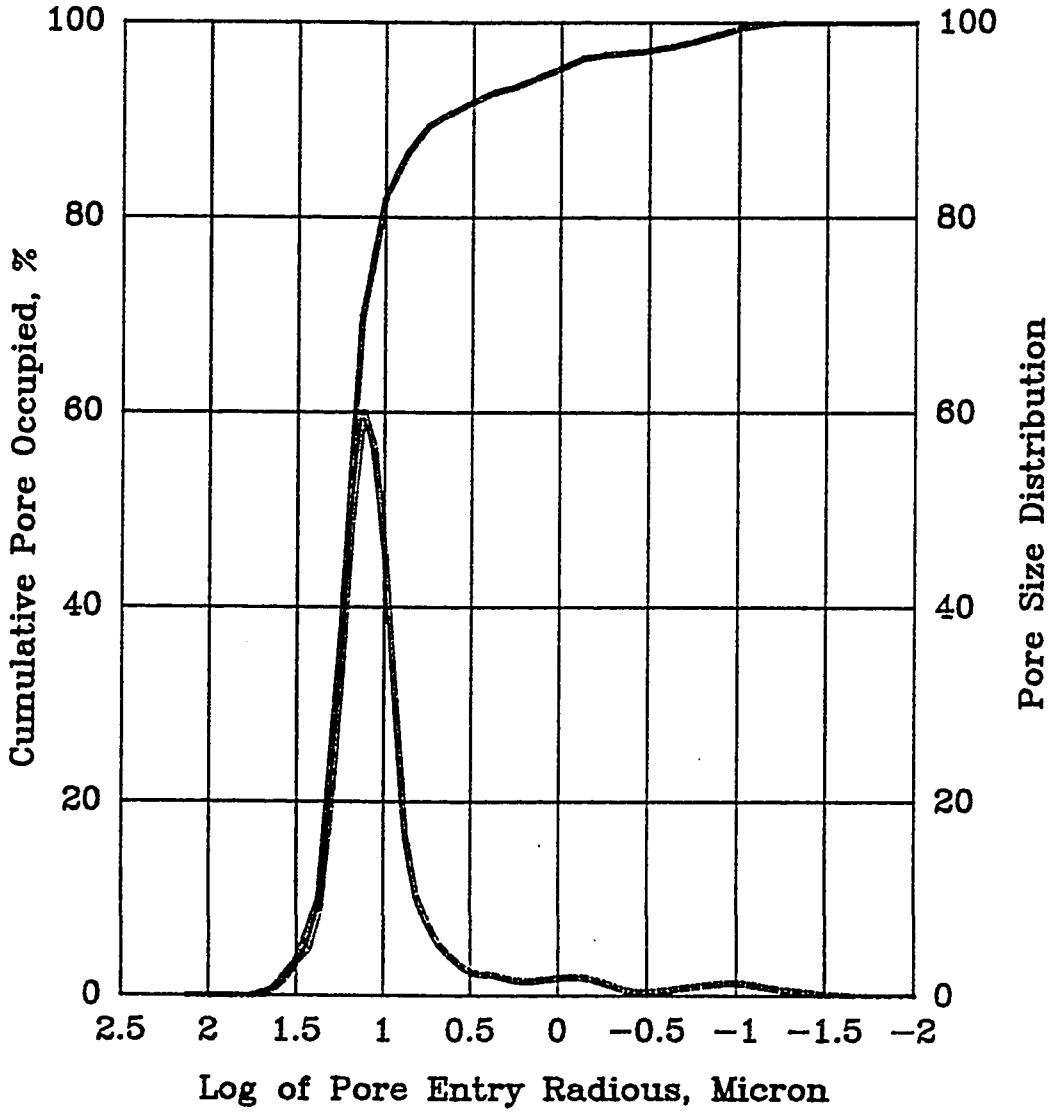

Fig (4.60). Pore Throat Size Distribution for Sample No. Bentheimer–4 cm

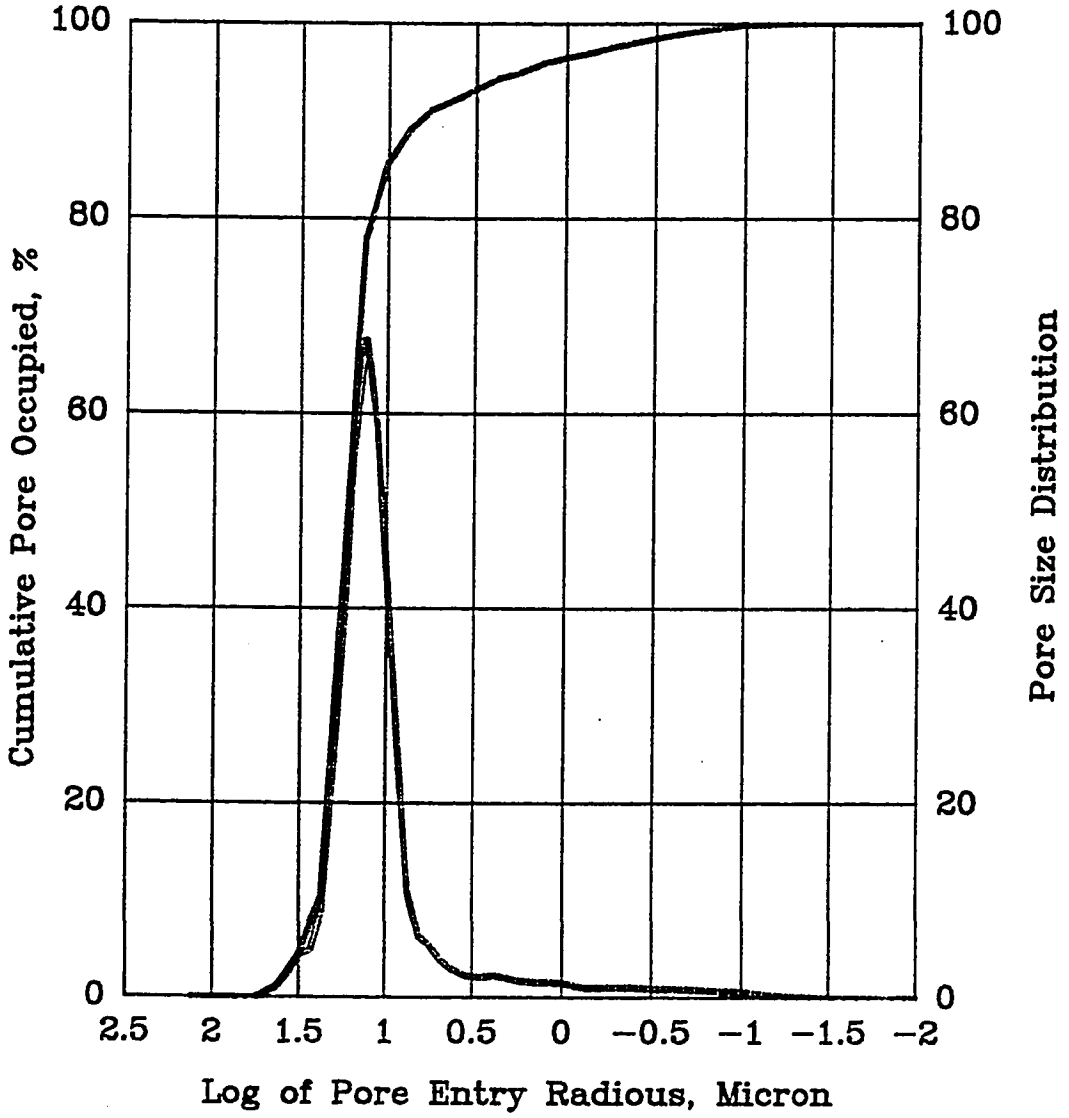

Fig (4.61). Pore Throat Size Distribution for Sample No. Bentheimer–6 cm

Table (4.3) Result Obtained From The Mercury Injection Capillary Pressure Data for Berea & Bentheimer Samples.

Sample #	Entry Pressure, psi	Displacement Pressure, psi	Swi (%)	PTS
S1	5	7	3	1.58
S6	5	7	5	1.622
S7	5	7	3	1.6
S10	3	6.5	4	1.581
S12	3	5	5	1.723
S13	2	6	5	1.57
S14	3	7	6	1.633
S16	3	7	4	1.713
S18	3	7	5	1.561
S20	3	5	6	1.754
S21	3	8	6	1.389
S22	3	7	6	1.699
B1	3	5	4	1.191
B2	3	5	6	1.136
B3	2	3	5	1.451
B4	2	4.5	3	1.149
B5	3	5	6	1.128
B6	2	4.5	5	1.269
B7	2	5	5	1.138
B8	2	4	4	1.183
B10	2	5	6	1.24
B12	2	5	6	1.257
B13	2	4.5	4	1.24
B14	2	5	5	1.178

Table (4.4) Result Obtained From The Mercury Injection Capillary Pressure Data for Carbonate samples.

Sample #	Entry Pressure, psi	Displacement Pressure, psi	Swi (%)	PTS
32	1	3	12	2.738
34	1	2	10	3.162
36	2	3.5	12	3.415
38	1	2	12	3.559
54	2	3	13	3.585
56	2	3.5	12	3.93
58	3	40	13	2.828
74	150	500	25	1.443
82A	100	200	50	1.69
82	200	300	50	1.79
90A	100	300	30	1.291
90	300	700	30	1.871
96	2	3	30	4.472
101A	30	50	45	2.582
101	60	170	45	1.86
105	2	4	5	4.472

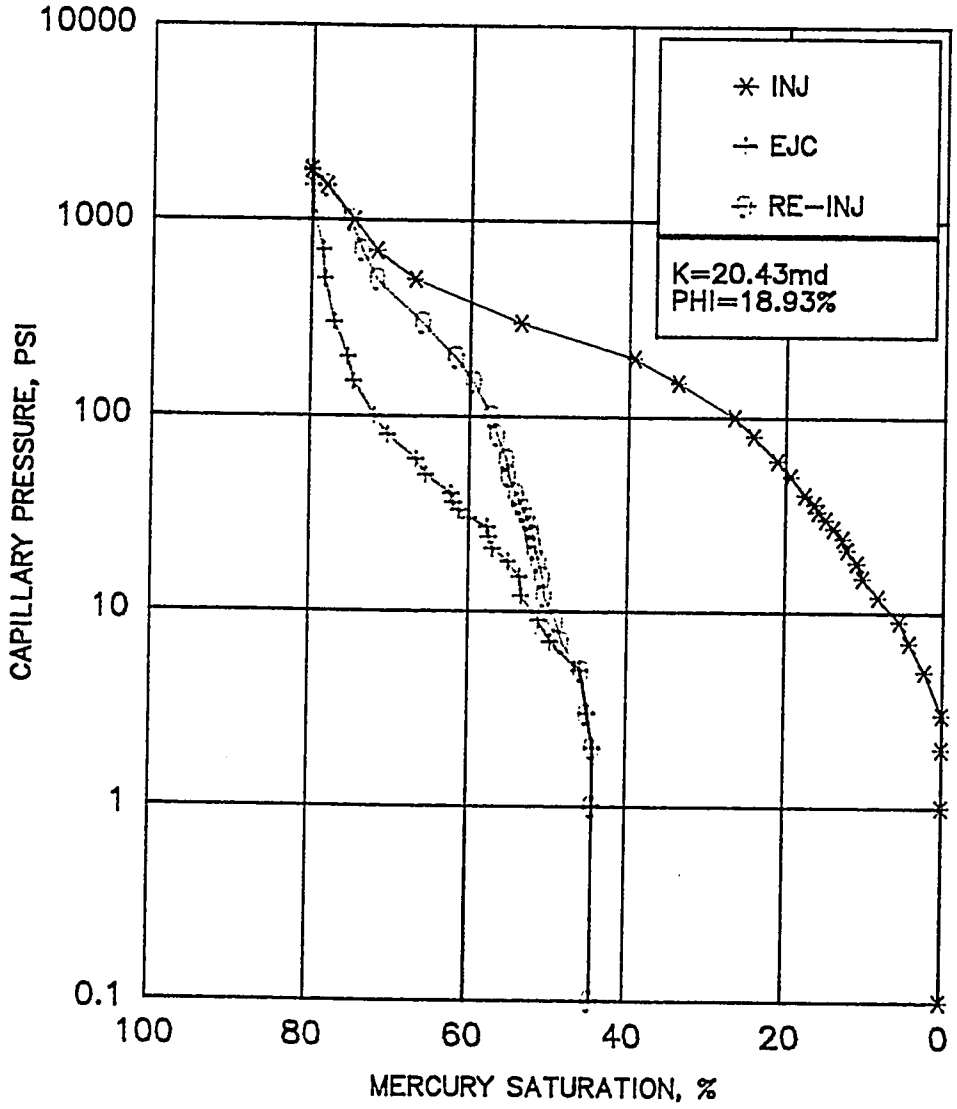

Fig(4.62). Injection, Ejection and Re-injection Capillary Pressure Curves for Carbonate Sample No. 58.

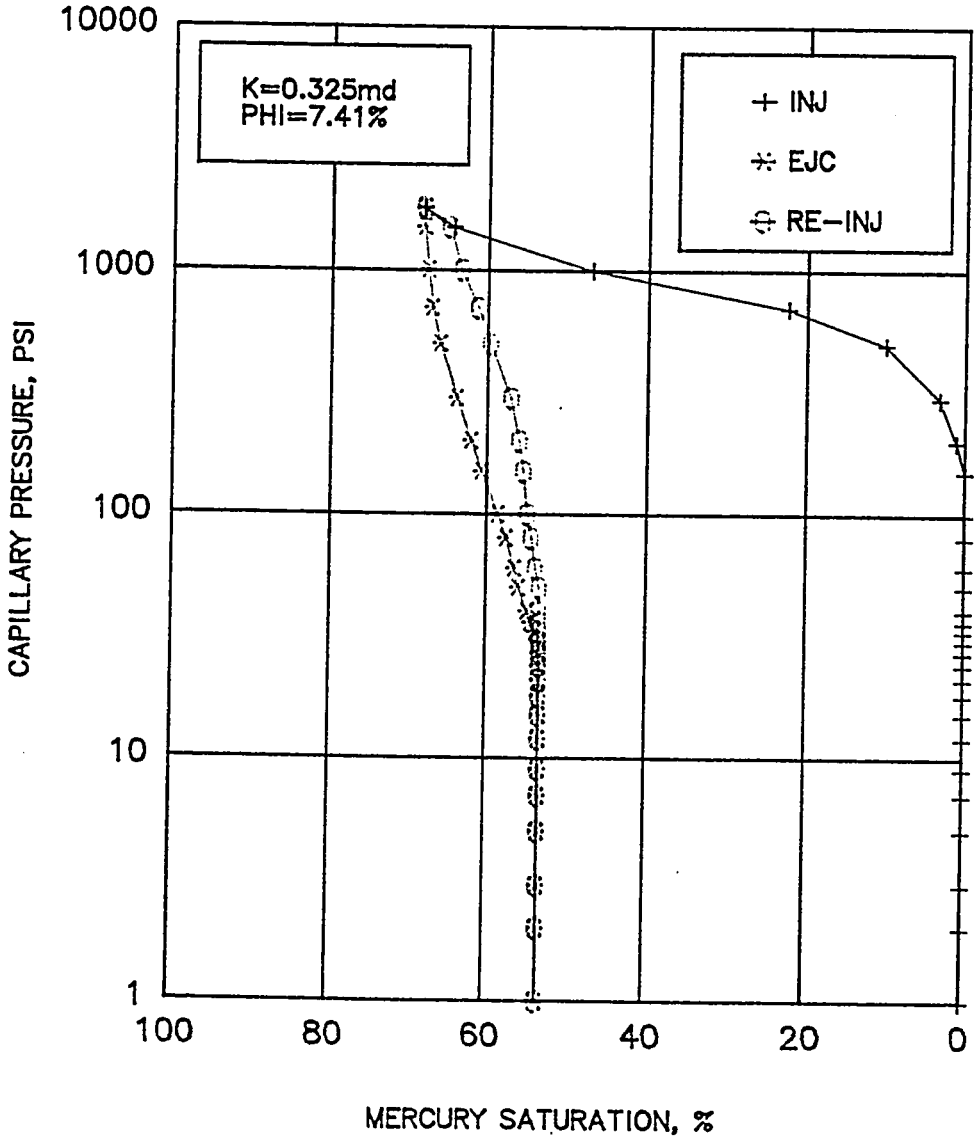

Fig(4.63). Injection, Ejection and Re-injection Capillary Pressure Curves for Carbonate Sample No. 74.

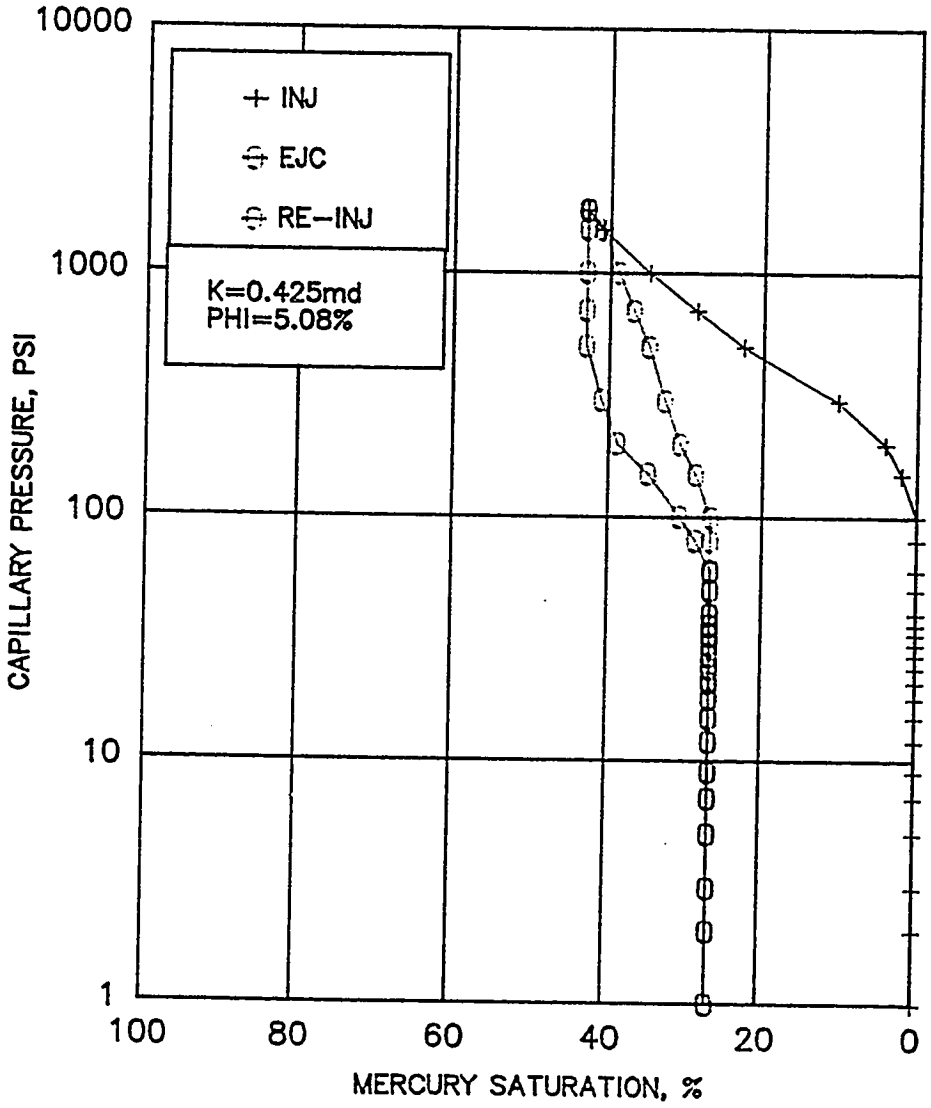

Fig(4.64). Injection, Ejection and Re-injection Capillary Pressure Curves for Carbonate Sample No. 82

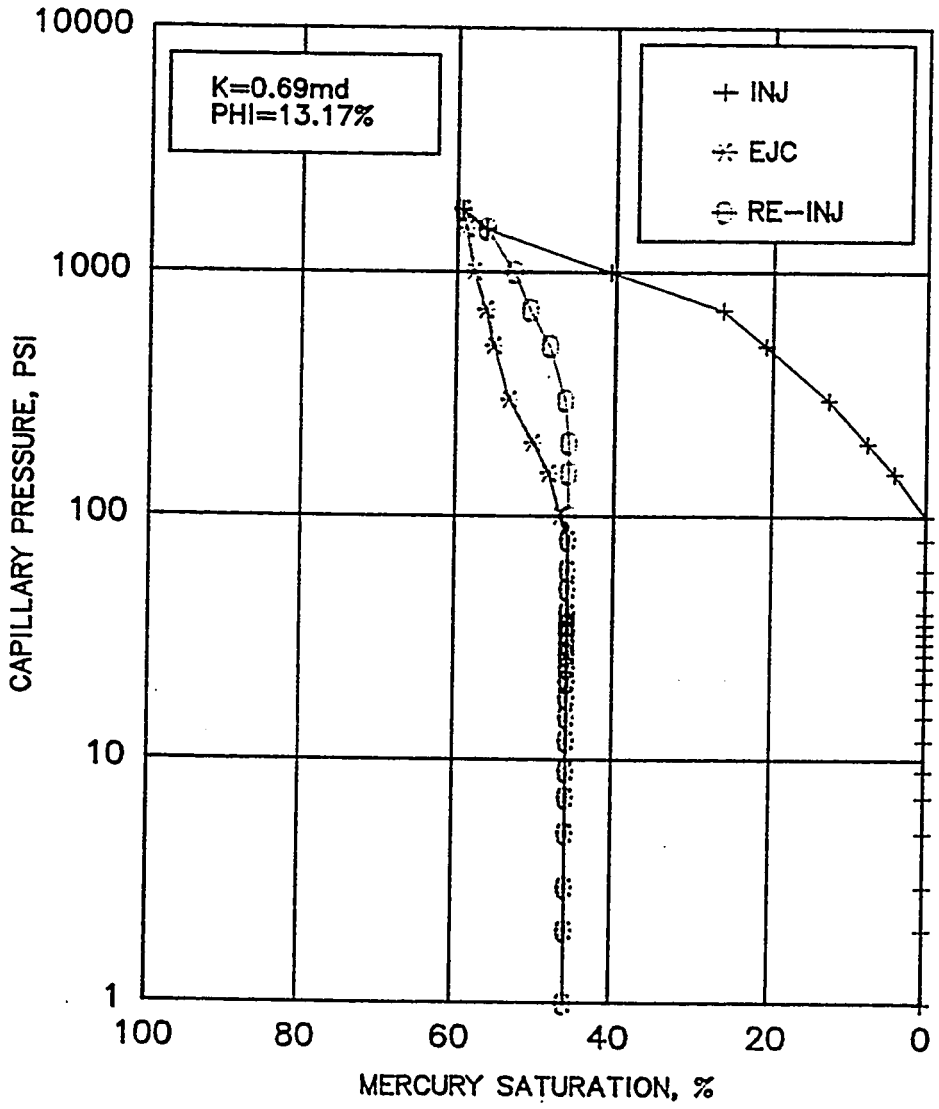

Fig(4.65). Injection, Ejection and Re-injection Capillary Pressure Curves for Carbonate Sample No. 90

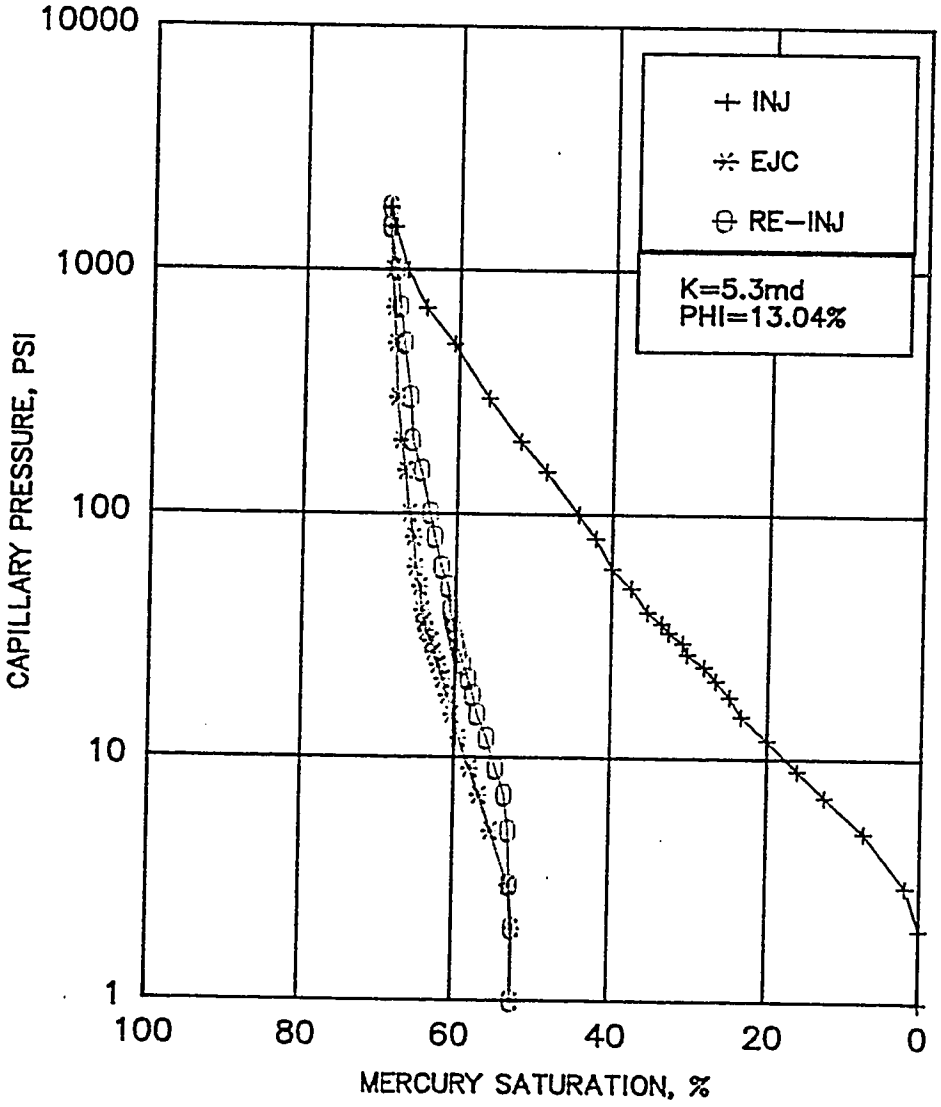

Fig(4.66). Injection, Ejection and Re-injection Capillary Pressure Curves for Carbonate Sample No. 96

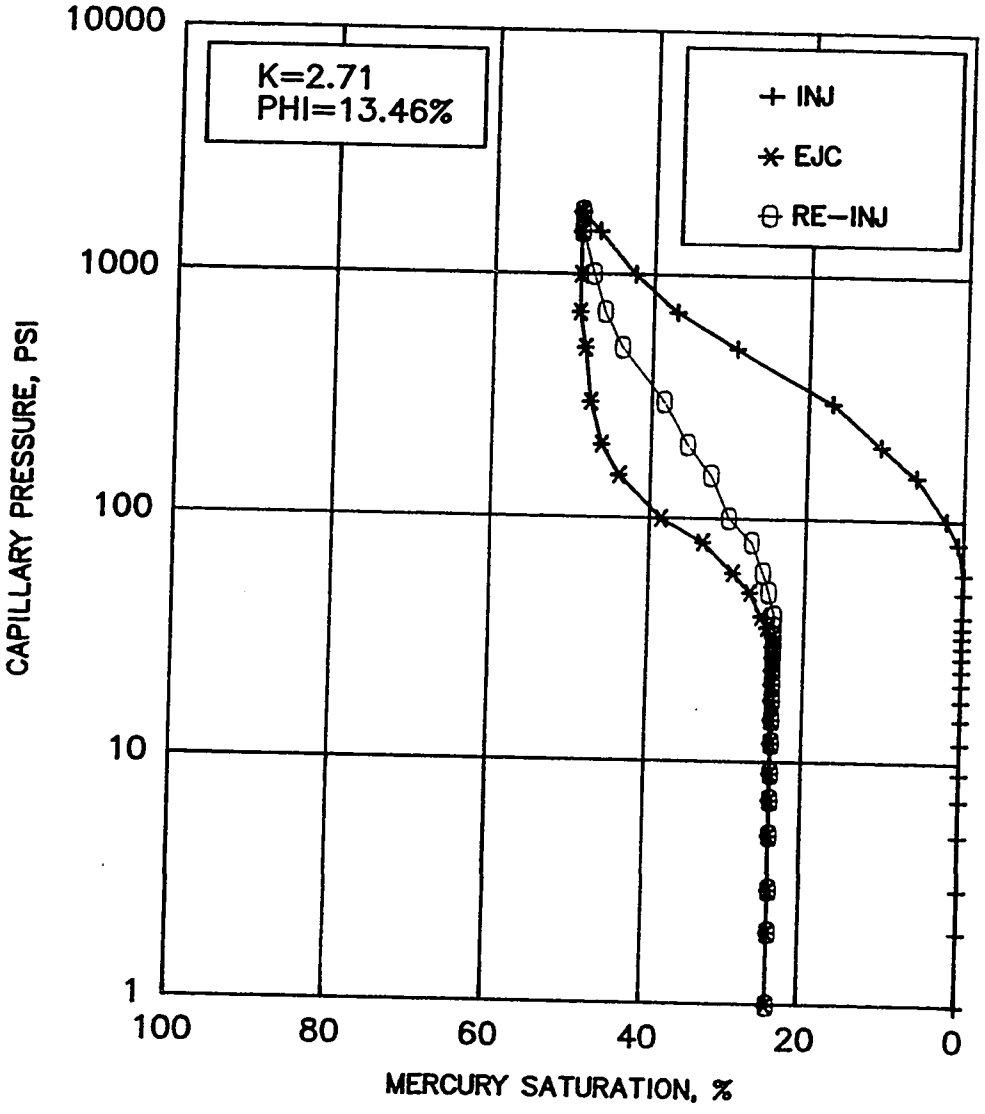

Fig(4.67). Injection, Ejection and Re-injection Capillary Pressure Curves for Carbonate Sample No. 101

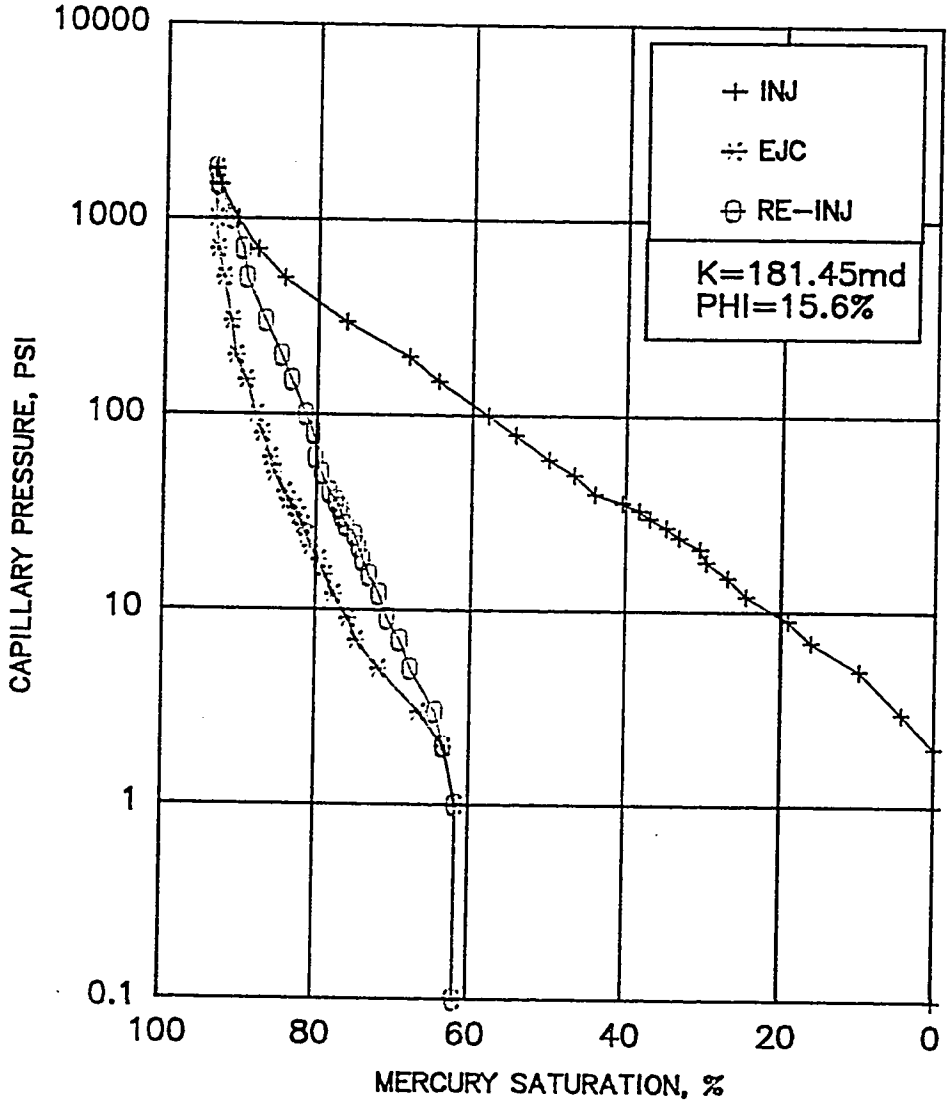

Fig(4.68). Injection, Ejection and Re-injection Capillary Pressure Curves for Carbonate Sample No. 105

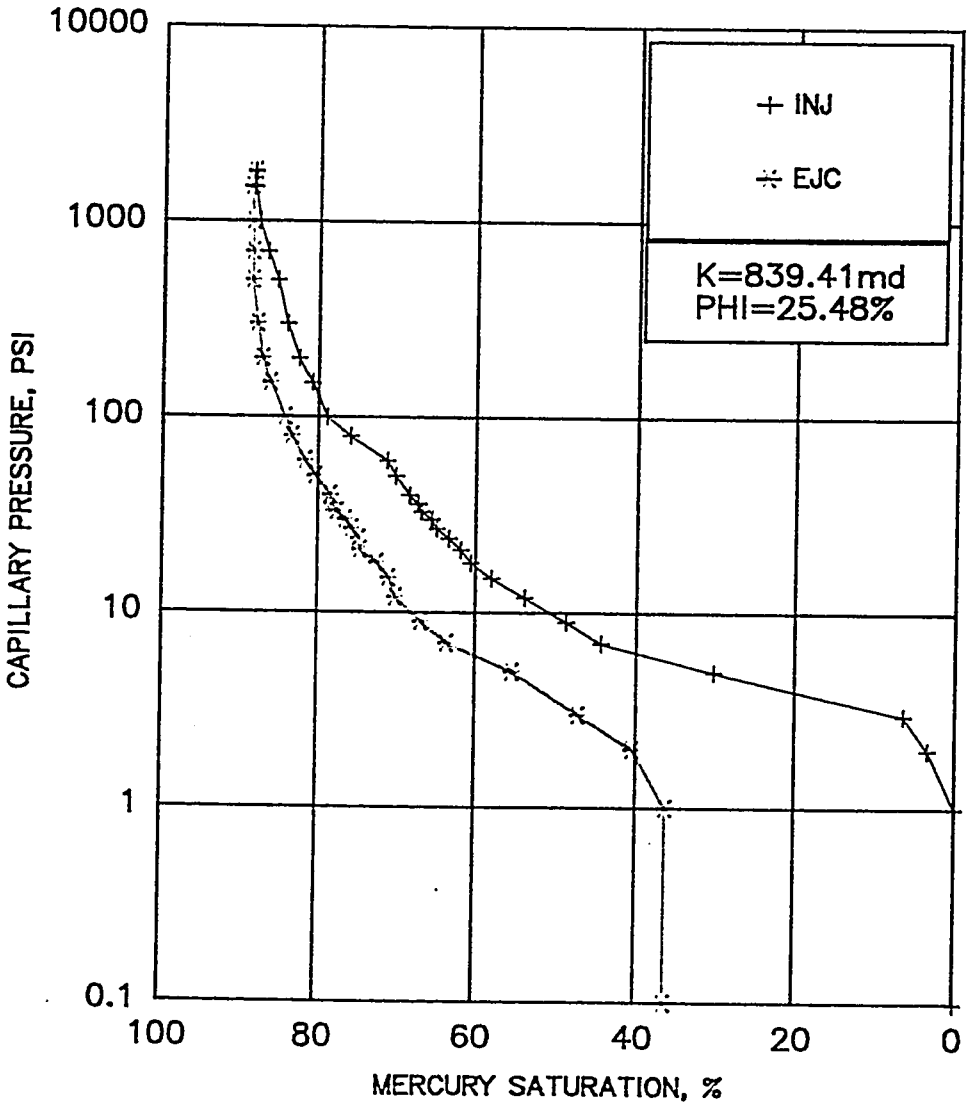

Fig(4.69). Injection and Ejection Capillary Pressure Curves for Carbonate Sample No. 32

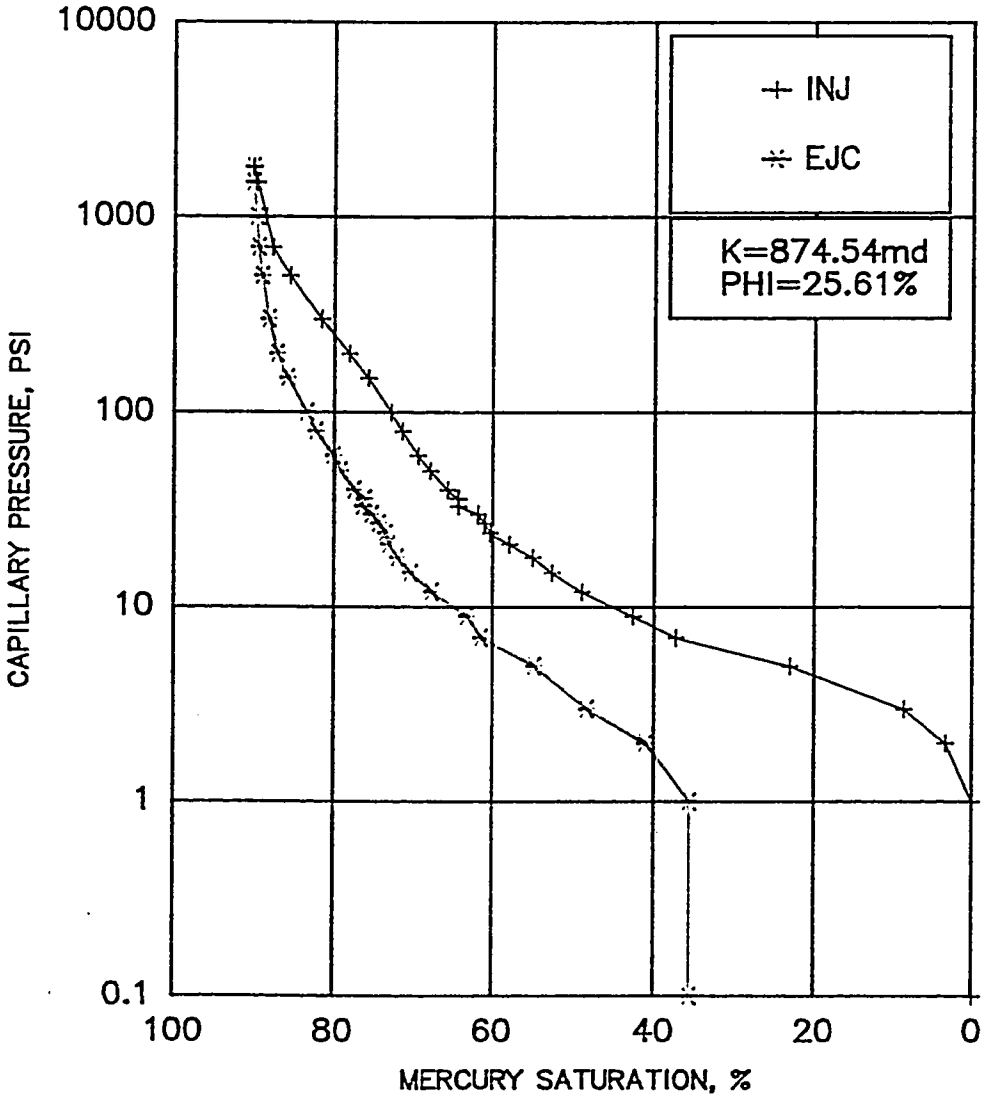

Fig(4.70). Injection and Ejection Capillary Pressure Curves for Carbonate Sample No. 34

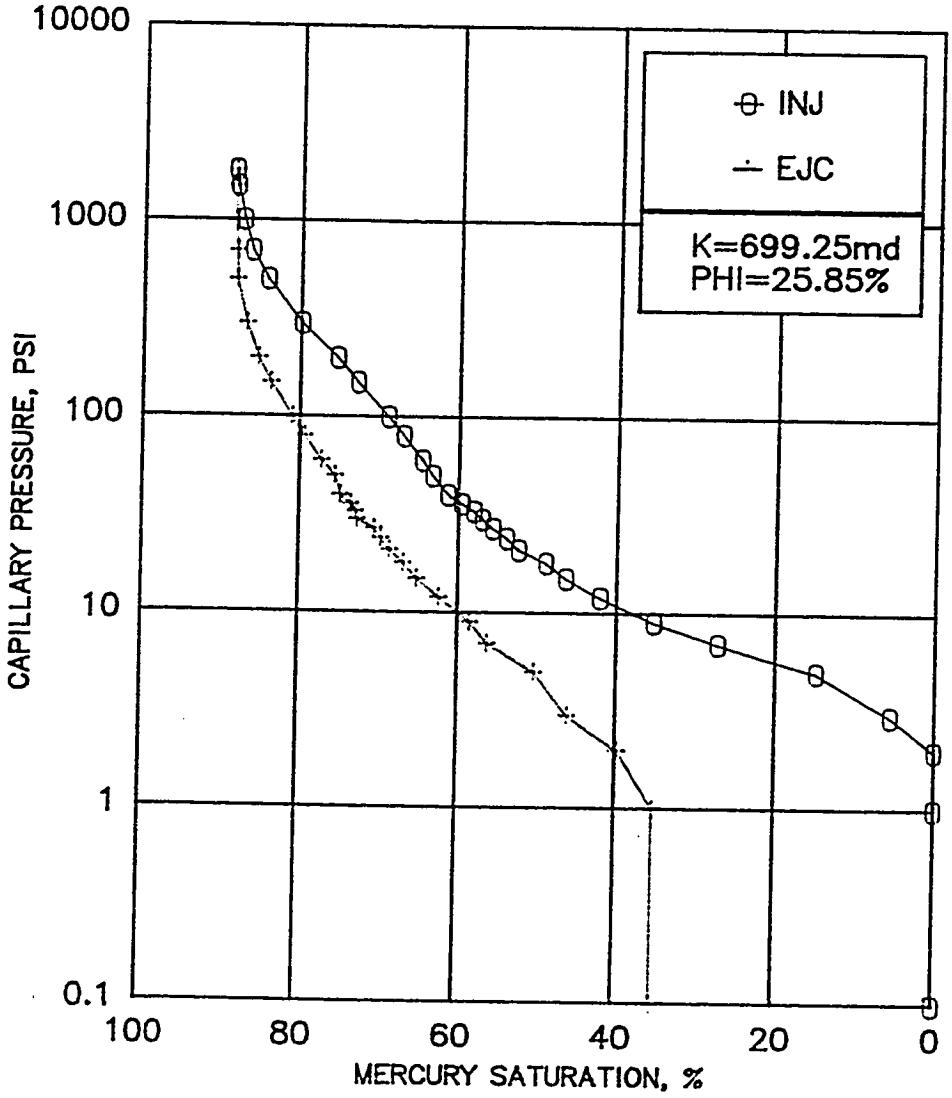

Fig(4.71). Injection and Ejection Capillary Pressure Curves for Sample No. Carbonate–36

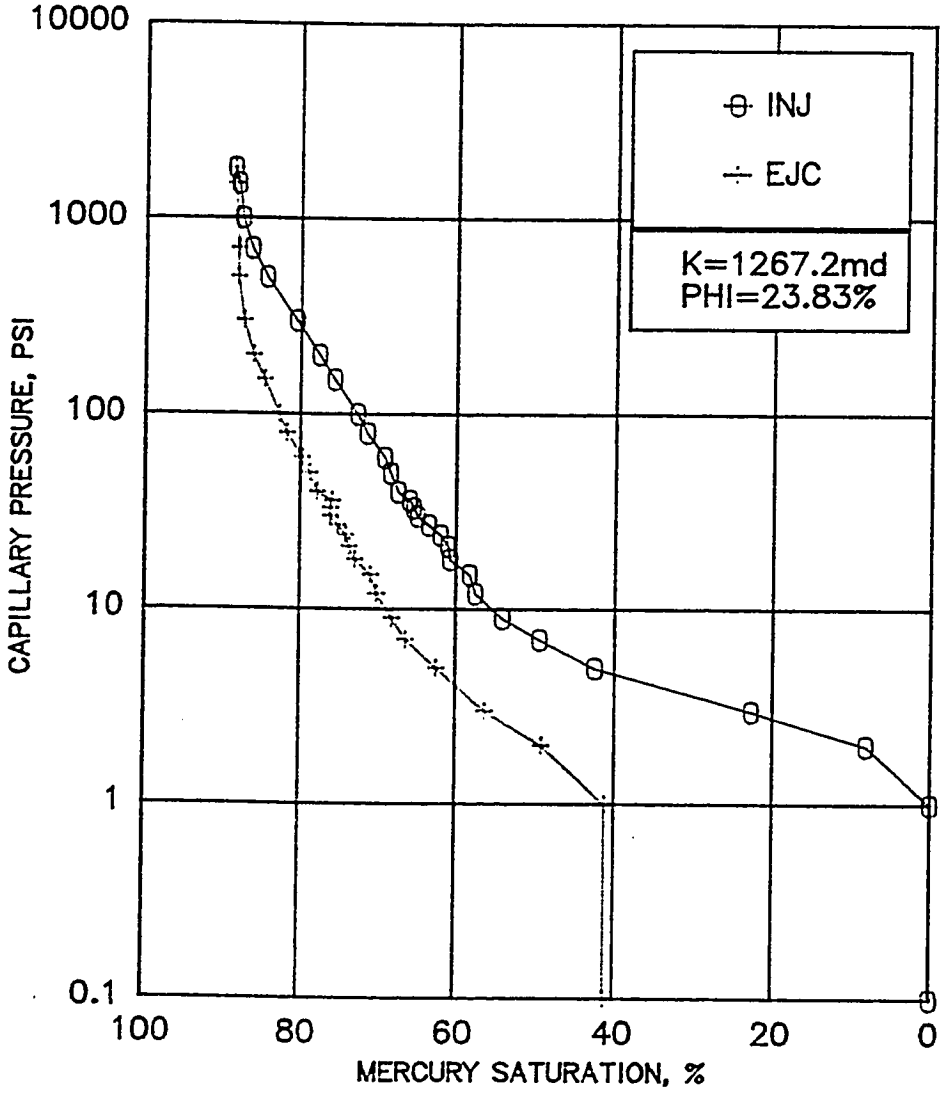

Fig(4.72). Injection and Ejection Capillary Pressure Curves for Sample No. Carbonate–38

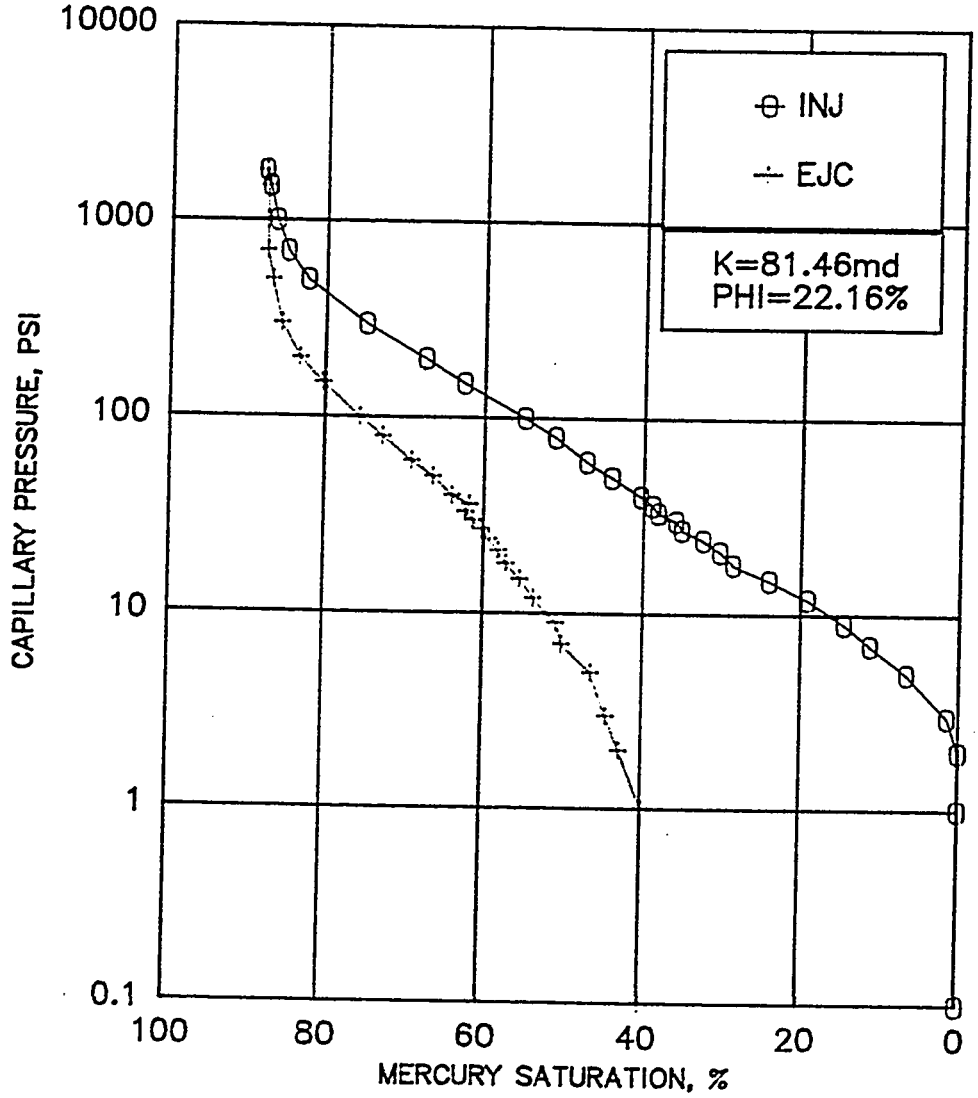

Fig(4.73). Injection and Ejection Capillary Pressure Curves for Sample No. Carbonate–54

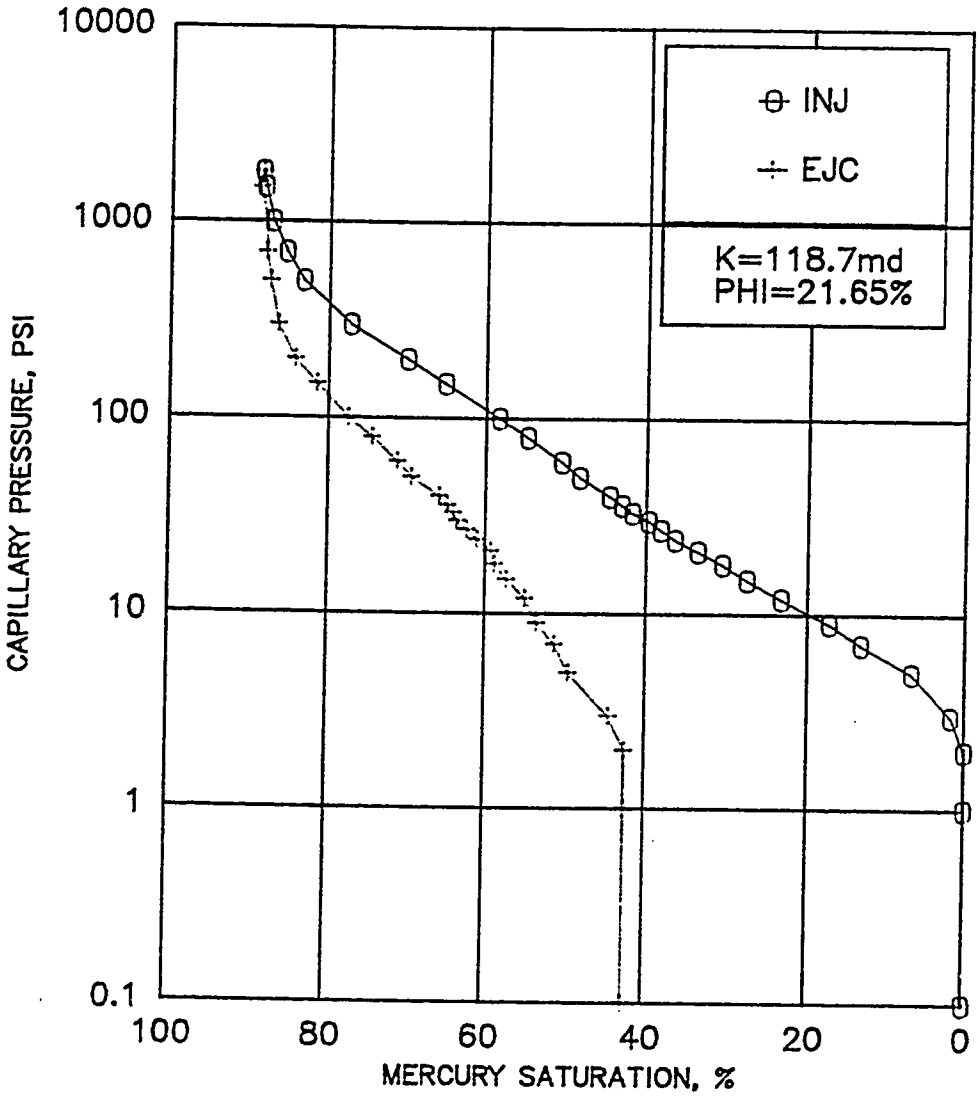

Fig(4.74). Injection and Ejection Capillary Pressure Curves for Sample No. Carbonate–56

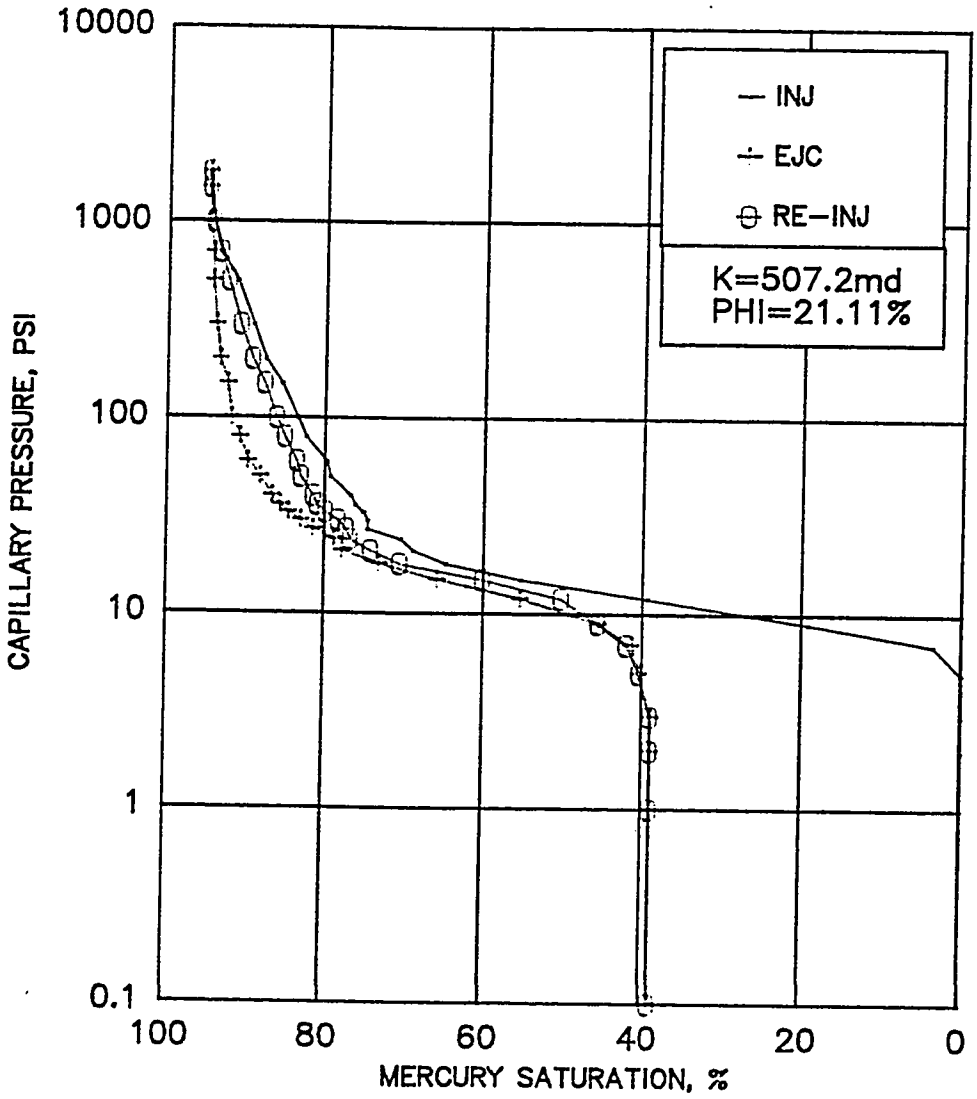

Fig(4.75). Injection, Ejection and Re-injection Capillary Pressure Curves for Sample No. Berea-2 cm

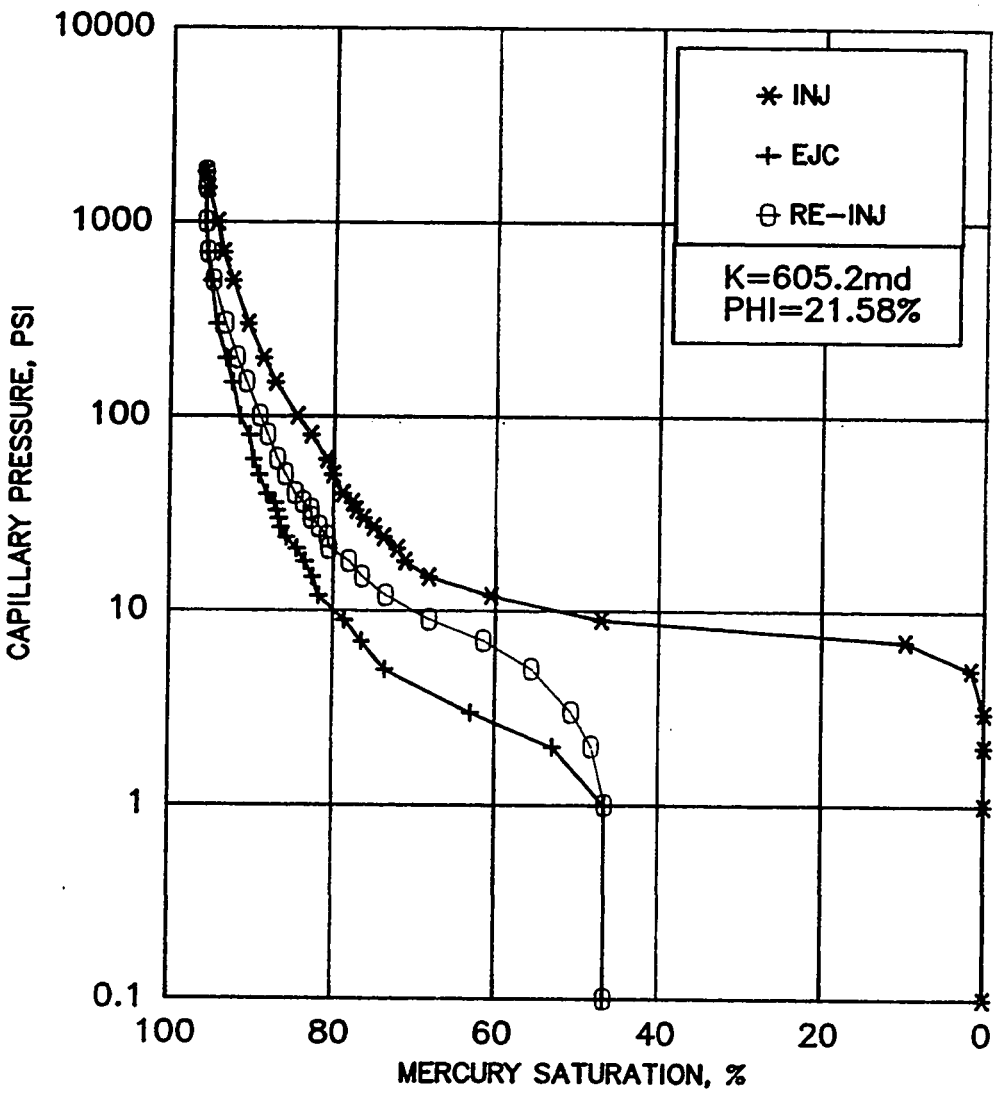

Fig(4.76). Injection, Ejection and Re-injection Capillary Pressure Curves for Sample No. Berea-4 cm

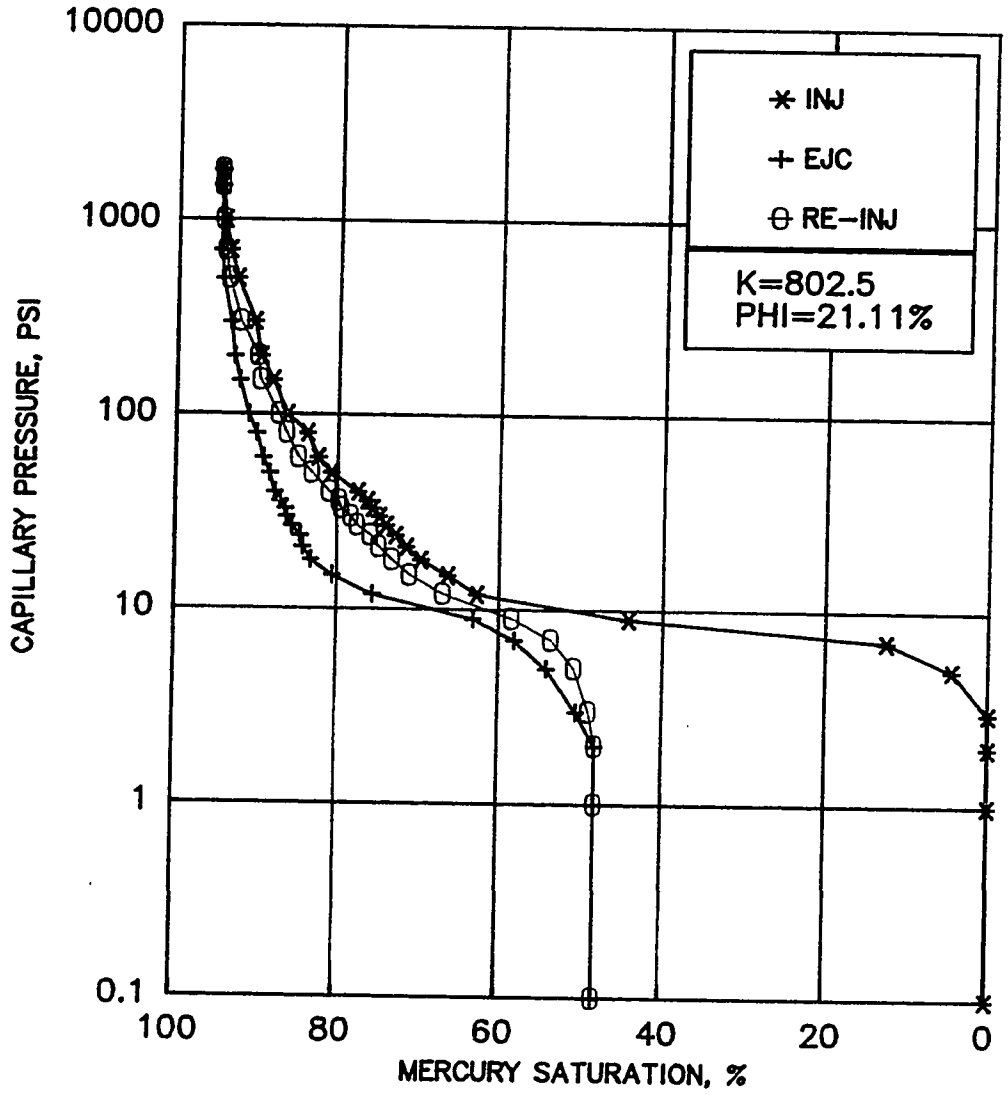

Fig(4.77). Injection, Ejection and Re-injection Capillary PressureCurves for Sample No. Berea-6 cm

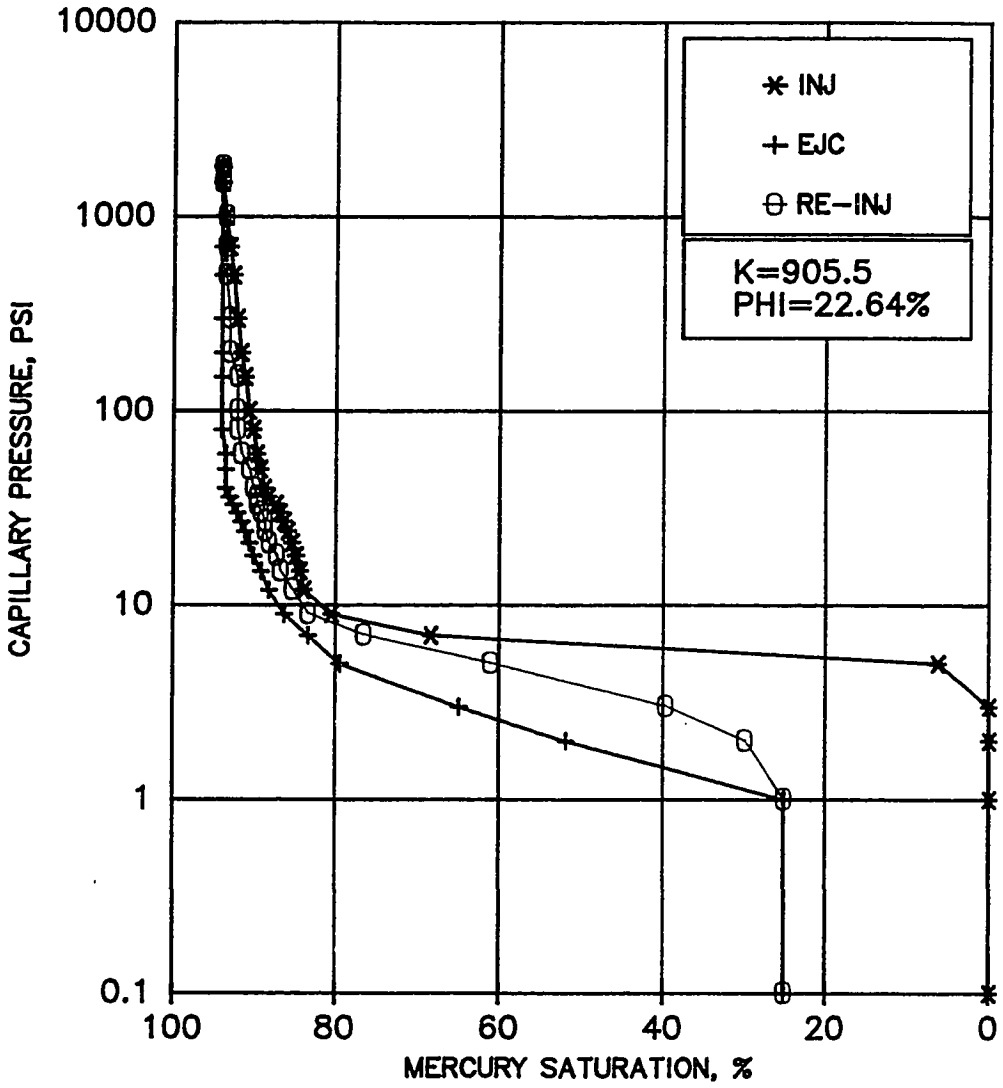

Fig(4.78). Injection, Ejection and Re-injection Capillary Pressure Curves for Sample No. Bentheimer-2 cm

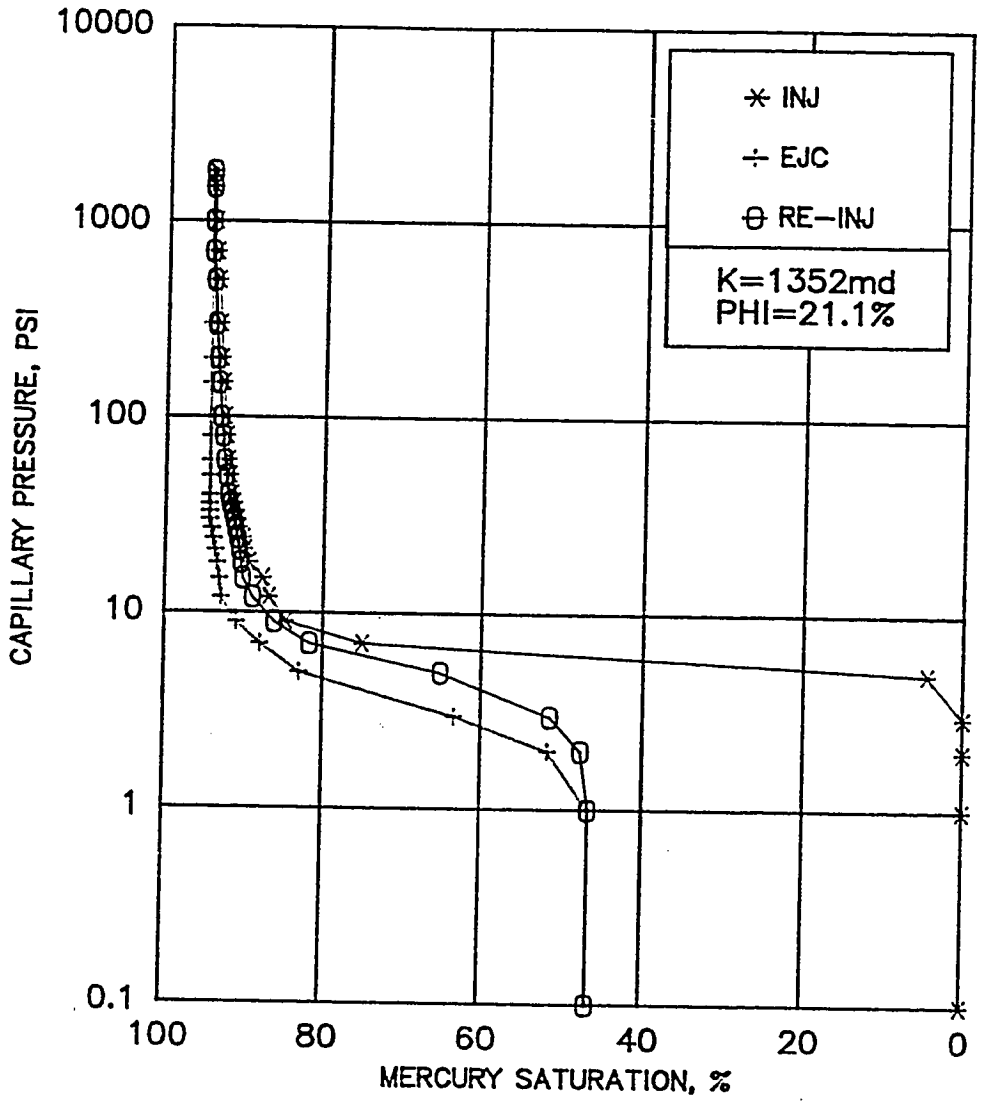

Fig(4.79). Injection, Ejection and Re-injection Capillary Pressure Curves for Sample No. Bentheimer-4 cm

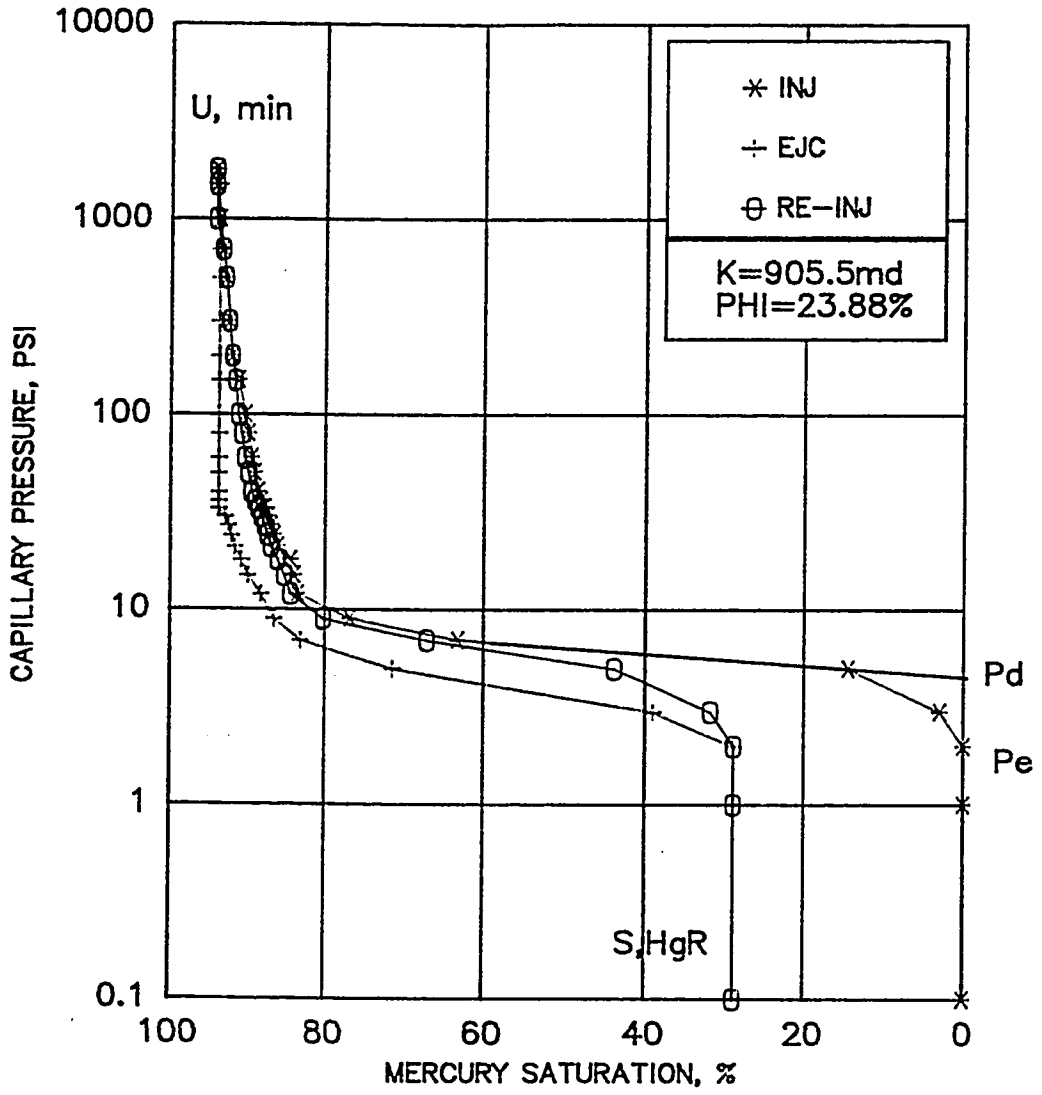

Fig(4.80). Injection, Ejection and Re-injection Capillary Pressure Curves for Sample No. Bentheimer-6 cm

sorted.

4.5 THE PARAMETERS INTERPRETED FROM CAPILLARY PRESSURE DATA

In this section, the importance of the capillary pressure data with respect to some key parameters will be discussed.

The most important parameters of the reservoir rocks are quantification of porosity and permeability but other factors which are porosity/permeability-related also help to enhance the reservoir rocks characteristic. These factors are described below and the values calculated from the capillary pressure curve are given in Tables (4.5) and (4.6).

(1) Entry Pressure - Pe

Entry pressure means an indication of the ability of the reservoir rock to accept nonwetting fluids. The sample starts to accept mercury into the pore system at this pressure.

Table (4.5) Result Obtained From The Mercury Injection Capillary Pressure Data for Berea & Bentheimer Samples.

Sample #	Umin %	Residual(Test), %	Residual (W), %	Pd	Withdrawal eff %
S1	2.21	23.89	36.27	7	75.56
S6	5.18	38.86	41.48	7	59.016
S7	2.85	29.77	30.705	6.5	69.34
S10	3.92	46.69	53.96	6.5	51.40
S12	5.16	33.91	39.21	6	64.25
S13	4.7	52.09	55.29	6.5	45.35
S14	5.43	48.23	45.15	6.5	49.01
S16	3.85	52.945	47.90	6.5	44.93
S18	5.103	48.198	34.42	4.5	49.21
S20	5.69	30.83	47.29	7.00	67.31
S21	5.37	30.81	53.21	7.5	67.44
S22	5.60	44.93	58.77	6.5	52.41
B1	3.78	25.41	38.27	5.00	73.60
B2	5.83	25.24	30.22	5.00	73.20
B3	5.12	32.07	32.56	3.00	66.20
B4	2.99	34.48	45.40	5.00	64.45
B5	5.59	46.58	37.67	6.50	50.66
B6	5.3	49.61	34.37	5.00	47.62
B7	4.77	37.84	42.65	5.00	60.26
B8	3.71	34.62	30.04	6.5	64.04
B10	5.8	28.86	64.90	5.0	69.37
B12	5.79	34.30	54.77	5.00	63.59
B13	4.83	39.88	74.67	4.5	58.10
B14	5.25	44.08	29.17	5.00	53.48

Table (4.6) Result Obtained From The Mercury Injection Capillary Pressure Data for Carbonate Samples

Sample #	Umin %	Residual(Test), %	Residual(W), %	Pd, psi	Withdrawal eff %
32	11.64	36.21	40.35	3	59.02
34	9.83	35.54	38.53	3	60.58
36	11.69	35.28	37.92	3.5	60.05
38	11.79	41.03	41.37	2	53.48
54	12.17	39.90	42.53	5	54.57
56	11.56	42.46	44.18	3	51.99
58	20.00	44.2	49.43	40	44.75
74	31.91	53.19	61.17	500	21.87
82A	57.08	26.57	96.35	200	38.10
82	56.40	19.82	148.81	300	54.55
90A	42.76	31.01	118.56	700	45.83
90	40.67	45.64	66.24	100	23.08
96	30.91	52.12	42.62	3	24.56
101A	49.18	32.94	84.73	100	35.19
101	50.62	23.92	67.22	170	51.56
105	6.52	61.68	61.34	4	34.01

(2) **Withdrawal Efficiency - W_d**

Withdrawal efficiency is expressed as :

$$W_d = \frac{Vol.\ of\ H_g\ extract\ sample\ at\ min.\ Pr.}{Vol.\ injected\ at\ max.\ Pr.}$$

It is an indication of the ability of the reservoir rock to release nonwetting fluids. Withdrawal efficiency strongly depends on residual mercury saturation. Withdrawal efficiency decreases with the increase in the residual saturation.

(3) **Unsaturated Pore Volume - U_{min}**

Unsaturated pore volume is the percentage of the pore volume that is not invaded by mercury at the maximum pressure attained (2000 psi).

(4) **Pore Throat Sorting - PTS**

Pore throat sorting means an evaluation of the uniformity of the pore throat size distribution.

The parameters as mentioned above can be obtained from the injection and withdrawal capillary pressure curves and are identified in Fig. (4.80).

(5) **Residual Non-wetting Phase Saturation - $S_{Hg R}$**

This is the volume of mercury remained in the pore system at the time when the minimum pressure was attained (0 psi).

(6) **The Displacement Pressure - P_d**

This is the pressure at which there is an abrupt change of gradient of the injection curve as a substantial volume of mercury begins to enter the sample. It can be estimated by extending the slope of the plateau to the right side of the y-axis.

(7) **Throat Size Diameter - d_T**

The capillary pressure corresponding to the throat diameter is given by the following expression :

$$P_c = \frac{4\sigma Cos0}{d_T}$$

The results from the Figs. (4.62) through (4.80) show that most of the sandstone samples with large withdrawal efficiency $W_d(>60)$ have relatively low displacement pressures ($\leq 7 psi$) However, the unsaturated pore volumes ($U_{\min}$) ranging from 2.2 to 5.6 were observed for those samples.

Examination of the correlation between pairs of variables such as permeability vs porosity, withdrawal efficiency vs permeability, withdrawal efficiency vs porosity, withdrawal efficiency vs displacement pressure and pore throat sorting vs withdrawal efficiency (the corresponding graphic plots are shown in Figs. (4.81) through (4.85)), lead to the conclusion that porosity is the only variable that correlates with the withdrawal efficiency for the carbonate rocks. But for the sandstone samples, no correlation exists between porosity and withdrawal efficiency. No significant correlation exists between permeability, displacement pressure, pore throat sorting and withdrawal efficiency.

4.6 THE ESTIMATION OF PERMEABILITY

Katz and Thompson [18] demonstrated the method as how to obtain the permeability from a mercury capillary pressure curve. In this section, Katz and Thompson's method will be used to calculate the permeability of 32 samples of Berea, Bentheimer and a few carbonate samples. The procedures for calculation are as follows :

The inflection point is located on the volume injected as a function of capillary pressure curve from the mercury injection. The graphs are shown in App-B1 and App-B2 in Appendix B. The pressure at the point as shown in the

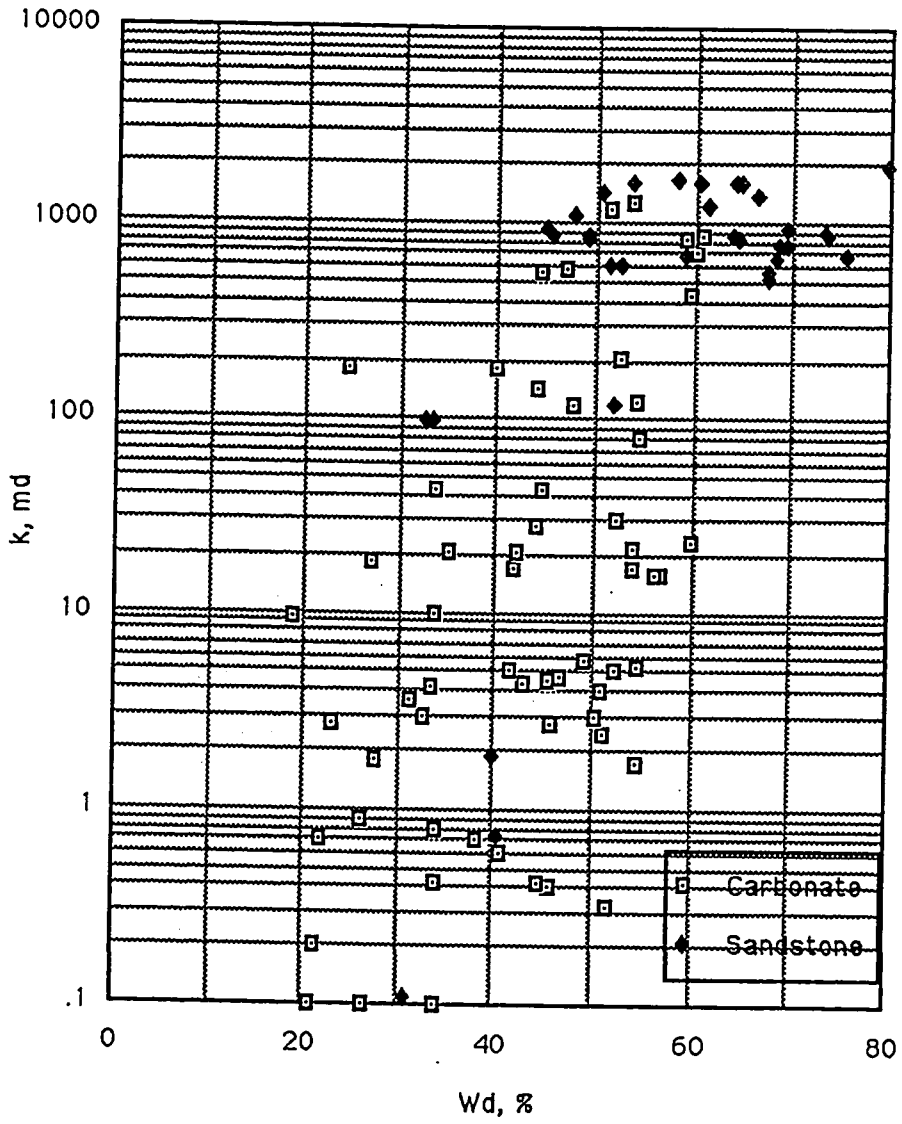

Fig (4.81). Relationship Between Permeability and Withdrawal Efficiency

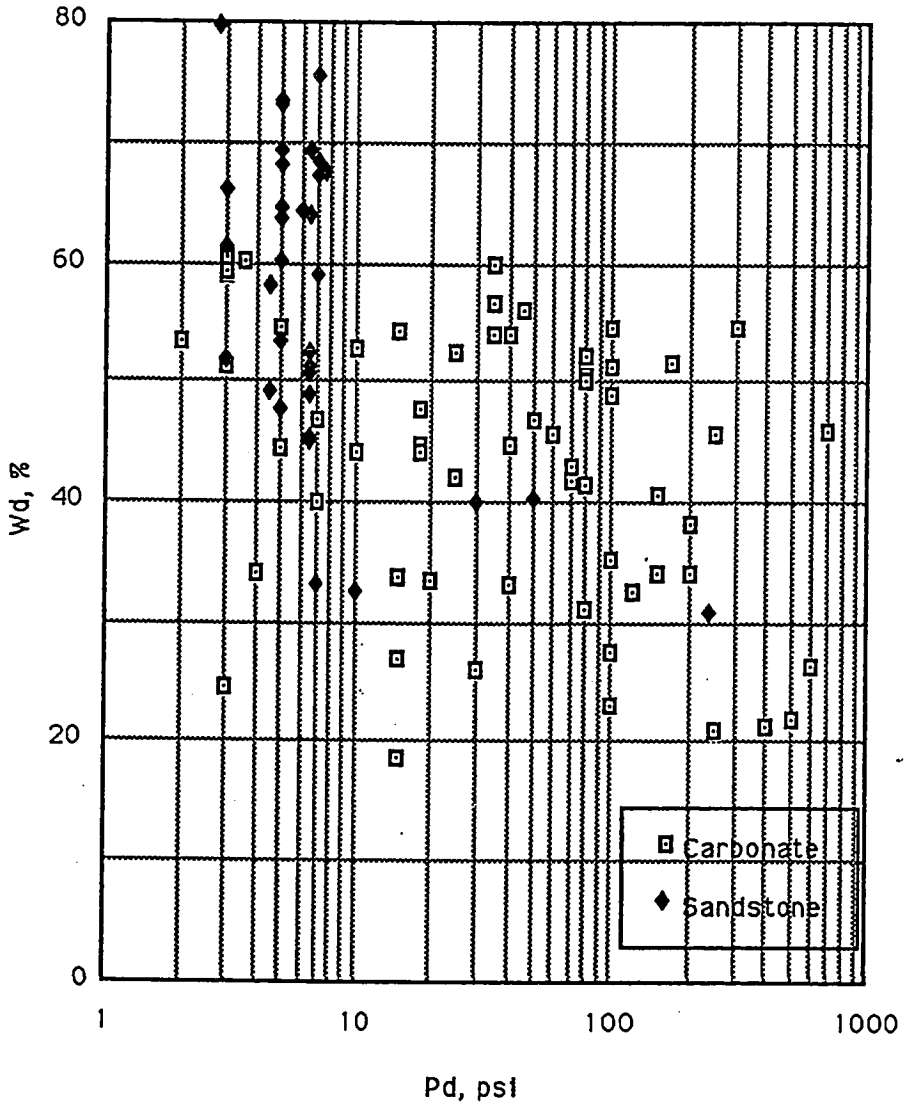

Fig (4.82). Relationship Between Withdrawal Efficiency and Displacement Pressure.

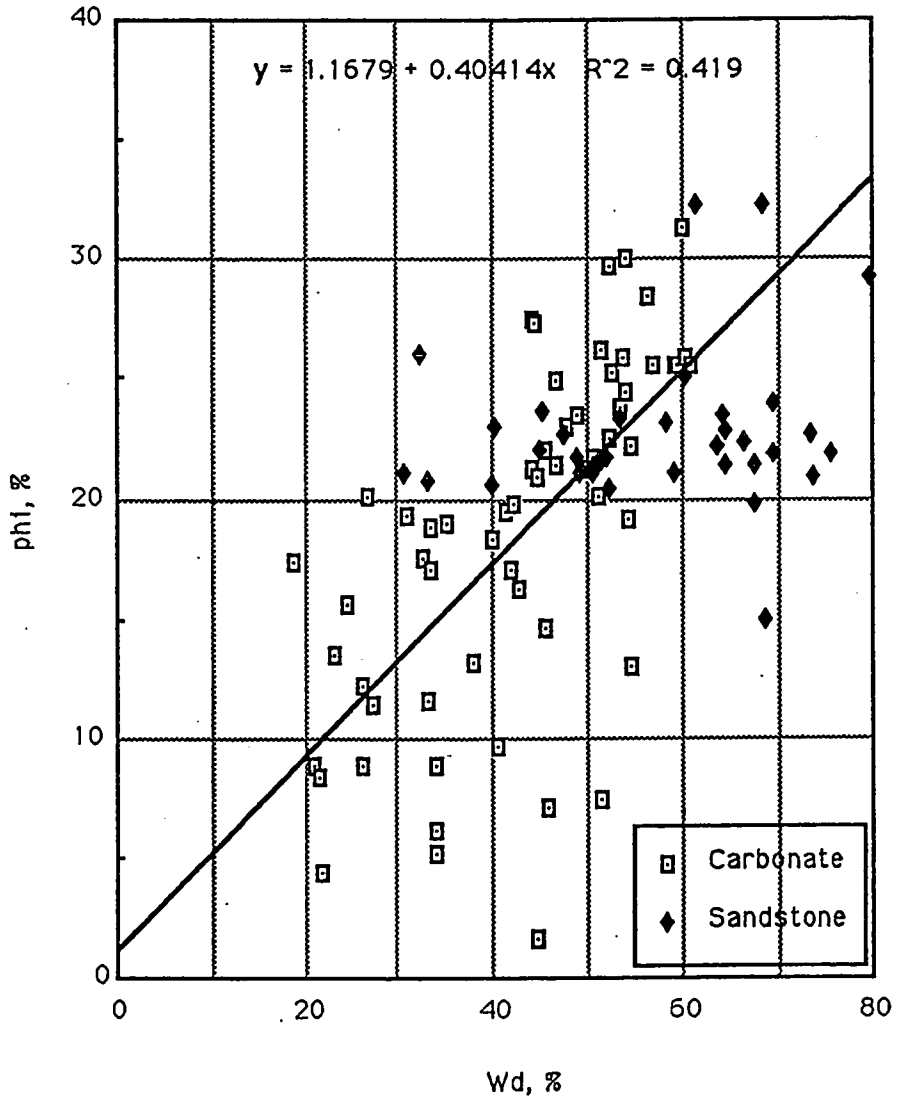

Fig (4.83). Porosity as a Function of Withdrawal Efficiency

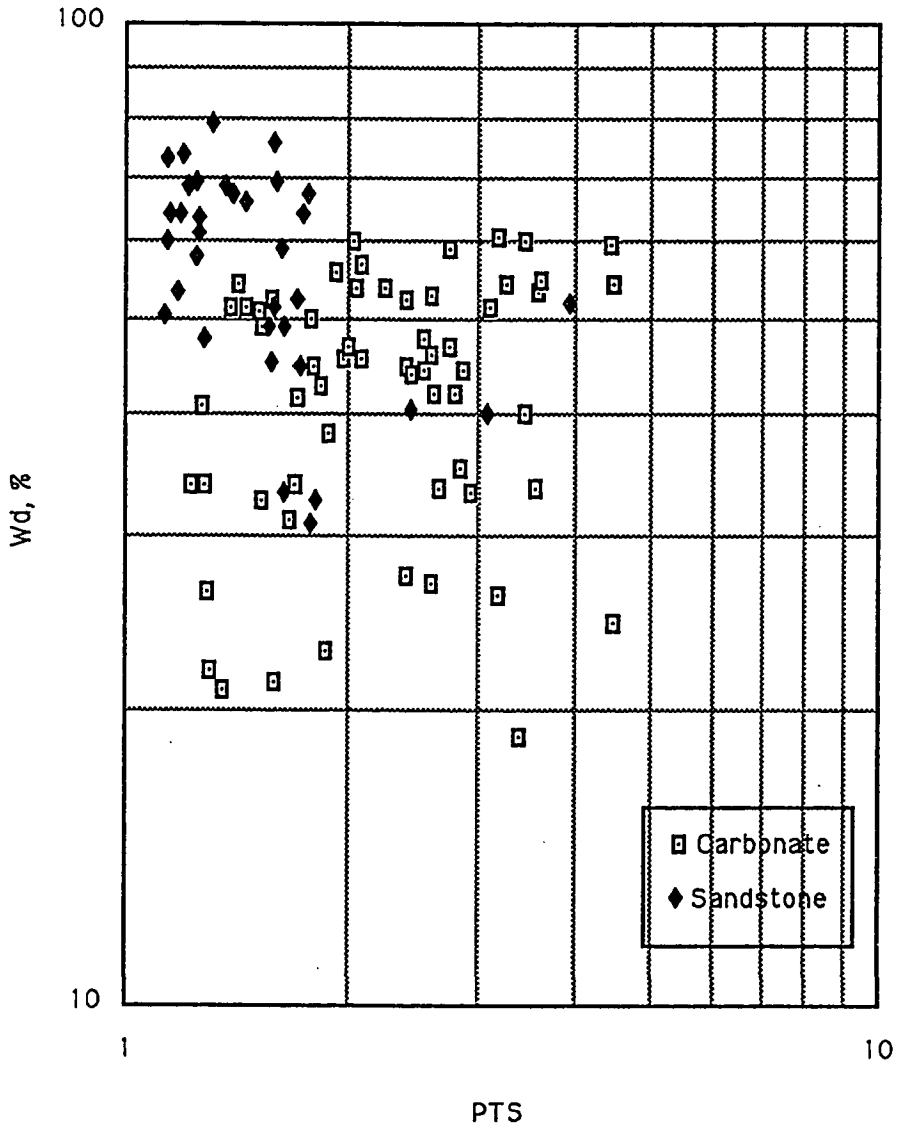

Fig(4.84). Relationship Between Withdrawal Efficiency and Pore Throat Sorting.

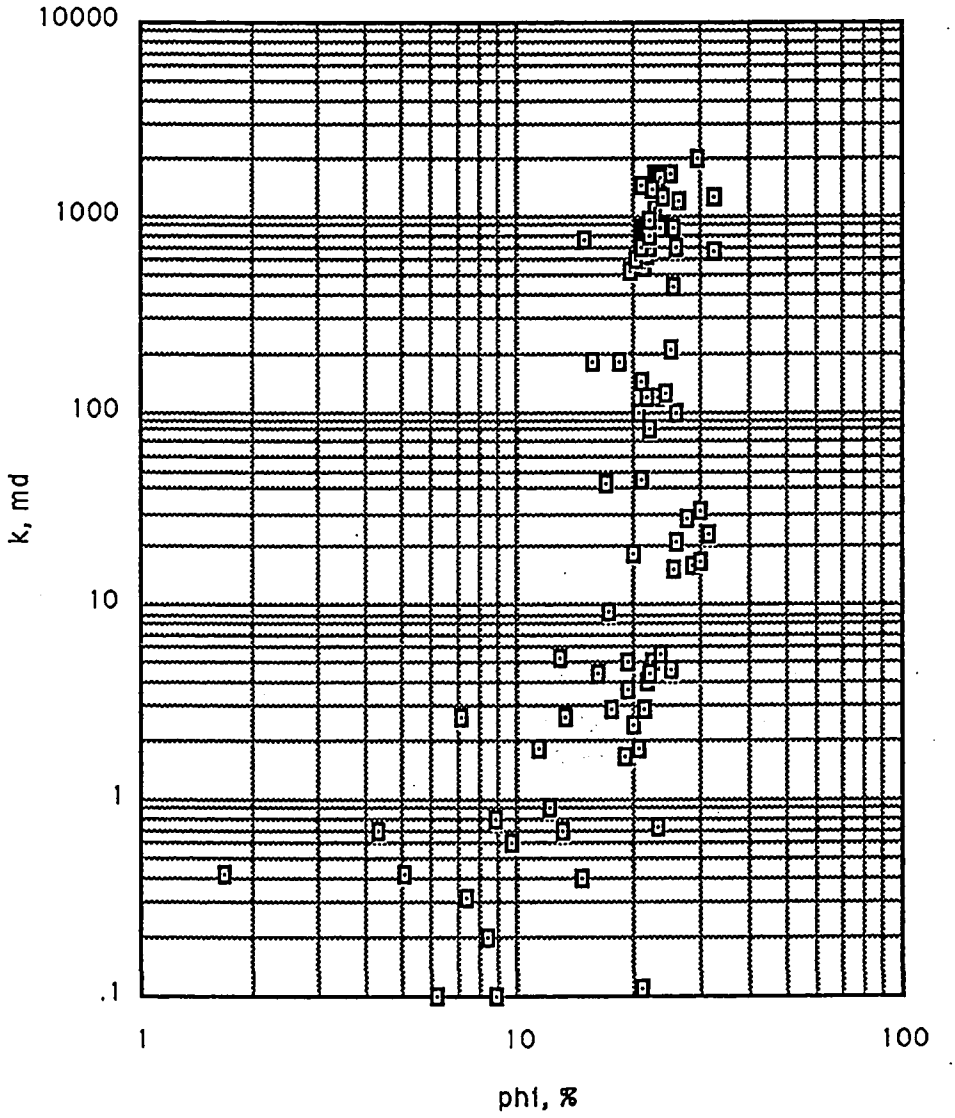

Fig(4.85). Permeability as a Function of Porosity for Both Sandstone and Carbonate Samples

graph is used to calculate the pore throat diameter. This diameter is equal to the percolation critical length, which is given by the following expression :

$$L_c = \frac{4\sigma Cos0}{P_c}$$

All the data points before attaining the critical pressure are discarded. After determination of the critical length from inflection point, the corresponding cumulative volume of mercury injected at inflection point is subtracted from the remaining data in the cumulative injected mercury column. Then the cumulative $H_g injected \times Diameter^3$ vs pore diameter is plotted. The graphs are shown in App-B3 and App-B4 in Appendix B.

From this graph, L^h_{max} , the diameter at the maximum peak, is obtained and $S(L^h_{max})$ is calculated using the equation below :

$$S(L^h_{max}) = \frac{\dfrac{Ordinate\ value\ of\ maximum}{diameter\ at\ maximum^3}}{Vol.\ of\ H_g\ injected\ at\ the\ higest\ pres. - vol.\ injected\ at\ the\ critical\ pres.}$$

Then the permeability can be obtained based on the following expression:

$$k = (\frac{1}{89})(L^h_{max})^2(\frac{L^h_{max}}{l_c})\varphi S(L^h_{max})$$

The results obtained from above procedures and the permeability calculation for some samples are given in App-B5 and App-B6 of Appendix B. Figure (4.86) presents the measured air permeability versus the calculated permeability using the above equation. the correlations were attempted with several statistical models. The best correlation coefficients were obtained when the power fit regression model was used. This model has the equation :

$$Y = b\, X^a$$

The measured and calculated permeability data are given in Table (4.7). A best fit curve of the data is expressed in the following equation :

$$k_{calc} = 1.0524 k_{mea}^{0.5669}$$

In this study, the estimated error has been found to be plus or minus a factor of 2. The error estimation agrees with that of Katz and Thompson's. The error is due to the following reasons :

1. Measurement of air permeability
2. l_c determination.

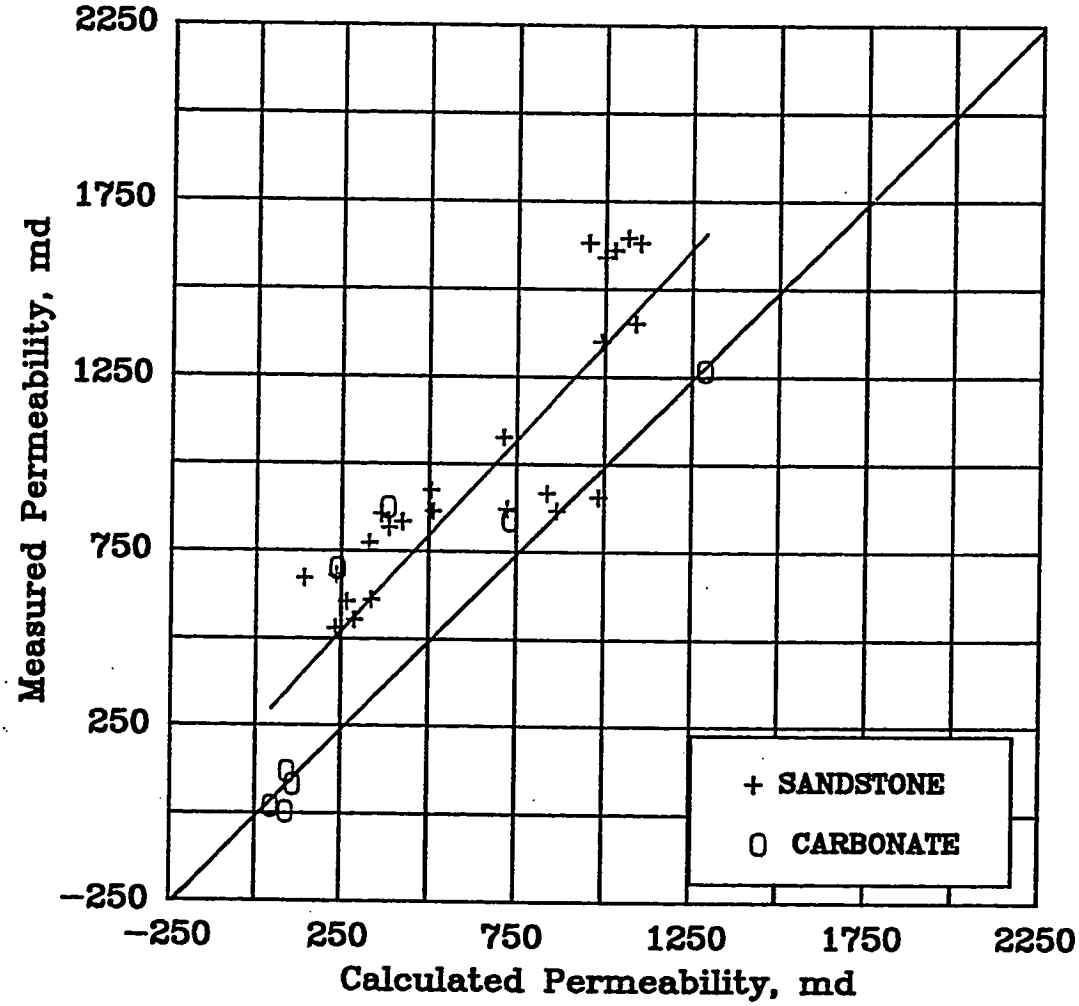

Fig(4.86). Permeability Correlation Between Measured and Calculated From Capillary Pressure Data Using Katz & Thompson's Method.

Table (4.7) Permeability Calculation Using Katz & Thompson's Method.

Sample #	Critical Length Lc, (cm)	Measured k (md)	Calculated k (md)
CAR-58	47.3926	20.43	46.91
CAR-96	46.1966	5.3	90.72
CAR-32	49.9805	839.41	732.43
CAR-34	41.0128	874.54	384.22
CAR-36	34.7736	699.25	239.76
CAR-38	80.9976	1267.2	1288.12
CAR-54	47.3926	81.46	111.08
CAR-56	36.1469	118.7	93.92
BENTHEIMER-1	32.4326	869	866.92
BENTHEIMER-2	32.4326	908	985.67
BENTHEIMER-3	46.6157	1352	991.81
BENTHEIMER-4	33.7134	1611	1028.43
BENTHEIMER-5	32.4326	1403	1088.81
BENTHEIMER-6	32.4326	1077	712.76
BENTHEIMER-7	33.7134	1632	1100.45
BENTHEIMER-8	33.7134	1591	998.35
BENTHEIMER-10	32.4326	917	837.32
BENTHEIMER-12	32.4326	871	723.28
BENTHEIMER-13	33.7134	1646	1064.89
BENTHEIMER-14	32.4326	1632	953.17
BEREA-1	24.1599	680	236.44
BEREA-6	23.4923	671	142.63
BEREA-7	24.1599	773	330.43
BEREA-10	24.8636	610	337.51
BEREA-12	31.2406	834	425.91
BEREA-13	24.1599	864	512.57
BEREA-14	24.1599	817	387.44
BEREA-16	24.8636	925	507.39
BEREA-18	24.1599	856	364.20
BEREA-20	24.8636	529	233.55
BEREA-21	19.0344	553	287.47
BEREA-22	20.9015	605.2	265.46

3. Surface tension, σ

4. Contact angle, θ

An explanation need to be given for the measurement of air permeability because of the inaccuracy of reading between flow rate and pressure drop across the sample. The flow rate vs pressure drop squared for some samples are given in App-B7 and App-B8 of Appendix B. The confining stress is also an important factor to be considered in calculating the permeability. As the confining stress increases, the slope of flow rate vs pressure drop increases and permeability increases. The second error comes from determination of l_c value. The positive to negative slope change of the curve occurs when the intruded mercury initially forms a connected cluster that spans the sample. Inflection point is located at the point at which the mercury first forms a cluster spanning the sample. The length scale l_c reflects the accuracy in the determination of the inflection point, which is a unique and well-defined experimental point. The largest errors in l_c are introduced by the roughness of the injection mercury capillary pressure curve. Smoothness of the curve is much important to pick up the actual inflection point. Therefore, cubic spline interpolation function was used to smooth the injection pressure curve. After smoothing the curve, the inflection points were determined. The estimated error was within the range. The third and last error comes from surface tension and contact angle. The mercury surface expands during injection and

contracts during withdrawal. Impurities affect the surface tension and contact angles. Surface impurities increase surface tension and contact angle during mercury injection. Therefore, the shape of the injection curve changes when surface tension and contact angle change.

Katz and Thompson's method applied in this work was compared with Swanson's [17] correlation method. The data of 32 samples, consisting of 24 sandstone and 8 carbonate samples, were used. Figure (4.87) displays the measured permeability against the calculated permeability using the correlation parameter $[S_b/P_c]_A$. This correlation parameter is the numerical value which represents the maximum length. It can be defined as the ratio of coordinates along a line drawn at 45° and the tangent to the capillary pressure curve intersects at point A. The correlation parameters determination for some samples are shown in App-C1 and App-C2 of Appendix C. The measured and calculated permeability data are shown in Table (4.8). The correlation relationship is shown below :

$$k_l = 1.6506\left[\frac{S_b}{P_c}_{A}\right]^{1.54804}$$

The overall deviation error was found 72 %; using the Katz and Thompson's, it was 45 %. From this point of view, the Katz and Thompson's gave better correlative result than the Swanson's. In Fig. (4.87), using

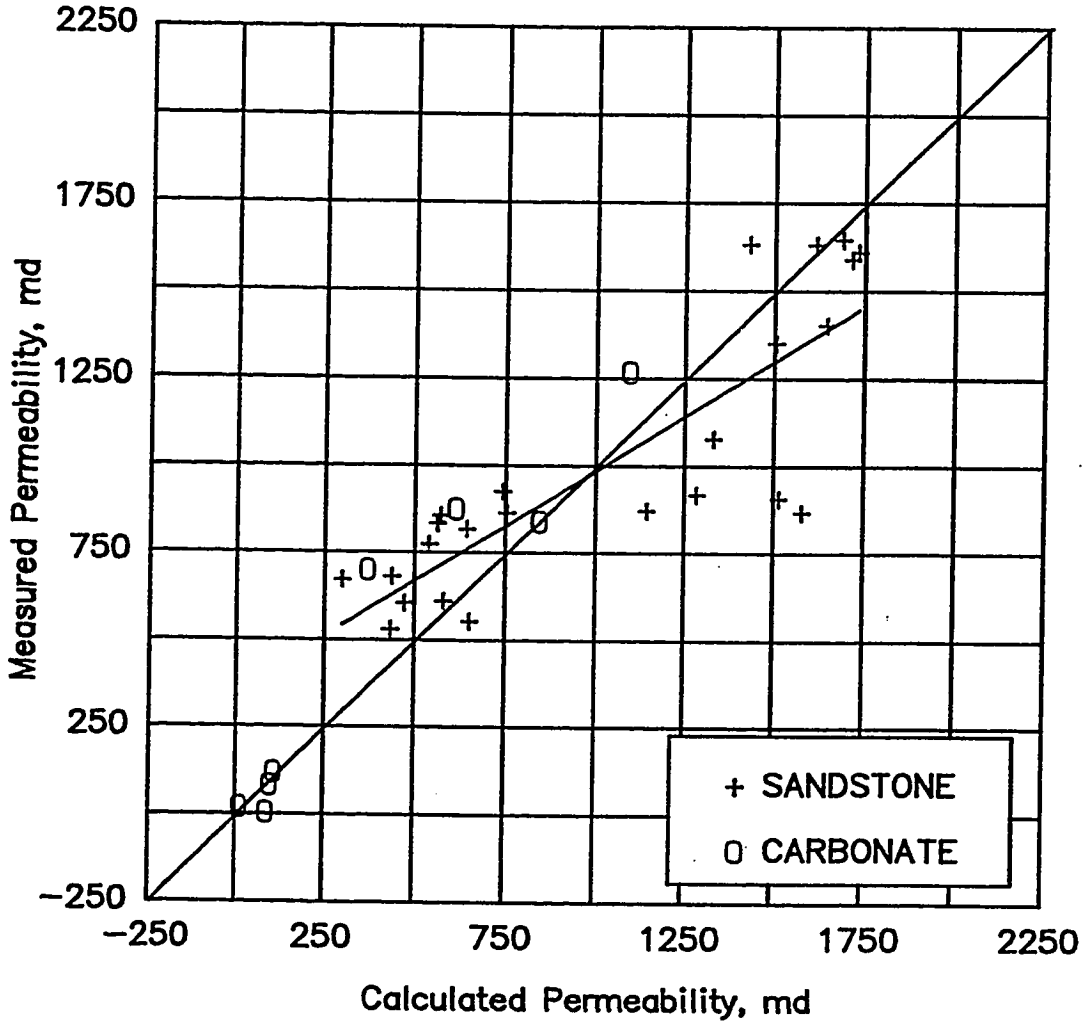

Fig.(4.87). Permeability Correlation Between Measured and Calculated From Capillary Pressure Data Using Swanson's Method.

Table (4.8) Permeability Calculation Using Swanson's Method.

Sample #	(SHg/ Pc) @ A (/ psi)	Measured k (md)	Calculated k (md)
CAR-58	0.40	20.43	10.83
CAR-96	1.53	5.3	86.66
CAR-32	6.67	839.41	843.32
CAR-34	5.43	874.54	613.92
CAR-36	3.92	699.25	370.72
CAR-38	7.89	1267.2	1095.85
CAR-54	1.65	81.46	97.12
CAR-56	1.76	118.7	107.79
BENTHEIMER-1	10.0	869	1579.99
BENTHEIMER-2	9.73	908	1513.47
BENTHEIMER-3	9.69	1352	1504.81
BENTHEIMER-4	10.61	1611	1732.92
BENTHEIMER-5	10.26	1403	1644.77
BENTHEIMER-6	8.95	1077	1330.68
BENTHEIMER-7	10.14	1632	1615.10
BENTHEIMER-8	10.54	1591	1714.00
BENTHEIMER-10	8.75	917	1284.93
BENTHEIMER-12	8.13	871	1145.66
BENTHEIMER-13	10.43	1646	1686.39
BENTHEIMER-14	9.38	1632	1429.76
BEREA-1	4.36	680	436.62
BEREA-6	3.41	671	299.04
BEREA-7	5.0	773	540.32
BEREA-10	5.24	610	580.65
BEREA-12	5.13	834	562.22
BEREA-13	6.20	864	753.82
BEREA-14	5.6	817	643.93
BEREA-16	6.14	925	741.81
BEREA-18	5.18	856	571.06
BEREA-20	4.33	529	432.9
BEREA-21	5.65	553	652.85
BEREA-22	4.58	605.2	471.69

Swanson's maximum length, most of the data fell on 45° line and in Fig. (4.86), using Katz and Thompson's critical length, most of the data fell above 45° line. The measured permeability used in both method was air permeability. Gas permeability was not corrected to liquid permeability using Klinkenberg gas slippage effect at infinite pressure. According to the Kamath [26] correction factors were required for each method.

The methods mentioned above can be used to estimate permeability for sandstone and carbonate samples without modification of the method. The Katz and Thompson's method is more realistic and more reliable and reasonable theory is behind their approach. However, the calculation is lengthy and the crucial thing is to be aware in finding out the inflection point. The Swanson's approach is also good and it is easy to find the maximum length from the curve, but it is just a correlation.

4.7 THE CORRELATION FUNCTION STUDY

In this section, J-function was applied in order to normalize the capillary pressure curves. As well-defined physical properties of the rock samples (pore structure, porosity and permeability) affect the capillary pressure curve, Leverett [1] proposed a correlation function in which capillary pressure data can be represented as a universal curve for all the concerned reservoir rocks. In

this J-function, the physical properties of the rock and fluid properties are used and the physical expression is obtained as :

$$J(S_w) = \frac{P_c}{\sigma}\sqrt{k/\varphi} \qquad unitless$$

Because the pore structure and rock characteristic change from one formation to another, Leverett's J-function cannot stand as a universal curve for all the types of rocks. However, Brown [5] modified the J-function in which the contact angle was included in the Leverett's function. The Leverett's correlation function thus becomes :

$$J(S_w) = \frac{P_c}{\sigma Cos\theta}\sqrt{k/\varphi} \qquad unitless$$

An improvement was observed in the correlation curve when the contact angle was used for all kinds of samples. He pointed out that more improvement can be obtained if the rock samples were divided according to their texturity basis.

Both there methods were employed to correlate capillary pressure data obtained from Berea, Bentheimer and some carbonate core samples. The porosities of these cores varied from 13.5 to 26.3 percentage, and the permeability varied from 0.325 to 1648 md. Plots of J-function versus mercury saturation data on semi-log paper for Leverett's function and modified J-

function are shown in Figs. (4.88) and (4.89) respectively. These figures show that since the correlation obtained for all the samples in this work has considerable dispersions of data points, no trends were observed. Although a separation has been made between sandstone and carbonate samples as Brown [5] suggested, the J-function did not fell into the trend. Therefore, the following modifications were made in this work using the J-function as proposed by Leverett.

The first modification used the expression as :

$$J(S_w)=\frac{P_c}{\sigma Cos\theta\varphi}\sqrt{k}$$

Throughout this study, the surface tension value of 480 dynes cm^{-1} and the contact angle, (0), value of 140° were used. The effect of the surface tension and contact angle that can vary the capillary pressure data is insignificant. The percentage of error is so small compared with the other parameters used in the equation. Figure (4.90) shows the results of J-curve obtained using the above equation. The scattering of points occurred in the low saturation range especially for those carbonate samples, which have low permeability and vuggy pore structures.

A simple modification was made in which the porosity term was removed from the Leverett's function for all the samples and the expression becomes :

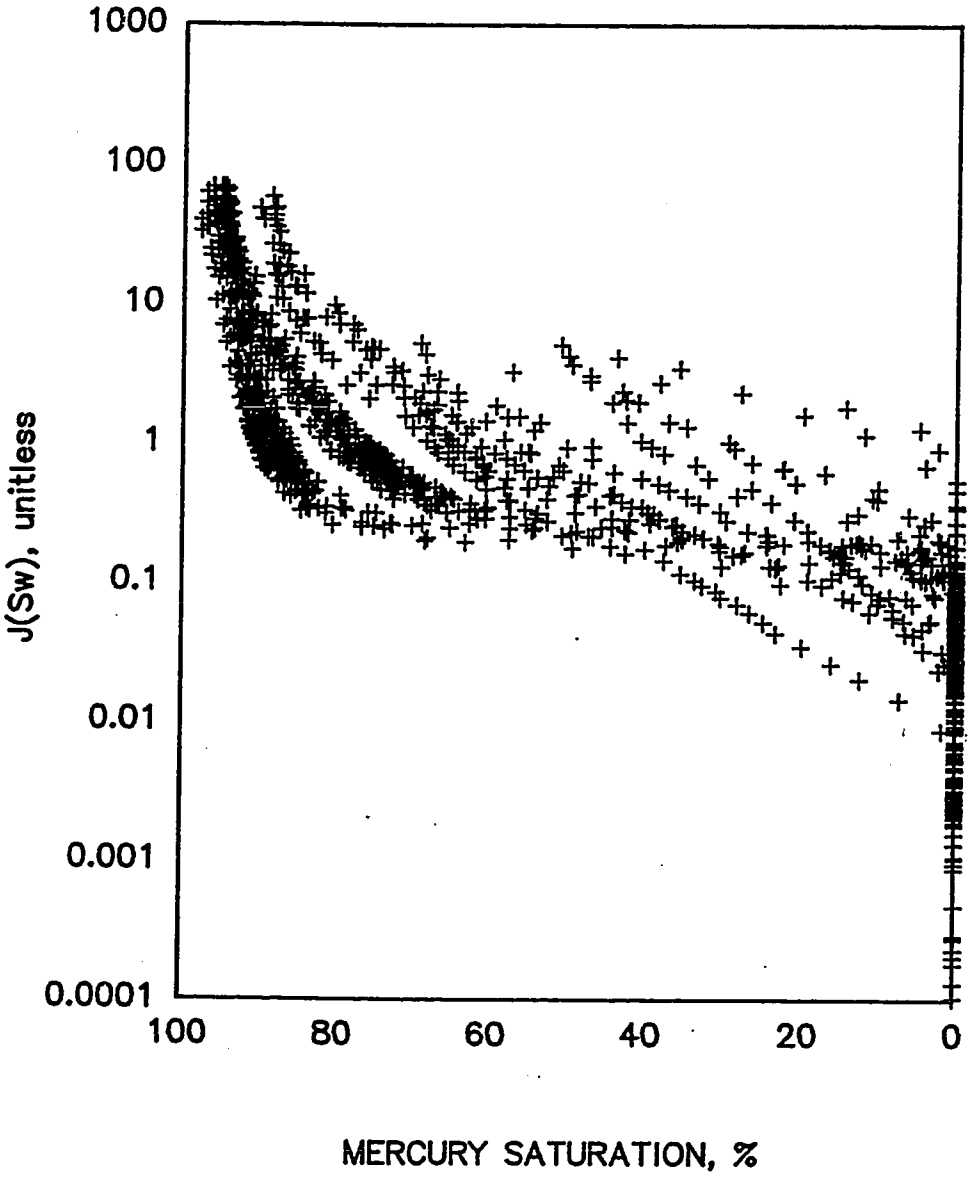

Fig.(4.88). J–Function Correlation For All Studied Samples Using Leverett's Original Function.

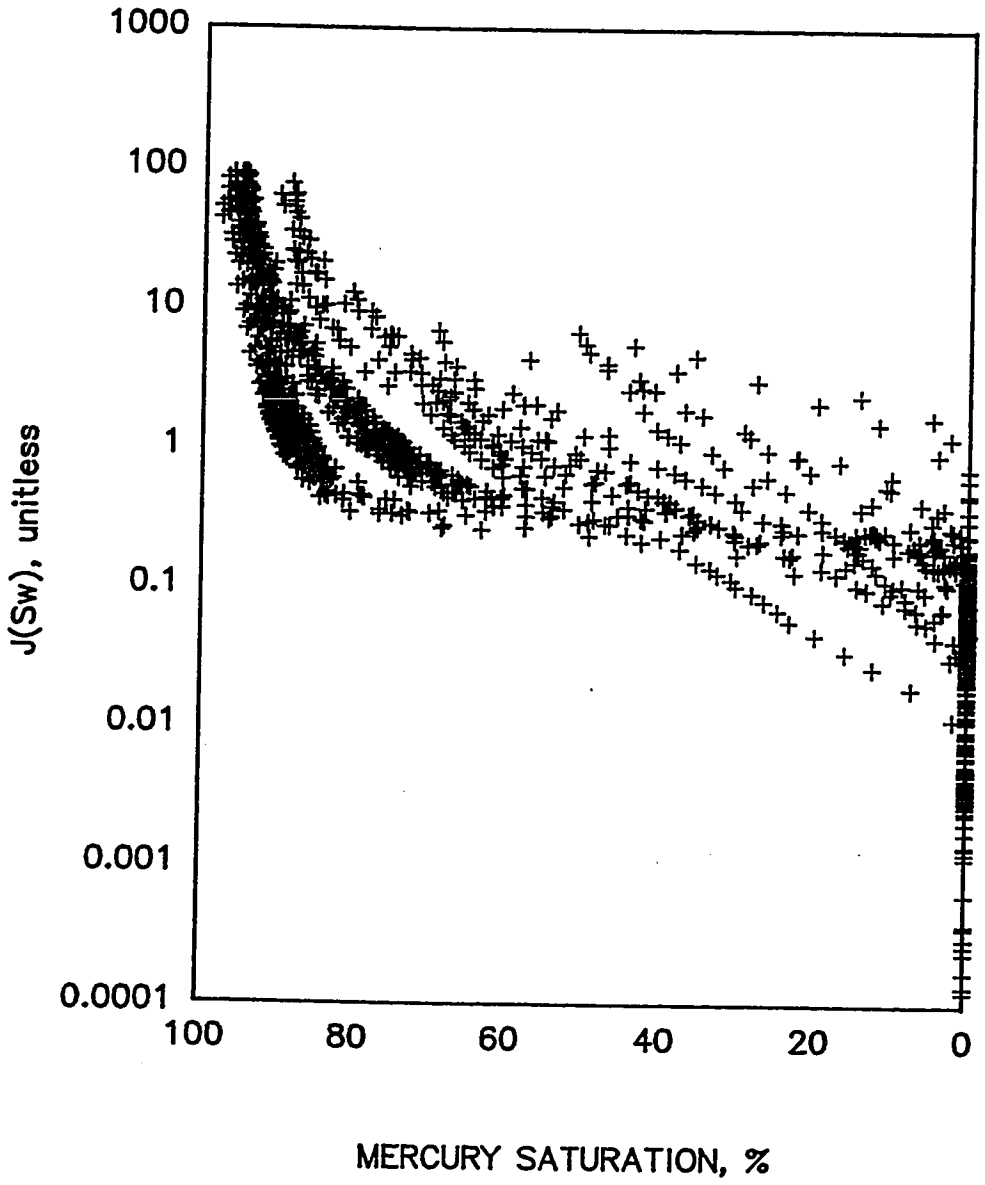

Fig.(4.89). J–Function Correlation For All Studied Samples Using Modified Brown's Function.

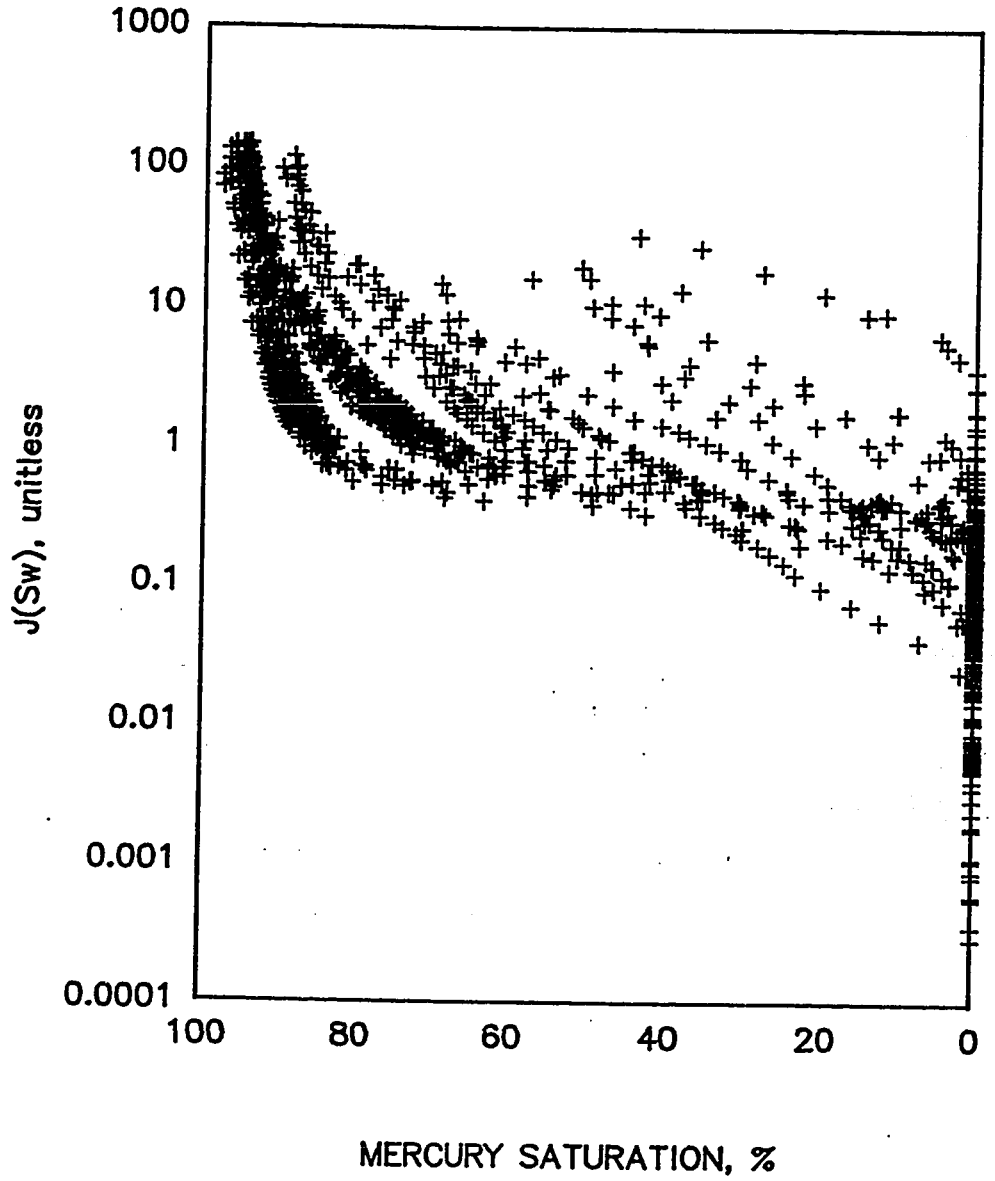

Fig.(4.90). J--Function Correlation For All Studied Samples Using Modified Function Developed in This Study.

$$J(S_w)=\frac{P_c}{\sigma}\sqrt{k}$$

The scattering of points was reduced considerably, giving very less spread of the data points as shown in Fig. (4.91). It was seen that J-curve was not only a function of permeability but also a function of porosity. Since the J-function modification did not give a good correlation, an extended J-function was carried out in the following section. The extended version of the J-function is as shown below :

$$J(S_w)=\frac{P_c}{\sigma}\sqrt{k/\varphi}PTS$$

and

$$J(S_w)=\frac{\frac{P_c}{\sigma}\sqrt{k/\varphi}}{PTS}$$

which differ slightly from each other.

The pore throat sorting (PTS) parameter, which is a numerical value and can be obtained from the slope of the plateau of the capillary pressure data, was added to the Leverett's J-function. Figures (4.92-a) and (4.92-b) show the results obtained by using the above equation. As shown in these figures, the spreading of the data points occurred in the low range of saturation up to

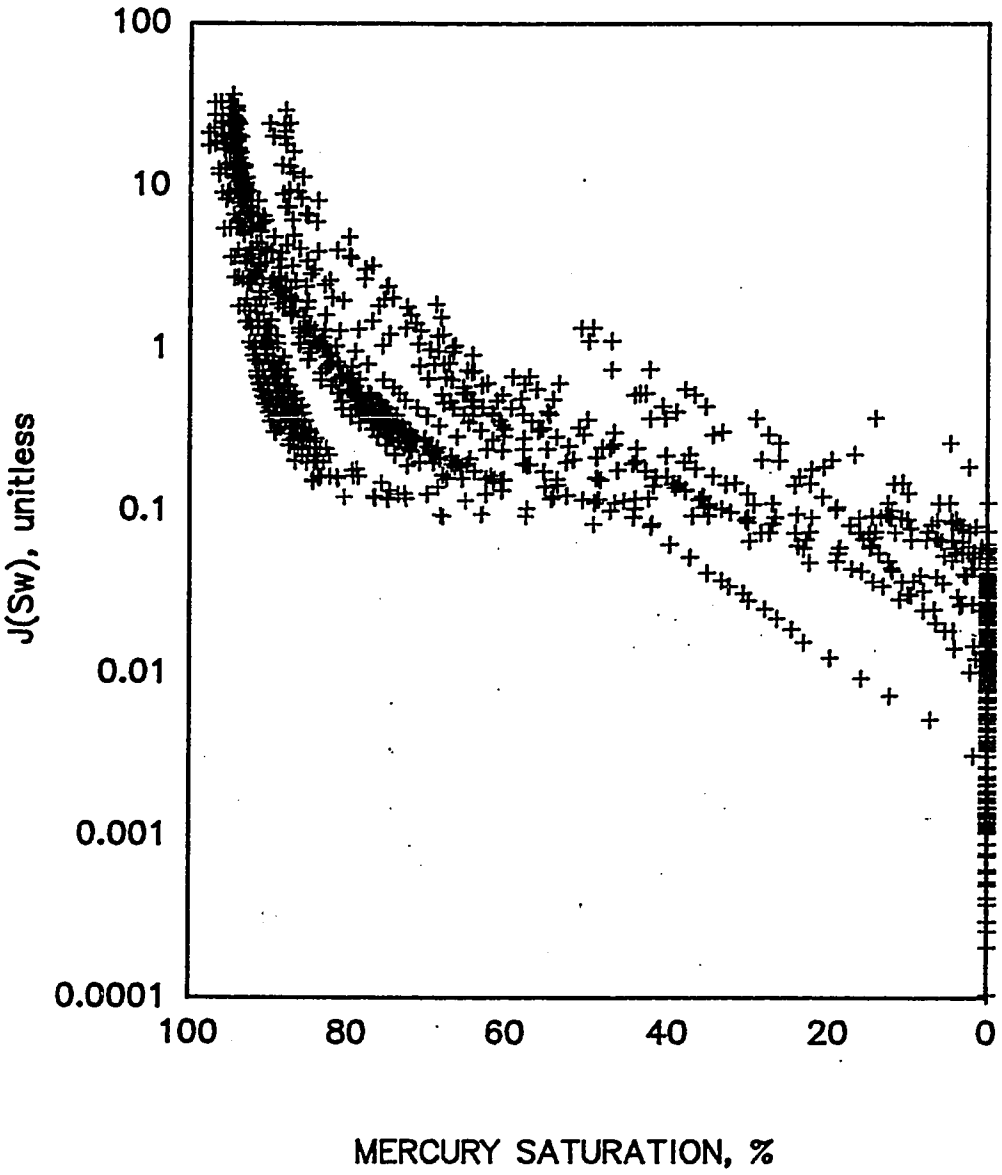

Fig.(4.91). J–Function Correlation For All Studied Samples Removing Porosity Term from Original Function.

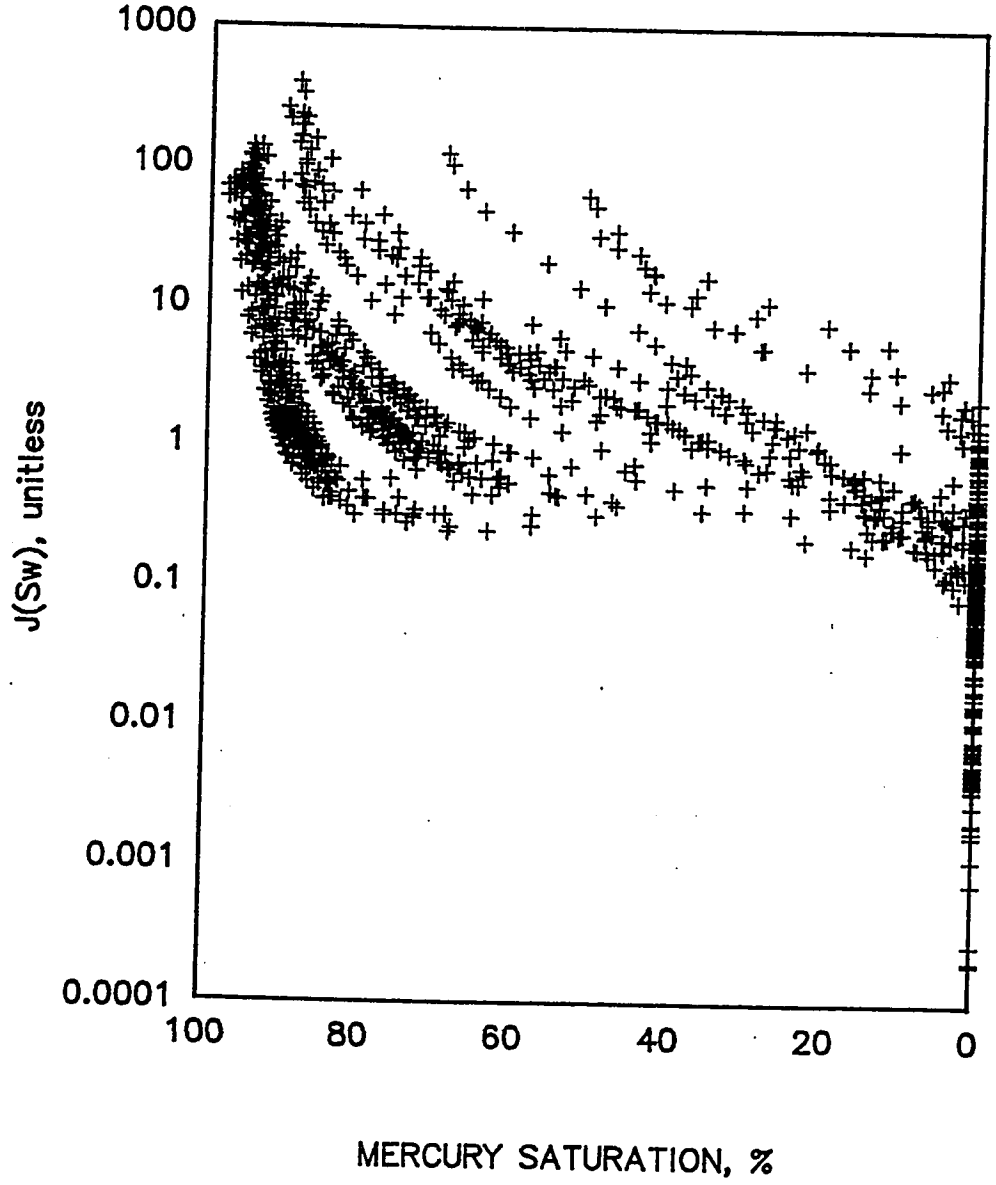

Fig(4.92–A). J–Function Correlation For All Studied Samples Using Pore Throat Sorting as a Multiplier Developed in This Study.

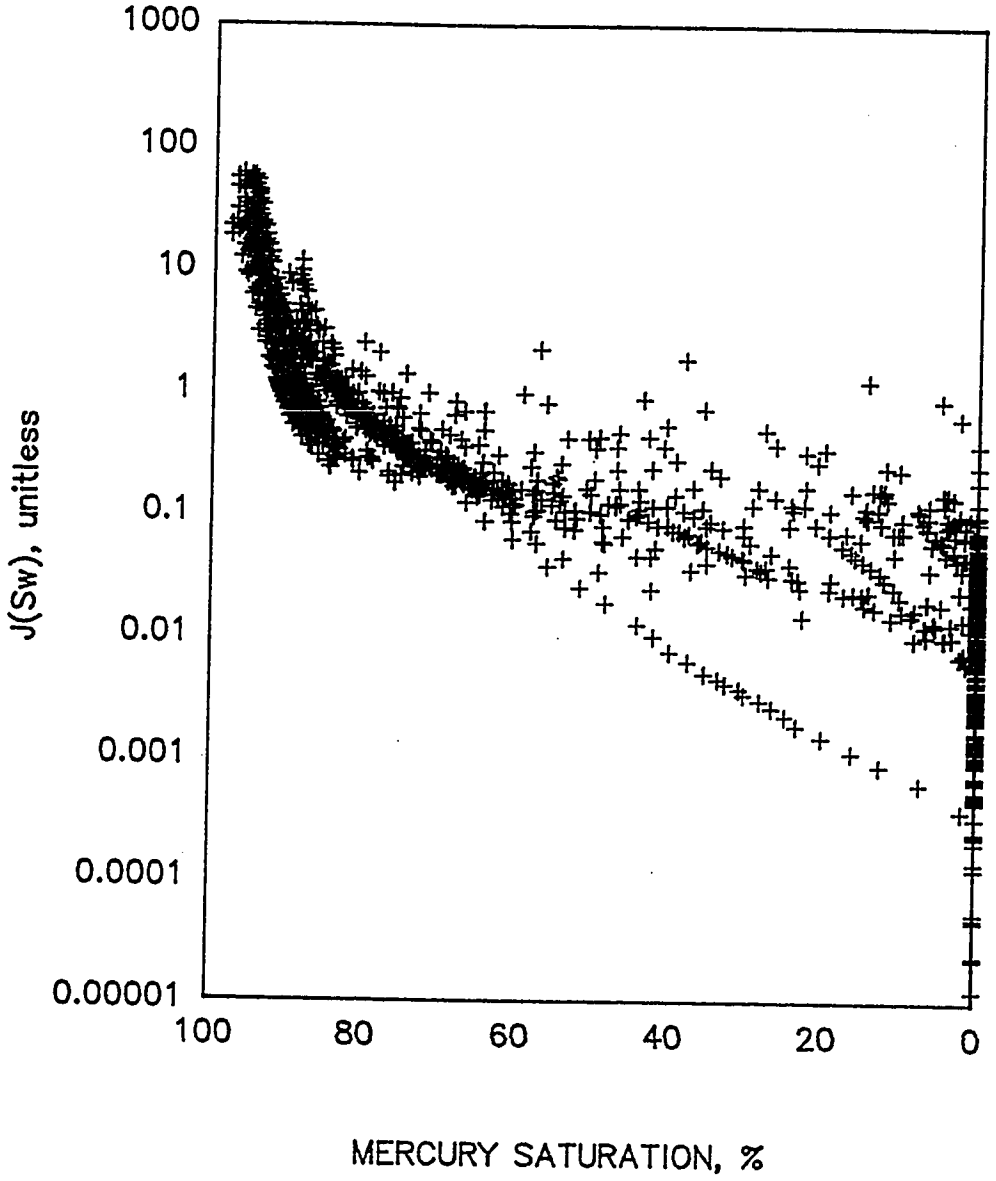

Fig.(4.92–B). J–Function Correlation For All Studied Samples Using Pore Throat Sorting as a Divider Developed in This Study.

60% when PTS was used as a dividing parameter and the dispersion of the points was greater in the saturation ranging from 50% and above, when PTS was used as a multiplication parameter. However, on plotting the J-function against mercury saturation for sandstone samples only, it was found that all the data points fell roughly along the same trend when PTS was used as a dividing parameter. For carbonate samples, the variations in porosity and permeability covered wide ranges. These samples were all carbonate rocks that can be classified as dolomite and the others were non-dolomite.

It is inferred from a comparison of the results of Leverett's J-function with that of the extended J-function study on the sandstone sample alone that the extended J-curve indicated a good correlation. To investigate this improvement quantitatively, the standard deviation error was calculated using the hyperbolic fit of iteration 27. The error was found to be 7.8% when Leverett's J-curve was used and when the extended J-curve was used, the error was reduced to 6.3%. The following expression was used and the graphs are shown in Figs (4.92-B.1) and (4.92-B.2).

$$Y = \frac{a + bX}{1.0 + cX}$$

While pore throat sorting (PTS) is normally obtained from capillary pressure curve, it can also be determined from the relationship with displacement pressure and permeability. PTS is a function of displacement

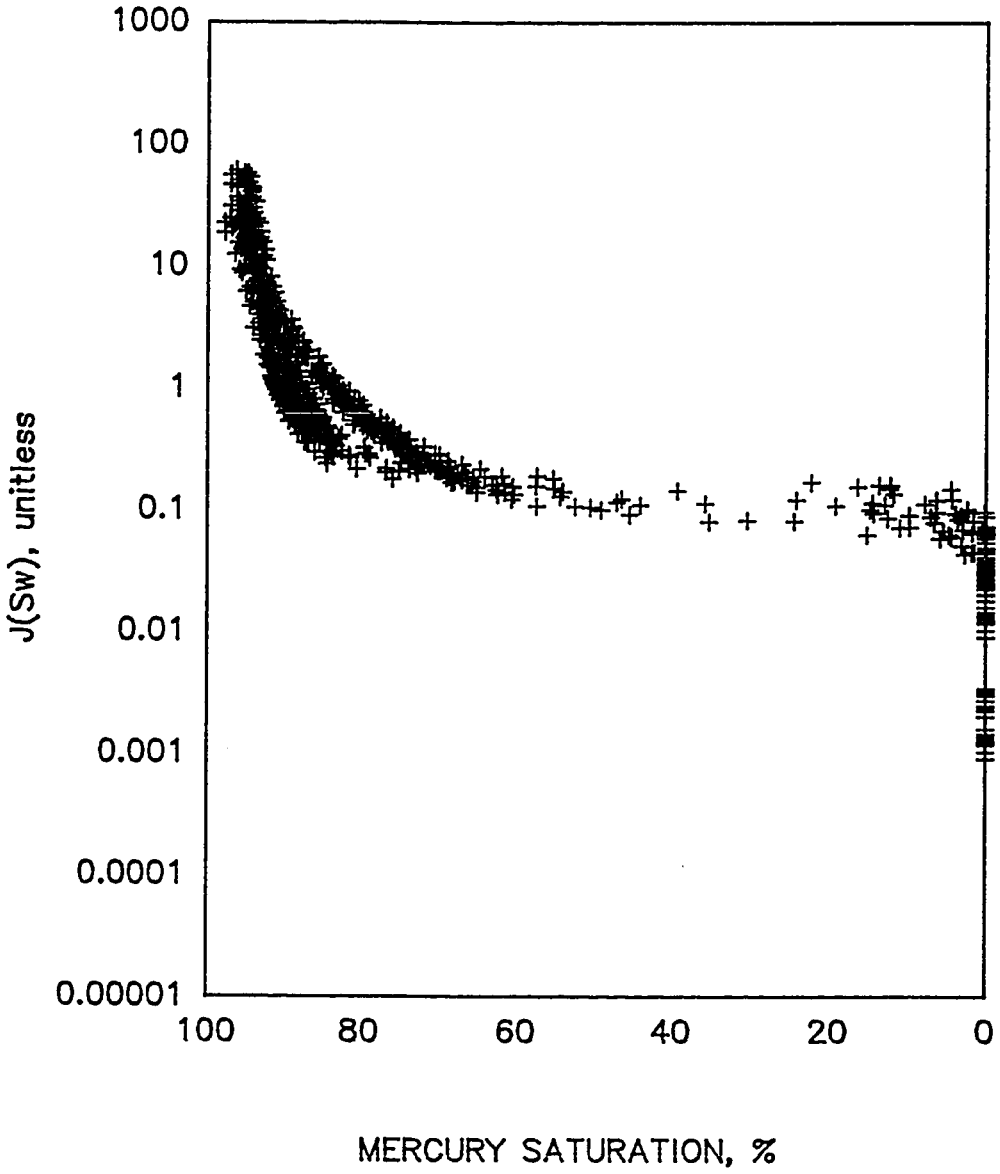

Fig.(4.92–B.1). J–Function Correlation For All Sandstone Samples Using Pore Throat Sorting as a Divider Developed in This Study.

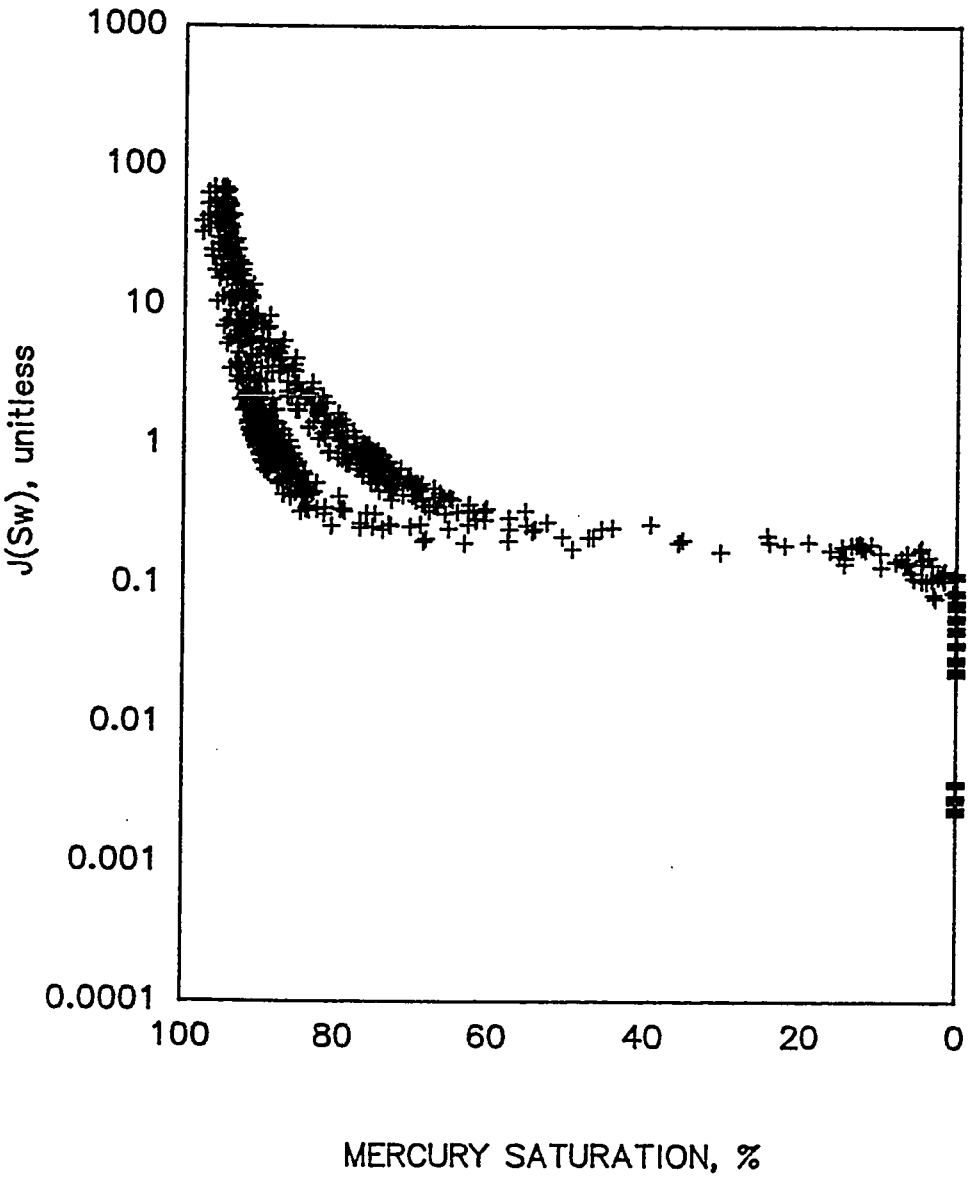

Fig.(4.92–B.2). J–Function Correlation For Sandstone Samples Using Leverett's Original Function.

pressure and permeability for sandstone samples as shown in Fig. (4.93-a). The displacement pressure correlated well with the sample permeability as shown in Fig. (4.93-b). The corresponding graphs for carbonate samples are shown in Figs. (4.93-c) and (4.93-d).

In Fig. (4.94), critical length, $l_{c,}$ which is determined from the capillary pressure curve where the inflection points occurred, was introduced into the J-function by removing of $\sqrt{k/\varphi}$ parameter from that original J-function. The equation becomes,

$$J(S_w)=\frac{P_c}{\sigma}l_c$$

It can be seen from the above figure that without separating the carbonate samples from sandstone samples, a wide range of scatter points occurred in the graph. The calculated J-function for sandstone and carbonate samples are shown in Fig. (4.94-a) and (4.94-b) respectively. The sandstone samples indicate a good correlation, while the carbonate samples exhibit a scattering of the data. The reason for this is that in the sandstone samples, the pore throats are distributed uniformly while in the carbonate samples, the pore throats are distributed in a peculiar form because of the vuggyness existing from one sample to another even though the samples were cut from the same core plug.

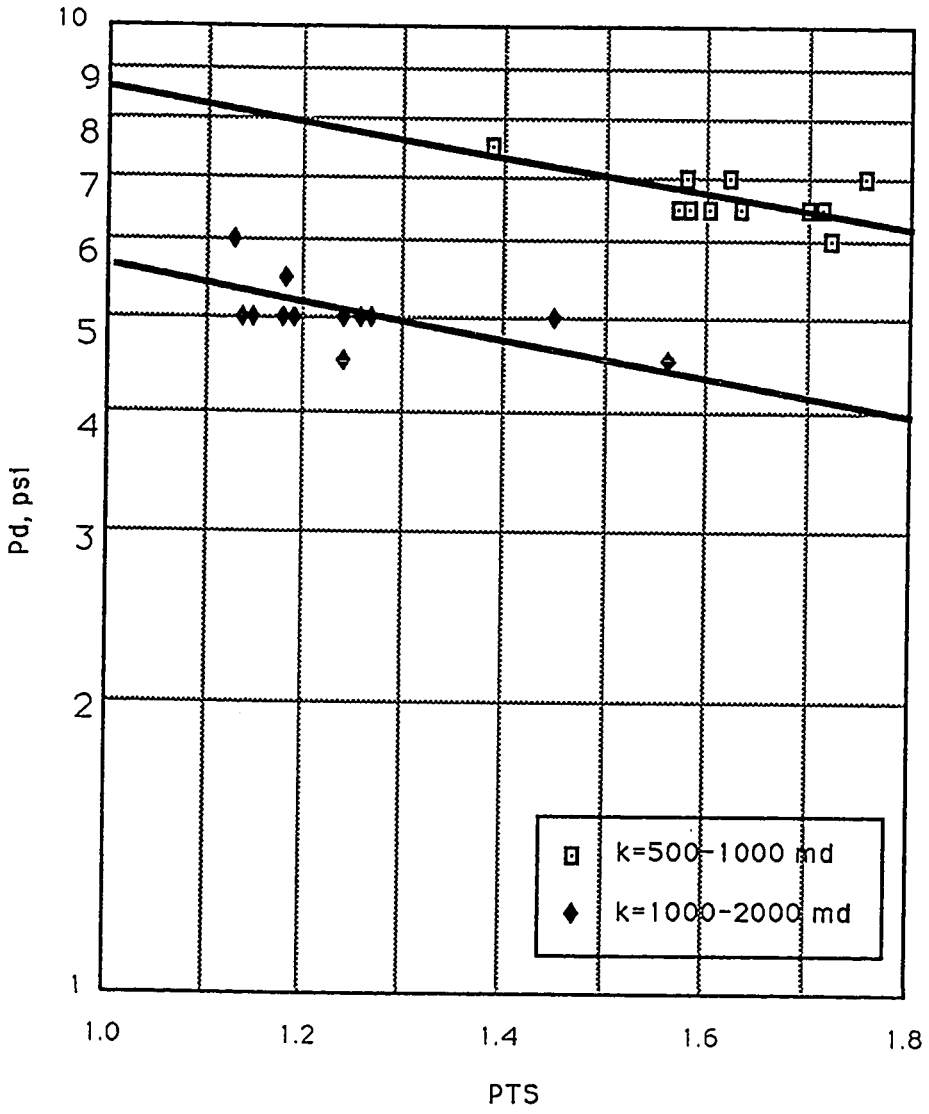

Fig(4.93-A). Displacement Pressure vs Pore Throat Sorting as a Function of Permeability for Sandstone

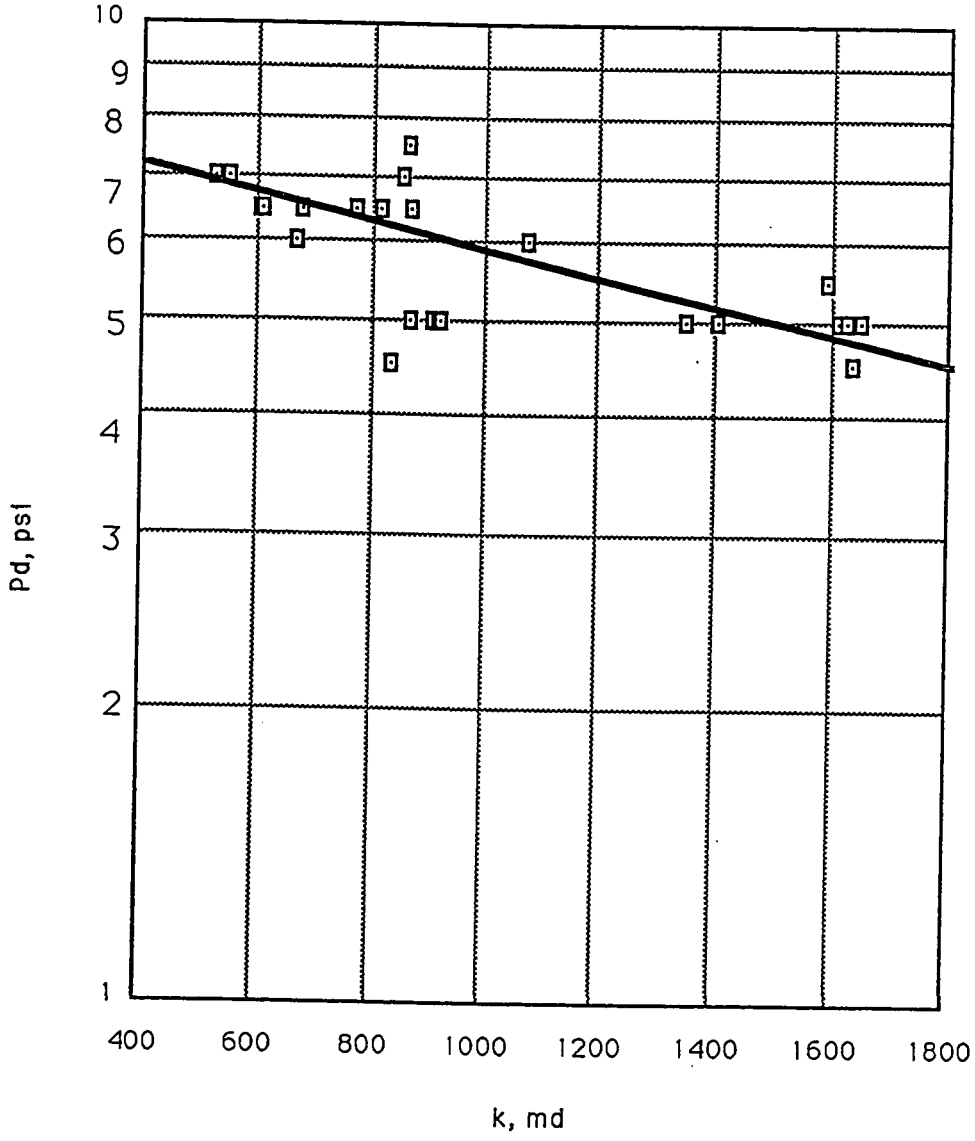

Fig(4.93-B). Displacement pressure vs permeability for Sandstone rocks

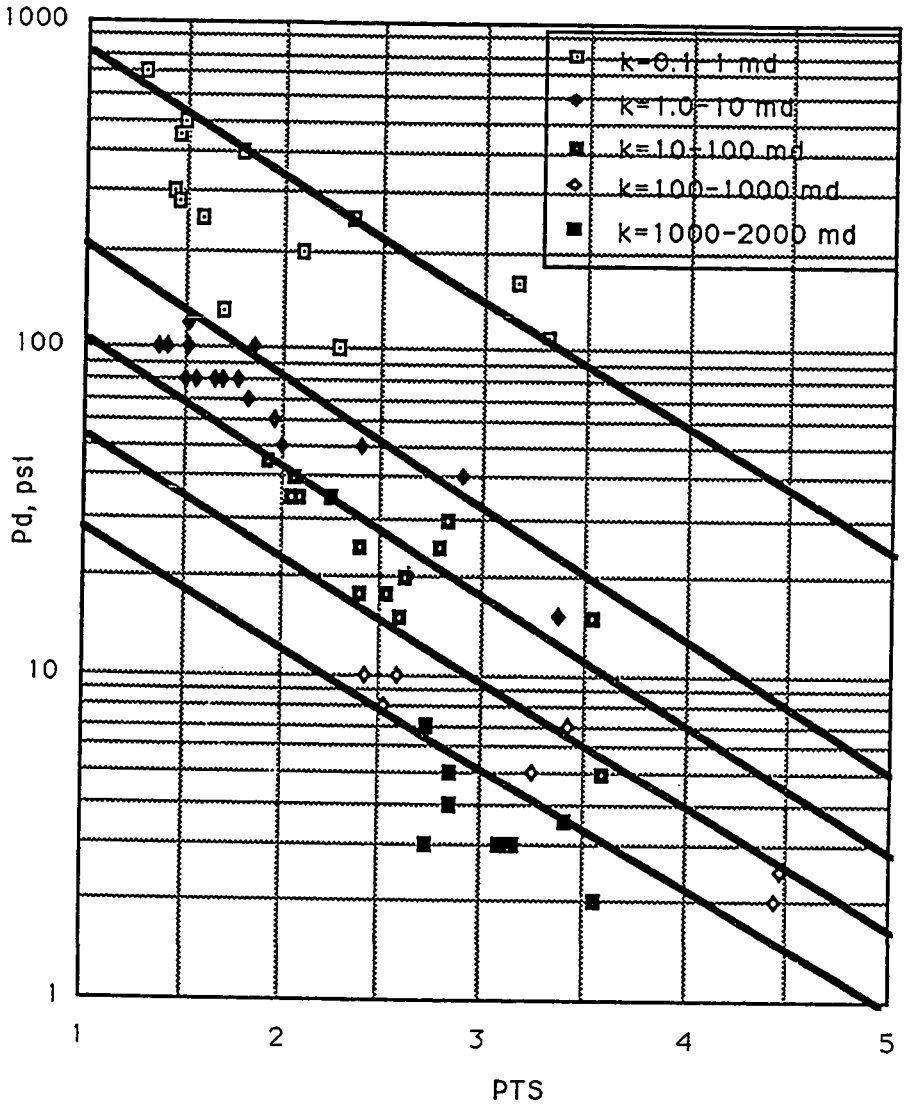

Fig(4.93-C). Displacement Pressure vs Pore Throat Sorting as a Function of Permeability for Carbonate Rocks

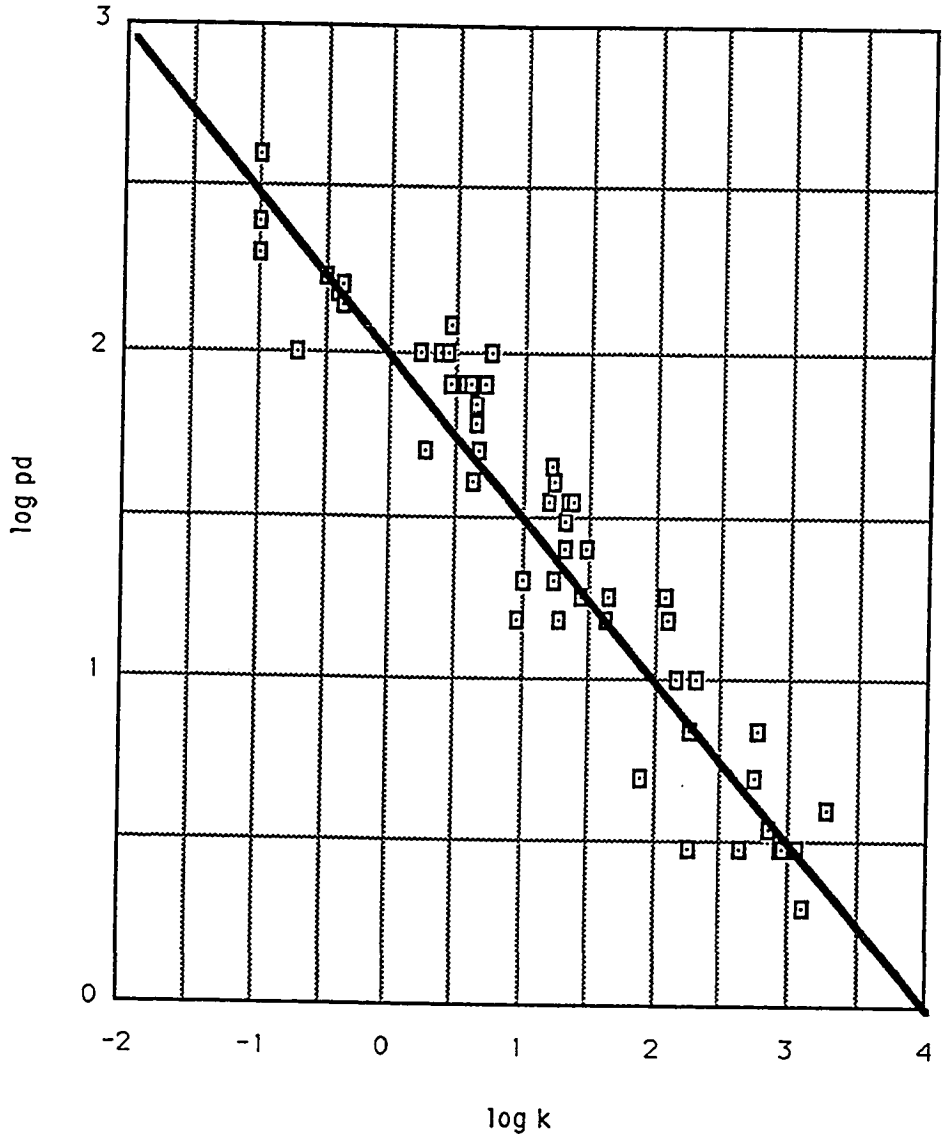

Fig(4.93-D). Displacement Pressure vs Permeability for Carbonate rocks

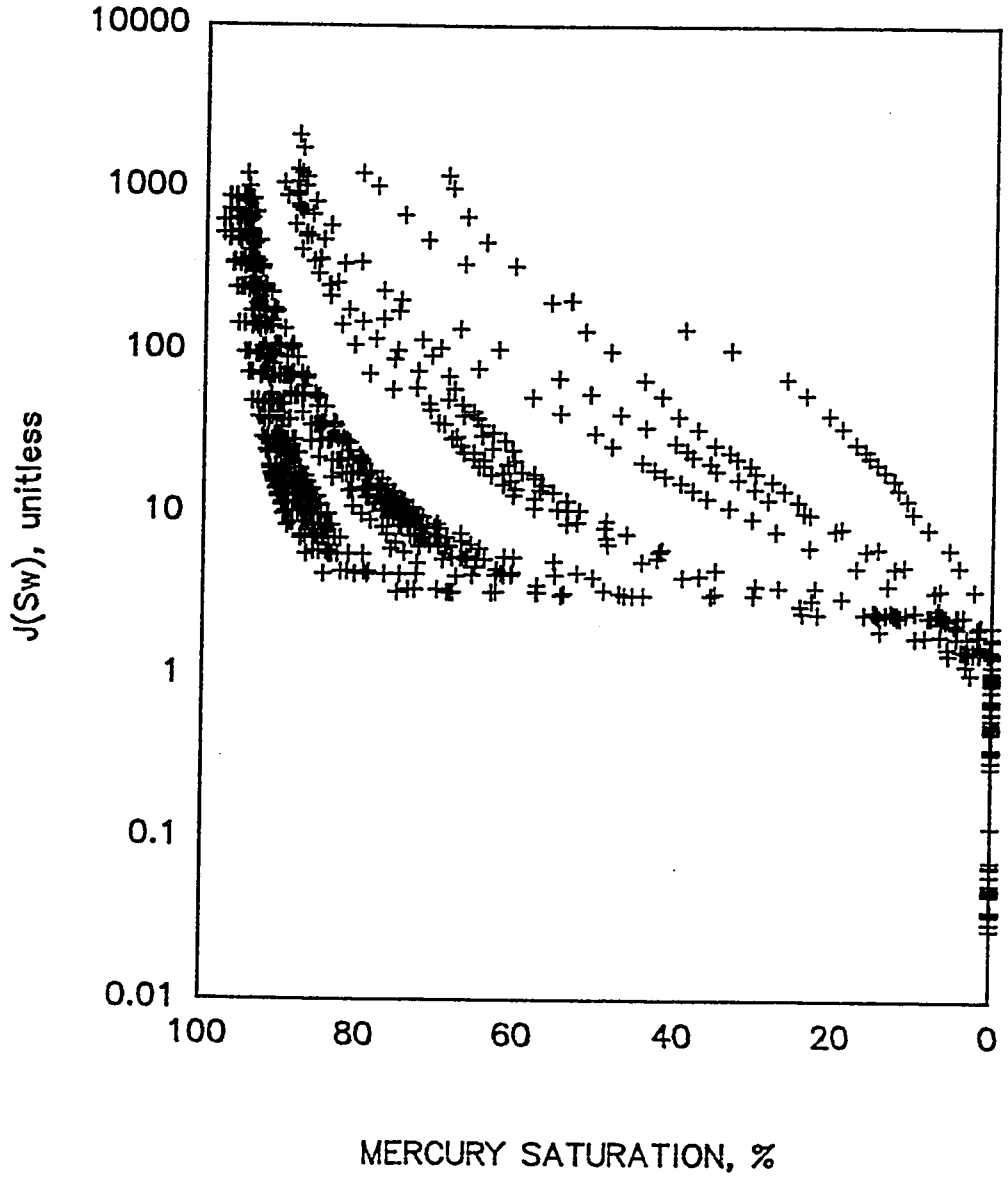

Fig.(4.94). J–Function Correlation For All Studied Samples Using Critical Length Developed in This Study.

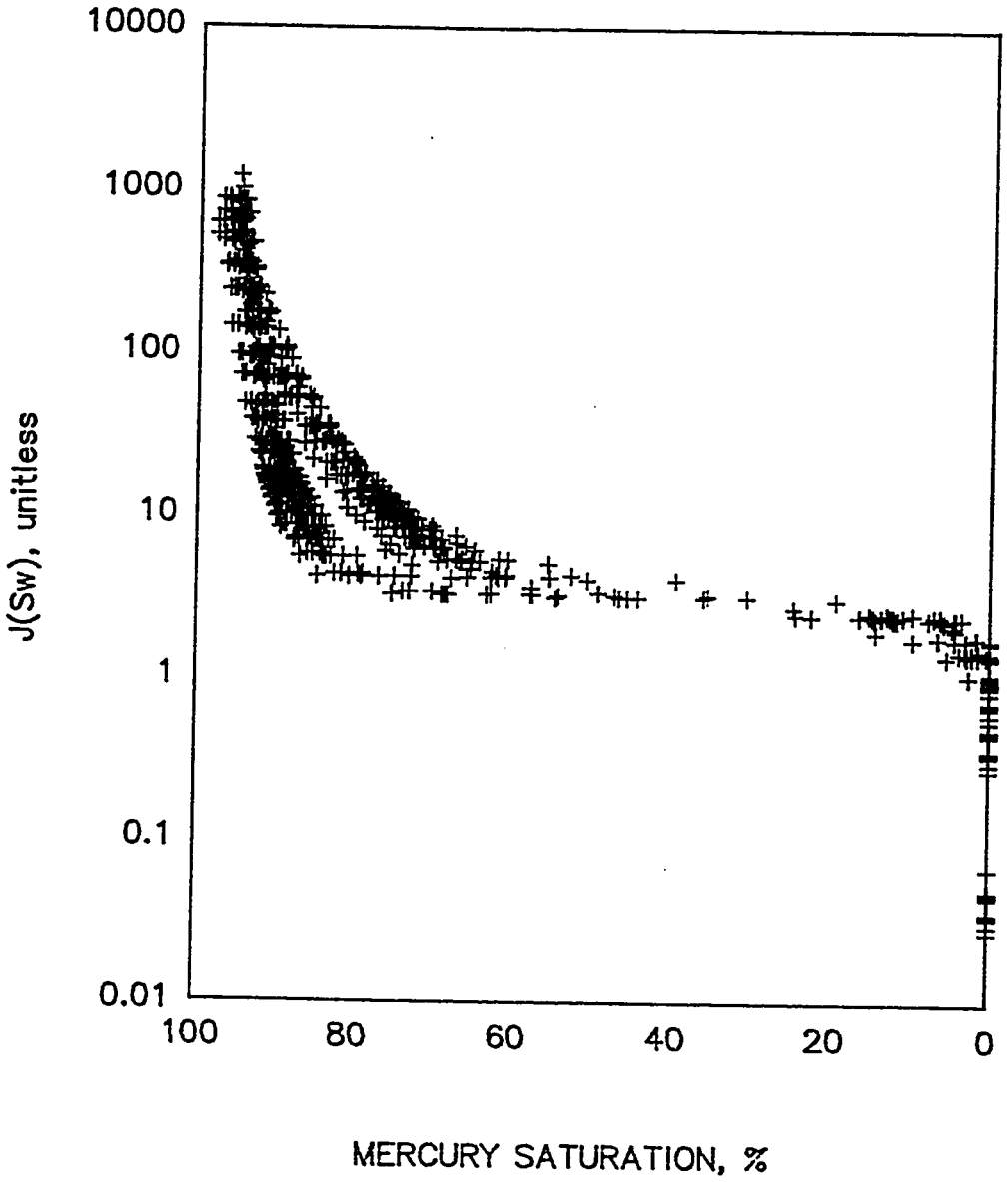

Fig.(4.94—A). J—Function Correlation For Sandstone Samples Using Critical Length Developed in This Study.

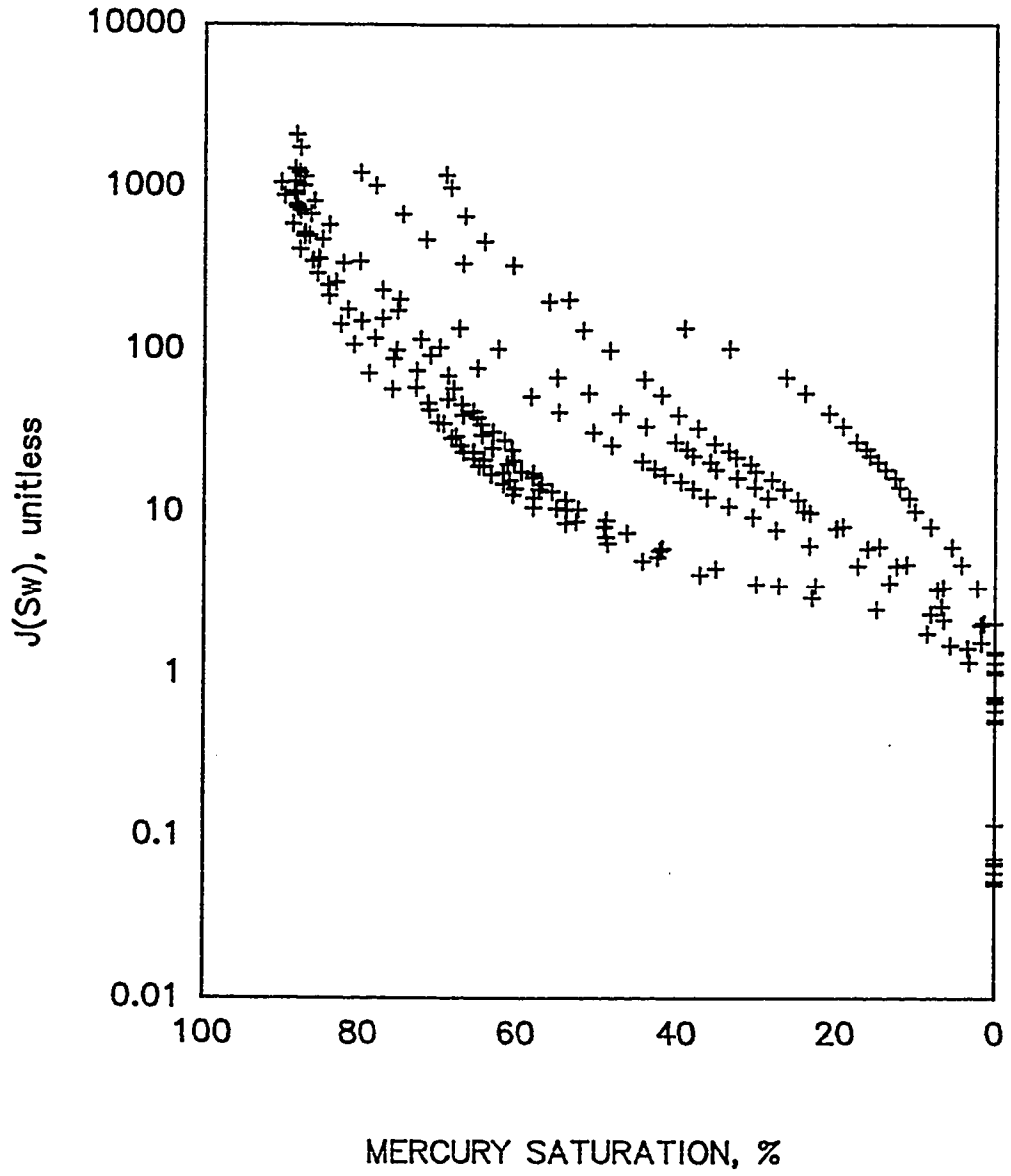

Fig.(4.94–B). J–Function Correlation For Carbonate Samples Using Critical Length Developed in This Study.

The effect of porosity as to whether the J-function can be improved was shown in Figs. (4.95) and (4.95-a). The equation used in Fig.(4.94) was modified by dividing by porosity. The expression thus becomes :

$$J(S_w) = \frac{P_c}{\sigma}\frac{l_c}{\varphi}$$

It is apparent that the porosity influenced the J-curve and gave more scattering in the correlation. Although the sandstone samples were separated from the carbonate samples, the dispersion of data points still existed as could be seen from Fig. (4.95-a).

Additional modifications were made in order to improve the correlation whereby the PTS as a parameter was used in the equation shown below :

$$J(S_w) = \frac{P_c}{\sigma}\frac{l_c}{PTS}$$

Figures (4.96) and (4.96-a) show the results obtained by using the above equation considering all the samples and the sandstone samples respectively. Both figures did not show a good correlation, especially for the carbonate samples. It is believed that carbonate samples contained cavities, vugs that differed from one sample to another and thus the deviations from the trends established in capillary pressure data were as expected.

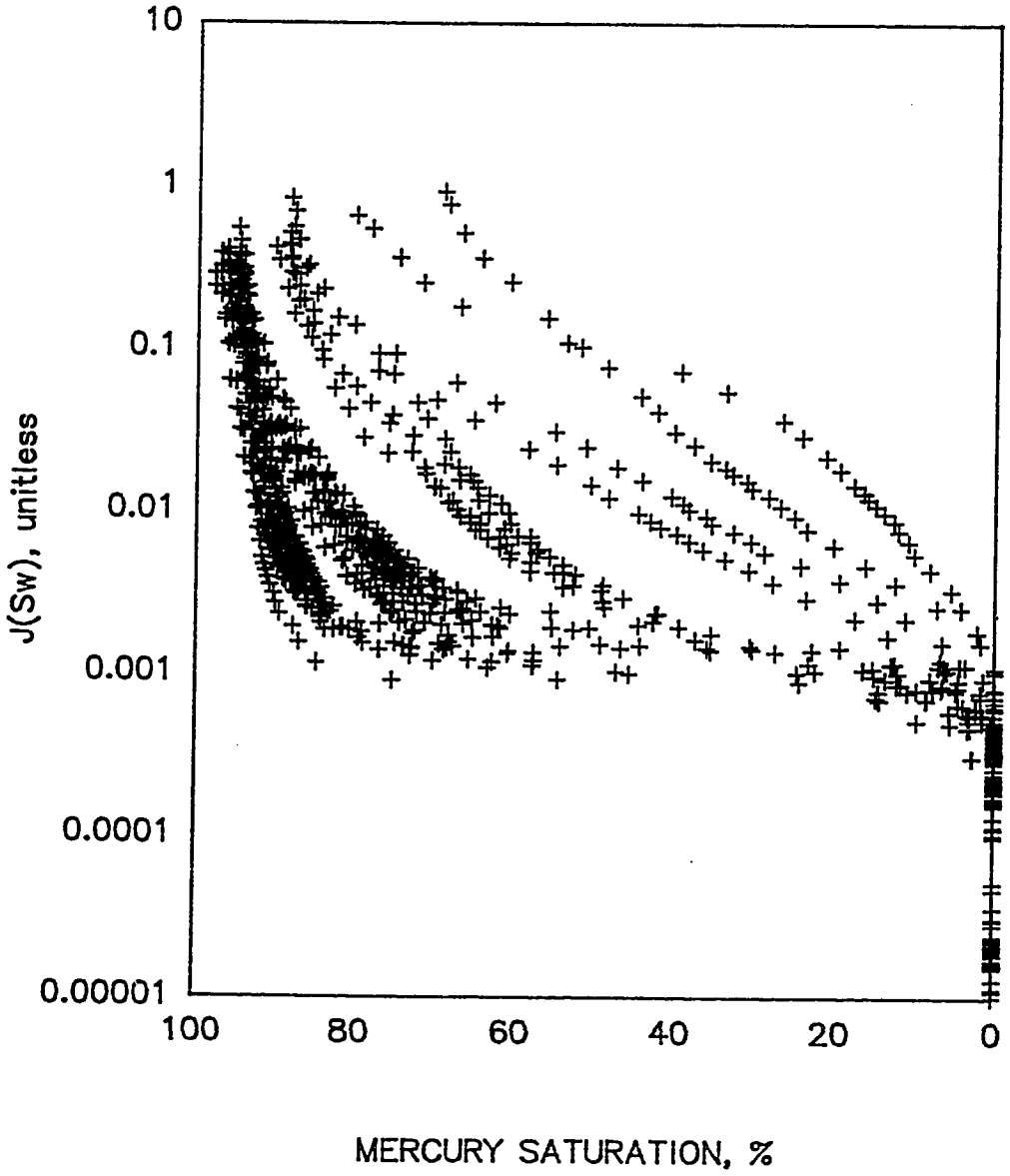

Fig.(4.95). J–Function Correlation For All Studied Samples Using Critical Length with Porosity Developed in This Study.

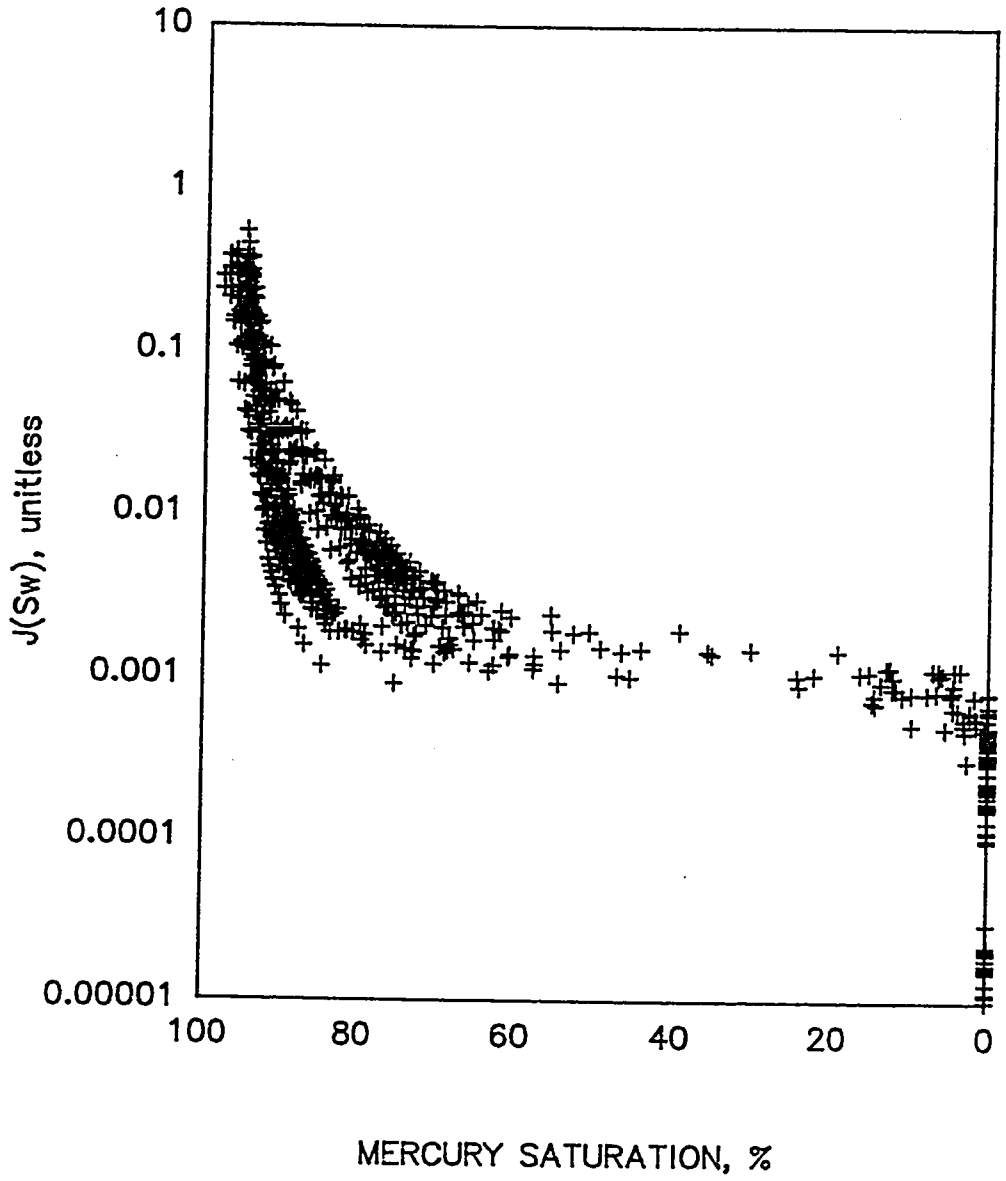

Fig.(4.95–A). J–Function Correlation For Sandstone Samples Using Critical Length with Porosity Developed in This Study.

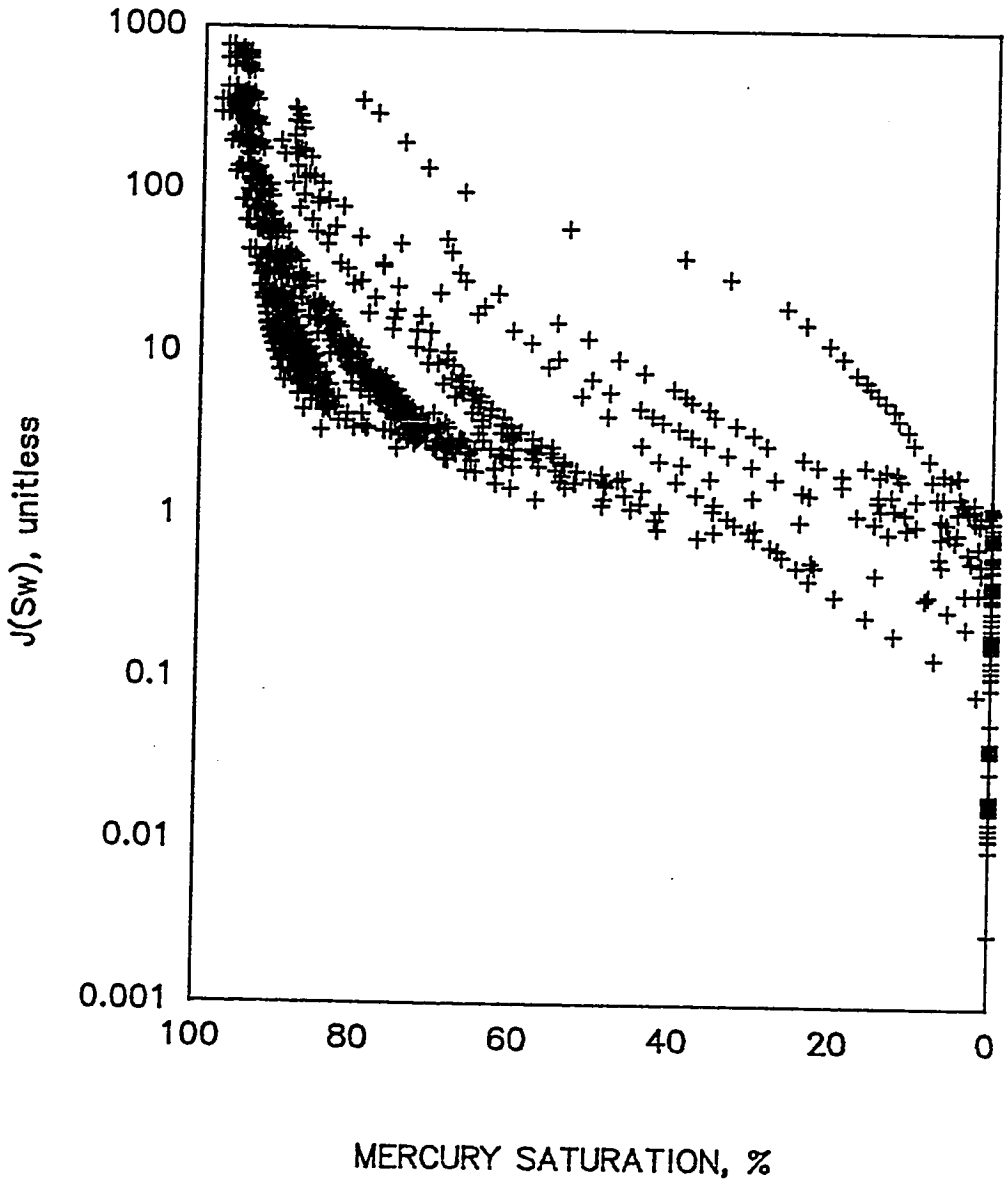

Fig.(4.96). J–Function Correlation For All Studied Samples Using Critical Length with PTS Developed in This Study.

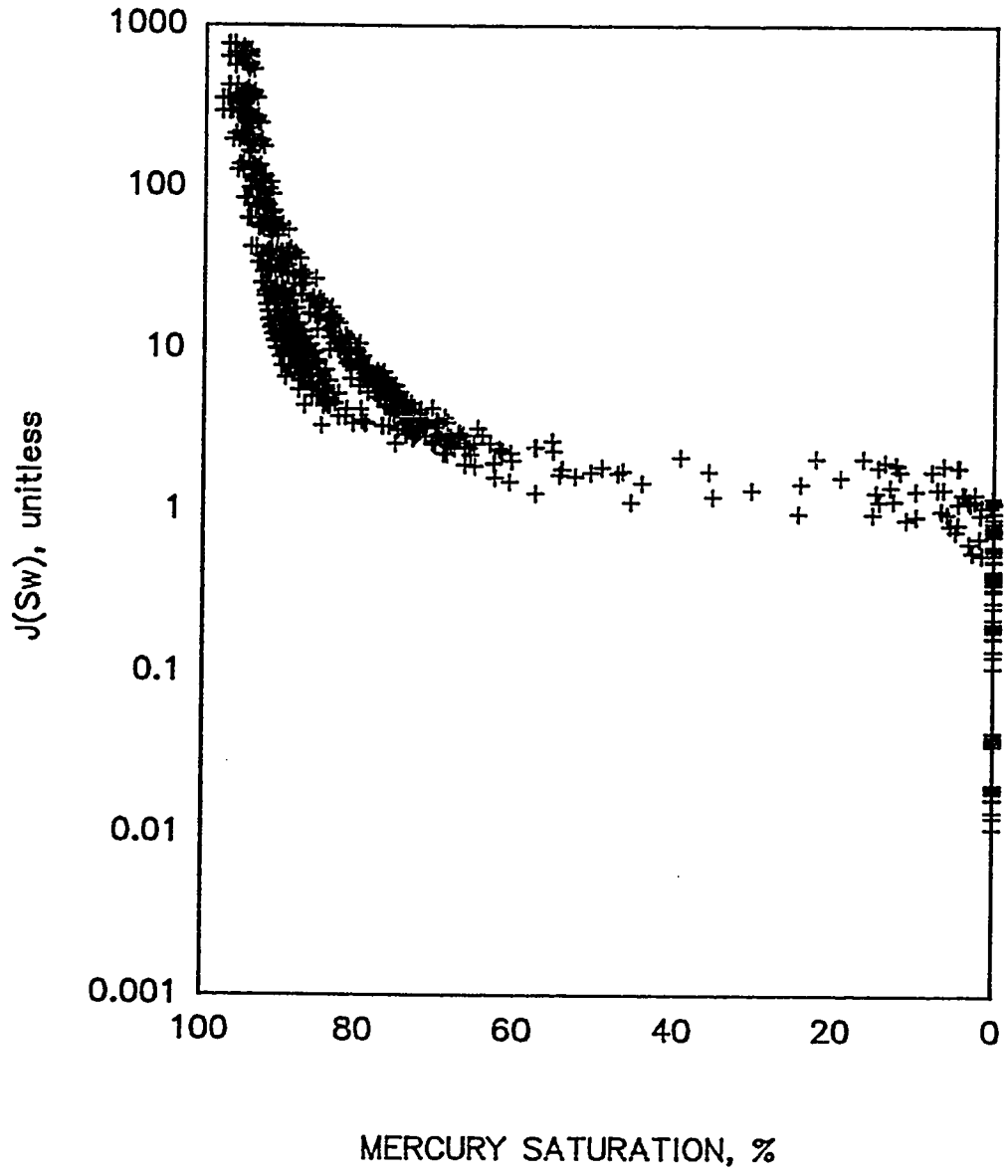

Fig.(4.96–A). J–Function Correlation For Sandstone Samples Using Critical Length with PTS Developed in This Study.

A correlation function was developed as an attempt to obtain a better correlation which is expressed as :

$$J(S_w) = \frac{P_c}{\sigma}\frac{k}{l_c \varphi}$$

Figure (4.97) shows the correlation obtained for all the samples. The correlation exhibits a scattering of the data in the range of low nonwetting phase saturations. Figures (4.97-a) and (4.97-b) are for sandstone and carbonate samples respectively. There is some dispersion of data points, but the trend of the correlation is good for both samples. The limitation of the correlation is that the permeability of the samples should be more than 20 md. For samples whose permeability is less than 10 md, the critical length (l_c) determination is not very accurate because of the difficulty in determining the inflection points of the capillary pressure curve.

A final attempt was made to obtain a better correlation which has the following modification. The displacement pressure was subtracted from the actual J-function proposed by Leverett.The expression so derived is :

$$J(S_w) - P_d = \frac{P_c}{\sigma}\sqrt{k/\varphi}$$

The J-curve for all the samples studies are shown in Fig. (4.98). The

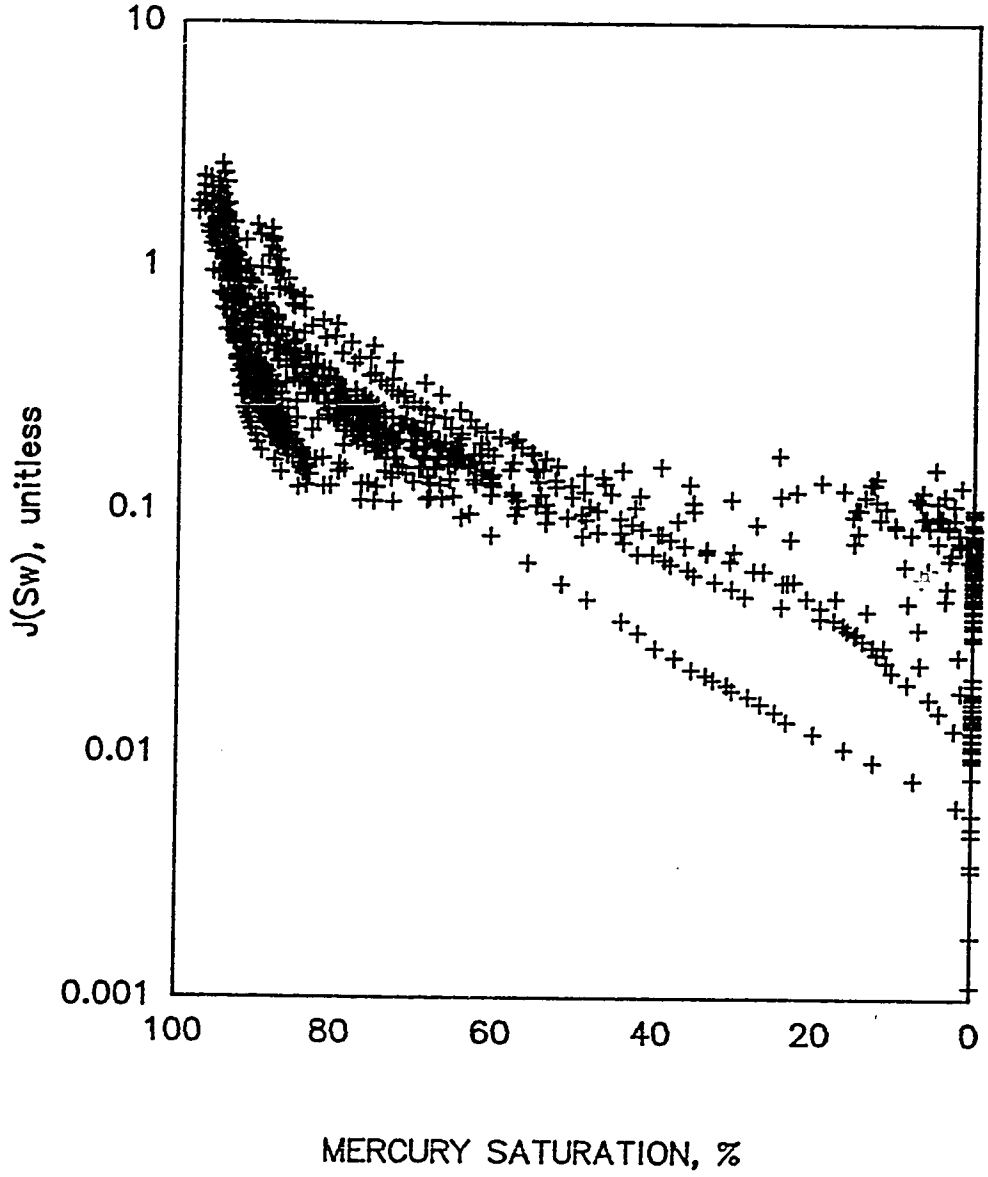

Fig.(4.97). J–Function Correlation For All Studied Samples Using Modified Correlation Developed in This Study.

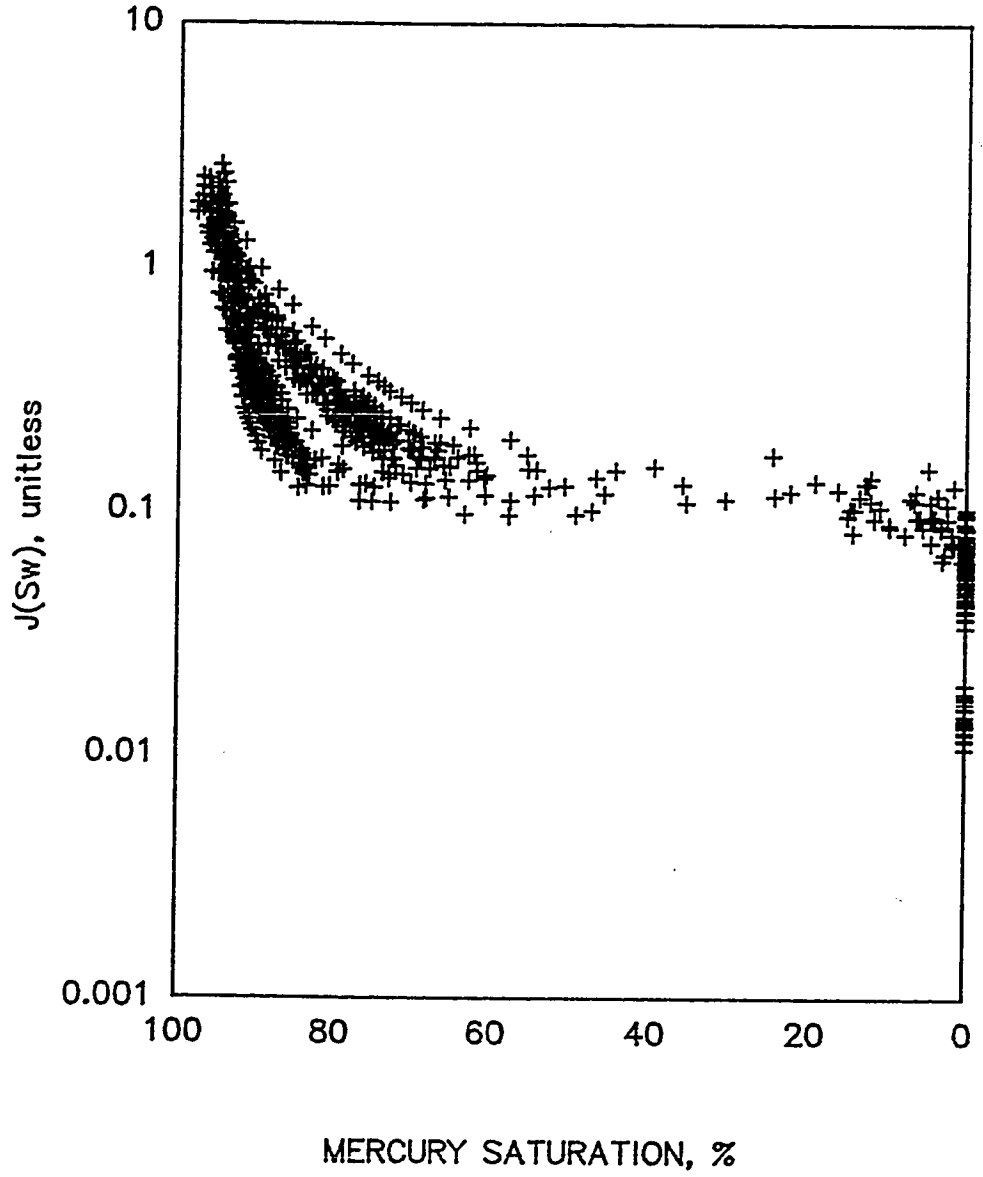

Fig.(4.97–A). J–Function Correlation For Sandstone Samples Using Modified Correlation Developed in This Study.

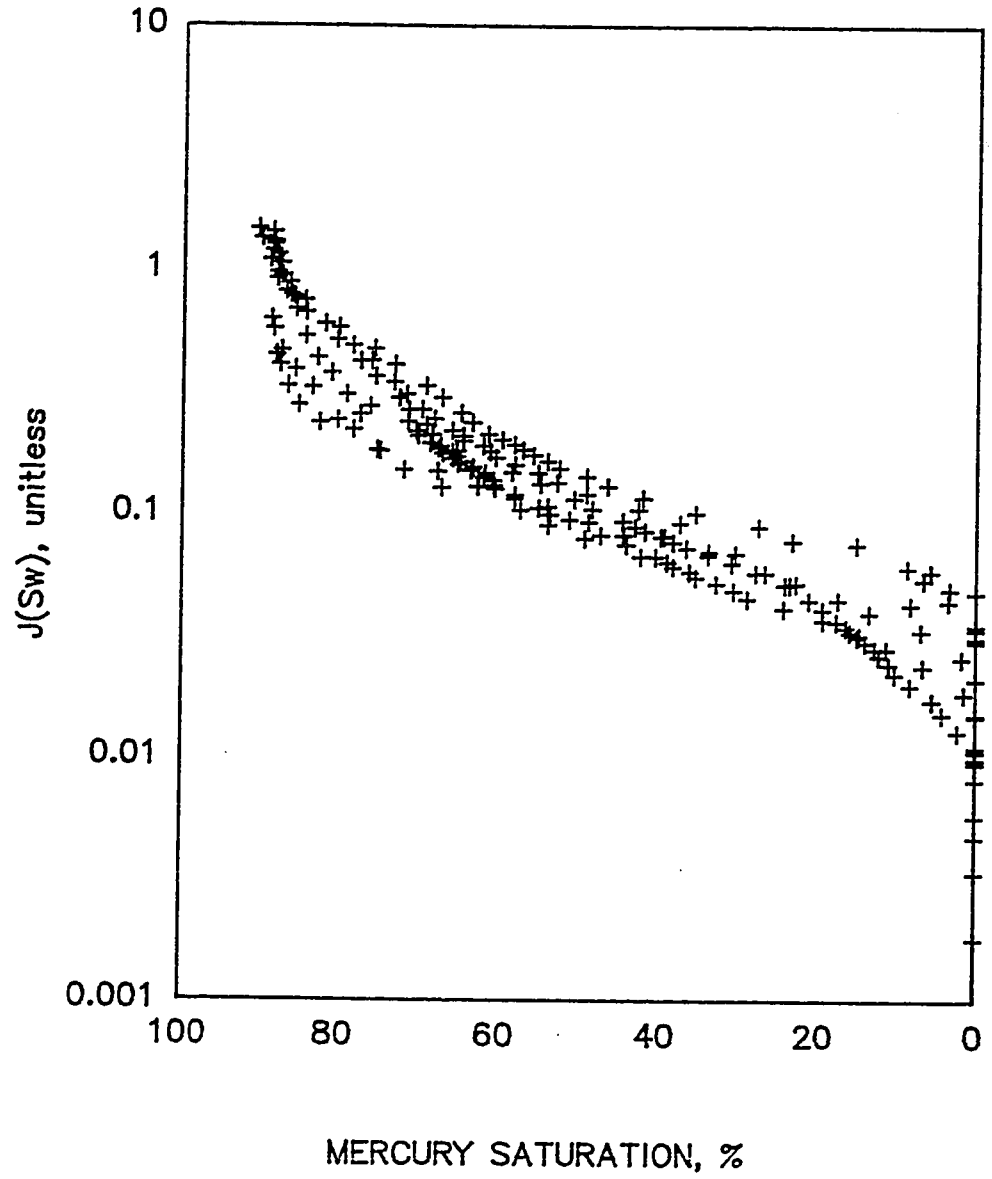

Fig.(4.97–B). J–Function Correlation For Carbonate Samples Using Modified Correlation Developed in This Study.

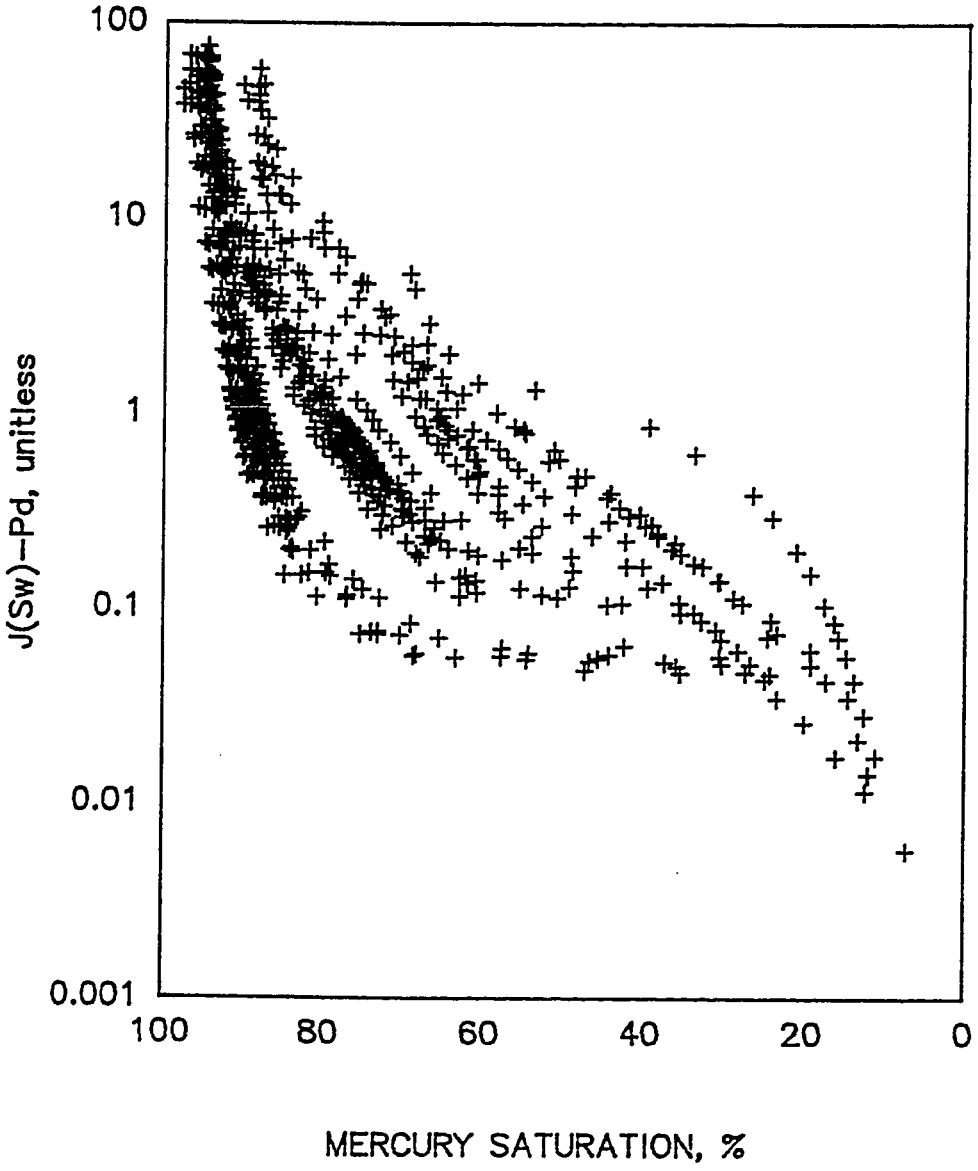

Fig.(4.98). J–Function Correlation For All Studied Samples Using Displacement Pressure as a Parameter.

scattering of the data points was reduced and the spreading became less except in the region of high saturation. An important question as to displacement pressure arises when the above expression is used because the displacement pressure value is included in the equation, and the displacement pressure cannot be determined from laboratory experiment unless the mercury capillary injection test was conducted for those samples which were used in J-function.

In summary, several attempted were made to obtain a modified J-function correlation for capillary pressure data because the capillary pressure can be obtained directly provided saturation of the sample is known without performing a laboratory experiment. The J-curve can be represented as a universal curve. Therefore, some of the literatures has been trying to find the correlation function. They concluded that no universal curve can be obtained and the J-curve should not be used for a group of closely related fields even in a single reservoir. According to this study, there is no suitable correlation existing and no curve can fit a group of samples. The parameters such as permeability, porosity, pore geometry, pore size distribution, pore throat sorting and apart from these, the contact angle of the samples which value do not stand the same throughout the rock life, and the surface tension have to be considered when J-curve is to be used.

An alternative way to determine capillary pressure was developed by Amyx, Bass, and Whiting [32] which method will be discussed in the following

section. Figure (4.99) represents the application of their method using the equation given below :

$$S_w = a\log k + c$$

For large capillary pressure, the data were converged in high permeability range as it was expected that larger capillaries had associated with high permeability. From the figure, by knowing the permeability and saturation value, the estimated capillary pressure can be obtained.

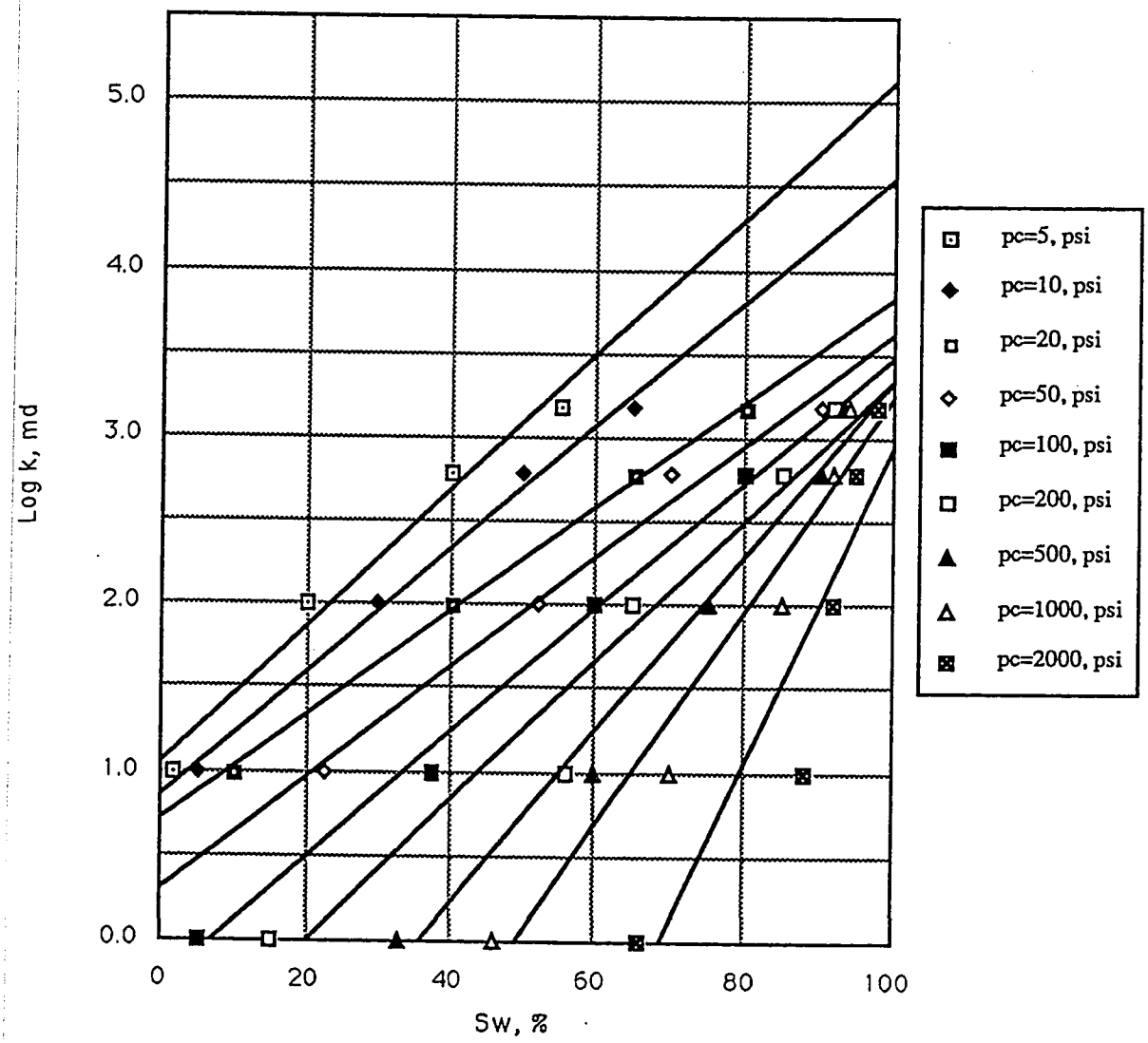

Fig(4.99). Permeability as a function of saturation for different capillary pressure.

CHAPTER 5

CHAPTER 5

CONCLUSIONS AND RECOMMENDATIONS

5.1 CONCLUSIONS

Based on the laboratory investigations and discussions presented in this study, the following conclusions are drawn:

1. The mercury injection provides the most reliable approach to obtain equilibrium capillary pressure data for injection, ejection and re-injection curves over a wide range of mercury saturation.

2. The variation of sample size did not show any shifting or movement in the injection capillary pressure curve for sandstone samples, but for carbonate samples, the variation of injection and ejection capillary pressure curves depends strongly on the pore throat diameter and the permeability of the samples.

3. For rapid rate of withdrawal capillary pressure curve, residual saturation increases along with the increase in the size of the sandstone sample, but the unsaturated pore volumes remain the same for all the sizes of the samples.

4. There is no significant effect on the capillary pressure curve studied due to the slow and the rapid injection as far as the sandstone sample is concerned.

5. The capillary pressure curve moves to a lower saturation range at a given pressure and the displacement pressure becomes lower with increasing sample size when the carbonate sample is coated with an epoxy on the surfaces which are least permeable.

6. The injection capillary pressure curve is insensitive to the sample size as well as the epoxy coating for sandstone sample. No surface effects were encountered between coated and uncoated sandstone samples which are highly permeable.

7. Porosity is the only variable that correlates well with withdrawal efficiency. No correlation exists between permeability, displacement pressure, pore throat sorting and withdrawal efficiency.

8. The estimation of permeability using Katz and Thompson's method shows that the calculated and measured values vary within the range as suggested by them. The Swanson's correlation method was utilized to compare the results with the previous method and it was found that The Katz and Thompson's method was more realistic to estimate the permeability than that of others.

9. The correlation function determination was improved in this study. The samples were separated into two groups of sandstone and carbonate and introducing pore throat sorting as a parameter for sandstone and critica length for carbonate samples.

5.2 RECOMMENDATIONS

From the results of this study, the following recommendations are made for the extension of the present work:

1. Capillary pressure measurements need to be conducted under high pressure around 10000 psi to understand better the capillary behavior of mercury-air in tight carbonate rocks.

2. The study of the capillary pressure on carbonate rock by mercury injection also suggests existance of some variations in the reservoir characteristics, but the small number of samples analyzed in this study may not be significantly sufficient to evaluate the rock characteristics.

NOMENCLATURE

a	Exponent
b	Multiplier
d_T	Throat Diameter, cm
$J(S_w)$	Correlation Function
k	Air Permeability, md
k_l	Liquid Permeability, md
k_{calc}	Calculated Permeability, md
k_{mea}	Measured Permeability, md
l_c	Critical Length, cm
L^h_{max}	Hydraulic Conductance, cm
P_c	Capillary Pressure, psi
P_d	Displacement Pressure, psi
PTS	Pore Throat Sorting
S_b	Saturation at the Tengent Intersect the 45° line Draw from Origin, %
$S(L^h_{max})$	Volume Fraction of Pore Sapce Filled with Mercury as a Function of P_c or Pore Diameter l, Fraction
σ	Surface Tension, Dynes/cm
0	Contact Angle, degree
φ	Porosity
$\frac{\sigma}{\sigma_o}$	Conductivity Formation Factor
$\frac{1}{89}$	Constant for Conversion

REFERENCES

1. Leverett, M.C. : " ***Capillary Behavior in Porous Solids*** , " Tulsa Meeting, Trans. AIME v.142 (October 1940) 152-169.

2. Hassler, G.L., and Brunner, E. : " ***Measurement of Capillary Pressure in Small Core Sample*** , " Los Angeles Meeting (October 1944) 114-123.

3. Purcell, W.R. : " ***Capillary Pressure-Their Measurement Using Mercury And The Calculation of Permeability Therefrom*** , " Transactions, AIME (February 1949) 39-48.

4. Rose Walter and Bruce, W.A. : " ***Evaluation of Capillary Character in Petroleum Reservoir Rock*** , " Petroleum Transactions, AIME (May,1949) 127-142.

5. Brown, Harry W. : " ***Capillary Pressure Investigations*** , " Petroleum Transactions, AIME Vol. 192, (1951) 67-74.

6. Pickell, J.J., Swanson, B.F., and Hickman, W.B. : " ***Application of Air-Mercury and Oil-Air Capillary Pressure Data In The Study of Pore Structure and Fluid Distribution*** , " Soc. Pet. Eng. J. (March 1966) 55-61.

7. Scientific Software Corporation : " ***Capillary Pressure Measurement***

Using Mercury (The Purcell Method) Permeability Estimation , " Reservoir Engineering Manual (September 1975) 2-47-2-51.

8. Wardlaw, N.C., and Taylar, R.P. : " ***Mercury Capillary Pressure Curves and The Interpretation of Pore Structure and Capillary Behavior in Reservoir Rocks*** , " Bulletin of Canadian Petroleum Geology, V.24, No.2 (June 1976) 225-262.

9. Wardlaw, N.C. : " ***Pore Geometry of Carbonate Rocks as Revealed by Pore Casts And Capillary Pressure*** , " Geologists Bulletin v.60, No.2 (February 1976) 245-257.

10. Wardlaw, N.C., and Cassan, J.P. : " ***Oil Recovery Efficiency and The Rock Pore Properties of Some Sandstone Reservoirs,*** " Bulletin Canadian Petroleum Geology, v.27, No.2 (June 1979) 117-138.

11. Wardlaw,N.C., and McKellar, M. : " ***Mercury Porosimetry and The Interpretation of Pore Geometry in Sedimentary Rocks and Artificial Model*** , " Powder Technology v.29 (1981) 127-143.

12. Larson, R.G., and Morrow, N.R. : " ***Effects of Sample Size on Capillary Pressure in Porous Media,*** " Powder Technology v.30 (1981) 123-138.

13. Sampath Krishnaswamy and Raible, Clarence.J. : " ***Measurement of Formation Characteristics of Western Tight Sands,*** " United State

Department of Energy (1May, 1981).

14. Swanson, B.F. : " *A Sample Correlation Between Permeabilities and Mercury Capillary Pressure* , " Journal of Petroleum Technology (December 1981) 2498-2504

15. Thomeer, J.H.M. : " *Air Permeability as a Function of Three Pore Network Parameters,* " Journal of Petroleum Technology (April 1983).

16. Swanson, B.F. : " *Microporosity in Reservoir Rocks-Its Measurement and Influence on Electrical Resistivity* , " SPWLA Twenty Sixth Annual Logging Symposium, (June, 1985).

17. Omorregie, Z.S. : " *Factors Affecting the Equivalency of Different Capillary Pressure Measurement Techniques* , " The 61st Annual Technical Conference and Exhibition of the Society of Petroleum Engineers, (October, 1986).

18. Katz, A.J. and Thompson, A.H. : " *Quantitative Prediction of Permeability in Porous Rock* , " Physical Review B, v.34, No.11 (December 1986) 8179-8181.

19. Katz, A.J. and Thompson, A.H. : " *Prediction of Rock Electrical Conductivity From Mercury Injection Measurements* , " Journal of Geophysical Research, v.92, No.B1 (January 1987) 599-607.

20. Thompson, A.H., Katz, A.J. and Krohn, C.E. : " ***The Microgeometry and Transport Properties of Sedimentary Rock,*** " Exxon Production Research, Co. U.S.A. (february, 1987).

21. Kent, D.M. : " ***Modelling Carbonate Reservoir Porosity for Enhance Recovery schemes*** , " The Journal of Canadian Petroleum Technology, (July-August, 1987).

22. Thompson, A.H., Katz, A.J. and Raschke, R.A. : " ***Estimation of Absolute Permeability From Capillary Pressure*** , " Journal of Petroleum Technology SPE 16794 (September 1987) 475-481.

23. Jennings, Jeffrey.B. : " ***Capillary Pressure Techniques : Application to Exploration and Development Geology*** , " The American Association of Petroleum Geologists Bulletin, v.71,No.10 (October 1987),p.1196-1209.

24. Mishra, B.K., and Sharma, M.M. : " ***Measurement of Pore Size Distributions From Capillary Pressure Curves*** , " AICHE Journal, Vol.34, No.4, (April 1988).

25. Tsang, Y.W., and Hale, F.V. : " ***A Study of the Application of Mercury Porosimetry Method to a Single Fracture*** , " Lawrence Berkeley Lab., Earth Sciences Division, University of California (June 1988).

26. Kamath, J. : " ***Evaluation of Estimating Air Permeability From Mercury Injection Data*** , " The 63rd Annual Technical Confrence and Exhibition of the Society of Petroleum Engineers, (October, 1988).

27. Chowdiah, P. : " ***Influence of Water-Desaturation Technique and Stress on Laboratory Measurement of Hydraulic Properties of Tight Sandstones*** , " SPE Formation Evaluation, (December, 1988).

28. Yuan, H.H., and Swanson, B.F. : " ***Resolving Pore Space Characteristics by Rate-Controlled Porosimetry*** , " SPE Formation Evaluation, (March, 1989).

29. Morrow, et al. : " ***Rock Matrix and Fracture Analysis of Flow in Western Tight Sands*** , " Annual Report, New Mexico Petroleum Revovery Research Center, (May, 1989).

30. Tsakiroglou, Christos.D., and Payatakes, Alkiviades, C. : " ***A New Simulator of Mercury Porosimetry for the Characterization of Porous Materials*** , " Journal of Colloid and Interface Sciences, Vol.137, No. 2, (July, 1990).

31. Maloney, D.R., Honarpour, M.M., and Brinkmeye, A.D. : " ***The Effects of Rock Characteristics on Relative Permeability*** , " National Inst. for Petroleum and Energy Research, Bartlesville, OK, (January, 1990).

32. Amyx, James W., Bass, Daniel M., and Whiting, Robert L. : " ***Petroleum Reservoir Engineering*** (***Physical Properties***) , " McGRAW-Hill, (March, 1960).

APPENDIX-A

App-A1.MERCURY CAPILLARY PRESSURE TEST DATA SHEET

Sample No	Berea S20		Caliper /Helium
Length (cm)	1.85	Bulk Volume (cc)	8.37
Diameter (cm)	2.4	Pore Volume (cc)	1.65
Dry Weight (g)	17.582	Grain Volume (cc)	6.72
Weight@End (g)	28.175	Grain Den. (g/cc)	2.62
Permeabl. (md)	507.3	Porosity (%)	19.77
		Pore Volume Used	1.6542

CAP PRESS (psi)	BLANK INJEC (cc)	BLANK EJECT (cc)	BLANK RE-INJ (cc)	TOTAL INJEC (cc)	TOTAL EJECT (cc)	TOTAL RE-INJ (cc)	NET INJEC (cc)	NET EJECT (cc)	NET RE-INJ (cc)
0.1	2.50	1.54	1.54	2.50	2.05	2.05	0.00	0.51	0.51
1	2.50	1.54	1.54	2.50	2.05	2.05	0.00	0.51	0.51
2	4.00	3.82	4.06	4.00	4.39	4.63	0.00	0.57	0.57
3	5.46	5.28	5.20	5.46	6.06	5.80	0.00	0.78	0.60
5	7.17	7.12	7.25	7.20	8.06	7.96	0.03	0.94	0.71
7	8.10	8.14	8.10	8.35	9.23	8.87	0.25	1.09	0.77
9	8.67	8.72	8.72	9.26	9.90	9.64	0.59	1.18	0.92
12	9.18	9.27	9.23	10.05	10.50	10.29	0.87	1.23	1.06
15	9.48	9.55	9.51	10.48	10.83	10.62	1.00	1.28	1.11
18	9.69	9.74	9.72	10.78	11.06	10.89	1.09	1.32	1.17
21	9.85	9.90	9.88	10.96	11.24	11.07	1.11	1.34	1.19
24	9.95	10.02	9.98	11.11	11.37	11.19	1.16	1.35	1.21
27	10.04	10.09	10.07	11.24	11.47	11.30	1.20	1.38	1.23
30	10.11	10.16	10.15	11.33	11.56	11.40	1.22	1.40	1.25
33	10.17	10.22	10.21	11.40	11.63	11.48	1.23	1.41	1.27
36	10.22	10.27	10.25	11.47	11.69	11.54	1.25	1.42	1.29
40	10.27	10.31	10.30	11.55	11.74	11.61	1.28	1.43	1.31
50	10.35	10.40	10.40	11.65	11.84	11.75	1.30	1.44	1.35
60	10.43	10.48	10.46	11.75	11.93	11.82	1.32	1.45	1.36
80	10.51	10.55	10.55	11.87	12.02	11.94	1.36	1.47	1.39
100	10.57	10.62	10.60	11.95	12.11	12.02	1.38	1.49	1.42
150	10.65	10.71	10.69	12.07	12.21	12.15	1.42	1.50	1.46
200	10.72	10.78	10.75	12.17	12.29	12.22	1.45	1.51	1.47
300	10.82	10.88	10.83	12.29	12.41	12.32	1.47	1.53	1.49
500	10.99	11.06	11.00	12.50	12.60	12.51	1.51	1.54	1.51
700	11.14	11.21	11.15	12.67	12.76	12.68	1.53	1.55	1.53
1000	11.35	11.41	11.35	12.90	12.97	12.90	1.55	1.56	1.55
1500	11.69	11.71	11.69	13.25	13.27	13.25	1.56	1.56	1.56
1800	11.80	11.80	11.80	13.36	13.36	13.36	1.56	1.56	1.56

App-A2. MERCURY CAPILLARY PRESSURE TEST DATA SHEET

			Hg/	Immers.
Sample No	Berea S1			
Length (cm)	2.24	Bulk Volume (cc)		10.34
Diameter (cm)	2.43	Pore Volume (cc)		2.26
Dry Weight (g)	21.031	Grain Volume (cc)		8.08
Weight@End (g)	32.13	Grain Den. (g/cc)		2.6028
Permeabl. (md)	507.3	Porosity (%)		21.857
		Pore Volume Used		2.26

CAP PRESS (psi)	BLANK INJEC (cc)	BLANK EJECT (cc)	BLANK RE-INJ (cc)	TOTAL INJEC (cc)	TOTAL EJECT (cc)	TOTAL RE-INJ (cc)	NET INJEC (cc)	NET EJECT (cc)	NET RE-INJ (cc)
0.1	0.66	0.66	0.66	0.66	1.20	1.20	0.00	0.54	0.54
1	0.66	0.66	0.66	0.66	1.20	1.20	0.00	0.54	0.54
2	3.39	3.39	3.39	3.39	3.93	3.93	0.00	0.54	0.54
3	5.13	5.13	5.13	5.13	5.67	5.67	0.00	0.54	0.54
5	7.15	7.15	7.15	7.15	7.85	7.85	0.00	0.70	0.70
7	8.24	8.24	8.24	8.40	9.49	9.26	0.16	1.25	1.02
9	9.02	9.07	9.07	9.83	10.53	10.35	0.81	1.46	1.28
12	9.79	9.82	9.80	11.04	11.40	11.28	1.25	1.58	1.48
15	10.02	10.18	10.16	11.47	11.83	11.75	1.45	1.65	1.59
18	10.54	10.57	10.56	12.09	12.26	12.24	1.55	1.69	1.68
21	10.78	10.82	10.80	12.43	12.55	12.51	1.65	1.73	1.71
24	10.92	10.96	10.94	12.61	12.72	12.68	1.69	1.76	1.74
27	11.10	11.12	11.10	12.81	12.89	12.86	1.71	1.77	1.76
30	11.20	11.24	11.20	12.93	13.06	12.98	1.73	1.82	1.78
33	11.30	11.36	11.30	13.07	13.20	13.10	1.77	1.84	1.80
36	11.38	11.42	11.40	13.17	13.28	13.22	1.79	1.86	1.82
40	11.45	11.52	11.45	13.28	13.40	13.30	1.83	1.88	1.85
50	11.60	11.65	11.60	13.46	13.58	13.48	1.86	1.93	1.88
60	11.71	11.79	11.71	13.60	13.76	13.63	1.89	1.97	1.91
80	11.86	11.95	11.86	13.78	13.95	13.81	1.92	2.00	1.95
100	11.95	12.01	11.95	13.89	14.07	13.92	1.94	2.06	1.97
150	12.07	12.15	12.07	14.07	14.24	14.11	2.00	2.09	2.04
200	12.15	12.23	12.15	14.17	14.34	14.23	2.02	2.11	2.08
300	12.26	12.35	12.26	14.35	14.49	14.38	2.09	2.14	2.12
500	12.46	12.54	12.46	14.59	14.70	14.61	2.13	2.16	2.15
700	12.63	12.71	12.63	14.79	14.89	14.80	2.16	2.18	2.17
1000	12.85	12.91	12.85	15.03	15.10	15.03	2.18	2.19	2.18
1500	13.18	13.22	13.18	15.39	15.43	15.39	2.21	2.21	2.21
1800	13.37	13.37	13.37	15.58	15.58	15.58	2.21	2.21	2.21

APPENDIX-B

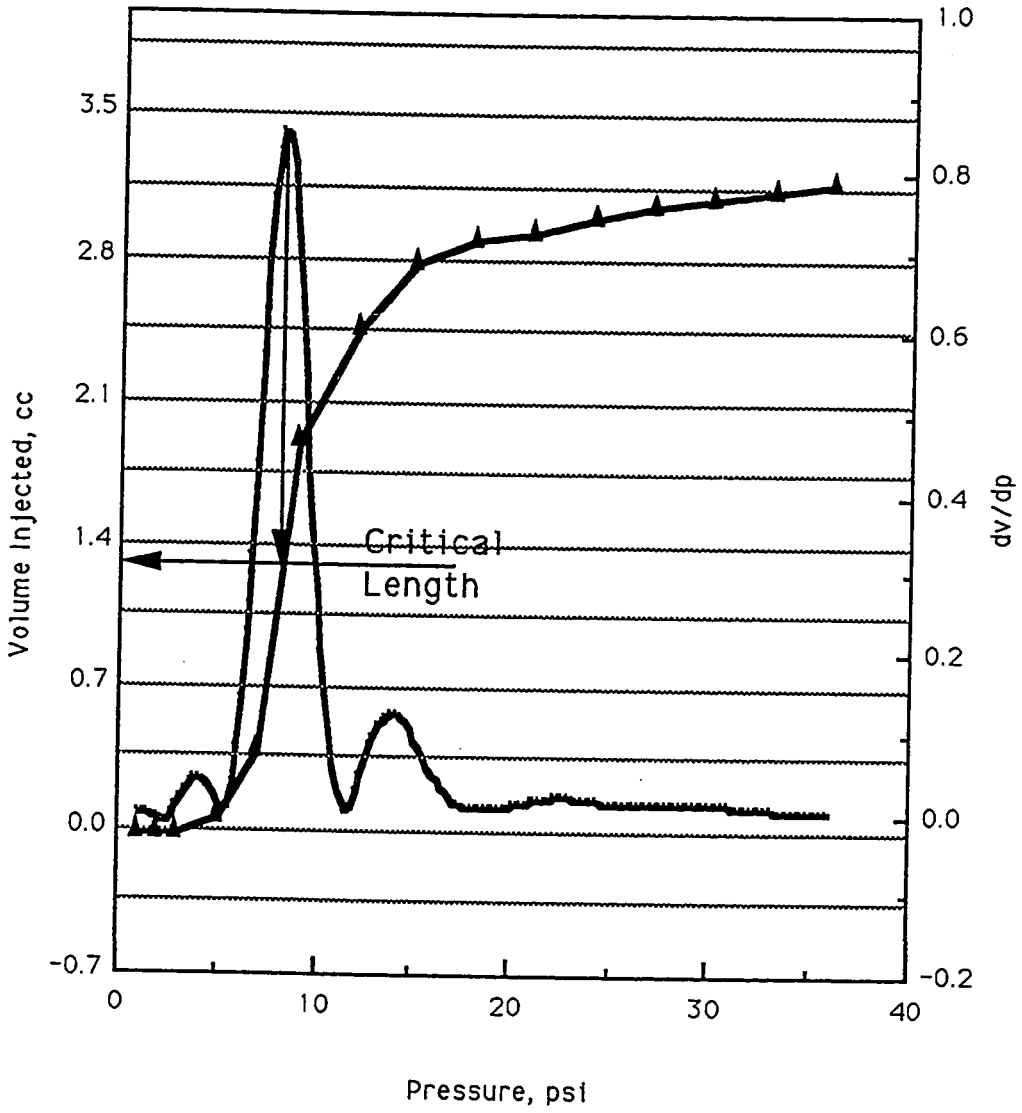

App-B1. Determination of Inflection Point from The Plot of Volume Injected vs Capillary Pressure for Berea Sample.

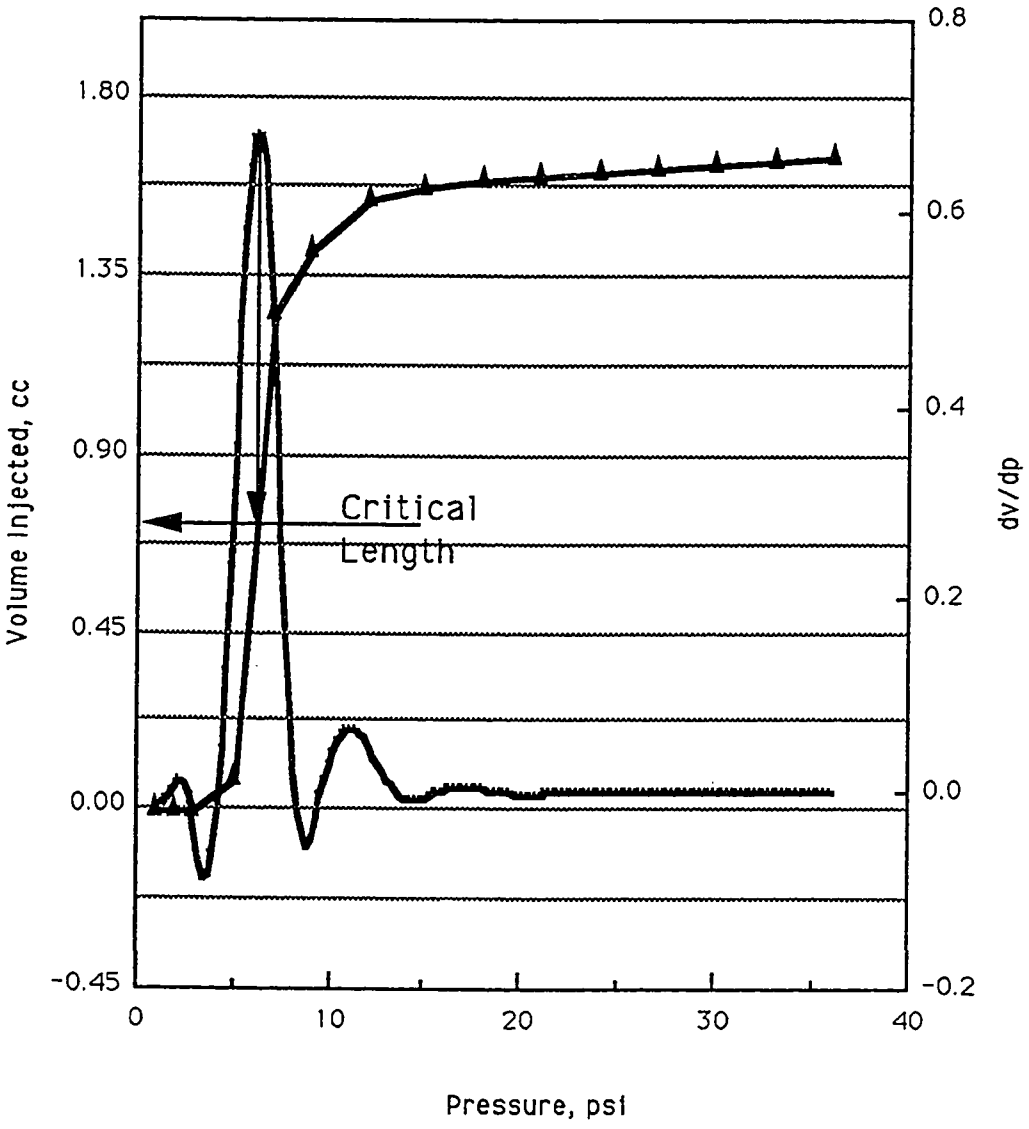

App-B2. Determination of Inflection Point from The Plot of Volume Injected vs Capillary Pressure for Bentheimer Sample.

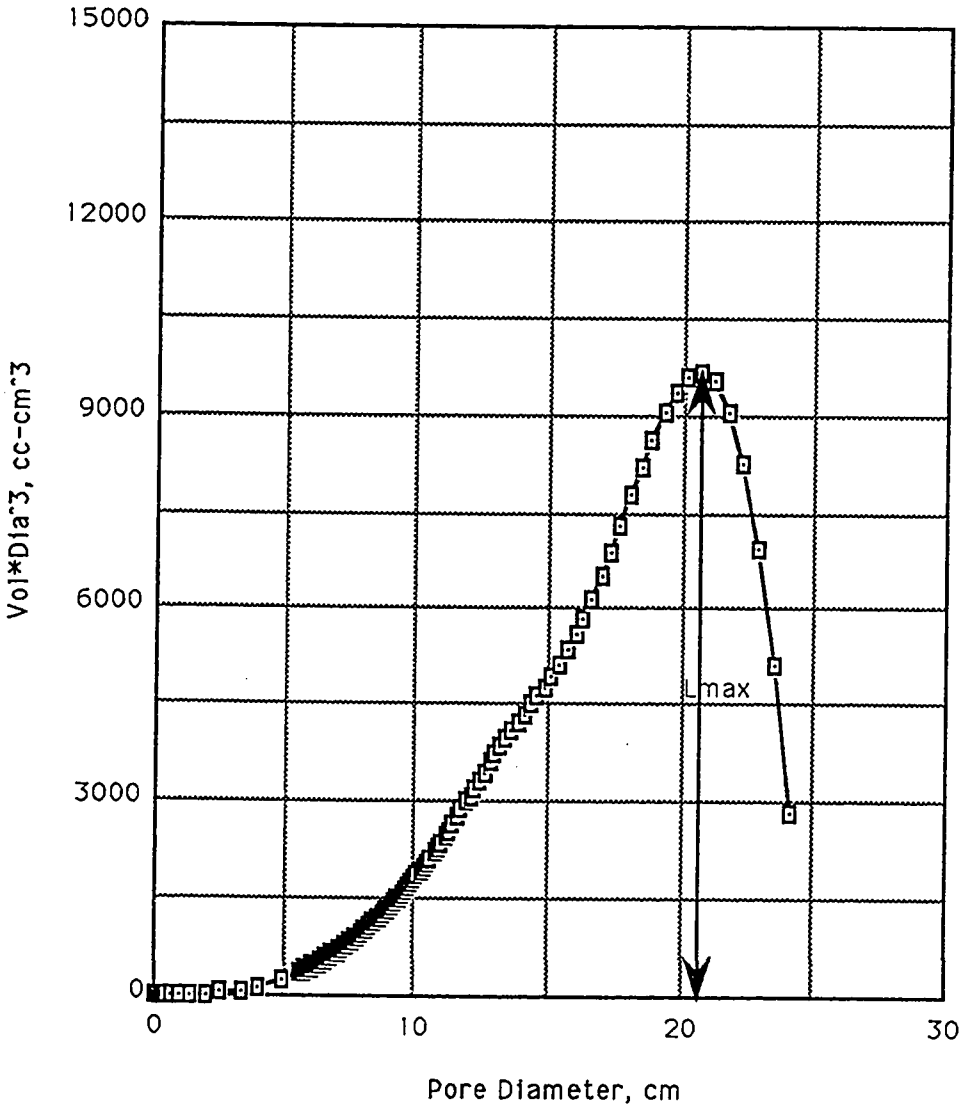

App-B3. Hydraulic Conductance Function Determination for Berea Sample from Volume Injected into Pore Spaces After the Inflection Point Was Obtained.

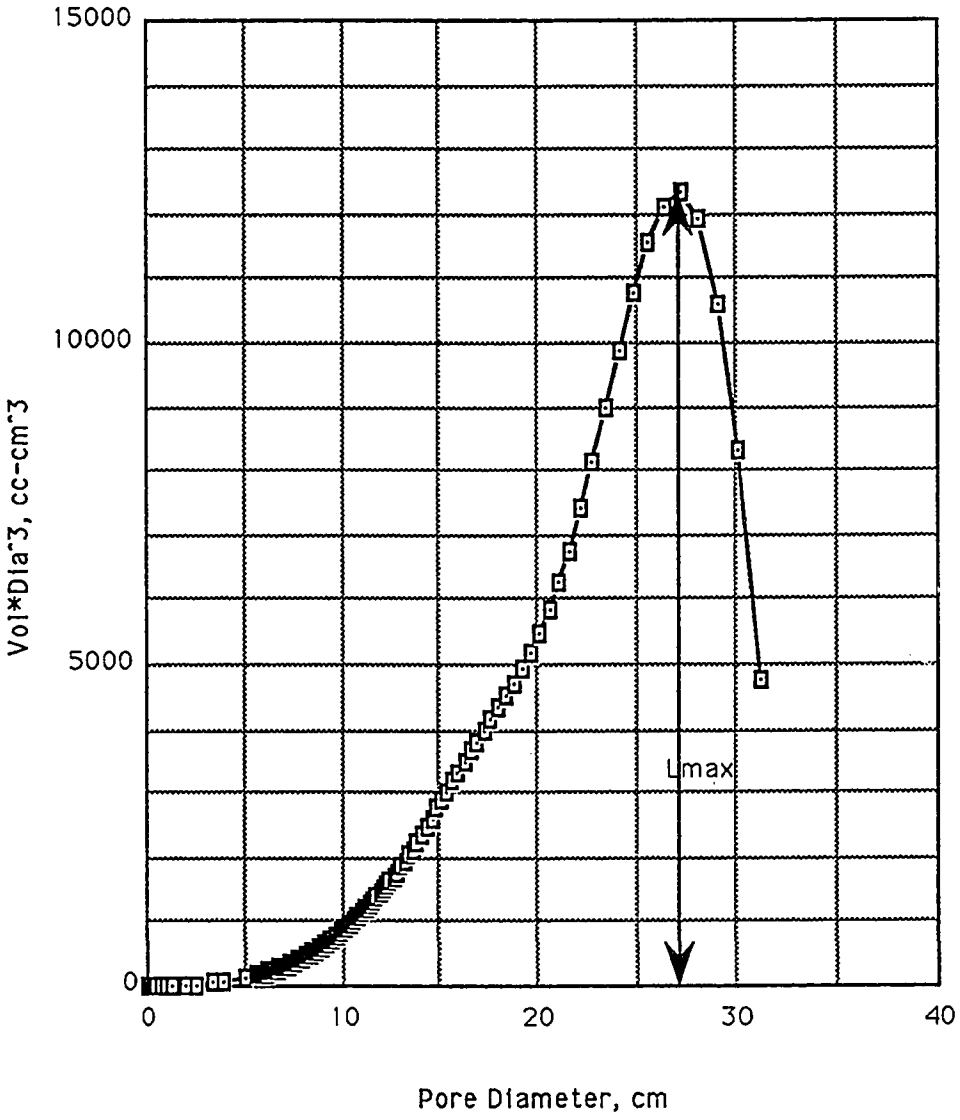

App-B4. Hydraulic Conductance Function Determination for Bentheimer Sample from Volume Injected into Pore Spaces After the Inflection Point Was Obtained.

App-B5. Katz and Thompson Method to Calculate Absolute Permeability							
Sample #	B1	Type:----	Berea		1 cm =	1.0E+04	uM
Measure Permeability:----			869	(md)	1 uM =	1.0E-06	M
Porosity:----------			20.88	(%)	1 md =	1.0E-11	cm^2
Interfacial Tension:-------			485	Dynes/cm	Pc =	6.1330	psi
Contact Angle:----------			135	Degree	Lc =	32.4326	uM
					Vol@lc =	0.7520	cc
Pressure	HG Vol.	Diameter			Vol@max=	1.7800	cc
(psi)	(cc)	(cm)			h'Lmax =	27.2478	uM
				12320.1	S(hlmax)=	0.5924	uM^2
1	0	198.909			k =	0.8669	uM^2
1.233	-0.002	161.321			k =	866.919	md
1.467	-0.003	135.589					
1.7	-0.002	117.005					
1.933	-0.001	102.902					
2.167	0.003	91.7901					
2.4	0.007	82.8788					
2.633	0.008	75.5447					
2.867	0.005	69.3788					
3.1	-0.006	64.1642					
3.333	-0.023	59.6787					
3.567	-0.042	55.7637					
3.8	-0.059	52.3445					
4.033	-0.068	49.3204					
4.267	-0.064	46.6157					
4.5	-0.044	44.202					
4.733	-0.002	42.026					
4.967	0.068	40.0461					
5.2	0.167	38.2518					
5.433	0.293	36.6113					
5.667	0.437	35.0995	Vol(cc)	Dia^3*Vol	Diameter		
5.9	0.593	33.7134		(cc^2)	(cm)		
6.133	0.752	32.4326	0	0	0		
6.367	0.909	31.2406	0.157	4786.95	31.2406		
6.6	1.055	30.1377	0.303	8294.21	30.1377		
6.833	1.183	29.1101	0.431	10631.8	29.1101		
7.067	1.287	28.1462	0.535	11929.2	28.1462		
7.3	1.361	27.2478	0.609	12320.1	27.2478		
7.533	1.411	26.405	0.659	12132.4	26.405		
7.767	1.441	25.6095	0.689	11572.4	25.6095		
8	1.453	24.8636	0.701	10774.9	24.8636		
8.233	1.454	24.16	0.702	9899.81	24.16		
8.467	1.446	23.4923	0.694	8997.77	23.4923		
8.7	1.434	22.8631	0.682	8150.62	22.8631		
8.933	1.423	22.2668	0.671	7407.89	22.2668		
9.167	1.415	21.6984	0.663	6773.23	21.6984		
9.4	1.413	21.1605	0.661	6263	21.1605		
9.633	1.415	20.6487	0.663	5837.05	20.6487		
9.867	1.421	20.159	0.669	5480.69	20.159		
10.1	1.431	19.694	0.679	5186.45	19.694		
10.333	1.443	19.2499	0.691	4929.05	19.2499		
10.567	1.457	18.8236	0.705	4702.17	18.8236		

	App-B5: Continue						
10.8	1.472	18.4175	0.72	4498.06	18.4175		
11.033	1.488	18.0286	0.736	4312.82	18.0286		
11.267	1.505	17.6541	0.753	4143.18	17.6541		
11.5	1.521	17.2964	0.769	3979.21	17.2964		
11.733	1.535	16.953	0.783	3815.04	16.953		
11.967	1.548	16.6215	0.796	3655.29	16.6215		
12.2	1.559	16.304	0.807	3497.5	16.304		
12.433	1.568	15.9985	0.816	3341.39	15.9985		
12.667	1.574	15.7029	0.822	3182.84	15.7029		
12.9	1.579	15.4193	0.827	3031.8	15.4193		
13.133	1.582	15.1458	0.83	2883.7	15.1458		
13.367	1.584	14.8806	0.832	2741.48	14.8806		
13.6	1.585	14.6257	0.833	2606.11	14.6257		
13.833	1.584	14.3793	0.832	2473.65	14.3793		
14.067	1.584	14.1401	0.832	2352.25	14.1401		
14.3	1.583	13.9097	0.831	2236.44	13.9097		
14.533	1.582	13.6867	0.83	2128.02	13.6867		
14.767	1.581	13.4698	0.829	2026.01	13.4698		
15	1.58	13.2606	0.828	1930.73	13.2606		
15.233	1.58	13.0578	0.828	1843.48	13.0578		
15.467	1.58	12.8602	0.828	1761.07	12.8602		
15.7	1.581	12.6694	0.829	1685.85	12.6694		
15.933	1.582	12.4841	0.83	1614.91	12.4841		
16.167	1.584	12.3034	0.832	1549.53	12.3034		
16.4	1.586	12.1286	0.834	1487.99	12.1286		
16.633	1.588	11.9587	0.836	1429.75	11.9587		
16.867	1.59	11.7928	0.838	1374.34	11.7928		
17.1	1.592	11.6321	0.84	1322.07	11.6321		
17.333	1.594	11.4757	0.842	1272.49	11.4757		
17.567	1.596	11.3229	0.844	1225.22	11.3229		
17.8	1.598	11.1747	0.846	1180.52	11.1747		
18.033	1.6	11.0303	0.848	1138.04	11.0303		
18.267	1.602	10.889	0.85	1097.44	10.889		
18.5	1.603	10.7518	0.851	1057.74	10.7518		
18.733	1.604	10.6181	0.852	1019.96	10.6181		
18.967	1.605	10.4871	0.853	983.824	10.4871		
19.2	1.606	10.3599	0.854	949.551	10.3599		
19.433	1.607	10.2356	0.855	916.876	10.2356		
19.667	1.607	10.1139	0.855	884.537	10.1139		
19.9	1.608	9.99543	0.856	854.828	9.99543		
20.133	1.608	9.87976	0.856	825.491	9.87976		
20.367	1.609	9.76625	0.857	798.296	9.76625		
20.6	1.609	9.65578	0.857	771.513	9.65578		
20.833	1.61	9.54779	0.858	746.786	9.54779		
21.067	1.61	9.44174	0.858	722.177	9.44174		
21.3	1.611	9.33846	0.859	699.55	9.33846		
21.533	1.611	9.23741	0.859	677.086	9.23741		
21.767	1.612	9.13811	0.86	656.246	9.13811		
22	1.613	9.04132	0.861	636.355	9.04132		
22.233	1.614	8.94657	0.862	617.273	8.94657		
22.467	1.614	8.85339	0.862	598.186	8.85339		
22.7	1.615	8.76252	0.863	580.627	8.76252		

	App-B5: Continue						
22.933	1.616	8.67349	0.864	563.761	8.67349		
23.167	1.617	8.58588	0.865	547.483	8.58588		
23.4	1.618	8.50039	0.866	531.906	8.50039		
23.633	1.619	8.41658	0.867	516.924	8.41658		
23.867	1.62	8.33407	0.868	502.447	8.33407		
24.1	1.62	8.25349	0.868	488.015	8.25349		
24.333	1.621	8.17446	0.869	474.676	8.17446		
24.567	1.622	8.0966	0.87	461.771	8.0966		
24.8	1.623	8.02053	0.871	449.394	8.02053		
25.033	1.624	7.94588	0.872	437.464	7.94588		
25.267	1.624	7.87229	0.872	425.422	7.87229		
25.5	1.625	7.80036	0.873	414.341	7.80036		
25.733	1.626	7.72973	0.874	403.649	7.72973		
25.967	1.627	7.66007	0.875	393.285	7.66007		
26.2	1.627	7.59195	0.875	382.885	7.59195		
26.433	1.628	7.52503	0.876	373.275	7.52503		
26.667	1.629	7.459	0.877	363.95	7.459		
26.9	1.63	7.39439	0.878	354.978	7.39439		
27.133	1.63	7.33089	0.878	345.912	7.33089		
27.367	1.631	7.26821	0.879	337.498	7.26821		
27.6	1.632	7.20685	0.88	329.397	7.20685		
27.833	1.633	7.14652	0.881	321.559	7.14652		
28.067	1.634	7.08694	0.882	313.939	7.08694		
28.3	1.634	7.02859	0.882	306.248	7.02859		
28.533	1.635	6.9712	0.883	299.146	6.9712		
28.767	1.636	6.91449	0.884	292.235	6.91449		
29	1.637	6.85894	0.885	285.571	6.85894		
29.233	1.637	6.80427	0.885	278.796	6.80427		
29.467	1.638	6.75023	0.886	272.515	6.75023		
29.7	1.639	6.69728	0.887	266.452	6.69728		
29.933	1.64	6.64515	0.888	260.571	6.64515		
30.167	1.641	6.5936	0.889	254.841	6.5936		
30.4	1.641	6.54306	0.889	249.026	6.54306		
30.633	1.642	6.4933	0.89	243.661	6.4933		
30.867	1.643	6.44407	0.891	238.429	6.44407		
31.1	1.644	6.39579	0.892	233.372	6.39579		
31.333	1.644	6.34823	0.892	228.204	6.34823		
31.567	1.645	6.30117	0.893	223.417	6.30117		
31.8	1.646	6.255	0.894	218.786	6.255		
32.033	1.647	6.20951	0.895	214.286	6.20951		
32.267	1.648	6.16448	0.896	209.892	6.16448		
32.5	1.648	6.12028	0.896	205.41	6.12028		
32.733	1.649	6.07672	0.897	201.279	6.07672		
32.967	1.65	6.03358	0.898	197.243	6.03358		
33.2	1.651	5.99124	0.899	193.335	5.99124		
33.433	1.651	5.94949	0.899	189.321	5.94949		
33.667	1.652	5.90813	0.9	185.607	5.90813		
33.9	1.653	5.86753	0.901	182.008	5.86753		
34.133	1.654	5.82747	0.902	178.504	5.82747		
34.367	1.655	5.78779	0.903	175.076	5.78779		
34.6	1.655	5.74882	0.903	171.563	5.74882		
34.833	1.656	5.71036	0.904	168.329	5.71036		

App-B5: Continue							
35.067	1.657	5.67226	0.905	165.165	5.67226		
35.3	1.658	5.63482	0.906	162.095	5.63482		
35.533	1.658	5.59787	0.906	158.927	5.59787		
35.767	1.659	5.56125	0.907	156	5.56125		
40	1.67	4.97273	0.918	112.883	4.97273		
50	1.68	3.97818	0.928	58.4255	3.97818		
60	1.69	3.31515	0.938	34.1754	3.31515		
80	1.70	2.48636	0.948	14.5714	2.48636		
100	1.71	1.98909	0.958	7.53928	1.98909		
150	1.72	1.32606	0.968	2.25718	1.32606		
200	1.73	0.99455	0.978	0.96208	0.99455		
300	1.74	0.66303	0.988	0.28798	0.66303		
500	1.75	0.39782	0.998	0.06283	0.39782		
700	1.76	0.28416	1.008	0.02313	0.28416		
1000	1.77	0.19891	1.018	0.00801	0.19891		
1500	1.78	0.13261	1.028	0.0024	0.13261		
1800	1.78	0.11051	1.028	0.00139	0.11051		

App-B6. Katz and Thompson Method to Calculate Absolute Permeability							
Sample #	S10	Type:----	Berea		1 cm =	1.0E+04	uM
Measure Permeability:----			610	(md)	1 uM =	1.0E-06	M
Porosity:----------			21.58	(%)	1 md =	1.0E-11	cm^2
Interfacial Tension:-------			485	Dynes/cm	Pc =	8.0000	psi
Contact Angie:----------			135	Degree	Lc =	24.8636	uM
					Vol@lc =	1.1420	cc
Pressure	HG Vol.	Diameter			Vol@max=	3.9300	cc
(psi)	(cc)	(cm)			h'Lmax =	22.3698	uM
				9649.17	S(hlmax)=	0.3092	uM^2
1	0	198.909			k =	0.3375	uM^2
1.233	0.001	161.321			k =	337.5157	md
1.467	0.001	135.589					
1.7	0.001	117.005					
1.933	0	102.902					
2.167	-0.001	91.7901					
2.4	-0.002	82.8788					
2.633	-0.003	75.5447					
2.867	-0.002	69.3788					
3.1	0.002	64.1642					
3.333	0.009	59.6787					
3.567	0.017	55.7637					
3.8	0.027	52.3445					
4.033	0.038	49.3204					
4.267	0.048	46.6157					
4.5	0.057	44.202					
4.733	0.065	42.026					
4.967	0.07	40.0461					
5.2	0.071	38.2518					
5.433	0.073	36.6113					
5.667	0.079	35.0995					
5.9	0.094	33.7134					
6.133	0.121	32.4326					
6.367	0.164	31.2406					
6.6	0.229	30.1377					
6.833	0.318	29.1101					
7.067	0.437	28.1462					
7.3	0.585	27.2478					
7.533	0.757	26.405	Vol(cc)	Dia^3*Vol	Diameter		
7.767	0.944	25.6095		(cc^2)	(cm)		
8	1.142	24.8636	0	0	0		
8.233	1.341	24.16	0.199	2806.36	24.16		
8.467	1.537	23.4923	0.395	5121.21	23.4923		
8.7	1.721	22.8631	0.579	6919.66	22.8631		
8.933	1.887	22.2668	0.745	8224.86	22.2668		
9.167	2.028	21.6984	0.886	9051.41	21.6984		
9.4	2.145	21.1605	1.003	9503.46	21.1605		
9.633	2.238	20.6487	1.096	9649.17	20.6487		
9.867	2.312	20.159	1.17	9585.06	20.159		
10.1	2.367	19.694	1.225	9356.99	19.694		
10.333	2.408	19.2499	1.266	9030.64	19.2499		
10.567	2.436	18.8236	1.294	8630.65	18.8236		

App-B6: Continue							
10.8	2.454	18.4175	1.312	8196.47	18.4175		
11.033	2.464	18.0286	1.322	7746.67	18.0286		
11.267	2.469	17.6541	1.327	7301.47	17.6541		
11.5	2.472	17.2964	1.33	6882.12	17.2964		
11.733	2.474	16.953	1.332	6489.95	16.953		
11.967	2.479	16.6215	1.337	6139.6	16.6215		
12.2	2.489	16.304	1.347	5837.84	16.304		
12.433	2.503	15.9985	1.361	5573.07	15.9985		
12.667	2.521	15.7029	1.379	5339.58	15.7029		
12.9	2.543	15.4193	1.401	5136.1	15.4193		
13.133	2.568	15.1458	1.426	4954.41	15.1458		
13.367	2.595	14.8806	1.453	4787.71	14.8806		
13.6	2.624	14.6257	1.482	4636.56	14.6257		
13.833	2.653	14.3793	1.511	4492.41	14.3793		
14.067	2.683	14.1401	1.541	4356.75	14.1401		
14.3	2.712	13.9097	1.57	4225.28	13.9097		
14.533	2.74	13.6867	1.598	4097.09	13.6867		
14.767	2.766	13.4698	1.624	3968.93	13.4698		
15	2.79	13.2606	1.648	3842.8	13.2606		
15.233	2.811	13.0578	1.669	3715.9	13.0578		
15.467	2.829	12.8602	1.687	3588.07	12.8602		
15.7	2.845	12.6694	1.703	3463.22	12.6694		
15.933	2.858	12.4841	1.716	3338.79	12.4841		
16.167	2.869	12.3034	1.727	3216.39	12.3034		
16.4	2.879	12.1286	1.737	3099.08	12.1286		
16.633	2.886	11.9587	1.744	2982.63	11.9587		
16.867	2.892	11.7928	1.75	2870.05	11.7928		
17.1	2.897	11.6321	1.755	2762.19	11.6321		
17.333	2.902	11.4757	1.76	2659.84	11.4757		
17.567	2.905	11.3229	1.763	2559.31	11.3229		
17.8	2.908	11.1747	1.766	2464.31	11.1747		
18.033	2.91	11.0303	1.768	2372.7	11.0303		
18.267	2.913	10.889	1.771	2286.55	10.889		
18.5	2.915	10.7518	1.773	2203.73	10.7518		
18.733	2.918	10.6181	1.776	2126.11	10.6181		
18.967	2.921	10.4871	1.779	2051.84	10.4871		
19.2	2.923	10.3599	1.781	1980.27	10.3599		
19.433	2.926	10.2356	1.784	1913.11	10.2356		
19.667	2.929	10.1139	1.787	1848.73	10.1139		
19.9	2.932	9.99543	1.79	1787.55	9.99543		
20.133	2.935	9.87976	1.793	1729.1	9.87976		
20.367	2.939	9.76625	1.797	1673.91	9.76625		
20.6	2.943	9.65578	1.801	1621.35	9.65578		
20.833	2.947	9.54779	1.805	1571.04	9.54779		
21.067	2.951	9.44174	1.809	1522.63	9.44174		
21.3	2.956	9.33846	1.814	1477.28	9.33846		
21.533	2.961	9.23741	1.819	1433.78	9.23741		
21.767	2.967	9.13811	1.825	1392.62	9.13811		
22	2.972	9.04132	1.83	1352.53	9.04132		
22.233	2.978	8.94657	1.836	1314.75	8.94657		
22.467	2.984	8.85339	1.842	1278.26	8.85339		
22.7	2.989	8.76252	1.847	1242.66	8.76252		

App-B6: Continue							
22.933	2.995	8.67349	1.853	1209.09	8.67349		
23.167	3.001	8.58588	1.859	1176.61	8.58588		
23.4	3.006	8.50039	1.864	1144.89	8.50039		
23.633	3.012	8.41658	1.87	1114.93	8.41658		
23.867	3.017	8.33407	1.875	1085.36	8.33407		
24.1	3.022	8.25349	1.88	1056.99	8.25349		
24.333	3.027	8.17446	1.885	1029.65	8.17446		
24.567	3.031	8.0966	1.889	1002.63	8.0966		
24.8	3.035	8.02053	1.893	976.697	8.02053		
25.033	3.039	7.94588	1.897	951.684	7.94588		
25.267	3.043	7.87229	1.901	927.439	7.87229		
25.5	3.047	7.80036	1.905	904.146	7.80036		
25.733	3.051	7.72973	1.909	881.655	7.72973		
25.967	3.054	7.66007	1.912	859.383	7.66007		
26.2	3.058	7.59195	1.916	838.409	7.59195		
26.433	3.061	7.52503	1.919	817.711	7.52503		
26.667	3.065	7.459	1.923	798.033	7.459		
26.9	3.068	7.39439	1.926	778.688	7.39439		
27.133	3.072	7.33089	1.93	760.375	7.33089		
27.367	3.076	7.26821	1.934	742.573	7.26821		
27.6	3.08	7.20685	1.938	725.422	7.20685		
27.833	3.084	7.14652	1.942	708.816	7.14652		
28.067	3.087	7.08694	1.945	692.302	7.08694		
28.3	3.091	7.02859	1.949	676.732	7.02859		
28.533	3.095	6.9712	1.953	661.644	6.9712		
28.767	3.099	6.91449	1.957	646.951	6.91449		
29	3.103	6.85894	1.961	632.773	6.85894		
29.233	3.107	6.80427	1.965	619.023	6.80427		
29.467	3.111	6.75023	1.969	605.623	6.75023		
29.7	3.115	6.69728	1.973	592.682	6.69728		
29.933	3.119	6.64515	1.977	580.123	6.64515		
30.167	3.123	6.5936	1.981	567.874	6.5936		
30.4	3.126	6.54306	1.984	555.757	6.54306		
30.633	3.13	6.4933	1.988	544.267	6.4933		
30.867	3.133	6.44407	1.991	532.785	6.44407		
31.1	3.137	6.39579	1.995	521.946	6.39579		
31.333	3.14	6.34823	1.998	511.156	6.34823		
31.567	3.143	6.30117	2.001	500.624	6.30117		
31.8	3.146	6.255	2.004	490.434	6.255		
32.033	3.149	6.20951	2.007	480.528	6.20951		
32.267	3.152	6.16448	2.01	470.852	6.16448		
32.5	3.155	6.12028	2.013	461.485	6.12028		
32.733	3.157	6.07672	2.015	452.149	6.07672		
32.967	3.16	6.03358	2.018	443.248	6.03358		
33.2	3.162	5.99124	2.02	434.412	5.99124		
33.433	3.164	5.94949	2.022	425.813	5.94949		
33.667	3.166	5.90813	2.024	417.409	5.90813		
33.9	3.168	5.86753	2.026	409.265	5.86753		
34.133	3.169	5.82747	2.027	401.139	5.82747		
34.367	3.171	5.78779	2.029	393.388	5.78779		
34.6	3.172	5.74882	2.03	385.684	5.74882		
34.833	3.174	5.71036	2.032	378.369	5.71036		

App-B6: Continue							
35.067	3.175	5.67226	2.033	371.027	5.67226		
35.3	3.176	5.63482	2.034	363.908	5.63482		
35.533	3.178	5.59787	2.036	357.146	5.59787		
35.767	3.179	5.56125	2.037	350.354	5.56125		
40	3.23	4.97273	2.088	256.753	4.97273		
50	3.28	3.97818	2.138	134.605	3.97818		
60	3.31	3.31515	2.168	78.9896	3.31515		
80	3.39	2.48636	2.248	34.5534	2.48636		
100	3.46	1.98909	2.318	18.2422	1.98909		
150	3.57	1.32606	2.428	5.6616	1.32606		
200	3.63	0.99455	2.488	2.44751	0.99455		
300	3.71	0.66303	2.568	0.74851	0.66303		
500	3.79	0.39782	2.648	0.16671	0.39782		
700	3.84	0.28416	2.698	0.0619	0.28416		
1000	3.87	0.19891	2.728	0.02147	0.19891		
1500	3.92	0.13261	2.778	0.00648	0.13261		
1800	3.93	0.11051	2.788	0.00376	0.11051		

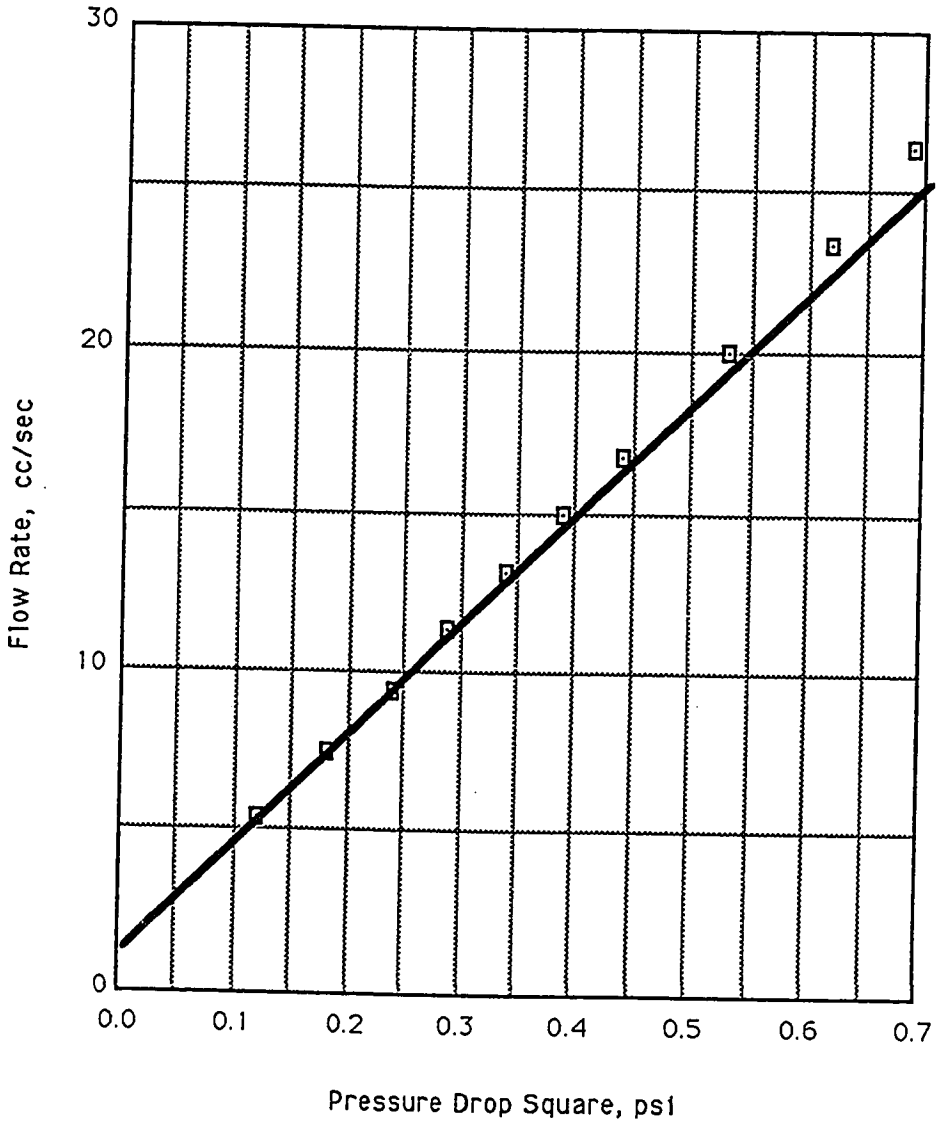

App-B7. Results Obtained from Gas Permeameter for Bentheimer Sample

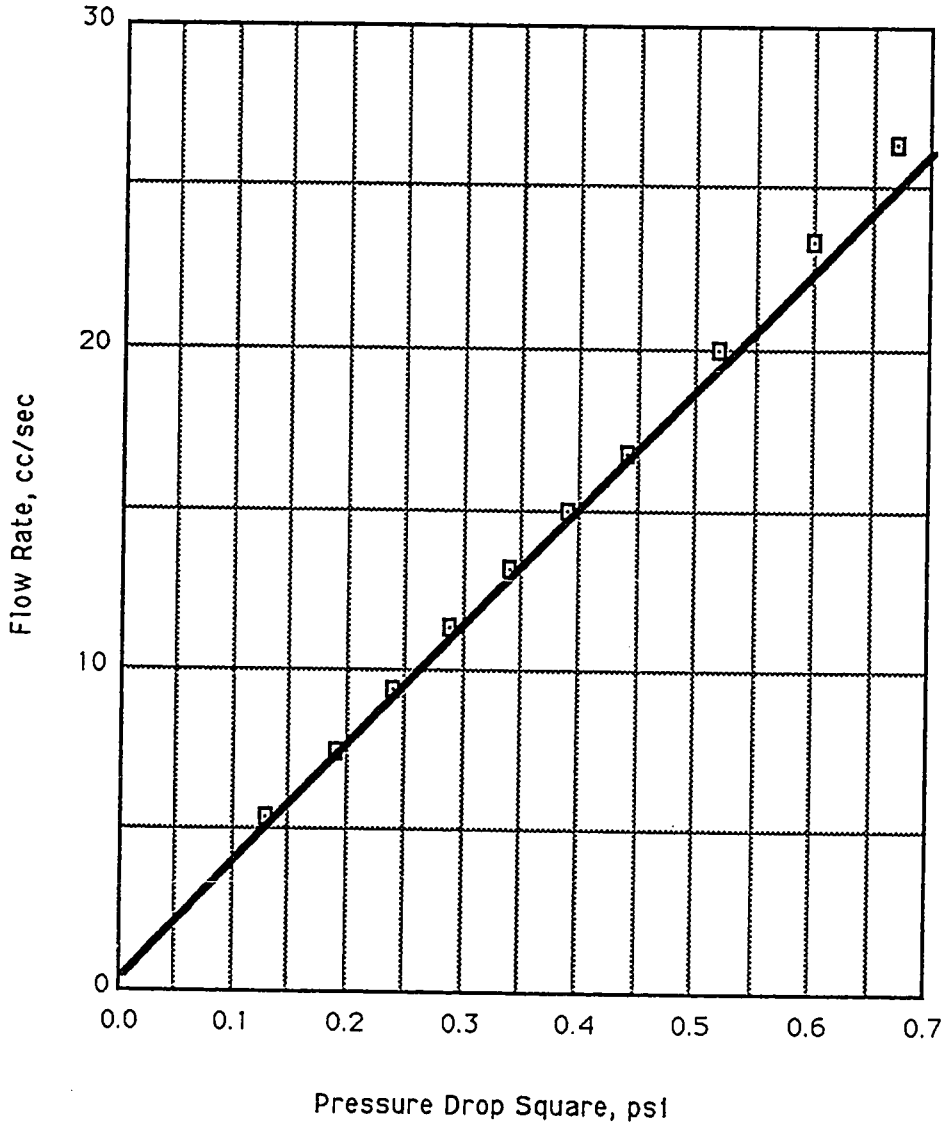

App-B8. Results Obtained from Gas Permeameter for Berea Sample.

APPENDIX-C

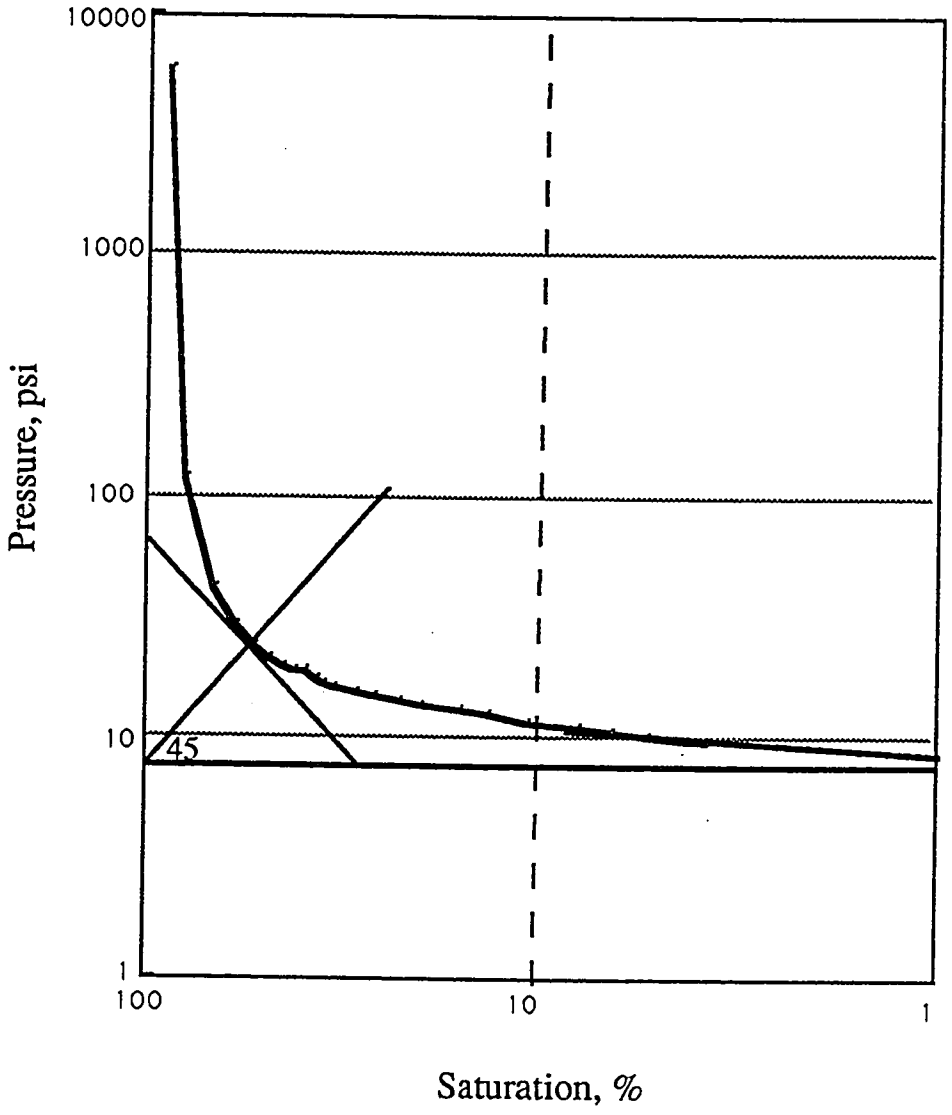

App-C1. Correlation Parameter Determination from Capillary Pressure Data for Berea Sample.

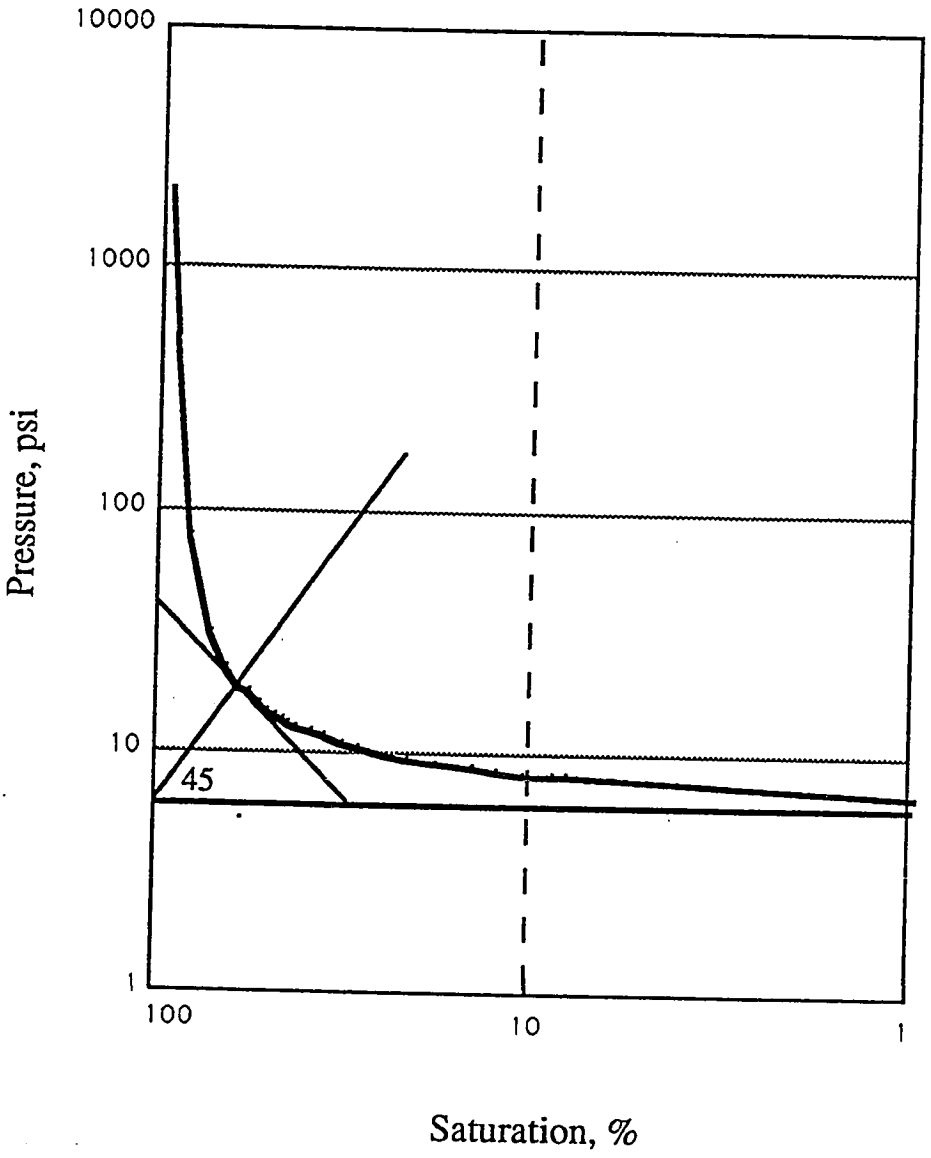

App-C2. Correlation Parameter Determination from Capillary Pressure Data for Bentheimer Sample.